Improving the Delivery of Molecularly-Targeted Agents to Effectively Treat Melanoma Brain Metastases

A Dissertation

SUBMITTED TO THE FACULTY OF

UNIVERSITY OF MINNESOTA

BY

Shruthi Vaidhyanathan

IN PARTIAL FULFILLMENT OF THE REQUIREMENTS

FOR THE DEGREE OF

DOCTOR OF PHILOSOPHY

Prof. William F. Elmquist

March 2015

Acknowledgements

First and foremost, I thank my advisor, Prof. William F. Elmquist for giving me this extraordinary opportunity, for his expert scientific guidance, for sharing his immense experience and foresight, and great patience when I was taking baby steps towards my research project, on my way towards shaping into a scientist.

I thank the members of my thesis committee, Prof. Richard Brundage, Prof. Jayanth Panyam and Prof. Jann Sarkaria for their contribution to my thesis work and education. I specially thank Prof. Sarkaria for his immense interest in my thesis project, his invaluable inputs, questions, and suggestions. Many of our discussions have been critical to the path my thesis has taken.

I thank members of the Elmquist lab, Rajendar Mittapalli, Brynna Wilken-Resman, Karen Parrish, Rajneet Oberoi, Ramola Sane and Sagar Agarwal for their invaluable inputs and discussions through different stages of my PhD project. Here, I specially like to thank Raj for his extraordinary patience and dedication in guiding me in all aspects of this project ranging from experiment planning to making presentations and drafting manuscripts. I am truly grateful to Raj.

I thank my friends, Mehak Mehta, Nidhi Sharda, Caroline Churchill, Tanmoy Sadhuka, Anuradha Gopalakrishnan, Guruprasad Somasundaram, Rohini Balachandran, Vignesh Ravindran, Vaidehi Venkatesan, and Arvind Sudarsanam for their company, encouragement and sharing their lives with me.

I thank my wonderful parents, Vaidhyanathan and Rukmini for their endless love, patience, faith in me, and their never give-up attitude. I thank my brother Shankar for his support during extremely tough times. I am always grateful to Sai, my husband, for his inputs, unbelievable support, relentless enthusiasm and willingness to play the mentor role.

Dedication

To Vidvath, my beautiful little friend. Although you left me too soon, you stay on in my heart touching my life in inexplicable ways every day.

Abstract

The FDA approval of molecularly-targeted drugs that specifically targeted aberrant signaling proteins has brought about new hope for the treatment of advanced melanoma. Historically, metastatic melanoma has been an untreatable devastating disease. Two BRAF inhibitors (vemurafenib and dabrafenib), a MEK inhibitor (trametinib), and a combination of dabrafenib and trametinib are currently in use and several other drugs are in clinical development. Melanoma is known to metastasize to distant organs such as the lung, liver and brain.

A critical challenge in the successful treatment of metastatic melanoma is the effective treatment of brain metastases. A significant proportion of melanoma patients have brain metastases at autopsy. It is also known that once patients develop clinical signs of CNS disease, they have an abysmally poor survival (less than 6 months). This brings about an important question about the efficacy of current drugs in treating brain metastases. The blood-brain barrier is comprised of a tight network of endothelial cells that are sealed together by tight-junction (TJ) protein complexes. The BBB also expresses several efflux transport proteins that utilize ATP to pump drug molecules against a concentration gradient. Together, the TJ proteins and ATP-dependent efflux transport proteins are known to effectively limit the permeability of several chemotherapeutics across the blood-brain barrier.

Of particular interest are two efflux transporters, P-glycoprotein (P-gp) and breast-cancer resistance protein (BCRP) that are known to be highly expressed at the BBB. One of the aims of this thesis project was to understand the factors that potentially limit the efficacy of molecularly-targeted drugs in treating deadly melanoma brain metastases. Through this work, we have shown that several molecularly-targeted agents are substrates for active efflux by P-gp and BCRP. Through a series of carefully planned in vitro experiments and elegant pharmacokinetic studies in mice we conclude that the limited brain distribution of vemurafenib, dabrafenib, trametinib, and GSK2126458 (a Pi3K/mTOR inhibitor) is due to their interaction with P-gp and BCRP. We also investigated potential differences in pharmacokinetics and pharmacodynamics of vemurafenib when administered as pharmacy grade Zelboraf® versus non-pharmacy grade vemurafenib. We observed that formulation differences that affect the solubility of a drug are extremely critical to designing and interpreting meaningful pre-clinical studies. Currently, we are conducting studies in a novel melanoma mouse model in order to understand the efficacy of molecularly- targeted drugs in treating brain metastases (single agent or in-combination). The findings of this thesis provide significant insight into the selection of rational drug combinations and are highly relevant to improving the treatment of melanoma brain metastases.

TABLE OF CONTENTS

LIST OF TABLES

LIST OF FIGURES

CHAPTER 1: IMPROVING THE DELIVERY OF MOLECULARLY-TARGETED AGENTS TO EFFECTIVELY TREAT MELANOMA BRAIN METASTASES

1. 1 Introduction

Metastases of melanoma into the central nervous system (CNS) are a common occurrence in the progression of metastatic melanoma. Brain metastases are a untreatable and lethal condition in most patients with advanced stages of melanoma. Surgery, stereotactic radiotherapy, and whole brain radiation have been the main treatment methods for brain metastases. More recently, understanding of the genetic drivers of melanoma has led to the development of molecularly targeted agents such as vemurafenib, dabrafenib, and trametinib have been approved by the FDA for use in patients with metastatic melanoma.

BRAF inhibitors that block the MAPK signaling pathway have certainly emerged as a new hope for this previously untreatable deadly disease. Vemurafenib and dabrafenib, the two BRAF inhibitors have shown remarkable results in reducing extra-cranial melanoma metastases (Chapman et al., 2011; Falchook et al., 2012; Hauschild et al., 2012), however, their efficacy in the treatment of brain metastases is questionable.

The success of these therapeutic agents in treating melanoma brain metastases greatly depends upon their delivery across the blood-brain barrier (BBB). The BBB is a physiological barrier that prevents the distribution of chemotherapeutic agents to the central nervous system. P-gp and BCRP are two important drug

efflux transporters that are highly expressed at the human BBB and are known to play an influential role in distribution of drugs to the brain (Uchida et al., 2011). Several chemotherapeutic agents do not cross the BBB due to their interaction with efflux transporters, thus making the brain a sanctuary site for metastatic tumor cells. Another significant concern is the development of resistance to molecularly targeted agents. Several other novel agents are currently in clinical development to be used in combination with BRAF inhibitors. One success story is that of the trametinib, a MEK inhibitor in combination with dabrafenib that significantly improved overall survival as compared to single agent dabrafenib (Flaherty et al., 2012a). Combination therapies that block alternate signaling pathways such as PI3K/mTOR is also a promising option for delaying resistance. In this chapter, current treatment options for melanoma brain metastases, the mechanisms that limit the brain delivery of these agents, and possible methods to overcome resistance and delivery challenges have been discussed.

1. 2 Melanoma

Melanoma is a neoplasm that originates in the pigment producing cells of the skin. Of the 3 million skin cancers that are diagnosed each year, basal and squamous cell carcinoma account for about 90% of the cases. Melanoma is the third most common skin cancer and has the highest mortality rate. It is estimated that 1 in 50 Americans will be diagnosed with melanoma at some point in their life-time (Siegel et al., 2014).

In the early stages of melanoma, localized disease is curable with a 5-year survival of greater than 90% while disseminated disease (metastatic melanoma) has an extremely poor prognosis with an overall survival of less than 1-year and 5-year survival of less than 15% (Balch et al., 2009). The incidence of melanoma has been steadily escalating and it is predicted that approximately 74,000 new cases and ~ 10,000 deaths from the disease are expected in 2015 (Siegel et al., 2015). After lung and breast cancer, melanoma is the third most common neoplasm to metastasize to the brain (Johnson and Young, 1996). Most melanomas arise from the skin and are called cutaneous melanomas. UV radiations are thought to play a significant causative role in cutaneous lesions. However, the exact role of UV radiations for acral lentiginous, mucosal and nodular type lesions is not well understood. Some of the risk factors for the development of CNS metastasis in melanoma patients include male sex, thickness or ulceration of primary lesion, site in the head and neck, mucosal or acral lentiginous tumors, and nodular primary lesions (Sampson et al., 1998).

1. 3 Melanoma brain metastases

More than 90% of melanoma patients develop brain metastases within three years of diagnosis of primary melanoma, and most of these patients die from progressive disease (Fife et al., 2004). Patients with one to three brain metastases are often treated with surgical resection or stereotactic radiosurgery, while those with several brain metastases typically receive whole brain radiation

(Gibney et al., 2012). Unfortunately, melanomas are highly resistant to radiation and chemotherapy, and patients with brain metastases have a dismal survival of the order of 4 months from first detection despite aggressive therapy (Sampson et al., 1998; Fife et al., 2004). Melanoma brain metastases are the cause of death in nearly 95 % of patients (Sampson et al., 1998). Patients with multiple brain metastases and extensive peripheral disease can have particularly poor survival, which can be as short as 1-2 months (Gupta et al., 1997; Fife et al., 2004). Incidentally, 50 to 70% of melanoma patients have brain metastases at autopsy (Fife et al., 2004).

After lung and breast cancer, melanoma is the third most common cancer to metastasize to the brain (Amer et al., 1978; Johnson and Young, 1996; Schouten et al., 2002). The presence of brain metastases in 50-70% of melanoma patients at autopsy is suggestive of a unmet medical need.

Drug delivery across the blood-brain barrier (BBB) is a crucial factor that has been severely overlooked for the success of novel targeted therapies in treating melanoma brain metastases. The success of many small molecule drugs in the effective treatment of central nervous system tumors is limited by their penetration across the blood-brain barrier, in particular by their interaction with efflux transporter proteins, including P-glycoprotein, and breast cancer resistance protein (BCRP) (Agarwal et al., 2011b).

The last decade has seen tremendous progress in the treatment of melanoma without much improvement in outcomes for patients with melanoma brain metastases. One important reason for this is the fact that patients with melanoma brain metastases have been systematically excluded from several clinical trials (Fife et al., 2004).

1. 4 Mechanism of Melanoma brain metastasis

The influence of the BBB and the natural tropism of melanoma to the brain are key factors that need to be well understood to improve the treatment of melanoma brain metastases. The "seed and soil" hypothesis proposed by Stephen Paget tried to explain the dissemination of tumor cells ("seed") from the primary site via the blood stream to distant organs based on an inherent biochemical affinity of cancer cells for a certain distant site ("soil") which further leads to the development of metastases (Fidler, 2003).

Metastasis is a multistage process where the cancer cells from the primary site disseminate to distant organs. The metastatic cascade in the formation of brain metastases is comprised of a series of sequential processes where tumor cells escape from the primary tumor, enter the blood circulation, attach to blood vessels, and extravasate along the BBB into the brain parenchyma. This is followed by invasion and interaction with the brain microenvironment leading to survival and proliferation of tumor cells **(Fig.1.1)**. Based on the characteristics of

the tumor cells, they can grow either by forming new blood vessels (angiogenesis), or develop by growing along pre-existing blood vessels (vascular co-option) (Joyce and Pollard, 2009; Fidler et al., 2010; Fidler, 2011). The invasion and growth of tumor cells in the brain parenchyma is facilitated by the interaction of tumor cells with endothelial cells.

1. 5 Recent improvements in the treatment of peripheral melanoma metastases

Recent discovery of activating mutations in the MAPK signaling pathway has led to the development of molecularly targeted agents that inhibit specific signaling proteins. The FDA approved BRAF inhibitors, vemurafenib and dabrafenib and a mitogen-activated protein kinase inhibitor, trametinib, have shown remarkable efficacy against peripheral melanoma tumors (Chapman et al., 2011; Falchook et al., 2012; Flaherty et al., 2012a; Hauschild et al., 2012) **(Fig.1.2)**. Vemurafenib and dabrafenib were approved after showing significant improvement in progression-free survival and overall survival (PFS) compared to dacarbazine. Dacarbazine (alkylating agent), an ineffective drug, was the standard of care for the treatment of advanced melanoma before the approval of vemurafenib (Serrone et al., 2000). Similarly, trametinib also showed a significant improvement in PFS leading to its approval. However, the emergence of resistance to BRAF inhibitors is a major hurdle in the long-term success of BRAF inhibitors. Resistance to BRAF inhibitors leading to eventual relapse is found to

usually occur within one year of single-agent therapy (Sullivan and Flaherty, 2013; Trunzer et al., 2013). Combination therapy with multiple molecularly targeted agents is a promising approach that has been pursued to overcome resistance and prolong survival. However, the efficacy of these agents in the treatment of melanoma brain metastases is poorly understood.

Effective combination therapy for melanoma brain metastases with targeted agents requires the sufficient delivery of all agents in the combination across the BBB to target sites in melanoma brain metastases that may reside behind an intact BBB.

1. 6 Failure of treatments for melanoma brain metastasis

1. 6. 1 Blood-brain barrier as a significant barrier to drug delivery

The BBB is comprised of endothelial cells that are joined together by tight-junctions, surrounded by extracellular matrix components, pericytes and astrocyte foot processes which together form the neurovascular unit. These tight junctions (zonula occludens) between endothelial cells make the BBB relatively impermeable to a large variety of drug molecules (Loscher and Potschka, 2005). In addition to the tight-junction proteins, the BBB also expressed a wide variety of transport proteins of the ATP Binding Cassette (ABC) family of proteins. These proteins are expressed on the basolateral and apical surface of the endothelial cells and play a critical role in efflux of several drugs that are used to treat brain diseases (Loscher and Potschka, 2005).

P-glycoprotein (P-gp, ABCB1, MDR1) , a 170 kDa phosphorylated glycoprotein and a 72 kDa half-transporter protein -BCRP (breast cancer resistance protein) are two important efflux transporters that are highly expressed at the human BBB, and are known to influence the CNS distribution of several drugs(Agarwal et al., 2011a; Uchida et al., 2011). The influence of these two efflux transporter proteins is known to play an important role in the treatment of CNS diseases such as HIV and glioma (Ohtsuki and Terasaki, 2007; Shaik et al., 2007; Agarwal et al., 2011b).

The presence of the BBB significantly impairs the delivery of several chemotherapeutic agents to brain metastases (Agarwal et al., 2011b). The BBB serves as a physical barrier and the ABC transporter proteins contribute to maintaining brain homeostasis by excluding potentially harmful endogenous and exogenous chemicals.

In successful treatment of melanoma brain metastases with rational combinations, it is important to ensure that all drugs in the combination achieve efficacious concentrations in all micrometastatic target sites in the brain. Microscopic subclinical brain metastases likely have a relatively intact BBB and also express functional efflux transporters **(Fig. 1.10)**. Melanoma cells that have been previously treated with chemotherapeutic agents have been known to express the ATP-dependent efflux transporter ABCB5, while a side-population of

stem cells from melanoma tumors are known to express ABCB1 and ABCB5 (Chartrain et al., 2012; Luo et al., 2012).

The lack of efficacy of chemotherapy in treating brain tumors can be attributed to this reason. In the context of melanoma brain metastases treatment, with the more recent molecularly-targeted agents regard, not much is known about the interaction of vemurafenib, dabrafenib, trametinib and GSK2126458 with P-gp and BCRP.

1. 6. 2 Current therapeutic options for melanoma

Until recently, the standard therapy for metastatic melanoma was the alkylating agent, dacarbazine which had a modest survival of 5-6 months, and an almost insignificant survival advantage with severe side effects and toxicities (Serrone et al., 2000). Also, high dose interleukin-2 (IL-2) has a poor survival of about a year with significant toxicities which include arrhythmias, hypotension, capillary leak syndrome and severe neurological changes, thus making it an extremely difficult treatment for patients. The toxicities of high-dose IL-2 requires ICU (intensive-care units)-level monitoring that still resulted in treatment related deaths in approximately 2% of patients in clinical trials (Atkins et al., 1999; Atkins et al., 2000). It is important to note here that high dose IL-2 has a really poor response rate of less than 5% in patients with melanoma brain metastases (Guirguis et al., 2002). Temozolomide, the alkylating agent which crosses the blood-brain barrier (BBB) has a dismally poor survival rate of 7% and a progression free survival of

1.2 months in patients with brain metastases with no prior treatment (Agarwala et al., 2004).

1. 6. 3 Molecularly-targeted agents

More recently, research effort has led to rapid progress in the development of molecularly targeted agents for the treatment of melanoma. The discovery and understanding of oncogenic driver mutations in melanoma has been crucial in the development of specific drugs that target the disease. In melanoma, oncogenic driver mutations in BRAF and NRAS in the MAPK (mitogen-activated protein kinase) signaling pathway, p53 mutations, and PTEN mutations have been identified to play an important role in the progression of the disease (Hodis et al., 2012).

The discovery of activating mutations in the mitogen-activated protein kinase (MAPK) pathway, particularly in melanoma has led to significant advanced in therapeutic strategies for metastatic melanoma. Novel therapies that target specific molecular drivers of cancer progression such as the MAPK and PI3K/mTOR (phosphoinositide 3-kinase) signaling pathways have brought new hope for improved treatment of metastatic melanoma in recent years.

The MAPK signaling pathway is known to be highly deregulated in about 80% of melanomas as well as in a wide range of other human cancers (Davies et al., 2002). BRAF is a serine-threonine kinase in the RAS-RAF-MEK-ERK signaling cascade. An important sequencing effort in 2001 identified important point-

mutations in the BRAF gene in melanoma; these mutations were also prevalent at differing frequencies in other human cancers such as colon, thyroid and ovarian cancer (Davies et al., 2002). Further genetic analysis led to the finding that point mutations in BRAF are the most commonly found somatic mutation in melanoma and its prevalence is about 50% (Hocker and Tsao, 2007). Also, it is known that ~ 90% of all identified BRAF mutations that occur in human cancers result in a V600 E/D/K amino acid substitution (Wellbrock et al., 2004). This mutation increases BRAF protein catalytic activity by approximately 50-200 fold as compared to wild-type resulting in constitutive activation of the MEK and ERK downstream proteins (Davies et al., 2002; Karasarides et al., 2004; Wan et al., 2004). The frequency of this activating mutation and the addiction of melanomas to this pathway make mutated BRAF an extremely important therapeutic target (Wan et al., 2004).

Normally, signaling via the MAPK pathway requires the binding of a growth factor, cytokine or hormone to a receptor tyrosine kinase which leads to the activation of RAS (**Fig. 1.3**). RAS is upstream of BRAF, and upon activation recruits BRAF to the cell membrane which further signals via MEK and ERK kinases leading to cell proliferation and growth. Activating mutations lead to constitutive signaling via the MAPK (mitogen-activated protein kinase) signaling pathway that stimulates nuclear translocation of phosphorylated extracellular

signal-regulated kinases, subsequent gene transcription, leading to uncontrolled tumor growth and proliferation (McCubrey et al., 2008).

1. 6. 3. 1 BRAF targeted therapy – Vemurafenib and Dabrafenib

A majority of melanoma patients with BRAF (v-raf murine sarcoma viral oncogene homolog B) mutations exhibit a valine to glutamic acid substitution at amino acid 600 (V600E; BRAF V600E). The prevalence of this mutation provided a new exiting target for therapy and led to the development of specific BRAF inhibitors. Over the last few years, the clinical development and FDA approval of two BRAF inhibitors, vemurafenib and dabrafenib has changed the landscape of melanoma treatment. Previously, sorafenib, a nonspecific RAF inhibitor, which was able to inhibit both, wild-type and mutant BRAF, yielded extremely poor clinical response when used as a single agent (Eisen et al., 2006).

Vemurafenib is a highly selective, potent and well-characterized small-molecule BRAF V600E inhibitor that was developed using a structure-guided drug discovery approach (Tsai et al., 2008). It was approved by the Food and Drug Administration in August 2011 for patients with late-stage melanoma harboring the V600E mutation. Vemurafenib showed a remarkable improvement in overall and progression free survival in a significant percentage of BRAF V600E positive melanoma patients (Chapman et al., 2011; Ribas et al., 2011).

An important factor that leads to near 100% mortality in patients with melanoma brain metastases is likely to be the limited brain permeability of therapeutic agents across the blood-brain barrier (BBB). In this context, it is important to understand the role of BRAF inhibitors for the treatment of melanoma brain metastases in addition to surgery and radiation therapy. In the case of vemurafenib, prior evidence through case studies in the literature suggest that there has been a potential lack of efficacy in the treatment of melanoma brain metastases (Rochet et al., 2012).

Dabrafenib (GSK2118436) is a potent ATP-competitive inhibitor of the BRAF kinase, the second BRAF inhibitor to be approved by the FDA after it showed comparable clinical response to that of vemurafenib (Chapman et al., 2011; Hauschild et al., 2012). The safety and clinical response of dabrafenib against peripheral melanoma metastases was greater than 50% (Hauschild et al., 2012). Interestingly, dabrafenib showed promising reduction in tumor size in ~90% of the patients with melanoma brain metastases (Falchook et al., 2012).

However, it is still not clear whether dabrafenib is effectively delivered to all micrometastatic sites, particularly those that a situated beyond an intact BBB. Given the potential lack of efficacy of vemurafenib in treating melanoma brain metastases and the insufficient information about dabrafenib in its potential survival benefit in patients with melanoma brain metastases, it is imperative to study the brain distribution of both these molecules in greater detail.

1. 6. 4 Resistance Mechanisms

Much of the current clinical data suggests that patients on BRAF inhibitors slowly stop responding to therapy due to the eventual development of resistance and relapse of disease (Puzanov et al., 2011). Several mechanisms may be responsible for this resistance. Mutations in upstream signaling proteins such as RAS or compensatory signaling from other growth factor receptors such as PI3K/mTOR may be driving the reactivation of the MAPK signaling pathway and strengthening the resistance to BRAF therapy (Flaherty et al., 2012a). Currently, several mechanisms have been suggested for the development of resistance to BRAF therapy, activating mutations in NRAS, upregulation of upstream RAS protein, platelet-derived growth factor receptor, phosphatidylinositol signaling (PI3K/mTOR), and loss of PTEN, upregulation of cyclinD1 and downregulation of $p27^{Kip1}$ (Aplin et al., 2011). Activating mutations in NRAS could potentially lead to signaling via CRAF, despite inhibition of BRAF using vemurafenib or dabrafenib. Also, the loss of PTEN is commonly found in melanoma which results in the increased signaling via the PI3K pathway (Villanueva et al., 2010).The occurrence of PTEN mutations with the concomitant maintenance of BRAF suggests that the PI3K pathway may be a potential driver of resistance **(Fig.1.4)**.

1. 7 Overcoming resistance

1. 7. 1 Targeting multiple signaling pathways

A rational combination of drugs that target multiple signaling pathways will eventually be the standard of care for the successful treatment of melanoma. However, in the context of treating melanoma brain metastases effectively, the challenge is the sufficient delivery of all agents in the combination across the BBB to the target sites in the brain that may reside behind an intact BBB.

Several new drug molecules are currently in development in combination with BRAF inhibitors, these include RAS, MEK, and PI3K/mTOR inhibitors **(Fig.1.5)** (Nikolaou et al., 2012).

In the context of delaying resistance, a recent success story is that of orally bioavailable MEK (MAPK kinase) inhibitor, trametinib, which was FDA approved as a single agents after it showed a 4.3 months progression free survival as compared to 1.5 months in the chemotherapy arm in phase 3 clinical trial in patients with BRAF V600E mutation (Flaherty et al., 2012b). MEK is a signaling protein that is downstream of BRAF in the MAPK signaling cascade. MEK on phosphorylation causes the phosphorylation of ERK which leads to gene transcription, cell division and growth.

Also, the combination of BRAF inhibitor dabrafenib and MEK inhibitor trametinib has shown significant improvement in progression-free survival in melanoma patients (9.4 months in the combination arm as compared to 5.8 months on

monotherapy) (Flaherty et al., 2012a) which led to the FDA approval of the combination.

However, acquired resistance to combinations is a significant problem that needs to be addressed as a top priority (Wagle et al., 2011). In the case of the dabrafenib and trametinib combination, a case study looking at the whole-exome sequencing (WES) and whole-transcriptome sequencing (RNA-seq) in 5 patients who had acquired resistance to the combination led to the identification of activating mutations in MEK2 in 3 of the 5 patients (Wagle et al., 2011; Wagle et al., 2014). This mutation was found to confer a profound resistance to the combination of dabrafenib and trametinib (Wagle et al., 2014).

In overcoming resistance to the combination of dabrafenib and trametinib, is the possibility of blocking downstream signaling proteins such as ERK or the addition of an inhibitor of other alternate signaling pathways that may be concomitantly deregulated **(Fig.1.6)**. In the case of melanoma, it is observed that the PI3K/AKT/mTOR inhibitor is frequently altered by a functional loss of PTEN or the amplification of AKT (Goel et al., 2006).

Simultaneously targeting of both the MAPK and the PI3K signaling pathways is an approach that has been proposed and actively being pursued in a subset of NRAS mutant melanomas **(Fig.1.7)** (Smalley et al., 2006).

The PI3K (phosphoinositide 3-kinase (PI3K) signaling pathway is found to be activated in several human cancers. The PI3K signaling pathway is a

downstream effector signaling molecule of the RAS pathway. PI3K phosphorylates a second messenger, phosphatidylinositol-4, 5-biphosphate, thereby generating phosphatidylinositol-3, 4, 5-triphosphate, which activates AKT. Activated AKT has several cellular and enzymatic substrates, which promote cellular proliferation, growth and survival **(Fig.1.8)**. In this context, GSK2126458, a highly potent and selective inhibitor of PI3Ks and the mammalian target of rapamycin (mTOR) may be a possible option to be considered for combination therapy. However, it is crucial to remember that the true success of combination therapy for treating melanoma brain metastases will depend on whether all drugs in the combination will be delivered across the BBB to all metastatic sites. Other signaling pathways driven by Akt and cyclin D-cyclin dependent kinases (4/6) complexes are being investigated intensely to identify novel targets that can improve combination therapy and delay resistance (Miller and Flaherty, 2014)**(Fig. 1.9.)**.

1. 7. 2 Immunotherapy: Targeting inhibitory immune receptors

Immune checkpoint blockade with antibodies has also been an important strategy that has been pursued to obtain durable response in the treatment of metastatic melanoma. Antibodies against inhibitory immune receptors, CTLA-4, PD-1 and PD-L1 have shown promising response in a subset of melanoma patients.

Normally, T-cell activation leads to an upregulation of CTLA-4 which in-turn causes the downregulation of T-cell function. The rationale for ipilimumab was the observation that blocking CTLA-4 could result in anti-tumor immunity in preclinical models.

Ipilimumab was the first approved anti-CTLA-4 antibody which showed an improvement in overall survival in two phase III clinical trials in melanoma patients (Hodi et al., 2010; Robert et al., 2011). Tremelimumab, a second anti-CTLA- 4 antibody did not show a statistically significant improvement in overall survival (Ribas et al., 2013).

The success with targeting CTLA-4 led to other approaches targeting immunological checkpoints. PD-1 and its ligand PD-L1 are negative regulators of T-cell based immune response. When engaged by its ligand, PD-1 leads to an inhibition of kinase activity, which further leads to the inhibition of T-cell activation. Broadly, there are two categories of anti-bodies that target the PD-1/PD-L1 axis; antibodies that inhibit PD-1 and those that target and inhibit PD-L1. Nivolumab and Pembrolizumab are PD-1 targeting anti-bodies that have shown durable response in a phase-I clinical trials in patients with solid tumors (Topalian et al., 2012; Topalian et al., 2014). The ability of the immune system to readily adapt to the changing tumor microenvironment is thought to be a reason for the durable response seen with immunotherapy as compared to the acquired mutations to molecularly targeted agents which make them ineffective. A

promising approach is to combine CTLA-4 and PD-1/PD-L1 antibodies for patients who benefit from immunotherapy. A combination of ipilimumab and nivolumab has shown durable response in melanoma patients (Wolchok et al., 2013). It remains to be seen whether immunotherapy can be effectively combined with molecularly-targeted agents to improve patient outcomes while keeping side effects under control.

1. 8 Statement of the problem

Melanoma brain metastases are a major cause of mortality in patients with advanced melanoma. The successful treatment of melanoma brain metastases has been extremely challenging and it is unclear whether the more recent and promising molecularly-targeted agents will be able to make an impact on improving the treatment of brain metastases. From previous experience with brain tumors, in particular glioblastoma, it is known that several chemotherapeutic agents that are known to be substrates of P-gp and BCRP are mostly ineffective due to their inability to cross the BBB.

In the case of the newer molecularly-targeted agents for melanoma, (vemurafenib, dabrafenib, trametinib, and GSK2126458) there is sparse clinical data about their efficacy treatment of melanoma brain metastases. It is critical to examine the brain distribution of these drugs in mouse models, with the hope that the preclinical evidence gained will help in choosing drugs and rational

combinations that can eventually provide a durable response for this devastating disease.

Also, the development of resistance is a significant problem which needs to be addressed for the rational selection of efficacious combination therapies. Effective combination therapy for melanoma brain metastases with targeted agents requires the sufficient delivery of all agents in the combination across the BBB. It is likely that brain metastases differ from peripheral mets in mechanisms and time course of development of resistance to different drug concentrations in brain versus peripheral mets. The problem in selection of drugs or rational combinations to obtain durable response in treating melanoma brain metastases requires that we have substantial information about the pharmacokinetics and brain distribution of these agents. Also, it is crucial to pursue strategies to improve their brain distribution.

1. 9 Research Objective

The objectives of this research program were:

1) To investigate and elucidate the crucial mechanisms affecting the brain distribution of several currently used molecularly-targeted anti-melanoma drugs. Of particular interest was to understand the influence of active efflux by P-glycoprotein (P-gp) and Breast cancer resistance protein (BCRP) on the pharmacokinetics of three classes of molecularly- targeted drugs (BRAF, MEK and Pi3K/mTOR inhibitors).

2) Based on the understanding gained in (1), to devise strategies to improve the brain distribution of these agents by inhibition of P-gp and Bcrp using known inhibitors in combination with these agents.

1. 9. 1 Research Plan

Vemurafenib and dabrafenib are potent FDA- approved BRAF inhibitors that are currently used for the treatment of metastatic melanoma, including patients with melanoma brain metastases. In order to understand the influence of active transport mechanisms on the brain distribution of these two agents, we quantitatively assessed the role of P-gp and BCRP mediated transport via elegant pharmacokinetic studies in chapter II (vemurafenib) and chapter III (dabrafenib).

Several clinical studies have observed that patients on BRAF inhibitors eventually stop responding to therapy. The development of resistance to BRAF inhibitors is a huge challenge that needs to be overcome in order to prolong treatment response. Blocking downstream signaling proteins or alternate signaling pathways is a strategy to delay resistance to therapy. MEK is downstream of BRAF in the MAPK signaling pathway and trametinib is a potent MEK inhibitor that is FDA-approved to be used as a single agent and in combination with dabrafenib for the treatment of advanced melanoma. In chapter IV, we pharmacokinetically assess the influence of active transport on the brain distribution of trametinib and a combination of dabrafenib and trametinib.

As a second strategy to overcome resistance, it is known that the Pi3K/mTOR signaling pathway play an important role in the progression of melanoma. The combined inhibition of the Pi3K/mTOR signaling besides BRAF and MEK inhibition is a strategy that is being investigated. Chapter V examines the influence of efflux transport proteins on the brain distribution of GSK2126458 (a potent Pi3K/mTOR inhibitor). We also attempt to improve the brain distribution of GSK212658 using elacridar (a dual inhibitor of P-gp and Bcrp).

The reformulation of crystalline vemurafenib into an amorphous solid dispersion led to a huge improvement in oral bioavailability. This formulation change was critical to enable the clinical use of vemurafenib. In chapter VI, we study the difference in pharmacokinetics and oral bioavailability of pharmacy grade vemurafenib versus non-pharmacy grade (crystalline powder) vemurafenib and its impact on vemurafenib brain distribution in a mouse model.

In summary, this dissertation attempts to provide a substantial understanding of the influence of active transport on the brain distribution and pharmacokinetics of important anti-melanoma drugs. From our findings, we will be able to make important recommendations regarding the rational use of these drugs as single agent and in combination for the treatment of melanoma brain metastases.

Figures

Figure 1.1: Various steps in the formation of melanoma brain metastasis (Fokas et al., 2013)

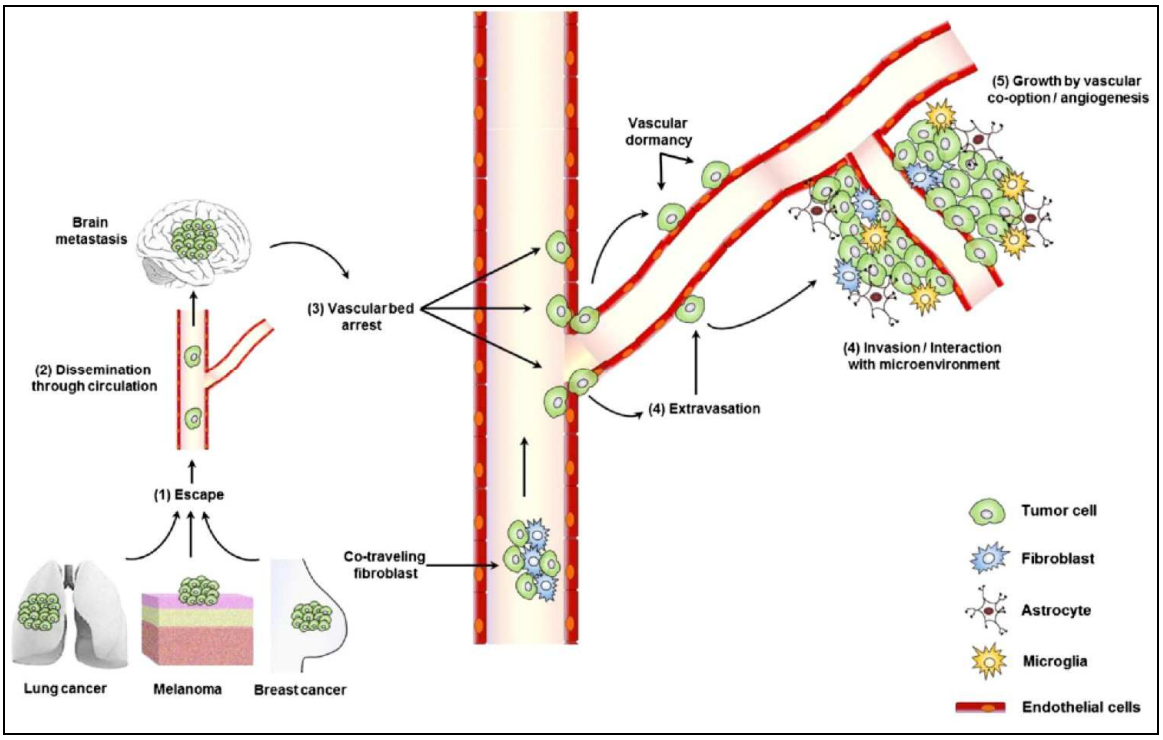

Figure 1.2: BRAF inhibitors (vemurafenib and dabrafenib) and MEK inhibitor (trametinib) block the MAPK signaling pathway

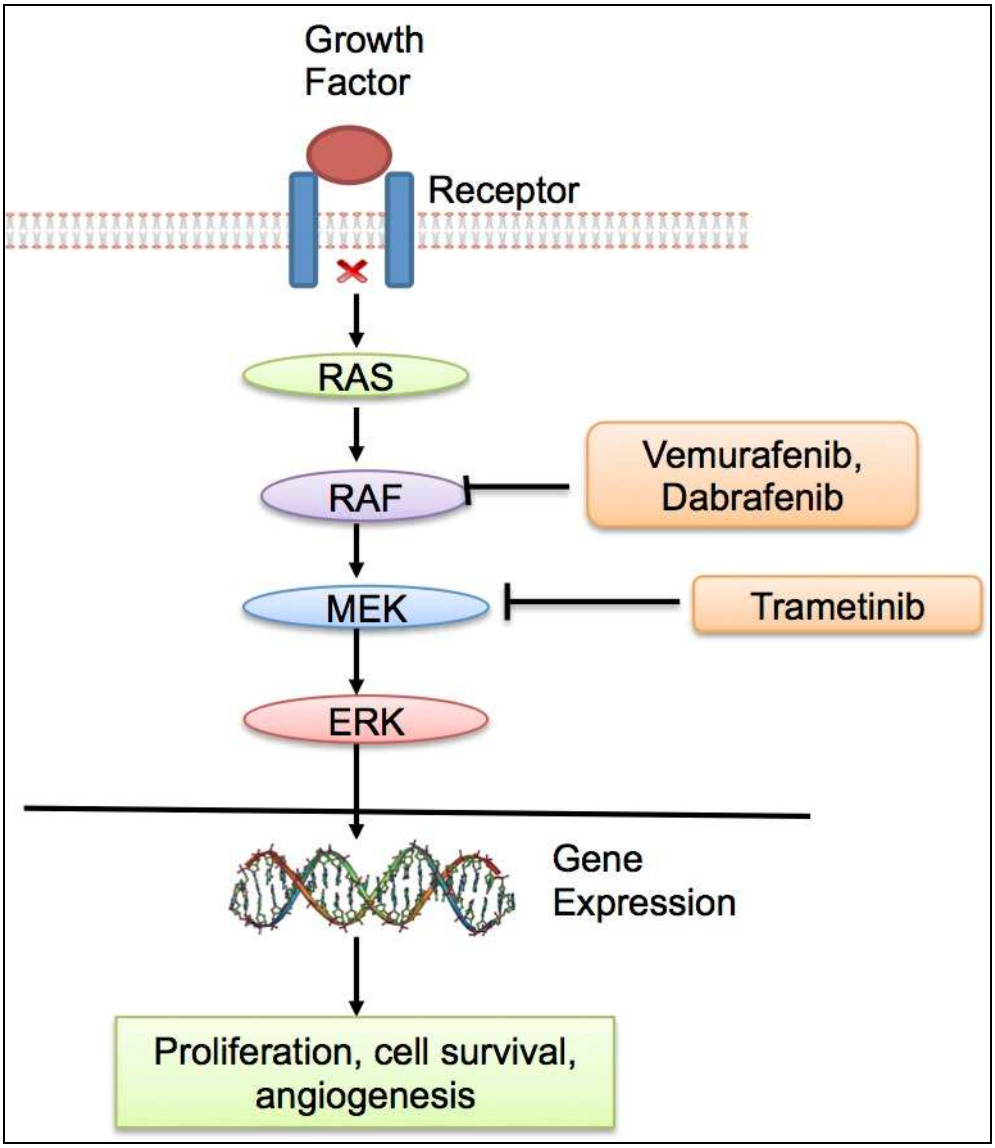

Figure 1.3: The RAF signaling pathway

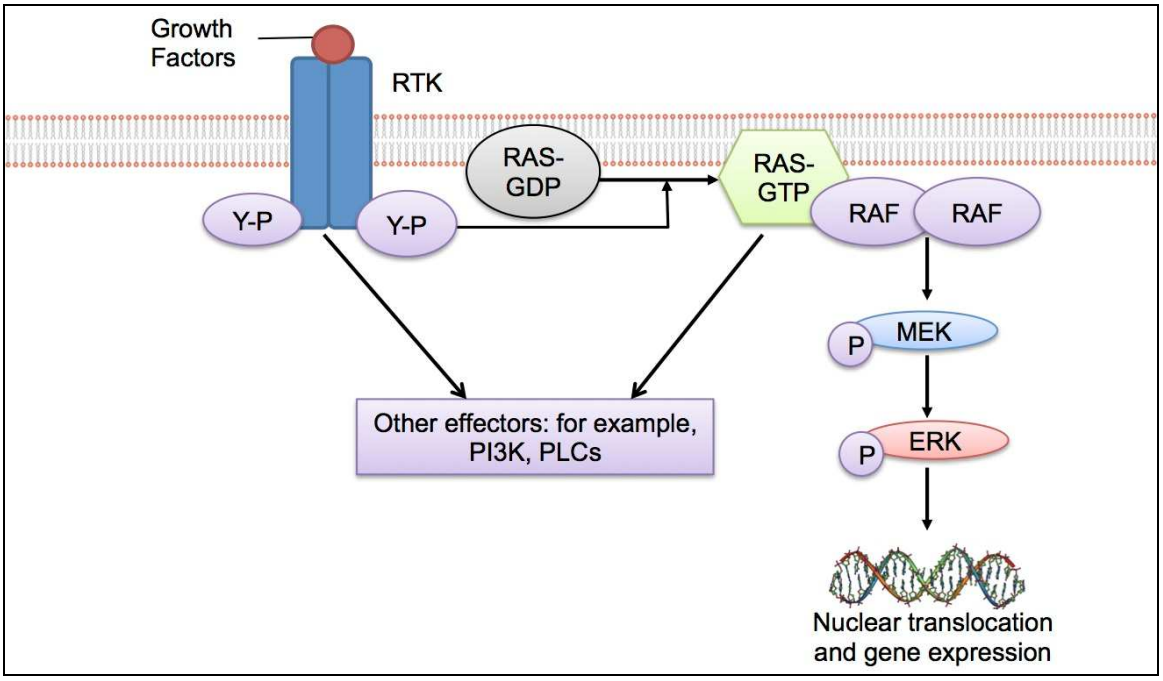

Binding of growth factor to receptor tyrosine kinases (RTK) leads to downstream signaling via RAS, RAF, MEK (mitogen-activated protein kinase (MAPK)/ERK kinase) and ERK (extracellular signal-regulated kinase) (Bollag et al., 2012)

Figure 1.4: Mechanism of acquired resistance to BRAF inhibitors

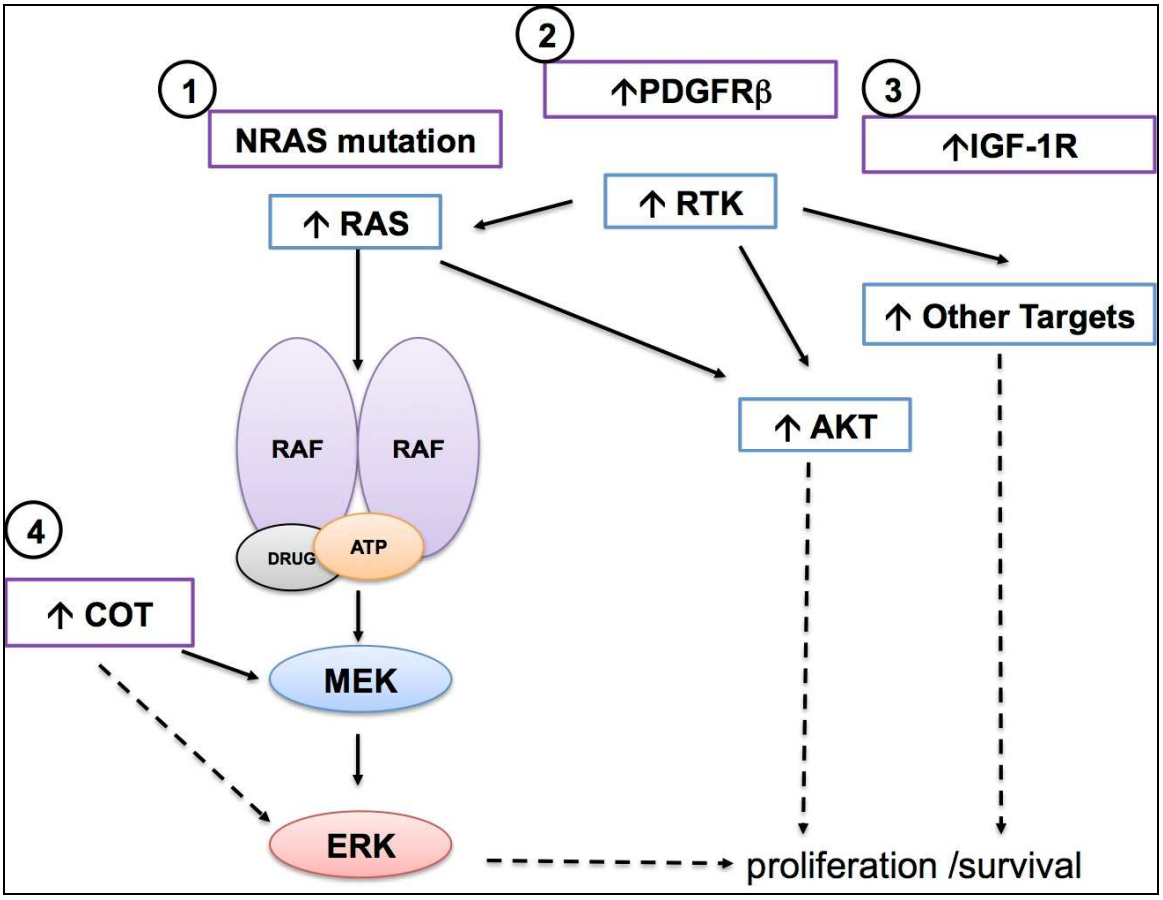

BRAF V600E melanoma tumors may acquire resistance via RAS mutation, RTK activation, COT activation (Poulikakos and Rosen, 2011).

Figure 1.5: Molecularly-targeted agents that inhibit the MAPK and PI3K signaling pathway

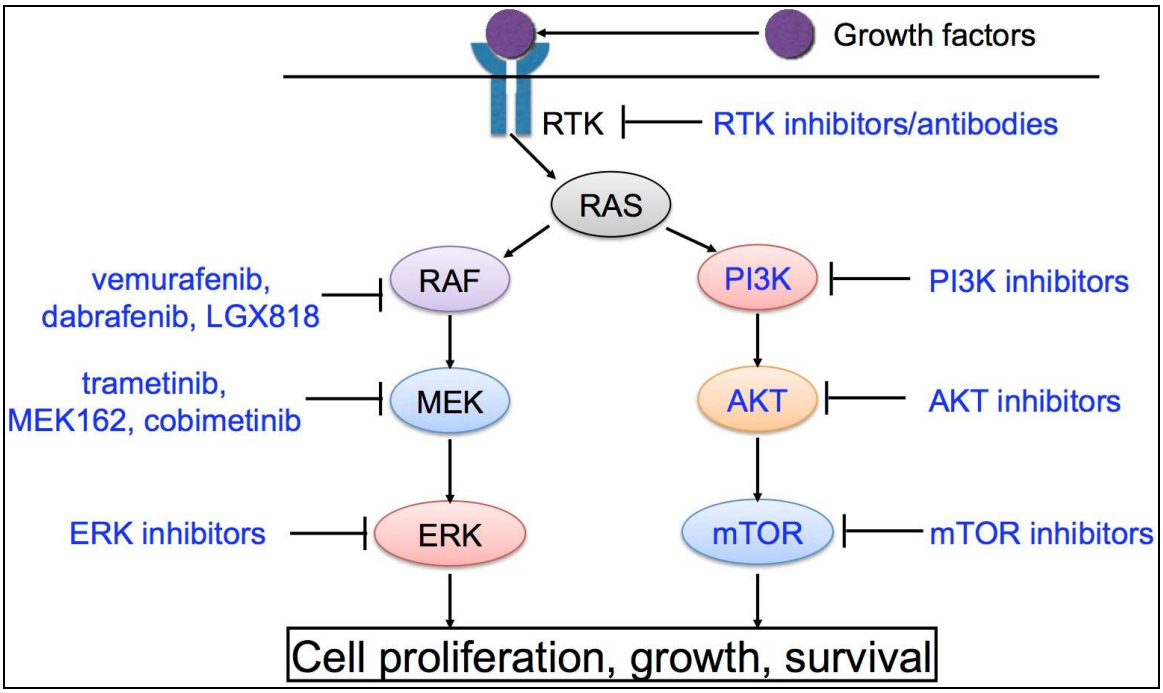

RAF and PI3K are downstream of RAS and are potential therapeutic targets that have to be rationally selected for single or combination treatment of melanoma brain metastases.

Figure 1.6: Important signaling pathways and therapeutic targets in melanoma

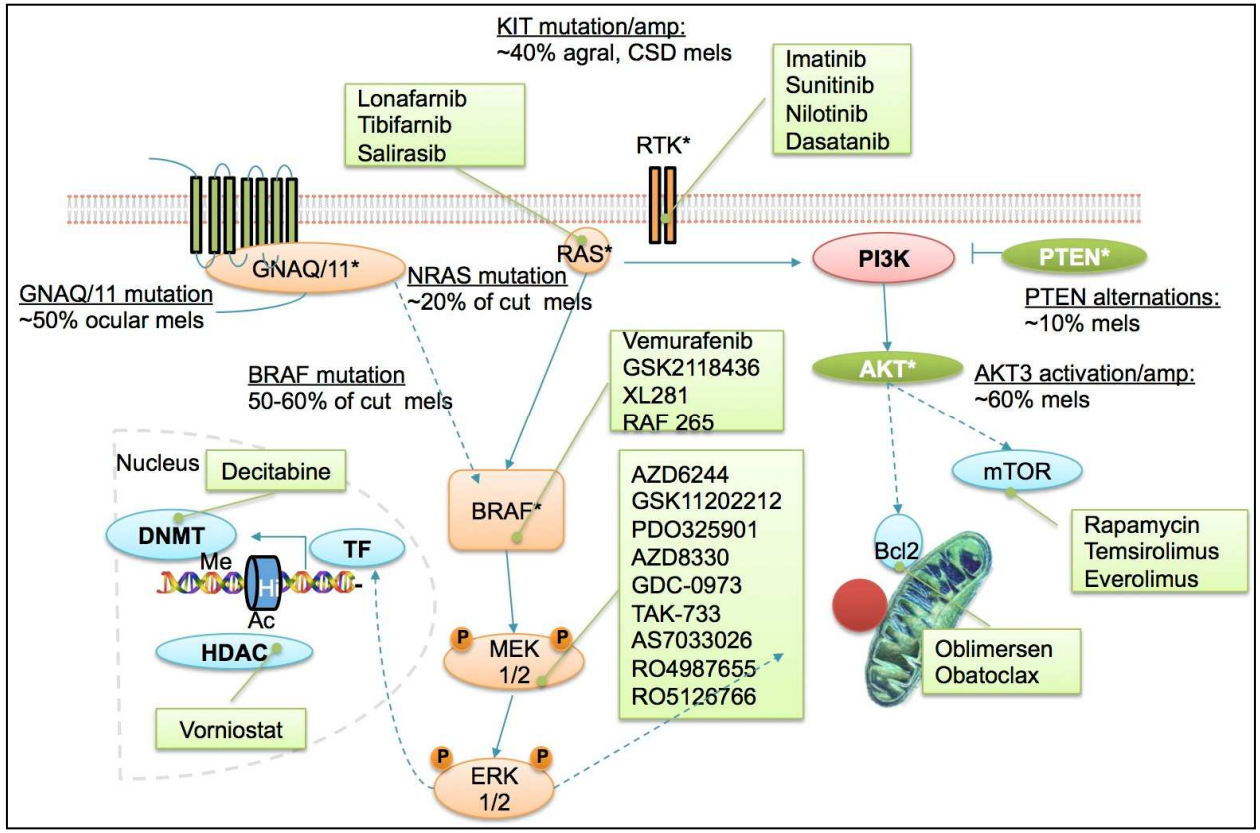

Activation of RTKs, lead to signaling via MAPK, PI3K. GNAQ and GNA11 mutations are mutated in ocular melanoma. In the nucleus, epigenetic silencing of tumor suppressor genes occurs through DNA methylation and histone acetylation by DNA methyltransferase (DNMT) and histone deactylase (HDAC), respectively(Nikolaou et al., 2012)

Figure 1.7: Schematic of the MAPK and PI3K pathways in melanoma and the clinical compounds available for their inhibition (Vultur et al., 2011)

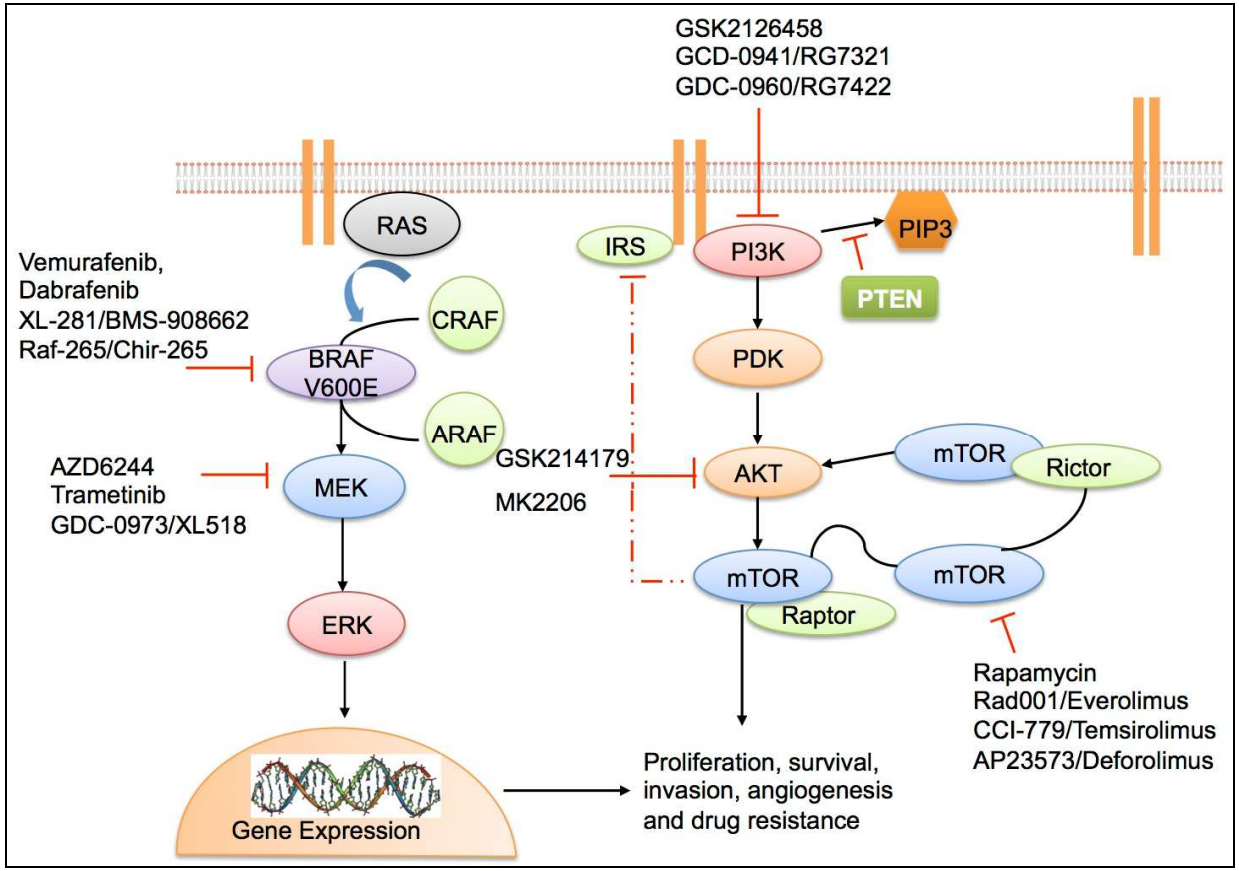

Figure 1.8: The PI3K signaling pathway

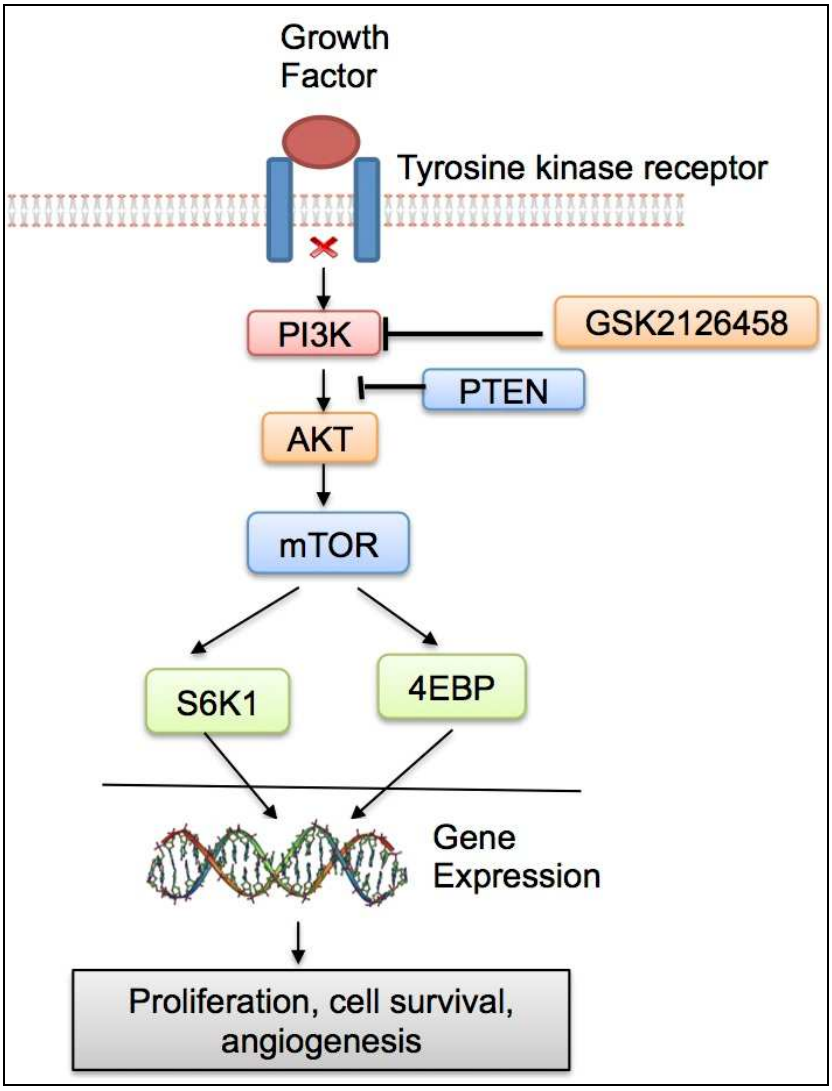

PI3K phosphorylates a second messenger, phosphatidylinositol-4, 5-biphosphate, thereby generating phosphatidylinositol-3, 4, 5-triphosphate, which activates AKT. Activated AKT has several cellular and enzymatic substrates, which promote cellular proliferation, growth and survival.

Figure 1.9: Currently targeted signaling pathways in melanoma therapy.

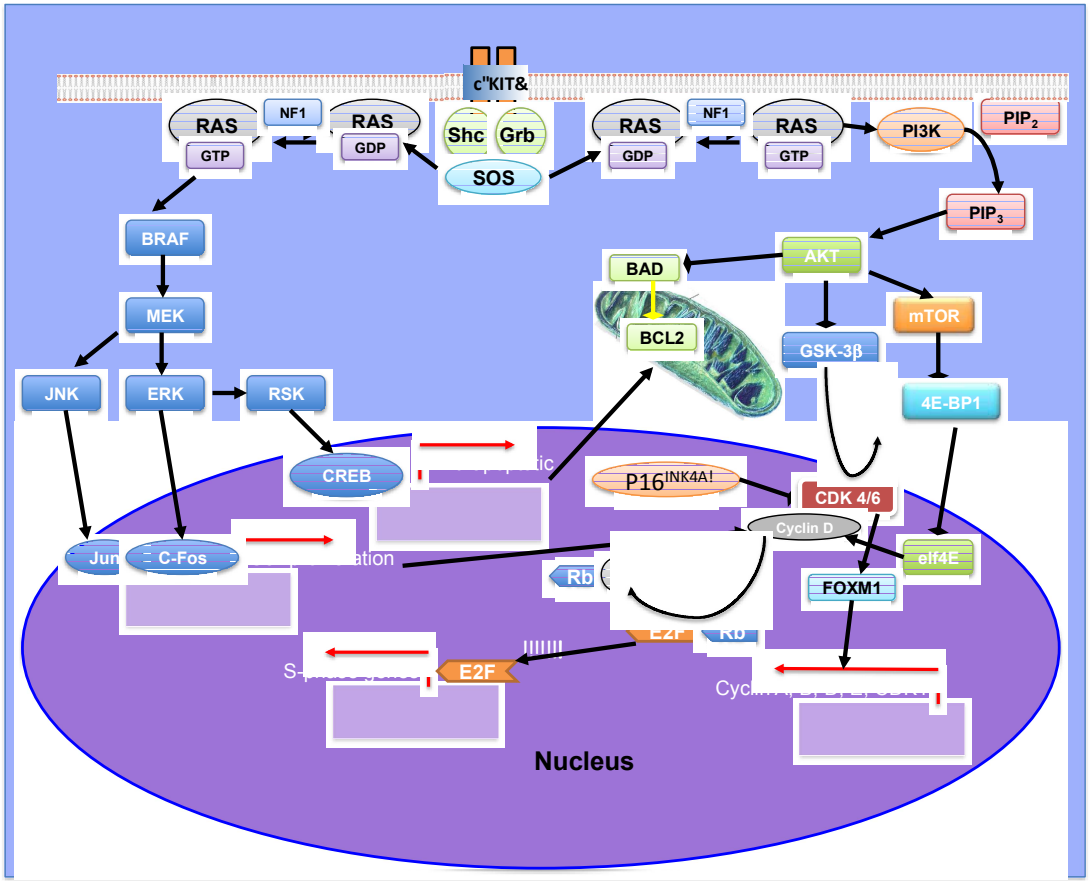

Figure 1.10: Barriers to drug delivery in treatment of melanoma brain metastases:

Shows the expression of efflux transporters, P-gp, Bcrp and MRPs at the BBB, ABCB5 known to be expressed by melanoma cells, and ABCB1 and ABCB5 expressed by the stem cell like side population of cells in melanoma tumors.

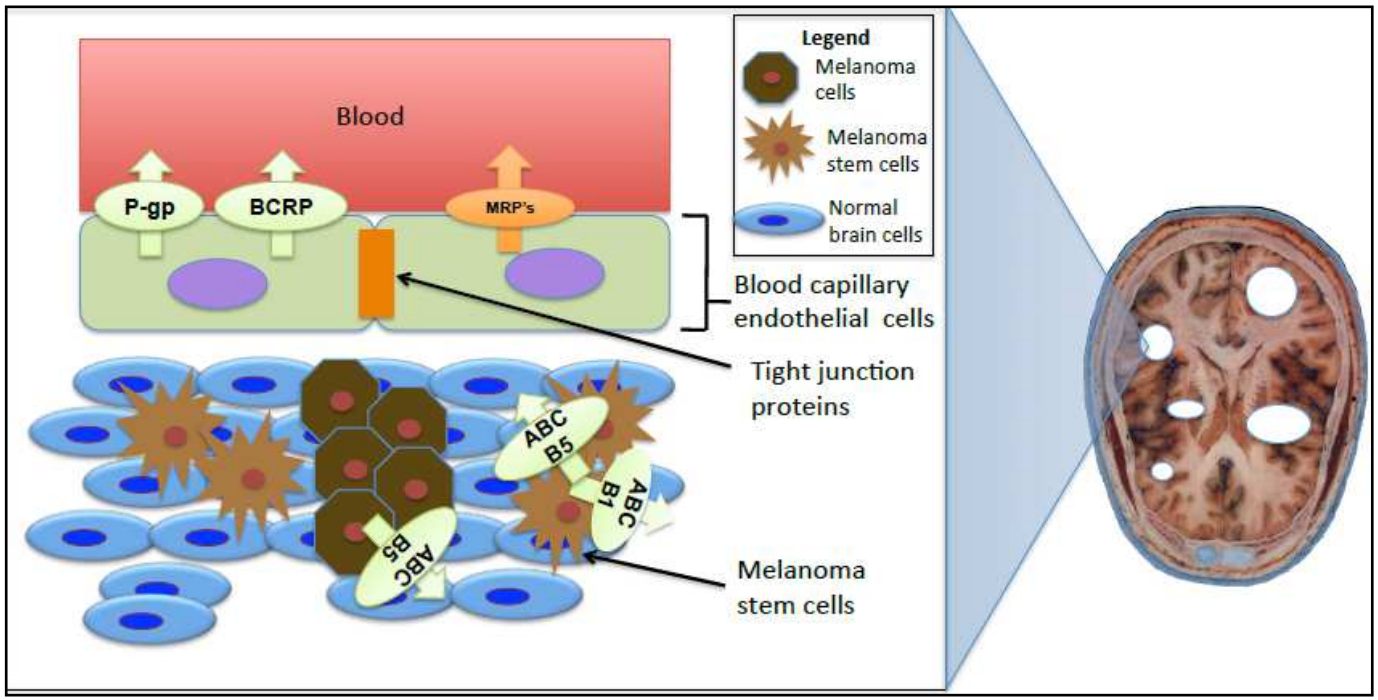

CHAPTER 2: IMPACT OF P-GLYCOPROTEIN (ABCB1) AND BREAST CANCER RESISTANCE PROTEIN (ABCG2) ON THE BRAIN DISTRIBUTION OF A NOVEL B-RAF INHIBITOR: VEMURAFENIB (PLX4032)

This manuscript has been published in the Journal of Pharmacology and Experimental Therapeutics, American Society for Pharmacology and Experimental Therapeutics

JPET 342:33–40, 2012

Vemurafenib (PLX4032) is a novel small molecule BRAF inhibitor, recently approved by US Food and Drug Administration (FDA) for the treatment of patients with metastatic melanoma with a $BRAF^{V600E}$ mutation. The objective of this study was to investigate the role of P-glycoprotein (P-gp) and breast cancer resistance protein (BCRP) on the distribution of vemurafenib to the central nervous system. *In vitro* studies conducted in transfected Madin-Darby canine kidney-II cells show that the intracellular accumulation of vemurafenib is significantly restricted due to active efflux by P-gp and BCRP. Bidirectional flux studies indicated greater transport in basolateral-to-apical direction than apical-to-basolateral direction due to active efflux by P-gp and BCRP. Selective P-gp and BCRP inhibitors zosuquidar and Ko143 were able to restore the intracellular accumulation and bidirectional net flux of vemurafenib. The *in vivo* studies revealed that the brain distribution coefficient (area under the concentration time profile of brain / area under the concentration time profile of plasma) of vemurafenib was 0.004 in wild-type mice. The steady-state brain-to-plasma ratio of vemurafenib was 0.035 ± 0.009 in *Mdr1a/b*$^{-/-}$ mice, 0.009 ± 0.006 in *Bcrp1*$^{-/-}$ mice, 1.00 ± 0.19 in *Mdr1a/b*$^{-/-}$*Bcrp1*$^{-/-}$ mice, compared to 0.012 ± 0.004 in wild type mice. These data indicate that the brain distribution of vemurafenib is severely restricted at the blood-brain barrier due to active efflux by both P-gp and BCRP. This finding has important clinical significance given the ongoing trials examining the efficacy of vemurafenib in brain metastases of melanoma.

2. 1 Introduction

Melanoma is a neoplasm that originates in the pigment producing cells of the skin. The incidence of melanoma is escalating. For example, in 2011, approximately 70,000 individuals were expected to be diagnosed with melanoma in the United States, and ~8800 were predicted to die from melanoma (Siegel et al., 2011). After lung and breast cancers, malignant melanoma is the third most common neoplasm that metastasizes to the brain (Johnson and Young, 1996). Approximately 50-75% of melanoma patients are found to have brain metastases at autopsy (Fife et al., 2004). Once the lesions have become established in the central nervous system (CNS), the median survival is less than 6 months (Fife et al., 2004; Raizer et al., 2008).

The current therapeutic options for melanoma patients include surgery, radiotherapy, and chemo or immunotherapy. The standard therapy using high dose interleukin-2 and dacarbazine proves to be unsuccessful in metastatic melanoma, with response rates of only 10 to 20% (Comis, 1976; Atkins et al., 1999; Garbe et al., 2011). The gene encoding the serine-threonine protein kinase B-RAF (BRAF) was found to be mutated in ~40-60% of melanomas (Wan et al., 2004). BRAF is an important component of RAF/MEK/ERK signaling pathway which regulates cell proliferation and growth (McCubrey et al., 2008). The mutated BRAF gene results in signaling pathways that promote tumor cell proliferation, invasion, and resistance. Among the BRAF mutations approximately

80% exhibit a valine to glutamic acid substitution (V600E; $BRAF^{V600E}$) resulting in constitutive expression of kinase activity (Davies et al., 2002). A recent study indicated that $BRAF^{V600E}$ is associated with poor patient survival (Long et al., 2011), and further studies show that the incidence of $BRAF^{V600E}$ mutation in brain metastases of melanoma is similar to that found in peripheral sites (Capper et al., 2011). Given the prevalence of $BRAF^{V600E}$ mutations in a large number of melanomas, BRAF has been an attractive treatment target for melanoma patients with V600E mutation, and as such many small-molecule inhibitors of BRAF have been developed.

Vemurafenib (previously known as PLX4032) is a small molecule $BRAF^{V600E}$ inhibitor that was developed using a structure-guided drug discovery approach (Tsai et al., 2008). It was approved by U.S. Food and Drug Administration (FDA) in August 2011 for late-stage melanoma patients with $BRAF^{V600E}$ mutation. Clinical trials with vemurafenib have shown remarkable responses in a high percentage of BRAF mutant melanoma cases (Ribas et al., 2011), with improved overall and progression-free survival (Chapman et al., 2011). A clinical trial evaluating the efficacy of vemurafenib in brain metastases of melanoma is currently recruiting patients (ClinicalTrials.gov identifier: NCT01378975). Whether or not vemurafenib will show clinical activity in brain metastases of melanoma is an important question that remains to be answered.

In this context, it is crucial to determine the mechanisms influencing the brain distribution of vemurafenib to further support the clinical investigations.

A major factor contributing to the rapid and near 100% mortality in melanoma patients with brain metastases has been the presumed limited permeability of chemotherapeutics across the blood-brain barrier (BBB). The BBB is a highly evolved vasculature structure which limits most molecules from distributing into the brain from the blood compartment. Anatomically, the vasculature of the BBB is unique in that it is comprised of endothelial cells, that are circumferentially sealed together by tight-junction protein complexes, that form the lumen of the vessel. Further, active efflux transporters that are present on the luminal side of capillary endothelium efficiently pump out the drugs from the brain to the blood circulation. Adenosine triphosphate-binding cassette proteins (ABC) such as P-glycoprotein (P-gp) and breast cancer resistance protein (BCRP) are major members of the efflux transporters present on the luminal membrane of the brain capillary endothelial cells (Schinkel and Jonker, 2003). Studies have shown that many therapeutic agents are substrates of these transporters and as a result have very limited brain distribution (Loscher and Potschka, 2005).

Vemurafenib can be considered a “sea-change” in the treatment of melanoma patients. However, important questions still remain regarding resistance and effective delivery to all sites of melanoma metastases, particularly in brain. In this

regard, there is a paucity of data regarding the delivery of anti-melanoma agents to brain metastases. Given the remarkable activity of the novel targeted $BRAF^{V600E}$ inhibitors in peripheral disease, it becomes critical to examine the mechanisms that may limit their delivery to brain metastases. Whether vemurafenib can cross the BBB to achieve therapeutic levels in the CNS remains unknown. This has motivated us to examine the interaction of vemurafenib with the two main BBB efflux transporters, namely P-gp and BCRP. Herein, using *in vitro* models, we show that vemurafenib is an avid substrate for both P-gp and BCRP. *In vivo* studies using genetic knockout mice indicate both transporters play a significant role in limiting the CNS distribution of vemurafenib.

2. 2 Materials and Methods

2. 2. 1 Chemicals

Vemurafenib (PLX4032) was purchased from Chemietek (Indianapolis, IN). [^{3}H]-Vinblastine was purchased from Moravek Biochemicals (La Brea, CA). [^{3}H]-Prazosin was purchased from Perkin Elmer Life and Analytical Sciences (Waltham, MA). KO143 was a generous gift from Dr. Alfred Schinkel (The Netherlands Cancer Institute, Amsterdam, The Netherlands) and zosuquidar [LY335979, (*R*)-4-((1*a*R, 6*R*,10*bS*)-1,2-difluoro-1,1*a*,6,10*b*-tetrahydrodibenzo-(*a*,*e*) cyclopropa(*c*)cycloheptan-6-yl)-((5-quinoloyloxy) methyl)-1-piperazine ethanol, trihydrochloride] was kindly provided Eli Lilly and Co.(Indianapolis, IN).

All other chemicals used were of high performance liquid chromatography or reagent grade and were obtained from Sigma-Aldrich (St. Louis, MO).

2. 2. 2 In vitro studies

All the *in vitro* studies were performed using polarized Madin-Darby canine kidney-II (MDCKII) cells. MDCKII-wild type (WT) and MDR1-transfected (MDCKII-MDR1) cell lines were kindly provided by Dr. Piet Borst (The Netherlands Cancer Institute). MDCKII-WT and Bcrp1-transfected (MDCKII-Bcrp1) cells were a kind gift from Dr. Alfred Schinkel (The Netherlands Cancer Institute). Cells were cultured in Dulbecco's modified Eagle's medium supplemented with 10% (v/v) fetal bovine serum and antibiotics (penicillin, 100 U/mL; streptomycin, 100 µg/mL; and amphotericin B, 250 ng/mL). Cells were grown in 25 mL tissue culture treated flasks before seeding for the experiments and were maintained at 37º C in a humidified incubator with 5% CO_2.

2. 2. 2. 1 In vitro accumulation studies

The intracellular accumulation of vemurafenib was performed in 12-well polystyrene plates (Corning Inc. Corning, NY) as described previously (Agarwal et al., 2010; Agarwal et al., 2011). Briefly, cells were seeded at a density of 2 x 10^5 cells and were grown until the cells were ~80% confluent. On the day of experiment the culture media was aspirated and the cells were washed two times with cell assay buffer (122 mM NaCl, 25 mM $NaHCO_3$, 10 mM glucose, 10 mM

HEPES, 3 mM KCl, 2.5 mM $MgSO_4$, 1.8 mM $CaCl_2$, and 0.4 mM K_2HPO_4). Then the cells were preincubated with assay buffer for 30 min, after which the buffer was aspirated and the experiment was initiated by adding 1 mL of vemurafenib (2 µM) to each well and further incubated for 60 min. The assay plates were incubated at 37º C on an orbital shaker (60 rpm) for the entire duration of the experiment. After the incubation period, the drug solution was aspirated and the cells were washed twice with ice cold PBS. Then the cells were lysed by adding 500 µL of 1% Triton X to each well. A 400 µL of solubilized cell fraction was sampled from each well and the concentration of vemurafenib was determined using LC-MS/MS as described below.

2. 2. 2. 2 Directional transport across MDKCII monolayers

The bidirectional flux studies were performed using 6-well Transwell® plates (Cornings Inc. Lowell, MA). The cells were seeded at a density of 2 $x10^5$ cells per well and the media was changed every other day until confluent monolayers were formed. On the day of experiment, the culture medium was aspirated and the cells were washed twice with assay buffer and after 30 min preincubation, the experiment was initiated by adding the vemurafenib solution (2 µM) in assay buffer to the donor compartment. Samples (200 µL) were collected from the receiver compartment at 0, 30, 60, 90, 120, and 180 minutes and replaced with drug-free assay buffer. Similarly, at the beginning of the experiment a 200 µL

sample was drawn from the donor compartment and replaced with 200 µL of drug solution. The Transwell® plates were incubated at 37 ºC on an orbital shaker for the duration of experiment except for the brief sampling times. When an inhibitor was used, the inhibitor was present in the both compartments during the pre and post incubation period.

The apparent permeability (P_{app}) for the directional transport was calculated as previously described (Agarwal et al., 2011). The permeabilities were calculated using the following equation

$$P_{\mathrm{app}} = \frac{\frac{dQ}{dt}}{AC_0} \qquad (1)$$

Where, (*dQ/dt*) is the slope obtained from the initial linear range from the amount transported versus time plot, A is the area of the Transwell® membrane, and C_0 is the initial donor concentration. The efflux ratio and corrected efflux ratio were calculated using eqs. 2 and 3, respectively,

$$\text{Efflux ratio} = \frac{P_{\mathrm{app}}(B \rightarrow A)}{P_{\mathrm{app}}(A \rightarrow B)} \qquad (2)$$

$$\text{Corrected flux ratio} = \frac{\left(\frac{B \rightarrow A}{A \rightarrow B}\right)_{\text{Transfected line}}}{\left(\frac{B \rightarrow A}{A \rightarrow B}\right)_{\text{Wild-type line}}} \quad (3)$$

where A→B represents permeability in apical to basolateral and B→A represents permeability in basolateral to apical direction.

2. 2. 2. 3 Competition assays using P-gp and Bcrp probes

Competition assays were performed using the prototypical probe substrates prazosin for BCRP and vinblastine for P-gp. Intracellular accumulation of these substrates at 60 min was determined in MDCKII-Bcrp1 or MDCKII-MDR1 cells in the presence of different concentrations of vemurafenib ranging from 1 μM to 25 μM. The increase in probe accumulation relative to control (i.e., no vemurafenib treatment) was reported as a function of vemurafenib concentration.

2. 2. 3 In vivo Studies

2. 2. 3. 1 Animals

All of the *in vivo* studies were performed in FVB (wild type), *Mdr1a/b*$^{-/-}$ (P-gp knockout), *Bcrp1*$^{-/-}$ (BCRP knockout), and *Mdr1a/b*$^{-/-}$*Bcrp1*$^{-/-}$ (triple knockout) mice of a FVB genetic background (Taconic Farms, Germantown, NY). All animals were 8 to 10 weeks old at the time of experiment. Animals were maintained in a 12 hr light/dark cycle with an unlimited access to food and water. All studies were carried out in accordance with the guidelines set by the *Principles of Laboratory*

Animal Care (National Institutes of Health, Bethesda, MD) and approved by the Institutional Animal Care and Use Committee of the University of Minnesota.

2. 2. 3. 2 Brain Distribution of vemurafenib in FVB mice

The dosing formulation of vemurafenib was prepared either in a vehicle containing 1% Tween 20 and 1% HPMC (for oral dosing) or in a vehicle containing 40% DMSO, 40% propylene glycol, and 20% saline (for i.v. studies). All vemurafenib formulations were freshly prepared on the day of experiment. In the first study, wild type, *Mdr1a/b*$^{-/-}$, *Bcrp1*$^{-/-}$, and *Mdr1a/b*$^{-/-}$*Bcrp1*$^{-/-}$ mice received an oral dose of 25 mg/kg and blood and brain samples were collected 1 and 4 hr post dose. At the end of the desired time point, the animals were euthanized using a CO_2 chamber. Blood was collected via cardiac puncture and collected in heparinized tubes. Plasma was obtained by centrifuging the blood at 7500 rpm for 10 min. Brains were rapidly removed from the skull, rinsed with ice cold PBS followed by a flash freeze in liquid nitrogen. Brain and plasma samples were stored at -80º C until further analysis.

In the i.v. dosing study, wild type and *Mdr1a/b*$^{-/-}$*Bcrp1*$^{-/-}$ mice were administered vemurafenib via the tail vein at a dose of 2.5 mg/kg. Blood and brain samples were processed after 5, 30, 90, 180, 300, and 480 minutes (n=4 for each time point) as mentioned above.

2. 2. 3. 3 Steady state brain distribution of vemurafenib

To determine the steady state brain and plasma concentrations of vemurafenib, Alzet osmotic mini pumps (Durect Corporation, Cupertino, CA) were loaded with vemurafenib (25 mg/mL dissolved in DMSO) to be released for 48 hrs at a rate of 1µL/hr. After vemurafenib loading, mini pumps were primed overnight in sterile saline at 37 º C. Pumps were implanted in the peritoneal cavity of wild type, *Mdr1a/b*$^{-/-}$, *Bcrp1*$^{-/-}$, and *Mdr1a/b*$^{-/-}$*Bcrp1*$^{-/-}$ mice as previously described (Agarwal et al., 2010; Agarwal et al., 2011). Briefly, mice were anesthetized using isofluorane and the abdominal cavity was shaved. A small midline incision was made in the lower abdomen under the rib cage. Then a small incision was made directly in the peritoneal membrane and the primed pump was inserted in the cavity. The incision was sutured and the skin was closed using surgical clips. The animals were allowed to recover on a heating pad and, once recovered, moved to their original cages. The animals were sacrificed 48 hrs after the implantation of the pumps, and brain and plasma samples were processed as described above.

2. 2. 3. 4 Analysis of vemurafenib using LC-MS/MS

The concentrations of vemurafenib in cell lysates, assay buffer, plasma and brain homogenate were determined using a sensitive and specific liquid chromatography coupled with tandem mass spectrometry (LC-MS/MS) assay. For brains, 3 volumes of 5% bovine serum albumin was added and homogenized

to get a uniform homogenate. For analysis of unknowns, an aliquot of cell lysate, cell assay buffer, brain homogenate or plasma was spiked with 50 ng of PLX4720 as an internal standard and alkalinized by addition of 2 volumes of pH 11 buffer (1 mM sodium hydroxide, 0.5mM sodium bicarbonate). The samples were then extracted by addition of 10 volumes of ethyl acetate followed by vigorous shaking for 5 min and centrifuged at 7500 rpm for 5 min at 4ºC to separate the organic layer. The organic layer was transferred to microcentrifuge tubes and dried under nitrogen. Samples were reconstituted in 100 µL of mobile phase and transferred into HPLC glass vials. Chromatographic analysis was performed using an AQUITY UPLC® system (Milford, MA, USA). The chromatographic separation was achieved using an Agilent Technologies Eclipse XDB-C18 column (4.6 x 50 mm) with 1.8 µm Zobrax Rx-SIL as the stationary phase. The mobile phase consisted of 20 mM ammonium formate with 0.1% formic acid and acetonitrile (30:70 v/v), and was delivered at a flow rate of 0.25 mL/min.

The column effluent was monitored using a Waters/Micromass Quattro™ Ultima mass spectrometer (Waters, Milford, MA). The instrument was equipped with an electrospray interface, and controlled by the Masslynx (Version 4.1) data system. The samples were analyzed using an electrospray probe in the negative ionization mode operating at a spray voltage of 2.96 kV for both vemurafenib and PLX4720 (internal standard). Samples were introduced into the interface through

a heated nebulized probe where the source and desolvation temperatures were set at 100 ºC and 275 ºC, respectively. The spectrometer was programmed to allow the [MH]- ion of vemurafenib at *m/z* 488.23 and that of internal standard at *m/z* 412.26 to pass through the first quadrupole (Q1) and into the collision cell (Q2). The collision energy was set at 27V for vemurafenib and 25V for PLX4720. The product ions for vemurafenib (*m/z* 380.89) and the internal standard PLX4720 (*m/z* 304.82) were monitored through the third quadrupole (Q3). The retention time for vemurafenib and the internal standard PLX4720 was 4.2 and 2.9 min, respectively. The assay was sensitive and linear over a range of 1.2 ng/mL to 1.2 µg/mL, with the coefficient of variation being less than 15% over the entire range.

2. 2. 4 Pharmacokinetic Calculations

Pharmacokinetic parameters and metrics were calculated by noncompartmental methods using Phoenix WinNonlin (Version 6.1) (Pharsight, Mountain View, CA). The area under the concentration time curve in both plasma and brain was calculated using the trapezoidal rule, and the area under the curve was determined up to the last measured time point ($AUC_{0\text{-tlast}}$). $AUC_{0\text{-tlast}}$ was used in determining brain to plasma distribution ratio. The area under the curve from time zero to infinity was also determined and the area extrapolated was less than 20% of the total area under the concentration curve. The terminal rate constants were determined using all the data points in the brain and the last three data points in

the plasma. In plasma, the concentration at zero time was extrapolated using the terminal rate constant to measure the area under the curve at time zero to the first measured time point.

2. 2. 5 Statistical Analysis:

Data in all experiments represent mean ± SD unless otherwise indicated. Comparisons between two groups were made using an unpaired t-test. One way ANOVA, followed by Bonferonni's multiple comparisons test, was utilized to compare multiple groups. A significance level of $p < 0.05$ was used for all experiments. (GraphPad Prism 5.01 software, San Diego, CA, USA). .

2. 3 Results:

2. 3. 1 Intracellular accumulation of vemurafenib:

The intracellular accumulation of vemurafenib was studied in MDCKII WT and P-gp or Bcrp overexpressing cell lines. [^{3}H]-prazosin and [^{3}H]-vinblastine were used as positive controls for Bcrp and P-gp, respectively. As expected, the accumulation of [^{3}H]-prazosin (**Fig. 2.1A**) was significantly lower in Bcrp overexpressing cell lines (WT: 100.0 ± 8.7; Bcrp: 8.0 ± 2.4, $p<0.0001$). Similarly, the accumulation of [^{3}H]-vinblastine (**Fig. 2.1B**) in P-gp overexpressing cells was ~80% lower compared to its WT line (WT: 110.0 ± 16.4; MDR1: 13.8 ± 4.1, $p = 0.0004$). Vemurafenib accumulation was ~ 77% lower in Bcrp overexpressing cell line compared to its WT line (WT: 100.0 ± 5.0; Bcrp: 12.9 ± 0.3, $P<0.0001$). The

difference in accumulation was abolished when a specific Bcrp inhibitor Ko143 was added (Bcrp: 8.0 ± 2.4; Bcrp with Ko143: 69.8 ± 3.0, $p<0.05$). Similarly, the accumulation of vemurafenib was ~20% lower in P-gp overexpressing line compared to its WT control (WT: 100.0 ± 2.6; MDR1: 73.6 ± 5.5, $p<0.05$), and the difference in accumulation was abolished (**Fig. 2.1B**) when a specific P-gp inhibitor LY335979 was added (MDR1: 73.6 ± 5.5; MDR1 with LY: 110.8 ± 2.9). The aggregate of these data indicates that vemurafenib is a substrate for both P-gp and Bcrp *in vitro.*

2. 3. 2 Competition assays:

The *in vitro* competition assays for vemurafenib were performed in MDCKII cells using vinblastine and prazosin as P-gp and Bcrp prototype probe substrates, respectively. The addition of increasing concentrations of vemurafenib resulted in a gradual increase in accumulation of prazosin and vinblastine in MDCKII-Bcrp1 cells and MDCKII-MDR1 cells, respectively. The fold increase in prazosin accumulation in MDCKII-Bcrp1 cells at 10 μM of vemurafenib was no different than the effect seen with 0.2 μM Ko143, a potent Bcrp inhibitor (**Fig. 2.2A**). Similarly, at 25 μM of vemurafenib, the fold increase in vinblastine accumulation was no different than the effect seen with the potent P-gp inhibitor LY335959 (**Fig. 2.2B**) in MDCKII-MDR1 cells. These data suggest that vemurafenib may share the same binding sites on the transporter proteins as these prototypical probe substrates.

2. 3. 3 Bidirectional flux across MDCKII monolayers:

The *in vitro* transport (apical to basolateral, A to B; and basolateral to apical, B to A) of vemurafenib was studied in MDCKII wild type, and P-gp or Bcrp overexpressing cell lines. **Fig. 2.3A** and **2.3B** demonstrate the transport of vemurafenib in the A to B and B to A direction in Bcrp1 and corresponding wild-type cell monolayers. In the wild type cells, there was minimal transport (less than 2.3% in 1.5 hrs) of vemurafenib in either direction (**Fig. 2.3A**). In case of the MDCKII-Bcrp1 cells, the permeability of vemurafenib in the B to A direction was significantly higher than the permeability in the A to B direction [A to B: ($0.02 \pm 0.003 \times 10^{-6}$ cm/s); B to A: ($9.9 \pm 6.8 \times 10^{-6}$ cm/s); $p < 0.05$; **Fig. 2.3C**]. The addition of 0.2 μM Ko143, a specific Bcrp inhibitor, resulted in partial inhibition of Bcrp mediated vemurafenib transport in these cells (**Fig. 2.3C**).

The transport of vemurafenib in the A to B and B to A direction in MDR1 and corresponding wild-type cell monolayers is depicted in **Fig. 2.3D** and **2.3E**. In the case of the MDCKII-MDR1 transfected line, the permeability of vemurafenib in B to A direction was significantly greater compared with permeability in A to B direction [A to B: ($0.21 \pm 0.16 \times 10^{-6}$ cm/s); B to A: ($16.7 \pm 2.1 \times 10^{-6}$ cm/s); $p < 0.05$; **Fig. 2.3F**] resulting in an efflux ratio of ~80. The addition of 1 μM LY335979, a potent inhibitor of P-gp, resulted in partial inhibition of P-gp mediated vemurafenib transport in these cell lines (**Fig. 2.3F**). The B to A permeability of vemurafenib was not significantly different from the A to B

permeability in the corresponding wild-type cells. The corrected flux ratio was found to be approximately 34 in control and 2 in cells treated with the P-gp inhibitor LY335979.

2. 3. 4 Brain distribution of vemurafenib in FVB wild type and Mdr1a/b$^{-/-}$ Bcrp1$^{-/-}$ mice after intravenous administration:

The brain distribution of vemurafenib was studied in FVB wild type mice after an i.v. dose of 2.5 mg/kg via the tail vein. **Fig. 2.4** shows the concentration time profile of vemurafenib in both plasma and brain at 5, 30, 90, 180, 300, and 480 minutes of post i.v dose. The plasma concentrations of vemurafenib were significantly higher (~3 log units) at all-time points compared to its brain concentrations, indicating the severely restricted brain distribution of vemurafenib. The brain to plasma partitioning (AUC_{brain} / AUC_{plasma}) was found to be ~0.004 in FVB wild type mice. The pharmacokinetic parameters are depicted in **Table 2.1**.

In a separate study, the brain distribution of vemurafenib in *Mdr1a/b*$^{-/-}$ *Bcrp1*$^{-/-}$ mice was examined after an i.v. dose of 2.5 mg/kg. As shown in **Fig. 2.5B**, the brain concentrations of vemurafenib in *Mdr1a/b*$^{-/-}$*Bcrp1*$^{-/-}$ mice were significantly higher than in wild type mice. The plasma concentrations were not different between the two types of mice (**Fig. 2.5A**). The brain to plasma (B/P) ratio of vemurafenib in wild-type mice was ~0.4%, significantly lower than the B/P ratio in *Mdr1a/b*$^{-/-}$*Bcrp1*$^{-/-}$ mice (**Fig. 2.5C**).

2. 3. 5 Brain distribution of vemurafenib after oral administration:

The brain distribution of vemurafenib was examined 1 and 4 hr post oral dose (25 mg/kg) of vemurafenib in FVB wild type, *Mdr1a/b*$^{-/-}$, *Bcrp1*$^{-/-}$, and *Mdr1a/b*$^{-/-}$ *Bcrp1*$^{-/-}$ mice. As shown in **Fig. 2.6A**, the brain concentrations of vemurafenib were significantly lower than plasma after 1 hr post dose in wild type, *Mdr1a/b*$^{-/-}$, and *Bcrp1*$^{-/-}$ mice with a B/P ratio of < 0.02. It should be noted that the brain concentrations were not corrected for the vascular content as the total brain distribution of vemurafenib was approximately equal to the vascular volume indicating the very limited brain distribution of vemurafenib. However, the B/P ratio of vemurafenib was significantly ($p < 0.0001$) higher in *Mdr1a/b*$^{-/-}$*Bcrp1*$^{-/-}$ mice [**Fig. 2.6A** and **2.6B**, B/P ratio at 1hr: 0.090 ± 0.036; at 4hr: 0.36 ± 0.07] than the wild type and single knockout mice at both 1 and 4 hr post dose. Importantly, the B/P ratio of *Mdr1a/b*$^{-/-}$*Bcrp1*$^{-/-}$ mice was 8-fold higher than wild type at 1 hr and 30-fold higher than wild type at 4hrs. These data show the important roles of both P-gp and Bcrp in restricting the delivery of vemurafenib across the BBB.

2. 3. 6 Steady state brain distribution of vemurafenib:

The steady state brain distribution of vemurafenib was studied after a constant intraperitoneal infusion using the Alzet osmotic pumps for 48 hrs. As shown in

Fig. 2.7A, the steady state brain concentrations of vemurafenib were significantly lower in wild type, *Mdr1a/b*$^{-/-}$, and *Bcrp1*$^{-/-}$ mice compared to their respective steady state plasma concentrations. The steady state B/P plasma ratio of vemurafenib in *Mdr1a/b*$^{-/-}$*Bcrp1*$^{-/-}$ mice equaled approximately 1(**Fig. 2.7B**), which is 80 fold ($p < 0.0001$) greater than the wild type and single knockout mice. [Wild type: 0.012 ± 0.004; *Mdr1a/b*$^{-/-}$: 0.035 ± 0.009; *Bcrp1*$^{-/-}$: 0.009 ± 0.006; *Mdr1a/b*$^{-/-}$ *Bcrp1*$^{-/-}$: 1.00 ± 0.19].

2. 4 Discussion:

The development of vemurafenib, a potent BRAF^{V600E} inhibitor, yields new hope for the melanoma patients who harbor this mutational status. However, the durable efficacy of vemurafenib depends on overcoming resistance (Wagle et al., 2011) and ensuring adequate delivery to all sites of metastases in melanoma patients, particularly the brain. Given the remarkable success in the early clinical trials (Chapman et al., 2011; Ribas et al., 2011), it is of particular interest to examine mechanisms that may limit the CNS distribution of vemurafenib to support further clinical trials. In the current study, we have evaluated how BBB efflux transporters influence the CNS distribution of vemurafenib using both *in vitro* cell culture models and *in vivo* using genetic knockout mice. We demonstrate that vemurafenib is a substrate for the ABC transporters P-gp and BCRP, and that active efflux by these two transporters at the BBB severely restricts the CNS distribution of vemurafenib.

Studies performed *in vitro* using MDCKII cells that overexpress human P-gp or murine BCRP revealed that vemurafenib is an avid substrate for the two efflux transporters. Using prototypical probe substrates (prazosin for BCRP and vinblastine for P-gp), we have seen a concentration-dependent increase in cellular accumulation of the probe with increasing concentrations of vemurafenib. We have examined the vectorial transport of vemurafenib across monolayers formed from MDCKII wild-type, MDCKII-MDR1 transfected cells and MDCKII-Bcrp1 transfected cells. The corrected flux ratio for vemurafenib in the MDR1 transfected line was ~34, and that ratio in the BCRP transfected line was 150, indicating that vemurafenib subject to significant efflux by each transporter across the monolayers. The selective P-gp and BCRP inhibitors zosuquidar and Ko143 were able to restore the intracellular accumulation and bidirectional net flux of vemurafenib. These *in vitro* results conclusively show that vemurafenib is a substrate for these two efflux transporters.

In vivo studies using FVB wild-type mice demonstrated that the CNS distribution of vemurafenib is significantly restricted across the blood-brain barrier. The brain concentrations of vemurafenib in FVB wild-type mice are significantly (~3 log units; **Fig. 2.5**) lower than the plasma concentrations. However, the brain concentrations were approximately ~8-30 fold higher in *Mdr1a/b*$^{-/-}$*Bcrp1*$^{-/-}$ mice than in the wild-type mice (**Fig. 2.7**). Steady state brain to

plasma ratios increased from approximately 0.01 in the wild-type mice to approximately 1 in the triple knockout mice. This remarkable 80-fold increase in targeted brain distribution of vemurafenib in *Mdr1a/b*$^{-/-}$*Bcrp1*$^{-/-}$ mice indicates the significant impact of P-gp and BCRP on CNS penetration of vemurafenib. It should be noted that the brain distribution of vemurafenib did not increase in *Bcrp1*$^{-/-}$ mice, it is increased by ~3-fold in *Mdr1a/b*$^{-/-}$ mice, indicating the "cooperative" role of these transporters at BBB. This type of "synergistic" effect of P-gp and BCRP was seen with other drugs; such as topotecan (de Vries et al., 2007), lapatinib (Polli et al., 2009), dasatinib (Chen et al., 2009), gefitinib (Agarwal et al., 2010) and sorafenib (Agarwal et al., 2011). One of the assumptions for this disproportional increase in brain distribution of the compounds is that the compensatory up- or down-regulation of active efflux and influx transporters in the single knockout (mice lacking either P-gp or BCRP) mice. However, in our previous study, using a quantitative proteomics approach, we have shown no compensatory changes in the BBB expression of relevant transporters in the single and combined knockout mice (Agarwal et al., 2012). The exact functional compensation between P-gp and BCRP at the BBB needs further investigation.

Although vemurafenib shows high initial response rates in melanoma patients with BRAF^{V600E} mutation, and has been shown to yield a durable response in a melanoma brain metastasis in one recent case study (Rochet,

2011), the development of resistance can occur quickly (Wagle et al., 2011). At the present time, several resistance mechanisms against BRAF inhibitors have been documented, some of which include the upregulation of NRAS, PDGFR, and IGFR-1/PI3K signaling (Johannessen et al., 2010; Nazarian et al., 2010; Villanueva et al., 2010). Therefore, the development of more effective combination therapies has been suggested (Vultur et al., 2011; Ji et al., 2012). In this context, the interaction of drugs such as vemurafenib with ABC transporters could be of great relevance for the rational design of therapeutic strategies in clinical setting. In the current study, we have shown that the brain distribution of vemurafenib is severely restricted at the blood-brain barrier due to active efflux by both P-gp and BCRP. This finding is clinically significant considering the ongoing trials on the efficacy of vemurafenib in brain metastases of melanoma.

Given the remarkable success thus far with vemurafenib, it will be crucial to find both the drug resistance and drug delivery liabilities to further improve progression free survival rates through rational drug development and design. In this particular case, the lack of treatment options and the aggressive course of this malignancy suggest that adjuvant treatment to improve delivery to the CNS through efflux inhibition may be a viable option to improve survival.

Figures:

Figure 2.1: Intracellular accumulation of vemurafenib in MDCKII cells

Panel A shows that accumulation of vemurafenib is significantly lower in Bcrp transfected lines compared to its WT control. The difference in accumulation was abolished when a specific Bcrp inhibitor Ko143 was used. Panel B shows that the accumulation of vemurafenib is ~20% less in MDR1 transfected cells than the WT controls and difference was abolished when MDR1 specific inhibitor LY335979 was used. Data represent mean ± SD, n=3-6 for all data sets.

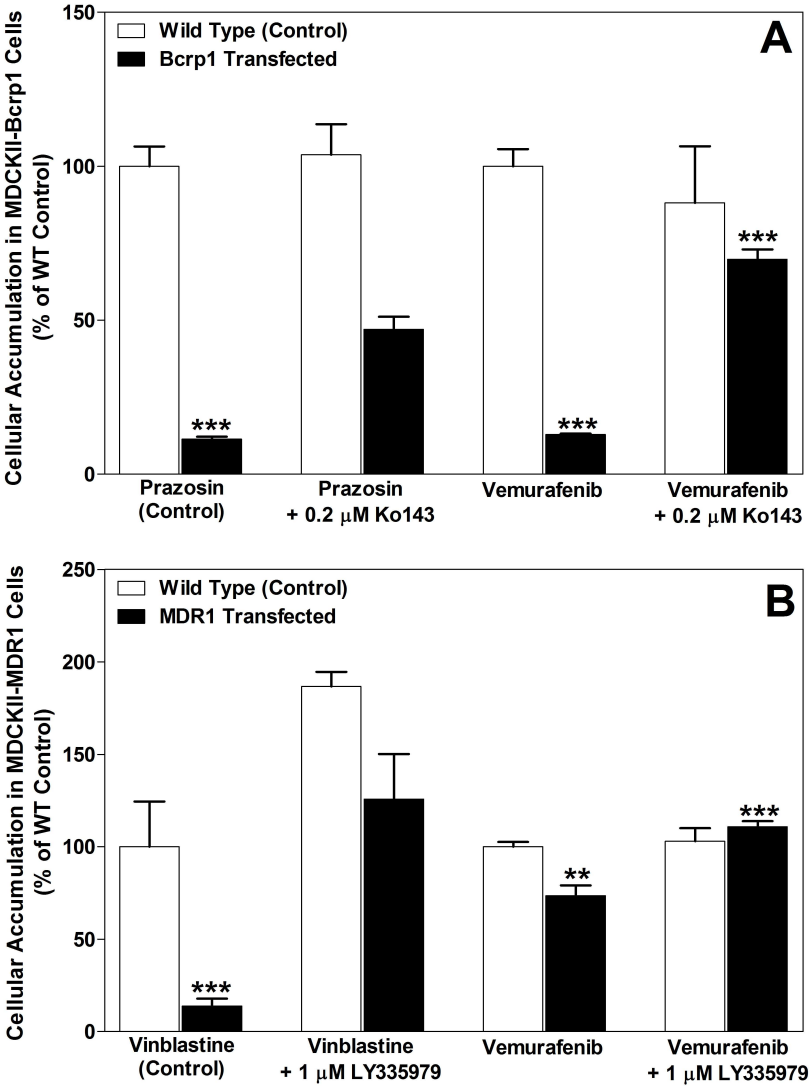
A
Wild Type (Control)
Bcrp1 Transfected
Cellular Accumulation in MDCKII-Bcrp1 Cells
(% of WT Control)
150
100
50
0
***
***
***
Prazosin
(Control)
Prazosin
+ 0.2 μM Ko143
Vemurafenib
Vemurafenib
+ 0.2 μM Ko143
B
Wild Type (Control)
MDR1 Transfected
Cellular Accumulation in MDCKII-MDR1 Cells
(% of WT Control)
250
200
150
100
50
0
***
**
***
Vinblastine
(Control)
Vinblastine
+ 1 μM LY335979
Vemurafenib
Vemurafenib
+ 1 μM LY335979

Figure 2.2: Competition assays for vemurafenib in MDCKII-MDR1 and MDCKII-Bcrp1 cells using [^{3}H]-vinblastine and [^{3}H]-prazosin as P-gp and Bcrp prototypical probe substrates respectively.

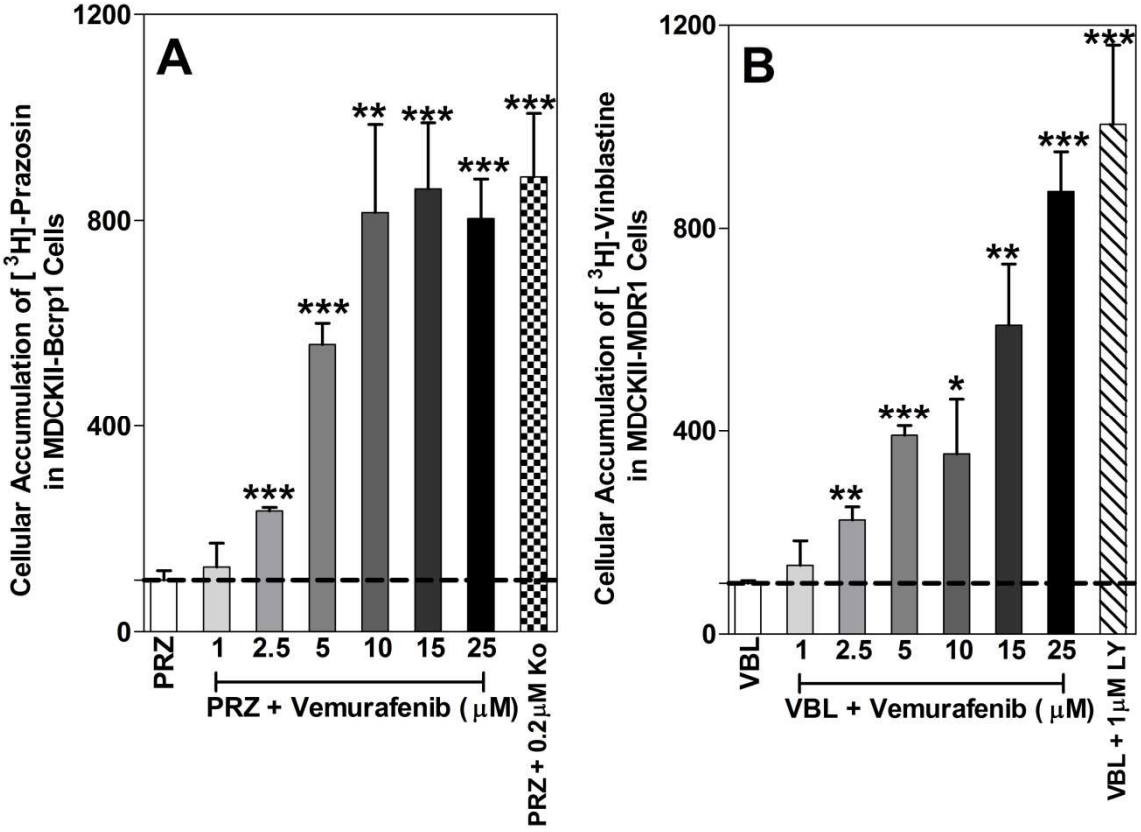

The addition of increasing concentrations of vemurafenib resulted in an increased accumulation of [^{3}H]-prazosin and [^{3}H]-vinblastine in Bcrp1 (Panel A) and MDR1 (Panel B) cells respectively. The data represent mean ± SD, n = 3 for all data sets. A *, **, and *** indicates a p value of <0.05, <0.01, and <0.0001, respectively.

Figure 2.3: Directional flux of vemurafenib in MDCKII cell monolayers.

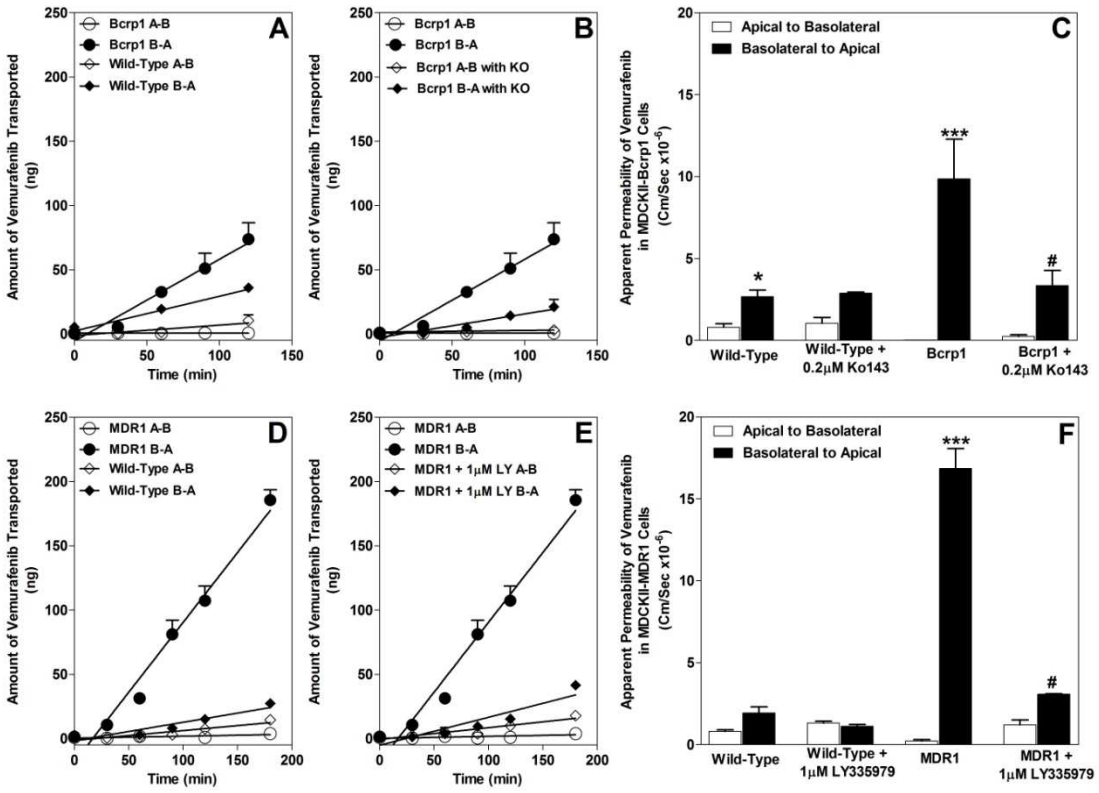

Panel **A** and **B** show the transport of vemurafenib in wild-type and Bcrp1-transfected cells. Panel **C** shows the apparent permeability of vemurafenib in wild-type and Bcrp1 cells in both A-to-B and B-to-A direction. In the Bcrp1 transfected cells, the B-to-A permeability of vemurafenib was significantly greater than the A-to-B permeability (***, $p < 0.05$). The addition of 0.2 μM Ko143, a potent bcrp inhibitor, decreased this directionality in flux due to bcrp (#, $p < 0.05$). Panel **D** and **E** show the transport of vemurafenib in wild-type and MDR1-transfected cells. Panel **F** shows the apparent permeability of vemurafenib in

wild-type and MDR1 cells in both A-to-B and B-to-A direction. In the MDR1 transfected cells, the B-to-A permeability of vemurafenib was significantly greater than the A-to-B permeability (***, $p < 0.05$). The addition of 1 μM LY335979, a potent P-gp inhibitor, abolished this directionality in flux due to P-gp (#, $p < 0.05$), such that there was no significant difference between in the permeability of vemurafenib in both directions. Data represent mean ± SE, n = 3-9 for all data sets.

Figure 2.4: Brain and plasma concentrations of vemurafenib after an i.v. dose of 2.5mg/kg in FVB wild type mice.

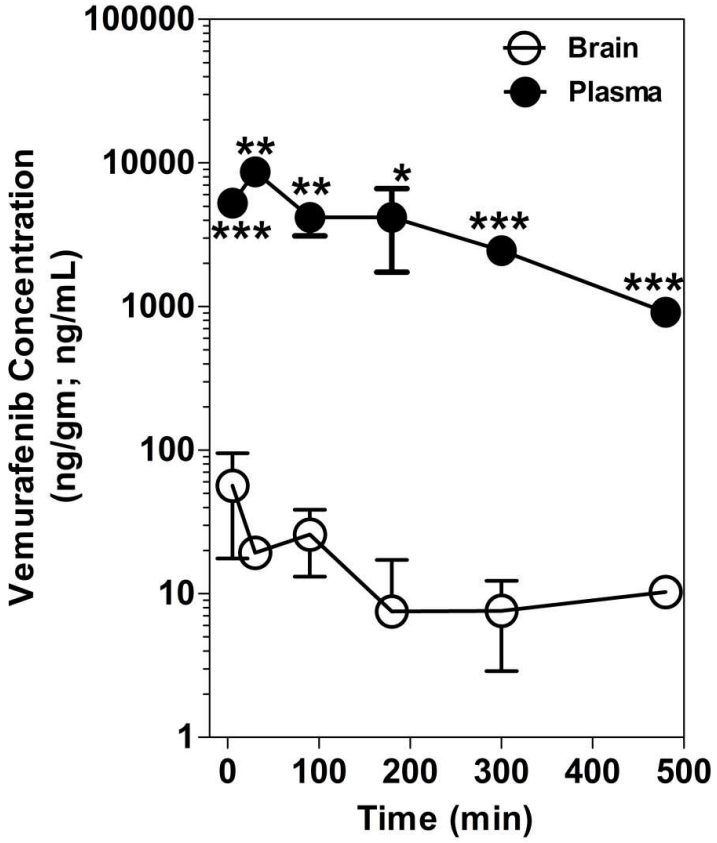

Whole brain and plasma were collected at 5, 30, 90, 180, 300, and 480minutes after dose and were analyzed using LC-MS/MS. The brain concentrations of vemurafenib were significantly lower than the plasma concentrations at all the time points. A *, **, and *** indicates a p value of <0.05, <0.01, and <0.0001 respectively. Data are mean ± SD; n=3-4 for all data point.

Figure 2.5: Comparison of vemurafenib brain distribution in wild-type and *Mdr1a/b$^{-/-}$Bcrp1$^{-/-}$* mice

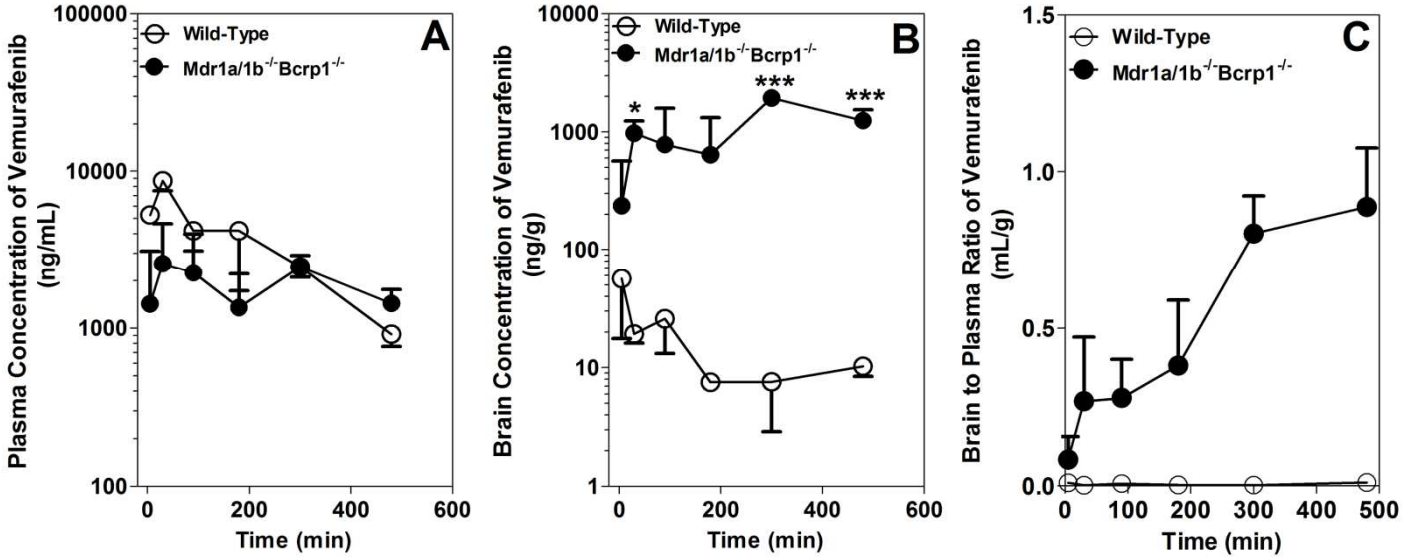

Vemurafenib was given i.v. at 2.5mg/kg and the concentrations in brain and plasma were determined using LC-MS/MS. Panel **A** and Panel **B** shows the plasma and brain concentrations of vemurafenib in wild-type and *Mdr1a/b$^{-/-}$Bcrp1$^{-/-}$* mice respectively. The B/P ratio for vemurafenib in wild-type and *Mdr1a/b$^{-/-}$Bcrp1$^{-/-}$* mice was shown in Panel **C.** Data represent mean ± SD; n=3-4 for all data points.

Figure 2.6: Brain to plasma ratios of vemurafenib after an oral dose of 25mg/kg in FVB wild type, *Mdr1a/b*$^{-/-}$, *Bcrp1*$^{-/-}$, and *Mdr1a/b*$^{-/-}$*Bcrp1*$^{-/-}$ mice.

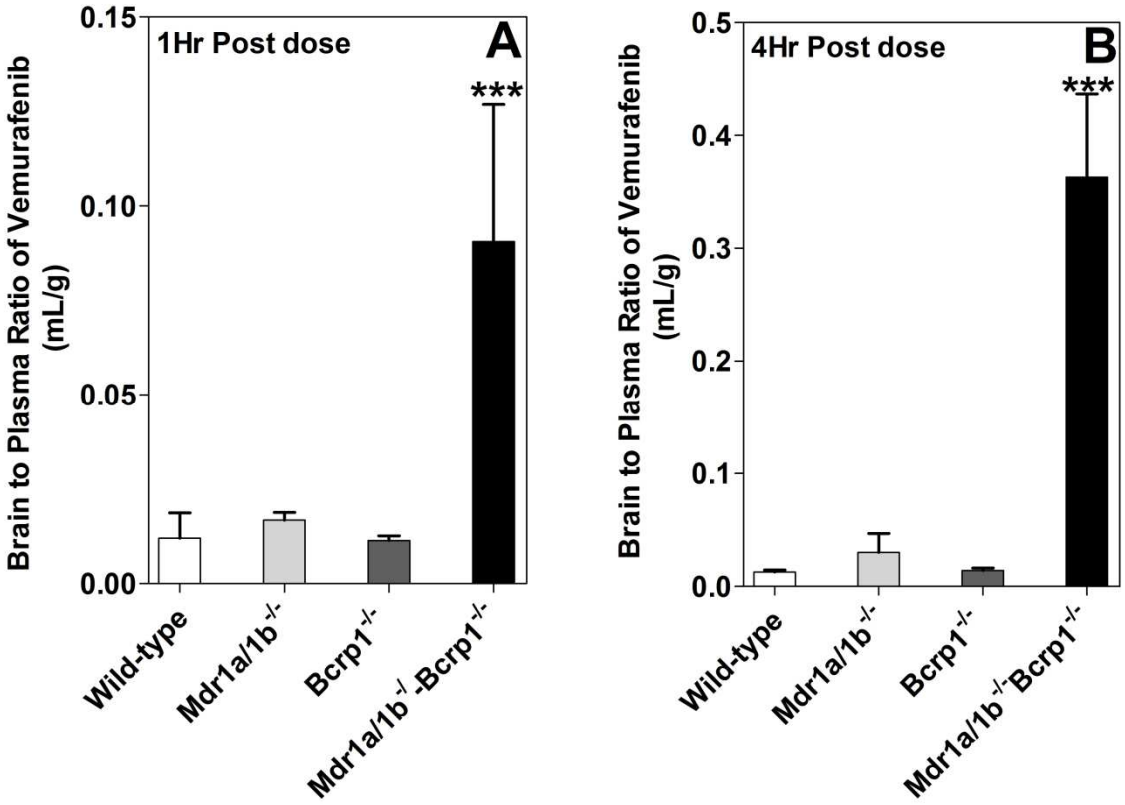

The mice were sacrificed after 1 (A) and 4hr (B) post dose of vemurafenib and the whole brain and plasma were analyzed using LC-MS/MS. The B/P ratios were significantly higher in *Mdr1a/b*$^{-/-}$*Bcrp1*$^{-/-}$ mice than the wild type mice at both 1 and 4hr post dose. A *** indicates a p value of <0.0001. Data are mean ± SD; n=3-4 for all data points.

Figure 2.7: Steady state brain distribution of vemurafenib in FVB wild type, *Mdr1a/b*$^{-/-}$ (P-gp knockout), *Bcrp1*$^{-/-}$ (BCRP knockout), and *Mdr1a/b*$^{-/-}$*Bcrp1*$^{-/-}$ (triple knockout) mice.

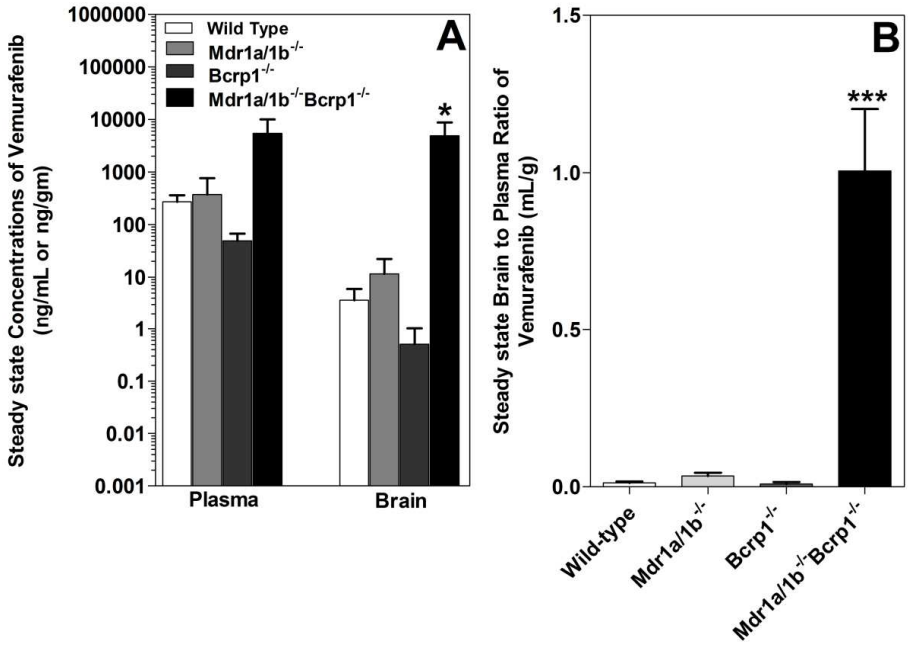

Vemurafenib was delivered at a constant infusion for 48 hrs at a rate of 25µg/hr, and the brain and plasma concentrations were determined thereafter. Panel A shows the steady state brain and plasma concentrations of vemurafenib, and panel B shows the B/P ratio in all four type mice. The B/P ratios were not significantly different in single knockout mice when compared to wild type mice. However the B/P ratio in triple knockout mice was significantly higher than the wild type mice, indicating the "cooperative" role of P-gp and Bcrp at the blood-brain barrier. A *, and *** indicates a p value of <0.01 and <0.0001 respectively. Data are mean ± SD; n=3-4 for all data points.

Table 2.1: Vemurafenib Pharmacokinetic Parameters after an I.V. dose of 2.5 mg/kg in FVB wild-type mice

	Plasma	Brain
Terminal rate constant (min^{-1})	0.0051	0.0047
Half-life (min)	136	148
Clearance (mL/min)	0.04	
Volume of Distribution (mL)	7.9	
$AUC_{0 \rightarrow t\ last}$ (min · µg/mL)	1663 ± 140*	6.5 ± 0.9*
AUC_{Brain}/AUC_{Plasma}	0.004	

Plasma and brain pharmacokinetic parameters were analyzed using non compartmental analysis after an i.v. dose of 2.5 mg/kg in FVB wild-type mice. The AUC_{brain} to AUC_{plasma} ratio of 0.004 indicates the severely restricted brain distribution of vemurafenib.`

***** Mean ± SE (standard error of the estimate)

CHAPTER 3: MECHANISMS LIMITING DISTRIBUTION OF THE BRAFV600E INHIBITOR DABRAFENIB TO THE BRAIN: IMPLICATIONS FOR THE TREATMENT OF MELANOMA BRAIN METASTASES

This manuscript has been published in the Journal of Pharmacology and Experimental Therapeutics, American Society for Pharmacology and Experimental Therapeutics JPET 344:655–664, 2013

Brain metastases are a common cause of death in stage IV metastatic melanoma. Dabrafenib is a BRAF inhibitor that has been developed to selectively target the valine 600 to glutamic acid substitution ($BRAF^{V600E}$) which is commonly found in metastatic melanoma. Clinical trials with dabrafenib are showing encouraging results, however the CNS distribution of dabrafenib remains unknown. Thus the objective of the current study was to evaluate the brain distribution of dabrafenib in mouse and to see whether active efflux by P-glycoprotein (P-gp) and Breast Cancer Resistance Protein (BCRP) restrict its delivery across blood-brain barrier (BBB). *In vitro* accumulation studies conducted in Madin-Darby canine kidney II (MDCKII) cells indicate that dabrafenib is an avid substrate for both P-gp and BCRP. Directional flux studies revealed greater transport in basolateral to apical direction with corrected efflux ratios of greater than 2 for both P-gp and Bcrp1 transfected cell lines. *In vivo,* the Kp (AUC_{brain} / AUC_{plasma}) of dabrafenib after an iv dose (2.5 mg/kg) was 0.023, which increased by 18-fold in Mdr1 *a/b*$^{-/-}$*Bcrp1*$^{-/-}$ mice to 0.42. Dabrafenib plasma exposure was ~2-fold greater in Mdr1 *a/b*$^{-/-}$*Bcrp1*$^{-/-}$ mice as compared to wild-type with an oral dose (25 mg/kg), however the brain distribution was increased by ~10-fold with a resulting Kp of 0.25. Further, compared to vemurafenib, another $BRAF^{V600E}$ inhibitor, dabrafenib has greater brain penetration with a similar dose. In conclusion, the dabrafenib brain distribution is limited in an intact BBB model and the data presented herein may have clinical implications in the prevention and treatment of melanoma brain metastases.

3. 1 Introduction

Melanoma is the most aggressive form of skin cancer as it accounts for more than 80% of deaths due to skin cancer. The incidence of melanoma has greatly increased over the past decade (Siegel et al., 2011). Extensive data in the literature point to the key role of mitogen-activated protein kinase (MAPK) pathway in melanoma pathogenesis. The MAPK pathway is involved in regulation of melanoma cell proliferation, growth, and survival. The downstream effectors of this signaling cascade include RAS-RAF-MEK-ERK (McCubrey et al., 2008). BRAF is a commonly mutated protein in melanoma, with ~80% carrying a V600E ($BRAF^{V600E}$) mutation (Davies et al., 2002). Thus, targeting this pathway represents an attractive therapeutic approach for melanoma.

Until recently, treatment options for melanoma were limited with no improvement in overall survival rates (Tsao et al., 2004; Garbe et al., 2011). However, in recent years there has been a tremendous improvement in the treatment of melanoma. Targeting $BRAF^{V600E}$ has proved to be a major advancement in the field of melanoma treatment (Flaherty et al., 2012; Sosman et al., 2012). For example, the recently US FDA approved drug, vemurafenib, a $BRAF^{V600E}$ inhibitor, showed remarkable efficacy against peripheral metastases (Chapman et al., 2011). However, brain metastases are prevalent in stage IV metastatic melanoma. This situation is alarming because ~50-75% of melanomas metastasize to the brain (Fife et al., 2004), and among those patients who have brain metastases, ~90% succumb to death (Skibber et al., 1996). The efficacy of vemurafenib in brain metastases of melanoma is under clinical investigation. Recent

preclinical studies have indicated that vemurafenib distribution is restricted at blood-brain barrier (BBB) (Durmus et al., 2012; Mittapalli et al., 2012).

Dabrafenib (GSK2118436A, **Figure 3.1**) targets both $BRAF^{V600E}$ and $BRAF^{V600k}$. Dabrafenib showed very encouraging results in a phase 1 dose escalation study (Falchook et al., 2012; Hauschild et al., 2012). The safety and clinical response of dabrafenib against peripheral metastases is comparable with that of vemurafenib, with an objective response of ~56% (Gibney and Sondak, 2012; Hauschild et al., 2012). Further, ~90% (9 out of 10 patients) of the patients with melanoma brain metastases had a reduction in tumor size (Falchook et al., 2012). However, important questions remain about the effective delivery to all sites of brain metastases, especially to the micro metastases which are situated beyond an intact blood-brain barrier (BBB). In a recent study, using preclinical model of brain metastases from breast cancer, it was shown that the blood-tumor barrier remains a significant impediment to chemotherapeutic drugs (Lockman et al., 2010). However, to date there are no data available in terms of drug delivery to brain metastases of melanoma. Further, it was shown that treatment of peripheral disease with targeted therapy increases the incidence of brain metastases (Rochet et al., 2012). A phase 2 clinical trial evaluating the efficacy of dabrafenib in brain metastases of melanoma is underway (Long et al., 2012) (clinicaltrials.gov identifier: NCT01266967). With this perspective, it is imperative to study the brain distribution of dabrafenib to provide a rationale to support clinical trials.

A critical challenge in treating brain metastases or in fact any neurological disorder is the delivery of drugs to the central nervous system. The BBB, an interface between blood and the brain, helps maintain homeostasis of the CNS and protects the brain from harmful toxins, metals and infectious agents (Deeken and Loscher, 2007). Together with capillary endothelial cells and tight junctions, it acts as a physical barrier (Hawkins and Davis, 2005). Further, with the expression of active efflux transporters such as P-glycoprotein (P-gp) and breast cancer resistance protein (BCRP), it acts a functional barrier (Schinkel and Jonker, 2003). Several anticancer agents have been shown to be substrates for both P-gp and BCRP and as such the brain distribution of these molecules is limited because of active efflux at the BBB (de Vries et al., 2007; Polli et al., 2009; Agarwal et al., 2010; Agarwal et al., 2011; Mittapalli et al., 2012).

In our previous study, we have shown that the brain distribution of vemurafenib is severely restricted at BBB due to active efflux by both P-gp and BCRP (Mittapalli et al., 2012). Given the highly encouraging clinical results with dabrafenib, the aim of the present study was to evaluate the brain distribution of dabrafenib in mouse, with the hope that these preclinical data would help in further improvement of a durable response in melanoma brain metastases patients. Using both *in vitro* transport studies and *in vivo* pharmacokinetic studies, we show that dabrafenib is a substrate for both P-gp and Bcrp and as such its brain distribution is limited in an intact BBB model. The data presented herein have clinical implications in the prevention or treatment of melanoma brain metastases because of concerns that sub-therapeutic concentrations

in the brain or at sites of micro metastases with an intact BBB would result in limited anti-tumor activity.

3. 2 Materials and Methods

3. 2. 1 Chemicals

Dabrafenib (GSK2118436A) was purchased from Chemietek (Indianapolis, IN). [^{3}H]-vinblastine and [^{3}H]-mitoxantrone were purchased from Moravek Biochemicals (La Brea, CA). [^{3}H]-prazosin was purchased from PerkinElmer Life and Analytical Sciences (Waltham, MA). [^{14}C]-Inulin was purchased from American Radiolabeled Chemicals, Inc. (St. Louis, MO). Ko143 was purchased from Tocris Bioscience (MO, USA). Zosuquidar [LY335979, (*R*)-4-((1*aR*, 6*R*,10*bS*)-1,2-difluoro-1,1*a*,6,10*b*-tetrahydrodibenzo-(*a*,*e*) cyclopropa (*c*)cycloheptan-6-yl)-((5-quinoloyloxy) methyl)-1-piperazine ethanol, trihydrochloride] was kindly provided Eli Lilly and Co.(Indianapolis, IN). All other chemicals used were of high performance liquid chromatography or reagent grade and were obtained from Sigma-Aldrich (St. Louis, MO).

3. 2. 2 In vitro studies

Polarized Madin-Darby canine kidney II (MDCKII) cells were used for all the *in vitro* studies. MDCKII-Wild-type (WT) and Bcrp1-transfected (MDCKII-Bcrp1) cells were a kind gift from Dr. Alfred Schinkel (The Netherlands Cancer Institute). MDCKII-WT and MDR1-transfected (MDCKII-MDR1) cell lines were kindly provided by Dr. Piet Borst (The Netherlands Cancer Institute). Cells were cultured in Dulbecco's modified Eagle's

medium supplemented with 10% (v/v) fetal bovine serum and antibiotics (penicillin, 100 U/mL; streptomycin, 100 µg/mL; and amphotericin B, 250 ng/mL). Cells were grown in 25 mL tissue culture treated flasks before seeding for the experiments and were maintained at 37º C in a humidified incubator with 5% CO_2. The growth media for MDCKII-MDR1 additionally contained 80 ng/ml of colchicine to maintain positive selection pressure of P-gp expression.

3. 2. 2. 1 In vitro cellular accumulation

Cellular accumulation studies were performed in 12-well polystyrene plates with a seeding density of 2 x 10^5 cells per well, and media was changed every other day until confluent monolayers are formed. The cells were washed two times with warm cell assay buffer (122 mM NaCl, 25 mM $NaHCO_3$, 10 mM glucose, 10 mM HEPES, 3 mM KCl, 2.5 mM $MgSO_4$, 1.8 mM $CaCl_2$, and 0.4 mM K_2HPO_4) on the day of the experiment, and preincubated with cell assay buffer for 30 min. The cell assay buffer was aspirated after pre-incubation period, and the experiment was initiated by adding one ml of 2 µM of dabrafenib to each well and further incubated for 60 min in an orbital shaker (60 rpm) that was maintained at 37º C. At the end of 60 min accumulation, the experiment was ended by aspirating the dabrafenib solution followed by washing twice with ice-cold PBS. Cell lysis was accomplished by adding 0.5 milliliters of 1 % Triton-X. When the inhibitor was present it was included in both pre-incubation and accumulation steps. The concentration of dabrafenib in solubilized cell fractions was analyzed using liquid

chromatography-tandem mass spectrometry (LC-MS/MS) as described below, and was normalized to the protein content.

3. 2. 2. 2 Bcrp and P-gp inhibition studies

Inhibition studies were performed using prototypical probe substrates, [^{3}H]-prazosin or [^{3}H]-mitoxantrone for Bcrp and [^{3}H]-vinblastine for P-gp. The intracellular accumulation of these probe substrates was evaluated in presence of varying concentrations of dabrafenib ranging from 0.1 to 50 μM. Briefly, the cells were pre-incubated with increasing concentrations of dabrafenib for 30 min. After pre-incubation the cells were incubated with radiolabelled probe substrate along with increasing concentrations of dabrafenib for 60 min. At the end of the incubation period, the radiolabelled probe substrate was aspirated; cell lysis was accomplished using 1% Triton-X. The radioactivity in solubilized cell fractions was determined by liquid scintillation counting (LS-6500; Beckman Coulter, Fullerton, CA). The radioactivity in cell fractions was normalized to protein concentrations in each well. The increase in cellular accumulation of probe substrate as compared to control (no treatment with dabrafenib) was measured and reported as a function of dabrafenib concentration.

3. 2. 2. 3 Directional flux studies

The bidirectional transport assays were performed in 12-well Transwell® plates (polyester membrane, 0.4 μM pore size, 1.12 cm^2 growth surface area; Corning Inc., USA). The cells were seeded at a density of 2 x10^5 cells per well and the media was

changed every other day until confluent monolayers were formed. The monolayer tightness was assessed by measurement of trans-epithelial electrical resistance (TEER). In parallel, the cell monolayer integrity was evaluated by analyzing the leakage of [^{14}C]-Inulin using the same passage cells seeded on the same day and at the same density.

On the day of the experiment, the cell monolayers were washed with pre-warmed cell assay buffer and preincubated for 30 minutes after which the experiment was initiated by adding 5 µM of dabrafenib solution in cell assay buffer to the donor compartment. Samples (100 µL) were collected from receiver compartment at 60, 120, and 180 min and replaced immediately with drug-free cell assay buffer. In addition, at the beginning of the experiment, 100 µL of sample was collected from donor compartment and replaced with 100 µL drug solution. The Transwell® assay plates were incubated in an orbital shaker (60 rpm) maintained at 37 °C for the duration of experiment except for the brief sampling times. In the inhibition experiments, either 0.2 µM Ko143 (selective Bcrp inhibitor) or 1 µM of zosuquidar (selective P-gp inhibitor) was added to both apical (A) and basolateral (B) compartments. Dabrafenib concentration was measured by LC-MS/MS. The apparent permeability (P_{app}), in A-to-B and B-to-A directions, was calculated as follows: $P_{app} = (dQ/dt)\ (1/A \times C_0)$, where dQ/dt is the slope obtained from the initial linear range from the amount transported versus time graph, A is the area of the Transwell® membrane, and C_0 is the initial donor concentration. The efflux ratio (ER) and the corrected efflux ratio (CFR) were calculated as follows: Efflux

ratio = [P_{app} (B → A) / P_{app} (A → B)]; Corrected efflux ratio = (Efflux ratio in transfected cells) / (Efflux ratio in wild-type cells); where, A→B represents permeability in apical to basolateral and B→A represents permeability in basolateral to apical direction.

3. 2. 2. 4 Equilibrium dialysis experiments

Unbound fractions in mouse plasma and brain homogenates were determined using equilibrium dialysis cassettes (Fisher Scientific, Acrylic, 1mL) as described by Kalvass et.al. (Kalvass et al., 2007). For initial pilot studies commercial mouse plasma (Valley Biomedical, Winchester, VA) and pooled brain homogenates from wild-type and knockout mice were used to determine the time to reach the equilibrium (**Supplemental Fig. 3.3**). Once the time to reach equilibrium was determined, the free fraction experiments were performed in plasma and brains isolated freshly from either wild-type or *Mdr1a/b*$^{-/-}$*Bcrp1*$^{-/-}$ mice. Spectra/por® dialysis membranes (MWCO: 12-14000 Da; Spectrum Laboratories, Inc. CA) were equilibrated in HPLC-water for 30 min followed by 30 min in ECF buffer (pH 7.4). Three volumes of ECF buffer was added to the brain tissue and homogenized to get a uniform homogenate. Dabrafenib was added to plasma and brain homogenate to achieve a final concentration of 2 µM; 1 ml was (n =3) loaded into the equilibrium dialysis cassette and dialyzed against an equal volume of ECF buffer (pH 7.4) in an orbital shaker (200 rpm) maintained at 37 °C. Equilibrium was achieved in ~ 6 hrs in both plasma and brain homogenates (**Supplemental Fig. 3.3**). At the end of the experiment, matrix (plasma or brain homogenate) and buffer samples

were removed from dialysis cassette and the concentrations of dabrafenib were measured using LC-MS/MS.

3. 2. 3 In vivo studies

All of the *in vivo* studies were performed in FVB (wild-type) and *Mdr1a/b*$^{-/-}$*Bcrp1*$^{-/-}$ (triple knockout) mice of either sex of a FVB genetic background (Taconic Farms, Germantown, NY). All animals were 8 to 10 weeks old at the time of experiment. Animals were maintained in a 12 hr light/dark cycle with an unlimited access to food and water. All studies were carried out in accordance with the guidelines set by the *Principles of Laboratory Animal Care* (National Institutes of Health, Bethesda, MD) and approved by the Institutional Animal Care and Use Committee of the University of Minnesota.

3. 2. 3. 1 Plasma and brain pharmacokinetics of dabrafenib after intravenous and oral administration

All dosing formulations of dabrafenib were prepared on the day of the experiment. Dabrafenib dosing formulations were prepared either as a solution in a vehicle containing DMSO, propylene glycol, and water (40:40:20; for i.v. dosing studies) or as a stable suspension in 1% carboxy methyl cellulose (for oral dosing studies).

In the first study, FVB wild-type and *Mdr1a/b*$^{-/-}$*Bcrp1*$^{-/-}$ mice were administered an i.v. dose of 2.5 mg/kg via the tail vein. Blood and brain samples were collected 5, 15, 30, 60, and 120 min post dose (n =4 at each time point). Animals were euthanized using

a CO_2 chamber at the desired time point. Blood was collected by cardiac puncture and plasma was harvested. Whole brain was removed from the skull and washed with ice-cold PBS; superficial meninges were removed by blotting with tissue paper. Plasma and brain specimens were stored at -80° C until further analysis.

In another study, FVB wild-type and *Mdr1a/b*$^{-/-}$*Bcrp1*$^{-/-}$ mice were administered 25 mg/kg dabrafenib via oral gavage. Blood and brain samples were harvested at 15, 30, 60, 120, and 240 min post dose (n =4 at each time point) as described above. Brain concentrations were corrected for residual drug in brain vasculature assuming a vascular volume of 1.4% in mouse brain (Dai et al., 2003).

3. 2. 4 LC-MS/MS Analysis

The concentrations of dabrafenib from all *in vitro* and *in vivo* studies were determined using a specific and sensitive LC-MS/MS assay. Brain samples were thawed to room temperature and homogenized with three volumes of 5% bovine serum albumin in PBS. An aliquot of sample (cell lysate, cell assay buffer, plasma, or brain homogenate) was spiked with 10 ng of internal standard [AG1478; (4-(3-chloroanilino)-6,7-dimethoxyquinazoline)] and liquid-liquid extraction was performed by addition of 10 volumes of ethyl acetate. After extraction, the supernatant organic layer was transferred to a micro-centrifuge tube and dried under gentle stream of nitrogen. The dried sample was reconstituted in 100 µL of mobile phase, vortex-mixed, centrifuged, transferred to auto sampler vials, and a 5 µL sample was injected onto the column, a Zorbax Eclipse XDB-C18 column (4.6 x 50 mm, 1.8 µm particle size; Agilent Technologies, Santa Clara,

CA). The aqueous mobile phase (A) was 20 mM ammonium formate with 0.1% formic acid and the organic mobile phase (B) was acetonitrile. The gradient was as follows: 50% B for the first 3 min, and increased to 90% B from 3 to 3.5 min and maintained at 90% B for 3 min, and decreased to 50% B within 0.5 min. The total run time was 11 min with a flow rate of 0.35 mL/min. The ionization was conducted in positive mode and the m/z transitions were 520.122 → 307.007, and 316.068 → 299.993 for dabrafenib and AG1478, respectively. The retention time of dabrafenib was 6.8 min and that of AG1478 was 2.8 min. The assay was sensitive and linear over a range of 2 ng/mL to 2 μg/mL, with the coefficient of variation being less than 20% over the entire range.

3. 2. 5 Pharmacokinetic calculations

Pharmacokinetic parameters and metrics from the concentration-time data in plasma and brain were obtained by non-compartmental analysis (NCA) performed using Phoenix WinNonlin 6.2 (Mountain View, CA). The area under the concentration-time profiles for plasma (AUC_{plasma}) and brain (AUC_{brain}) were calculated using the linear trapezoidal method. The sparse sampling module in WinNonlin 6.2 (Pharsight, Mountain View, CA) was used to estimate the standard error around the mean of the AUCs (Bailer, 1988; Nedelman et al., 1995).

3. 2. 6 Statistical Analysis

Data in all experiments represent mean ± SD unless otherwise indicated. One way ANOVA, followed by Bonferonni's multiple comparisons test, was utilized to compare

multiple groups. Comparisons between two groups were made using an unpaired t-test. A significance level of $p < 0.05$ was used for all experiments. (Graph Pad Prism 5.01 software, San Diego, CA, USA).

3. 3 Results:

3. 3. 1 In vitro accumulation of dabrafenib in MDCKII-Bcrp1 and MDCKII-MDR1 cells

The cellular accumulation of dabrafenib in MDCKII- wild-type, Bcrp1, and MDR1 transfected cell lines is summarized in **Fig. 3.2**. [^{3}H]-prazosin and [^{3}H]-vinblastine were used as positive controls for Bcrp and MDR1, respectively, and as expected, the cellular accumulation of these probe substrates were significantly lower as compared to wild-type controls [WT: (100 ± 8); Bcrp1: (16.7 ± 1.4); MDR1: (11.6 ± 3.1);] confirming significant transporter activity in these transfected cell lines. We choose a concentration of 2 μM for dabrafenib accumulation studies as the pilot studies revealed that no saturation of transporters occur up to 75 μM of dabrafenib (**Supplemental Fig. 3.1**). Dabrafenib accumulation was significantly lower in Bcrp1 cells [**Fig. 3.2A,** Bcrp: (11.3 ± 1.4); WT: (100 ± 10); $p < 0.001$] when compared to corresponding wild-type controls. The addition of 0.2 μM of Ko143, a specific Bcrp1 inhibitor, increased dabrafenib accumulation, such that it was not significantly different than wild-type control. Likewise, dabrafenib accumulation in MDR1 transfected cell lines (**Fig. 3.2B**) was ~ 65% lower when compared wild-type control and the difference was abolished when 1 μM of

LY335979 was used. These data indicate that dabrafenib is a substrate for both P-gp and Bcrp1 and inhibition of these efflux transporters enhance the cellular delivery of dabrafenib.

3. 3. 2 Competition assays using prototypical probe substrates

The effect of increasing concentrations of dabrafenib on the cellular accumulation of prototypical probe substrates (prazosin or mitoxantrone for Bcrp, vinblastine for P-gp) was assessed in MDCKII-wild-type, Bcrp1 and MDR1 transfected cell lines. Increasing concentrations of dabrafenib did not increase the accumulation of [^{3}H]-prazosin in both Bcrp cells as well as the respective wild-type control cells (**Fig. 3.3A**). Similarly, increasing dabrafenib concentrations did not increase the accumulation of [^{3}H]-vinblastine until 25 μM was reached, however at 50 μM of dabrafenib, there was ~1.5 and 2.5 fold increase in vinblastine accumulation in wild-type and MDR1 cells, respectively (**Fig. 3.3B**). Furthermore, dabrafenib did not change the cellular accumulation of mitoxantrone in Bcrp1 cells (**Supplemental Fig. 3.2**).

3. 3. 3 Directional transport studies

The directional transport of dabrafenib was assessed using monolayers of MDCKII-wild-type, Bcrp1, and MDR1 transfected lines grown on Transwell® permeable membranes. Confluent monolayers were formed in 3 to 4 days with intact tight junctions. Paracellular leakage was assessed by measuring the transport of [^{14}C]-Inulin across the cell monolayers and the inulin transported in 60 min was found to be less than 1%. The

directional permeability of dabrafenib was very similar between A-to-B and B-to-A directions in the wild-type cells (11.5 ± 1.4 vs 14.1 ± 1.4 x 10^{-6} cm/s for A-to-B and B-to-A, respectively; **Table 3.1**). However in the Bcrp1 transfected cell line, the apparent permeability of dabrafenib in B-to-A direction was significantly higher than the permeability in A-to-B direction [A-to-B: (1.3 ± 0.3); B-to-A: 27.3 ± 4.1), $p < 0.05$; **Table 3.1**) with and efflux ratio of 21. Treatment with Ko143 significantly ($p < 0.05$) reduced the Bcrp1-mediated efflux of dabrafenib in B-to-A direction and increased the A-to-B permeability with a resulting efflux ratio of 0.7. The corrected efflux ratio was found to be ~18 for Bcrp1 mediated transport. Similarly, in MDR1 cells the B-to-A permeability was significantly higher compared to A-to-B permeability with an efflux ratio of 11. Addition of LY335979, a specific P-gp inhibitor, abolished the difference in directional permeabilities with a resulting efflux ratio of 1 (**Table 3.2**). The corrected efflux ratio was ~4. These results conclusively indicate that dabrafenib is an avid substrate for both Bcrp1 and P-gp.

3. 3. 4 Plasma protein and brain tissue binding

Since it is the unbound drug concentration that results in pharmacological action, we determined the free fraction (f_u) in plasma and brain tissue homogenates. Dabrafenib is highly bound to plasma proteins as well as brain tissue. No significant difference was observed in free fraction in plasma and brain tissue homogenate when compared between wild-type and *Mdr1a/b*$^{-/-}$*Bcrp1*$^{-/-}$ mice genotypes [Wild-type: ($f_{u,\ plasma}$ = 0.004 ±

0.001), ($f_{u,brain\ homogenate}$ = 0.02 ± 0.003); *Mdr1a/b*$^{-/-}$*Bcrp1*$^{-/-}$: ($f_{u,\ plasma}$ = 0.006 ± 0.004), ($f_{u,brain\ homogenate}$ = 0.02 ± 0.005)].

3. 3. 5 Brain distribution of dabrafenib in FVB wild-type and Mdr1a/b$^{-/-}$Bcrp1$^{-/-}$ mice

The brain and plasma dabrafenib concentration time profiles after an i.v. dose of 2.5 mg/kg in FVB wild-type mice are summarized in **Fig. 3.4**. The brain concentrations of dabrafenib were significantly lower than the corresponding plasma concentrations at all measured time points. The pharmacokinetic parameters were summarized in **Table 3.3**. The brain-to-plasma partitioning (K_p, AUC_{brain} / AUC_{plasma}) was found to be 0.023, indicating the limited distribution of dabrafenib to the brain. We also investigated the brain distribution of dabrafenib in *Mdr1a/b*$^{-/-}$*Bcrp1*$^{-/-}$ mice after a 2.5 mg/kg i.v. dose of dabrafenib. The plasma concentrations were no different between wild-type and *Mdr1a/b*$^{-/-}$*Bcrp1*$^{-/-}$ mice (**Fig. 3.5A**), however the brain concentrations of dabrafenib in *Mdr1a/b*$^{-/-}$*Bcrp1*$^{-/-}$ mice (**Fig. 3.5B**) were significantly higher than the corresponding brain concentrations observed in wild-type mice. The K_p in *Mdr1a/b*$^{-/-}$*Bcrp1*$^{-/-}$ mice increased to ~0.4 which was 18-fold greater than what was observed in wild-type mice indicating the influence of P-gp, Bcrp or both on the brain distribution of dabrafenib.

Dabrafenib is administered to patients orally (Falchook et al., 2012) and we sought to determine the brain and plasma pharmacokinetics after an oral dose. Hence, in a separate study, we investigated the brain distribution of dabrafenib after an oral dose of 25 mg/kg in wild-type and *Mdr1a/b*$^{-/-}$*Bcrp1*$^{-/-}$ mice, and the results are summarized in **Fig. 3.6** and **Table 3.4**. The AUC_{plasma} in *Mdr1a/b*$^{-/-}$*Bcrp1*$^{-/-}$ mice (31 ± 5

μg x min/mL) was ~2-fold higher as compared to the wild-type mice (16 ± 3 μg x min/mL). This indicates that P-gp and Bcrp may have some influence on the oral absorption or systemic clearance of dabrafenib at 25 mg/kg dose. Dabrafenib brain concentrations were significantly enhanced in *Mdr1a/b*$^{-/-}$*Bcrp1*$^{-/-}$ mice compared with those in wild-type. The AUC_{brain} in wild-type mice was 0.69 μg x min/mL which increased approximately 10-fold in *Mdr1a/b*$^{-/-}$*Bcrp1*$^{-/-}$ to 7.6 μg x min/mL. The K_p in wild-type mice was 0.044, which increased by 6 fold in *Mdr1a/b*$^{-/-}$*Bcrp1*$^{-/-}$ mice to 0.25. The aggregate of these data suggests that the brain distribution of dabrafenib is significantly limited at BBB due to active efflux by both P-gp and BCRP after either intravenous or oral administration.

3. 3. 6 Comparison of brain distribution of dabrafenib with vemurafenib

We compared the brain distribution of dabrafenib after single oral dose with our previously published results for vemurafenib (Mittapalli et al., 2012) and the data were shown in **Fig. 3.7**. The plasma concentrations, for both dabrafenib and vemurafenib, were higher in the *Mdr1a/b*$^{-/-}$*Bcrp1*$^{-/-}$ mice as compared to wild-type mice (**Fig. 3.7A**). It should be noted that the plasma concentrations of dabrafenib were not significantly different as compared to vemurafenib in either type of the mice. Since the total brain distribution of vemurafenib was approximately equal to the brain vascular volume, for comparison purposes, the data shown in this particular case was not corrected for vascular content for both dabrafenib and vemurafenib. The brain concentrations of dabrafenib were significantly higher as compared to vemurafenib brain concentrations in

both wild-type and *Mdr1a/b*$^{-/-}$*Bcrp1*$^{-/-}$ mice (**Fig. 3.7B**). The brain-to-plasma concentration ratio for dabrafenib is ~10, ~4 fold greater compared to vemurafenib brain to plasma ratio in wild-type and *Mdr1a/b*$^{-/-}$*Bcrp1*$^{-/-}$ mice, respectively [Wild-type: dabrafenib: (0.1 ± 0.03); vemurafenib: (0.008 ± 0.001); *Mdr1a/b*$^{-/-}$*Bcrp1*$^{-/-}$: dabrafenib: (0.3 ± 0.04); vemurafenib: (0.07 ± 0.02);]. The aggregate of these data indicate that dabrafenib has greater brain penetration than vemurafenib.

3. 4 Discussion

Brain metastases are a common cause of death from stage IV metastatic melanoma (Skibber et al., 1996; Davies et al., 2011). Until 2011, the only FDA approved therapies for metastatic melanoma were dacarbazine and interleukin-2, which showed response rates of only 10-20% (Comis, 1976; Atkins et al., 1999; Garbe et al., 2011). However, therapies for metastatic melanoma have been changed dramatically with the development of highly selective inhibitors of BRAF^{V600E}, the most commonly found mutation in melanoma patients. The first of these selective BRAF^{V600E} inhibitors, vemurafenib was approved by US FDA in 2011, and showed remarkable efficacy in clinical trials (Chapman et al., 2011). A second BRAF^{V600E} inhibitor, dabrafenib, showed similar results when compared to vemurafenib, with fewer adverse effects in clinical trials (Falchook et al., 2012; Hauschild et al., 2012). Further, dabrafenib showed remarkable efficacy in reducing the tumor size in brain of patients with brain metastases (Falchook et al., 2012). However, a durable response depends on effective delivery of therapies to all the sites of metastases in brain, especially to the micrometastases (less

than 1 mm in diameter) that have an intact BBB (Gibney and Sondak, 2012) with functional efflux transporters. Furthermore, in a recent study, Rochet and colleagues reported that treatment of melanoma patients with vemurafenib resulted in development of metastatic disease in the brain (Rochet et al., 2012). From these data, it appears that the brain remains at least in part a pharmacological sanctuary site due to the continued presence of an intact BBB where some metastatic sites reside. The efficacy of dabrafenib in brain metastases of melanoma is under investigation in a phase 2 clinical trial. With this perspective, it is critical to determine the mechanisms that limit the brain distribution of dabrafenib. In the current study, using both *in vitro* and *in vivo* models, we demonstrate that dabrafenib is a dual substrate for BCRP and P-gp and its brain distribution is limited due to active efflux at the BBB. Furthermore, our data indicate that dabrafenib has greater brain distribution when compared to vemurafenib and as such dabrafenib might have some advantages for treating patients with melanoma brain metastases. To the best of our knowledge, this is the first report to show the brain distribution of dabrafenib and its interactions with Bcrp and P-gp.

The experiments performed in transfected MDCKII cells that overexpress either murine Bcrp or human P-gp revealed that dabrafenib is a dual substrate for both Bcrp and P-gp (**Fig. 3.2, Tables 1** and **2**). Interestingly, inhibition studies conducted using prototypical probe substrates (prazosin and mitoxantrone for Bcrp, and vinblastine for P-gp) showed no increase in probe substrate accumulation with increasing concentrations of dabrafenib up to a concentration of 50 and 25 μM in Bcrp1 and MDR1 cells,

respectively. In both wild-type and MDR1 cells, using vinblastine as a probe substrate, dabrafenib showed significant increase in accumulation at 50 μM. However, it should be noted that this concentration is not pharmacologically relevant, as the clinically observed concentrations of dabrafenib (given 150 mg/kg twice daily) are ~ 2 μM (Falchook et al., 2012).

It should be noted that specific Bcrp (Ko143) and P-gp (LY335979) inhibitors were able to increase cellular accumulation of dabrafenib (**Fig. 3.2**), as well as the probe substrates (**Fig. 3.3**), in both Bcrp1 and MDR1 cells, respectively, indicating that Ko143 and LY335979 bind to multiple binding sites on the transporter proteins. The fact that dabrafenib is a substrate for both Bcrp and P-gp, but does not inhibit these transporter proteins for some prototypical probe substrates, may indicate that dabrafenib is binding to a different site on the transporter protein as compared to the probe substrates tested. It is noteworthy to recognize how screening assays using specific binding site probe substrates can be misleading. In our previous studies, we have shown that differences exist in the inhibition of BCRP depending on both the inhibitor used and the substrate under evaluation (Giri et al., 2009).

With this knowledge from *in vitro* data, we next investigated the *in vivo* brain distribution of dabrafenib in mouse. After an i.v. dose, the brain concentrations of dabrafenib in FVB wild-type mice were significantly lower than the corresponding plasma concentrations (**Fig. 3.4**), with a K_p of 0.023. However, the brain distribution of dabrafenib was significantly improved when the same dose was administered in

Mdr1a/b$^{-/-}$*Bcrp1*$^{-/-}$ mice, with a resulting K_p of 0.42 (**Table 3.3**). It is worth noting that the unbound brain-to-plasma partition ratio (K_p,uu) in wild-type and *Mdr1a/b*$^{-/-}$*Bcrp1*$^{-/-}$ mice were ~0.1 and ~1.7, respectively. These data indicate that dabrafenib brain distribution is limited in an intact BBB model through the action of efflux transporter mediated clearance.

Since the clinical use of dabrafenib utilizes chronic oral dosing, we next determined the brain distribution of dabrafenib after oral administration. The AUC_{plasma} in *Mdr1a/b*$^{-/-}$*Bcrp1*$^{-/-}$ mice is ~2-fold higher (**Fig. 3.6A; Table 3.4**) as compared to wild-type mice after oral administration. As the systemic clearance is no different between the genotypes after an i.v. dose (see **Fig. 3.5; Table 3.3**), the observed higher plasma exposure in Mdr1a/b-/-Bcrp1-/- mice after oral dose indicate that BCRP and P-gp may have some influence on oral absorption of dabrafenib at 25 mg/kg dose. This phenomenon was observed with other drugs that are dual substrates of BCRP and P-gp, such as dasatinib (Lagas et al., 2009) and vemurafenib (Durmus et al., 2012). However the brain concentrations are ~12-fold higher in *Mdr1a/b*$^{-/-}$*Bcrp1*$^{-/-}$ mice resulting in a ~6-fold increase in B/P ratio as compared to wild-type mice. Taken together, all these data indicate that dabrafenib brain distribution is limited in an intact BBB model. In this regard, use of pharmacological inhibitors such as elacridar, a dual P-gp and Bcrp inhibitor, may have significant value in improving the CNS distribution of dabrafenib.

Since both dabrafenib and vemurafenib are showing remarkable results in clinical trials, it is appropriate to compare these two molecules in terms of their brain

distribution. In our previous study, we have shown that both BCRP and P-gp have a significant impact on the brain distribution of vemurafenib (Mittapalli et al., 2012), which was further supported by a recently published report by another group (Durmus et al., 2012). Compared to vemurafenib (Mittapalli et al., 2012) the B/P ratio of dabrafenib is significantly higher in both wild-type and *Mdr1a/b*$^{-/-}$*Bcrp1*$^{-/-}$ mice (**Fig. 3.7**). While the B/P ratio in this case was measured only at one time point, we also observed a greater AUC_{brain} to AUC_{plasma} of dabrafenib in wild-type mice after a similar i.v. dose as compared vemurafenib (**Table 3.5**). Given the *in vitro* potency of dabrafenib, which is at least 40 times higher than vemurafenib against $BRAF^{V600E}$ [vemurafenib IC_{50}: 31 nM (Bollag et al., 2010); dabrafenib IC_{50}: 0.8 nM (Laquerre et al., 2009)], and greater brain penetration than vemurafenib, dabrafenib might be beneficial in treating melanoma brain metastases, however this prediction warrants further preclinical and clinical investigation.

Currently, the duration of response with single agent therapy has been limited because the development of resistance is inevitable, as reported in case of vemurafenib (Johannessen et al., 2010; Nazarian et al., 2010; Villanueva et al., 2010). Further, studies have shown that mutations in upstream signaling proteins such as RAS or compensatory signaling from other growth factor receptors such as PI3K/mTOR drive the reactivation of the MAPK signaling pathway and build up the resistance to BRAF therapy (Flaherty et al., 2012). Thus, understanding the key molecular aberrations associated with resistance will be crucial in designing the rational combinations using

two or more drugs to simultaneously block multiple pathways, such as the clinical trial evaluating the combination of dabrafenib with the MEK inhibitor trametinib (NCT01072175). Also, the evaluation of combinations of immune therapies such as ipilimumab (Margolin et al., 2012) and rational choices of molecularly-targeted agents would be valuable in overcoming the low response rates of immune therapy and short durations of response associated with targeted therapies.

The development of $BRAF^{V600E}$ inhibitors has been a major breakthrough for the treatment of melanoma patients. However, challenges still remain in delivering these targeted therapies to melanoma micro metastases in brain that could be growing behind an intact BBB. Given the success rate so far with both dabrafenib and vemurafenib, it will be essential to determine the both the resistance mechanisms and CNS delivery issues that need to be addressed to achieve a durable response. Multiple drugs / cocktails need to be evaluated for rational combinations (e.g., a BRAF inhibitor and/or MEK inhibitor and/or PI3K/mTOR inhibitor) to decrease resistance in peripheral or systemic disease. At the same time, there is also a critical need to examine the CNS delivery of combinations to see if one agent influences the brain delivery of another, or one or more drug(s) in the combination does not reach the brain, leading to heightened resistance. The successful and durable treatment of melanoma requires that the brain does not become a pharmacological sanctuary site for melanoma metastases.

Figures:

Figure 3.1: Chemical structure of dabrafenib (GSK2118436A)

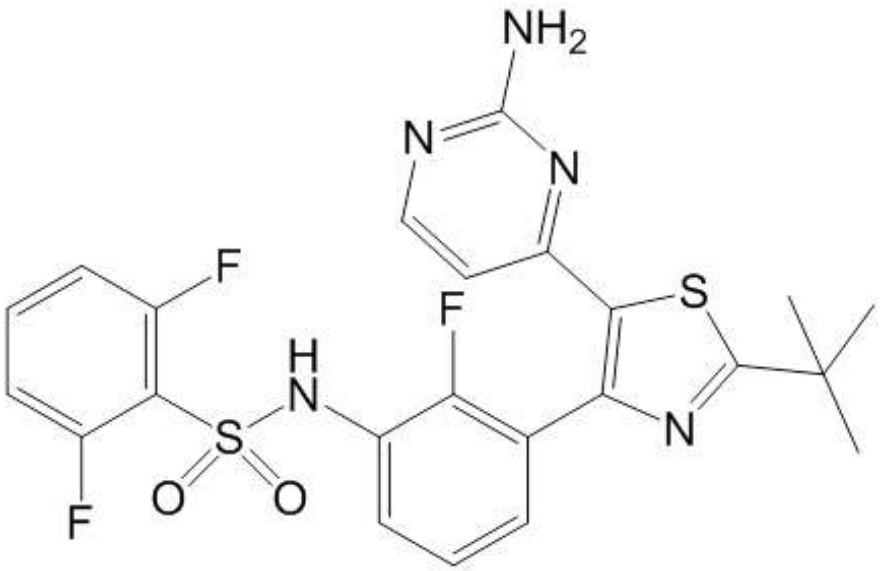

Figure 3.2: *In vitro* cellular accumulation of dabrafenib.

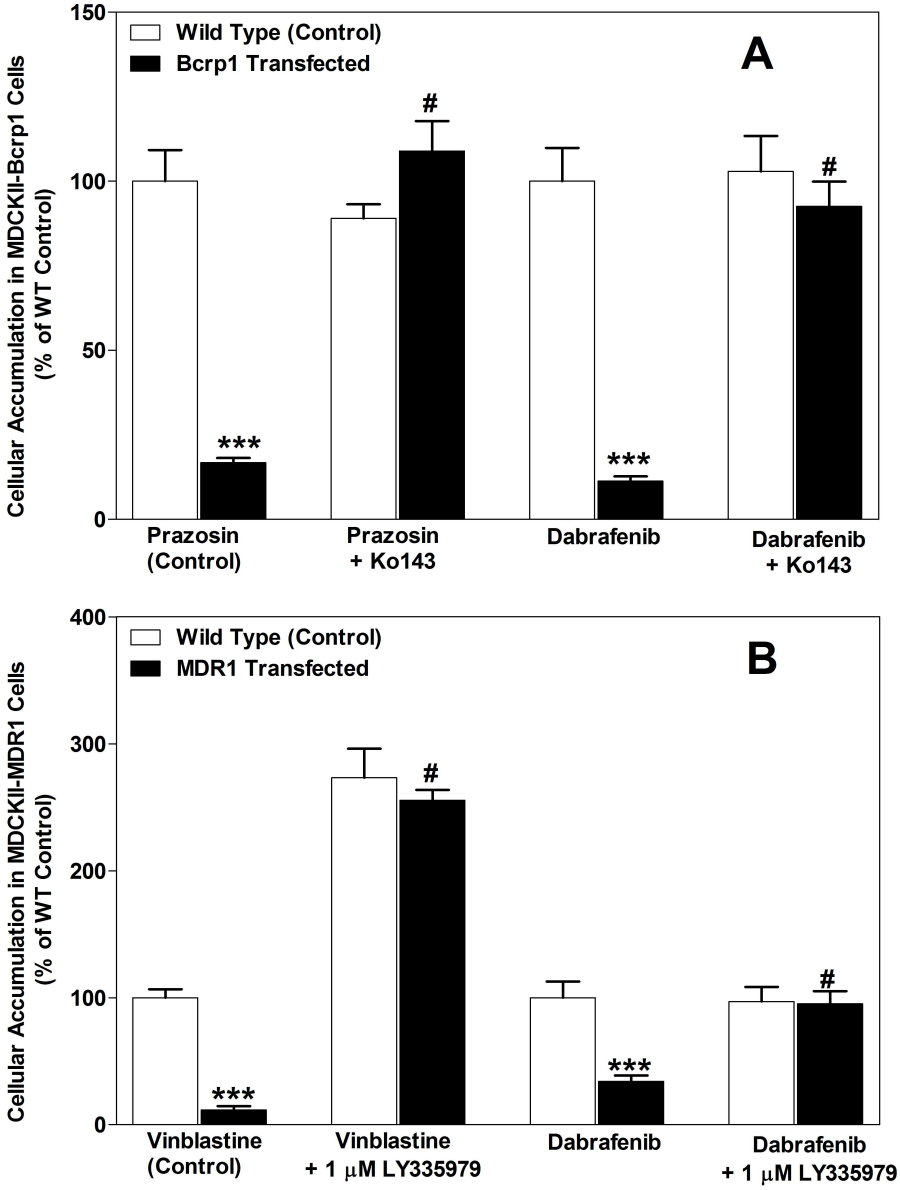

Panel A shows the accumulation of prazosin (prototypical Bcrp probe substrate; positive control), and dabrafenib in MDCKII-wild-type and Bcrp1-transfected cell lines with and

without Bcrp inhibitor Ko143 (0.2 μM). The accumulation of dabrafenib and vinblastine (probe substrate for P-gp) in MDR1 cells with and without P-gp inhibitor LY335979 (1 μM) is shown in Panel B. Data represent mean ± SD; n = 6 for all data points. ***, $p < 0.001$ compared to respective wild-type control. #, $p < 0.001$ compared to untreated transfected cell line.

Figure 3.3: Competition assays using prototypical probe substrate molecules

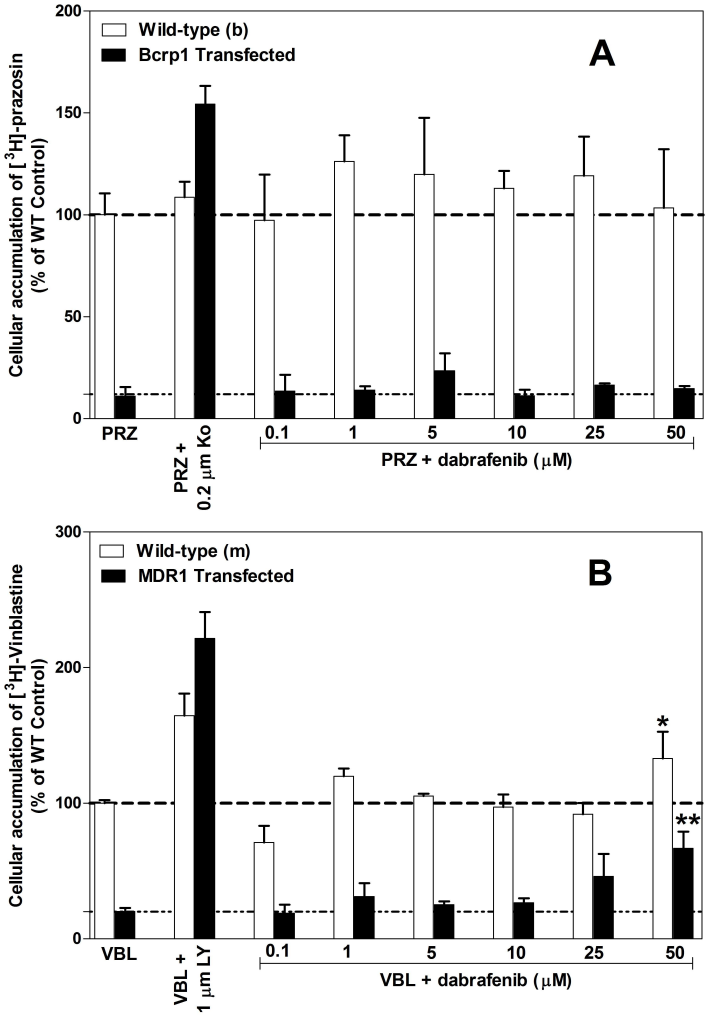

Intracellular accumulation of [^{3}H]-prazosin (Bcrp probe substrate), [^{3}H]-vinblastine (P-gp probe substrate) in Bcrp1-transfected (Panel A) and MDR1-transfected (Panel B) cell lines with increasing concentrations of dabrafenib from 0.1 μM to 50 μM. Ko: Bcrp inhibitor Ko143; LY: P-gp inhibitor LY335979. Data represent mean ± SD; n = 3 for all data points. **, p =0.0439 compared to untreated wild type cells. **, p =0.003 compared to untreated MDR1 cells.

Figure 3.4: Brain and plasma concentration vs time profiles of dabrafenib

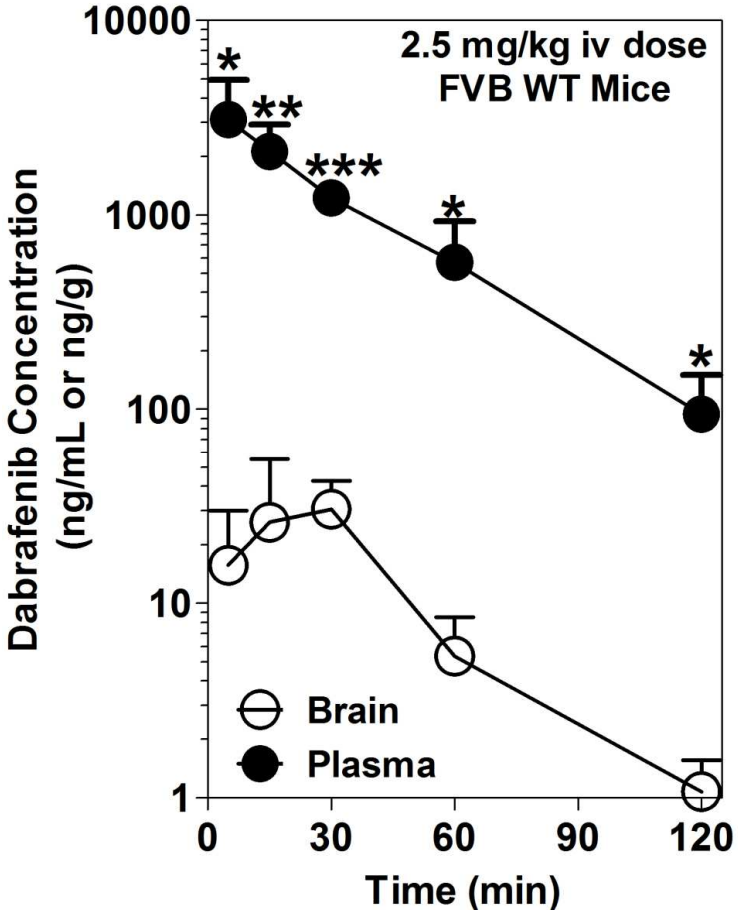

Brain and plasma concentrations of dabrafenib after an i.v. dose of 2.5 mg/kg in FVB wild-type mice at 5, 15, 30, 60, and 120 minutes post dose. Brain concentrations of dabrafenib are significantly lower than plasma concentrations at all measured time points. Data represent mean ± SD, n = 3-4. *, **, ***, represent $p < 0.05$, $p < 0.001$, $p < 0.0001$, respectively.

Figure 3.5: Brain distribution of dabrafenib in FVB wild-type and *Mdr1a/b*$^{-/-}$*Bcrp1*$^{-/-}$ mice.

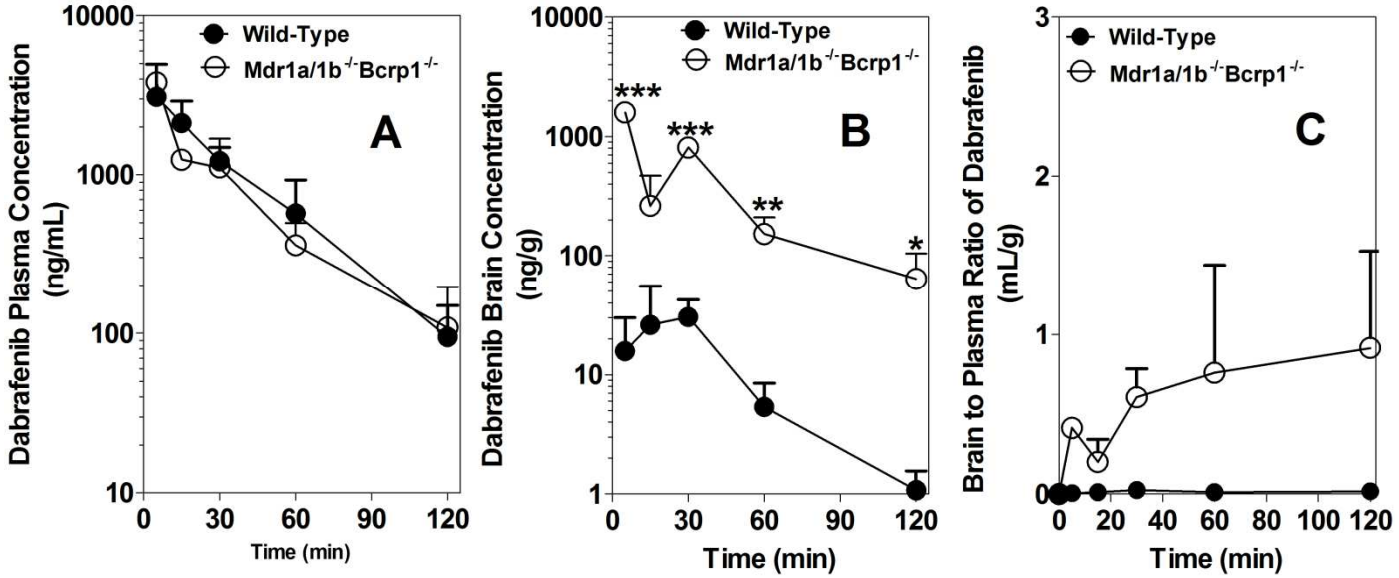

Plasma concentration vs time (A), brain concentration vs time (B), and brain-to-plasma concentration ratios (C) of dabrafenib in wild-type and *Mdr1a/b*$^{-/-}$*Bcrp1*$^{-/-}$ mice after an iv dose of 2.5 mg/kg. Plasma and brain concentrations were determined using LCMS/MS at 5, 15, 30, 60, and 120 minutes post dose of dabrafenib. Data represent mean ± SD, n = 3-4. *, **, ***, represent $p< 0.05$, $p< 0.001$, $p<0.0001$, respectively.

Figure 3.6: Brain distribution of dabrafenib in FVB wild-type and *Mdr1a/b*$^{-/-}$*Bcrp1*$^{-/-}$ mice after an oral dose.

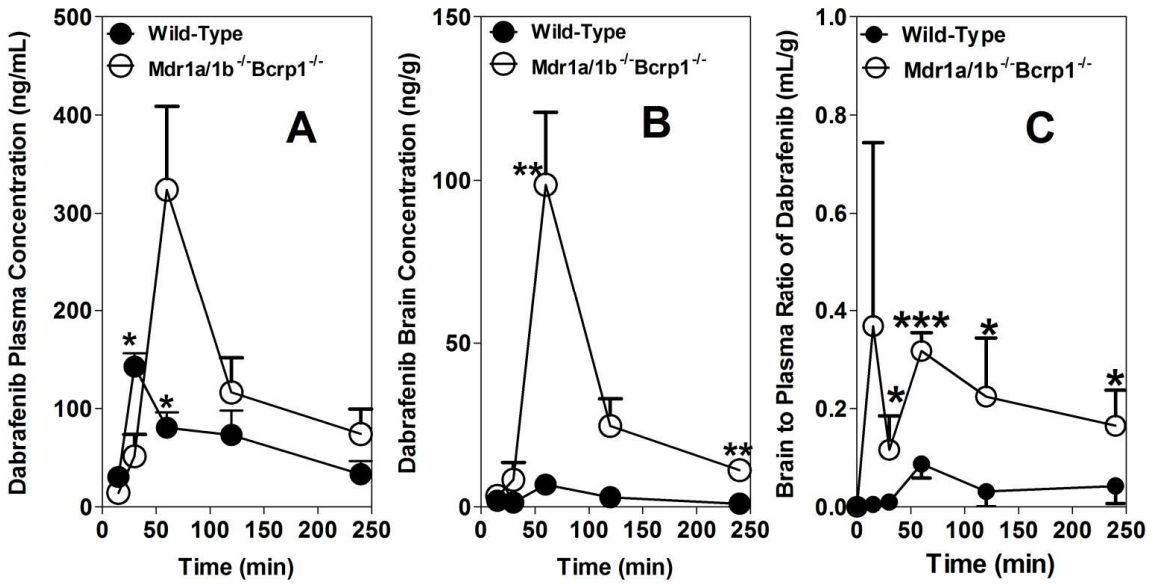

Plasma (A), brain (B) concentration vs. time profiles, and brain-to-plasma concentration ratios (C) of dabrafenib in wild-type and *Mdr1a/b*$^{-/-}$*Bcrp1*$^{-/-}$ mice after an oral dose of 25 mg/kg. Plasma and brain concentrations were determined using LCMS/MS at 15, 30, 60, 120, and 240 minutes postdose of dabrafenib. Data represent mean ± SD, n = 3-4. *, **, ***, represent $p< 0.05$, $p< 0.001$, $p<0.0001$, respectively.

Figure 3.7: Comparison of the brain distribution of dabrafenib and vemurafenib.

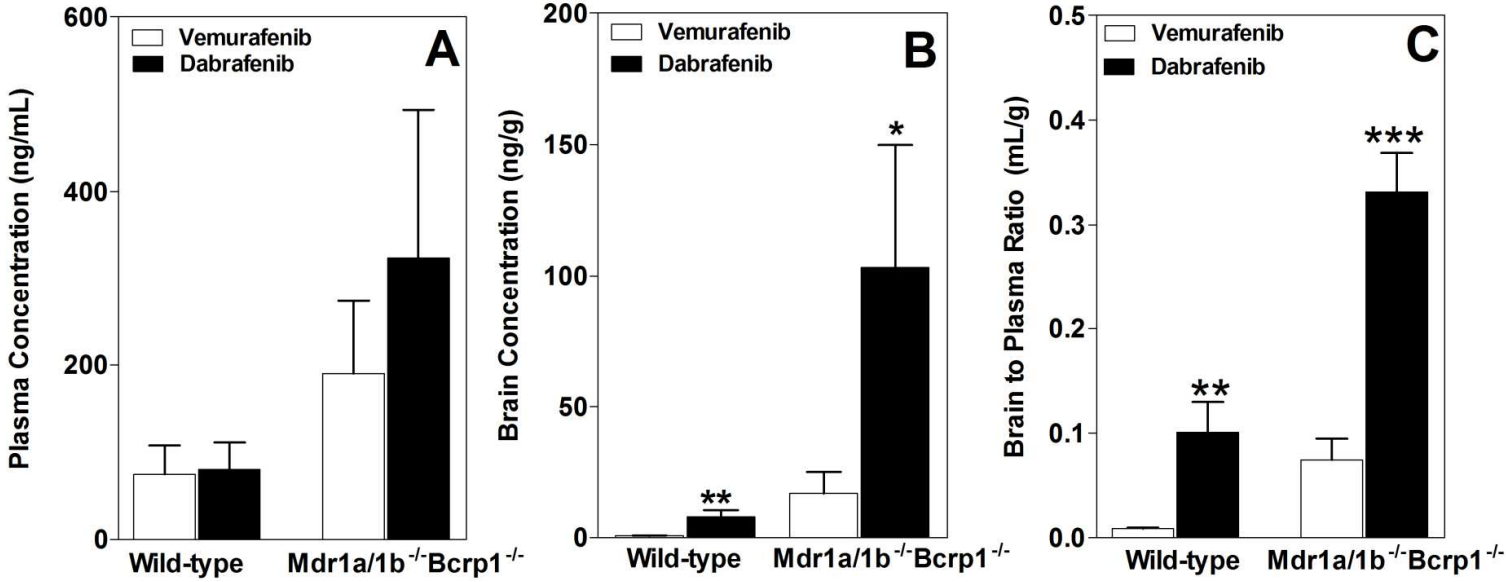

Plasma (A), brain (B), and brain to plasma concentration ratios (C) of dabrafenib and vemurafenib in wild-type and *Mdr1a/b*$^{-/-}$*Bcrp1*$^{-/-}$ mice after 1 hr postdose in separate animals (25 mg/kg, oral dose). Vemurafenib data is from our previously published results (Mittapalli et al., 2012). Data represent mean ± SD, n = 3-4. A *, **, ***, represent $p< 0.05$, $p< 0.001$, $p<0.0001$, respectively.

Table 3.1: Directional flux of dabrafenib in MDCKII-WT and MDCKII-Bcrp1 transfected cell lines.

Cell line	P_{app} (cm/s x10^{-6})		ER	CFR
	A-to-B	B-to-A		
MDCKII-WT	11.5 ± 1.4	14.1 ± 1.4	1.2	-
MDCKII-WT + 0.2 μM Ko143	16.4 ± 0.9	15.3 ± 2.6	0.9	
MDCKII-Bcrp1	1.3 ± 0.3*	27.3 ± 4.1*	21.0	17.5
MDCKII-Bcrp1 + 0.2 μM Ko143	13.2 ± 2.1#	9.6 ± 0.33#	0.7	

Note:
ER-Efflux ratio
CFR: Corrected efflux ratio
Papp: apparent permeability of dabrafenib
*significantly different compared to respective wild-type control cells
significantly different compared to untreated Bcrp1 control cells
Data represent mean ± SD; n = 3

Table 3.2: Directional flux of dabrafenib in MDCKII-WT and MDCKII-MDR1 Cells.

Cell line	P_{app} (cm/s x10^{-6})		ER	CFR
	A-to-B	B-to-A		
MDCKII-WT	2.6 ± 1.0	7.7 ± 1.6	3.0	-
MDCKII-WT + 1 µM LY335979	5.5 ± 0.4	5.2 ± 0.7	0.90	
MDCKII-MDR1	0.7 ± 0.3*	7.9 ± 1.9	11.4	3.8
MDCKII-MDR1 + 1 µM LY335979	4.9 ± 0.52#	5.2 ± 1.4	1.1	

Note:
ER-Efflux ratio
CFR: Corrected efflux ratio
Papp: apparent permeability of dabrafenib
*significantly different compared to respective wild-type control cells
significantly different compared to untreated MDR1 control cells
Data represent mean ± SD; n = 3

Table 3.3: Comparison of Pharmacokinetic Parameters of Dabrafenib in FVB Wild-type and *Mdr1a/b*$^{-/-}$*Bcrp1*$^{-/-}$ Mice After an i.v. dose of 2.5 mg/kg.

	Wild-type		*Mdr1a/b*$^{-/-}$*Bcrp1*$^{-/-}$ Mice	
	Plasma	**Brain**	**Plasma**	**Brain**
Terminal rate Constant (min^{-1})	0.03	0.036	0.024	0.026
Half-life (min)	23.7	19.1	28.3	26.6
Clearance (mL/min/kg)	24.2		28.4	
Volume of Distribution (L/kg)	0.83		1.2	
$AUC_{0 \rightarrow t\ last}$ (µg · min /mL)[1]	120.9 ± 15.8	2.8 ± 0.4	101.4 ± 8.7	42.1 ± 3.4*
K_p[2]	0.023		0.42	
K_p Ratio[3]	18.3			

1. Area under the curve from time zero to 2 hour post dose
2. Kp = AUC_{brain}/AUC_{plasma}
3. Kp Ratio = (Kp in *Mdr1a/b*$^{-/-}$*Bcrp1*$^{-/-}$ mice) / (Kp in wild-type mice)
4. *, $p < 0.05$ compared to wild-type AUC_{brain}

Table 3.4: Pharmacokinetic metrics in FVB wild-type and *Mdr1a/b*$^{-/-}$*Bcrp1*$^{-/-}$ Mice after Oral Dosing with 25 mg/kg Dabrafenib (Data presented as Mean ± SEE)

Mouse Genotype	Tissue	C_{max} (µg/mL)	AUC_{last}[1] (µg.min/mL)	Kp[2]	Kp Ratio[3]
Wild-type	Plasma	0.143 ± 0.014	15.8 ± 3.0	0.044	5.7
Wild-type	Brain	0.007 ± 0.001	0.69 ± 0.22		
***Mdr1a/b*$^{-/-}$ *Bcrp1*$^{-/-}$**	Plasma	0.324 ± 0.085	31.1 ± 5.1[#]	0.25	
***Mdr1a/b*$^{-/-}$ *Bcrp1*$^{-/-}$**	Brain	0.098 ± 0.022	7.6 ± 1.3*		

1. Area under the curve from time zero to 4 hour post dose
2. Kp = AUC_{brain}/AUC_{plasma}
3. Kp Ratio = Kp in TKO Mice / Kp in WT Mice
4. [#], p = 0.0414 compared to WT plasma
5. *, p = 0.002 compared to WT brain

Table 3.5: Comparison of brain distribution of vemurafenib and dabrafenib in FVB wild-type mice after an i.v. dose of 2.5 mg/kg.

	Dabrafenib		Vemurafenib[#]	
	Plasma	**Brain**	**Plasma**	**Brain**
Terminal rate Constant (min^{-1})	0.031	0.036	0.0051	0.0047
Half-life (min)	23.7	19.1	136	148
Clearance (mL/min/kg)	24.2		1.6	
Volume of Distribution (L/kg)	0.83		0.316	
$AUC_{0 \rightarrow t\ last}$ (min · µg/mL)	120.9 ± 15.8	2.8 ± 0.4	1663 ± 140	6.5 ± 0.9
K_p	0.023		0.004	

[#] From previously published data (Mittapalli et al., 2012).

Supplemental Figure 3.1:

Accumulation of different concentrations (0.5 to 75 μM) of dabrafenib in MDCKII-wild type and Bcrp1 transfected cell lines. The data show a linear correlation between concentration and cellular accumulation indicating that no saturation of efflux transporters. Data represent Mean ± SD; n= 3 for all data sets.

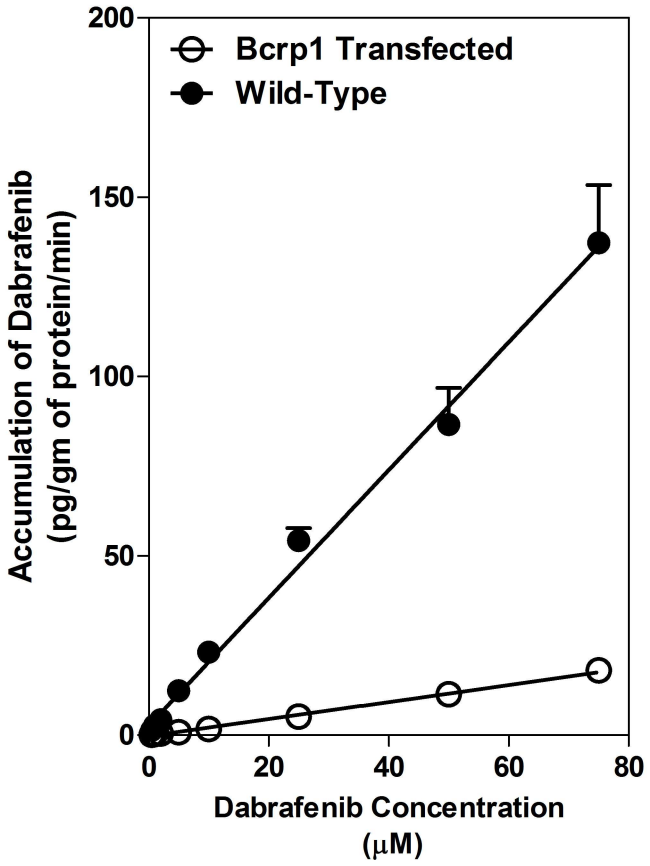

Supplemental Figure 3.2:

Intracellular accumulation of [^{3}H]-mitoxantrone (MTX; Bcrp probe substrate) in Bcrp1-transfected cell lines with increasing concentrations of dabrafenib from 0.1 µM to 50 µM. Ko: Bcrp inhibitor Ko143; Data represent mean ± SD; n = 3 for all data points.

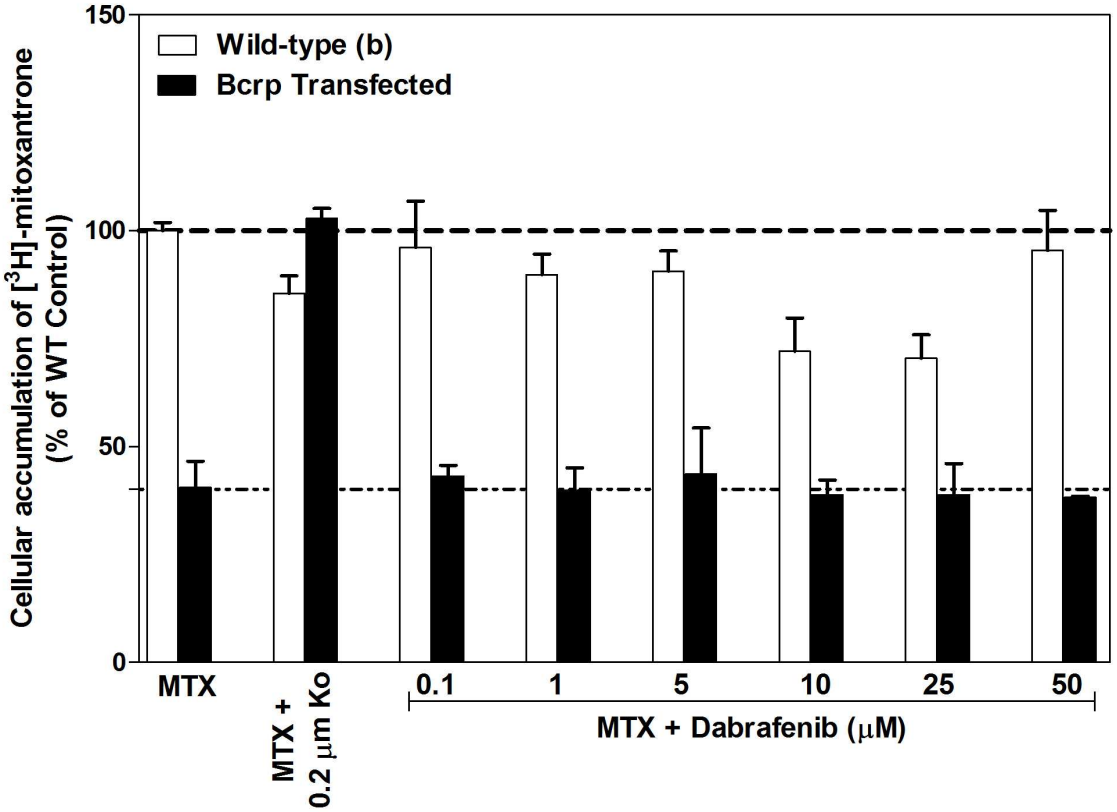

Supplemental Figure 3.3:

Equilibrium dialysis in plasma and brain homogenate: The graph shows the free fraction of dabrafenib (fraction unbound, f_{ub}) in plasma and brain homogenate with respect to time. The data indicate that equilibrium is achieved in ~6hrs in both plasma and brain homogenate.

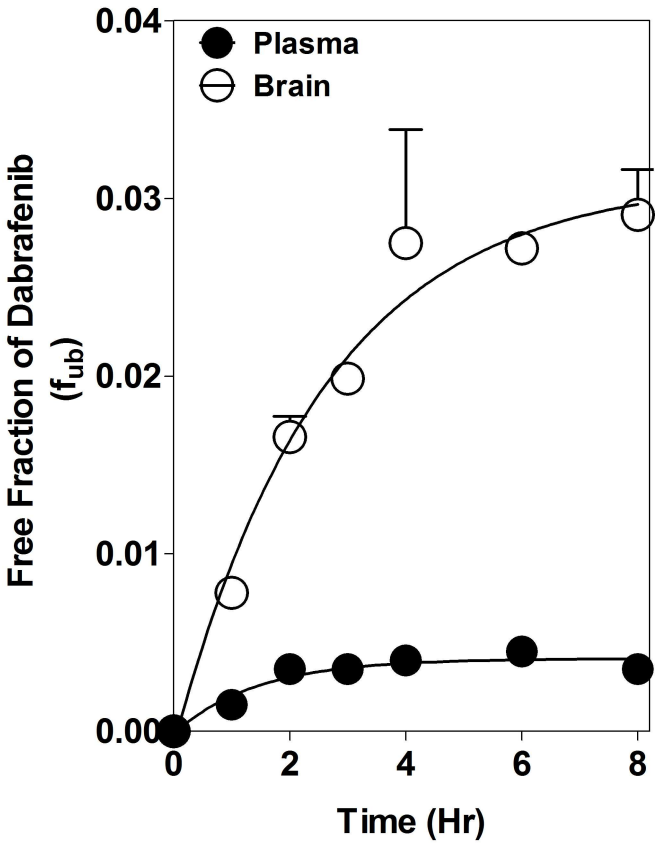

Chapter 4: Factors influencing the CNS distribution of a novel MEK 1/2 Inhibitor: Implications for combination therapy for melanoma brain metastases

This manuscript has been published in Drug Metabolism and Disposition August 2014, 42:1292-1300.

Brain metastases are a major cause of mortality in patients with advanced melanoma. Adequate brain distribution of targeted agents for melanoma will be critical for treatment success. Recently, improvement in overall survival led to FDA-approval of the BRAF inhibitors, vemurafenib and dabrafenib, and the MEK1/2 inhibitor, trametinib. However, brain metastases and emergence of resistance remain a significant problem. MEK1/2 is downstream of BRAF in the MAPK signaling pathway, making it an attractive target to combat resistance. The recently approved combination of dabrafenib and trametinib has shown improvement in progression-free survival; however, adequate brain distribution of both compounds is required to effectively treat brain metastases. In previous studies, we found limited brain distribution of dabrafenib, the purpose of the current study was to investigate factors influencing the brain distribution of trametinib. *In vitro* studies indicated that trametinib is a substrate for both P-gp and Bcrp; efflux transporters found at the blood-brain barrier. *In vivo* studies in transgenic mouse models confirmed that P-gp plays an important role in restricting brain distribution of trametinib. The brain-to-plasma partition coefficient (AUC_{Brain}/AUC_{Plasma}) was approximately 5-fold higher in *Mdr1a/b*$^{(-/-)}$ (P-gp knock-out) and *Mdr1a/b*$^{(-/-)}$*Bcrp1*$^{(-/-)}$ (triple knock-out) mice when compared with wild-type and *Bcrp1*$^{(-/-)}$ (Bcrp knock-out) mice. The brain distribution of trametinib was similar between the wild-type and Bcrp knock-out mice. These results show that P-gp plays an important role in limiting brain distribution of trametinib and

may have important implications for use of trametinib as single agent or in combination therapy for treatment of melanoma brain metastases.

4. 1 Introduction

Melanoma is the deadliest skin cancer with a remarkably high propensity for brain metastasis. Approximately 94% of melanoma patients develop brain metastases within 3 years of diagnosis of primary melanoma, and more than 90% of these patients die from progressive disease (Fife et al., 2004). Patients with 1 to 3 brain metastases are often treated with surgical resection or radiosurgery, while those with multiple brain metastases typically receive whole brain irradiation (Gibney et al., 2012). Unfortunately, melanoma is resistant to radiation and chemotherapy, and patients with brain metastases have a median survival of about four months despite aggressive therapy (Sampson et al., 1998; Fife et al., 2004). Thus, identifying therapies specifically effective for melanoma brain metastases could provide significant benefit for these patients.

The recent discovery of activating mutations in the MAPK pathway in melanoma has led to significant advances in treatment options for metastatic melanoma. These activating mutations cause deregulated constitutive signaling via the MAPK pathway that stimulates nuclear translocation of phosphorylated ERK, subsequent gene transcription, and ultimately tumor growth and proliferation (McCubrey et al., 2008). BRAF is mutated in greater than 50% of patients with metastatic melanoma (Davies et al., 2002). A majority of patients with BRAF

mutations exhibit a valine to glutamic acid substitution at amino acid 600 (V600E; BRAF ^{V600E}) (Davies et al., 2002). The FDA-approved BRAF inhibitors (vemurafenib and dabrafenib) and a MEK inhibitor, trametinib (GSK1120212; Fig. 4.1), have shown remarkable initial efficacy against peripheral BRAFV600E mutant tumors (Flaherty et al., 2010; Johannessen et al., 2010; Kim et al., 2010; Nazarian et al., 2010; Villanueva et al., 2010; Chapman et al., 2011; Gowrishankar et al., 2012). Vemurafenib and dabrafenib were both approved after showing a significant improvement in progression-free survival and overall survival as compared to dacarbazine in phase 3 clinical trials (Chapman et al., 2011; Hauschild et al., 2012). Similar to vemurafenib and dabrafenib, trametinib showed a 4.3 month progression-free survival as compared to 1.5 months in the chemotherapy group in phase 3 clinical trials in patients with V600 BRAF mutations (Flaherty et al., 2012). Emergence of resistance to BRAF inhibitor therapy commonly occurs through hyperactivation of downstream MEK signaling, and concurrent therapy with the BRAF inhibitor dabrafenib and the MEK inhibitor trametinib significantly prolongs survival compared to single agent therapy. Other mechanisms of BRAF-inhibitor resistance also have been defined involving hyperactivation of receptor tyrosine kinases, NRAS, or PI3K/mTOR, and these discoveries suggest that various combinations of molecular targeted agents will become the standard of care for melanomas (Johannessen et al., 2010; Gowrishankar et al., 2012).

The efficacy of many molecularly targeted agents in central nervous system tumors is limited by penetration across the blood brain barrier. The BBB is comprised of a monolayer of endothelial cells connected by tight junctions that serve as a physical barrier protecting the brain. In addition, these endothelial cells express multiple efflux transporters, including p-glycoprotein (P-gp) and breast cancer resistance protein (BCRP) that are known to exclude many anticancer agents from the brain.(Ohtsuki and Terasaki, 2007; Agarwal et al., 2011) We have previously demonstrated that vemurafenib and dabrafenib are restricted in brain distribution due to their efflux by P-gp and BCRP in an intact BBB (Mittapalli et al., 2012; Mittapalli et al., 2013). Microscopic subclinical brain metastases likely have a relatively intact BBB, and the limited accumulation of these BRAF inhibitors in the brain suggest that they may not be particularly effective in preventing emergence of new brain metastases. Consistent with this observation, there are clinical data suggesting an increased incidence of brain metastases in patients in whom peripheral disease is effectively controlled with these BRAF inhibitors (Rochet et al., 2012). However, there are sparse data about the efficacy of trametinib in the treatment of brain metastases, and no reports on factors influencing its brain distribution.

Effective combination therapy of melanoma brain metastases with targeted agents requires the sufficient delivery of all agents in the combination across the BBB to the target sites in melanoma brain metastases that may reside behind an

intact BBB. The latency time from the initial seeding of undetectable micro-metastatic melanoma in the brain to the first detection by MRI, and the subsequent poor survival after detection, suggests the deadly nature of occult disease and the importance of prevention of clinically-detectable brain metastases. Since trametinib is a highly efficacious combination partner for treatment of melanoma, the purpose of this study was to evaluate the factors limiting the brain distribution of trametinib in mice with the goal that this information will inform development of effective combination therapies that might include trametinib for patients with melanoma brain metastases.

4. 2 Materials and Methods

4. 2. 1 Chemicals

Trametinib and dabrafenib (GSK2118436A) were purchased from Chemietek (Indianapolis, IN). [^{3}H]-Prazosin and [^{3}H]-digoxin were purchased from Perkin Elmer Life and Analytical Sciences (Waltham, MA). [^{3}H]-Vinblastine and [^{3}H]-mitoxantrone were purchased from Moravek Biochemicals (La Brea, CA). [^{14}C] dasatinib was kindly provided by Bristol-Myers Squibb Co. (Princeton, NJ) and [^{14}C]-inulin was purchased from American Radiolabeled Chemicals, Inc. (St. Louis, MO). Ko143 [(3S,6S,12aS)-1,2,3,4,6,7,12,12aoctahydro-9-methoxy-6-(2-methylpropyl)-1,4-dioxopyrazino(1',2':1,6) pyrido(3,4-b)indole-3-propanoic acid 1,1-dimethylethyl ester] was purchased from Tocris Bioscience (Ellisville, MO) and zosuquidar [LY335979, (*R*)-4-((1*aR*, 6*R*,10*bS*)-1,2-difluoro-1,1*a*,6,10*b*-tetrahydrodibenzo-(*a*,*e*) cyclopropa(*c*)cycloheptan-6-yl)-**α**-((5-quinoloyloxy) methyl)-1-piperazine ethanol, trihydrochloride] was kindly provided Eli Lilly and Co.(Indianapolis, IN). Cell culture reagents were purchased from Invitrogen (Carlsbad, CA). All other chemicals used were of high performance liquid chromatography or reagent grade and were obtained from Sigma-Aldrich (St. Louis, MO).

4. 2. 2 In vitro studies

In vitro studies were performed using polarized Madin-Darby canine kidney-II (MDCK-II) cells. MDCKII-WT and Bcrp1-transfected (MDCKII-Bcrp1) cell lines were gifts from Dr. Alfred Schinkel (The Netherlands Cancer Institute). MDCKII-wild type (WT) and MDR1-transfected (MDCKII-MDR1) cell lines were kindly provided by Dr. Piet Borst (The Netherlands Cancer Institute). Cells were cultured in Dulbecco's modified Eagle's medium supplemented with 10% (v/v) fetal bovine serum and antibiotics (penicillin, 100 U/mL; streptomycin, 100 µg/mL; and amphotericin B, 250 ng/mL). Cells were grown in 25 mL tissue culture treated flasks before seeding for the experiments and were maintained at 37º C in a humidified incubator with 5% CO_2. The growth media for MDCKII-MDR1 additionally contained 80 ng/ml of colchicine to maintain positive selection pressure of P-gp expression

4. 2. 2. 1 In vitro accumulation studies

The intracellular accumulation of trametinib was performed in 12-well polystyrene plates (Corning Inc. Corning, NY). Briefly, cells were seeded at a density of 2 x 10^5 cells per well and were grown until the cells were ~80% confluent. On the day of experiment the culture media was aspirated and the cells were washed two times with cell assay buffer (122 mM NaCl, 25 mM $NaHCO_3$, 10 mM glucose, 10 mM HEPES, 3 mM KCl, 2.5 mM $MgSO_4$, 1.8 mM $CaCl_2$, and 0.4 mM K_2HPO_4). Then the cells were preincubated with assay buffer

for 30 min, after which the buffer was aspirated and the experiment was initiated by adding 1 mL of trametinib (2 μM) to each well and further incubated for 60 min. The assay plates were incubated at 37º C on an orbital shaker (60 rpm) for the entire duration of the experiment. When the inhibitor was present, it was included in both pre-incubation and accumulation steps. After the incubation period, the drug solution was aspirated and the cells were washed twice with ice cold PBS. Then the cells were lysed by adding 500 μL of 1% Triton X to each well. The solubilized cell fraction was sampled from each well and the concentration of trametinib was determined using liquid chromatography-tandem mass spectrometry (LC-MS/MS) and normalized to protein content (BCA protein assay).

4. 2. 2. 2 Bcrp and P-gp inhibition studies

Inhibition assays were performed using radiolabeled prototypical probe substrates [^{3}H]-prazosin for Bcrp, [^{3}H]-digoxin for P-gp and [^{14}C] dasatinib or dabrafenib (2 μM) as dual substrates. The intracellular accumulation of these probe substrates was evaluated in the presence of varying concentrations of trametinib ranging from 0.1 to 25 μM. Briefly, the cells were pre-incubated with increasing concentrations of trametinib for 30 min. After pre-incubation the cells were incubated with substrate along with increasing concentrations of trametinib for 60 min. At the end of the incubation period, the buffer was aspirated and cells were lysed using 1% Triton-X. The radioactivity in solubilized cell fractions was

determined by liquid scintillation counting (LS-6500; Beckman Coulter, Fullerton, CA). The concentration of dabrafenib in the solubilized cell fraction was determined using liquid chromatography-tandem mass spectrometry (LC-MS/MS) by a method previously described by Mittapalli et.al (Mittapalli et al., 2013). The concentration of dabrafenib and radioactivity of probe substrates in cell fractions was also normalized to protein content in each well. The increase in cellular accumulation of substrate as compared to control (no treatment with trametinib) was measured and reported as a function of trametinib concentration.

4. 2. 2. 3 Directional transport across MDCKII monolayers

The bidirectional flux studies were performed using twelve well Transwell® plates (polyester membrane, 0.4 μM pore size, 1.12 cm^2 growth surface area); (Corning Inc., Lowell, MA). The cells were seeded at a density of 2 $x10^5$ cells per well and the media was changed every other day until confluent monolayers were formed. On the day of experiment, the culture medium was aspirated and the cells were washed twice with cell assay buffer. After a 30 min pre-incubation, the experiment was initiated by adding the trametinib solution (5 μM) in assay buffer to the donor compartment. Samples (100 μL) were collected from the receiver compartment at 0, 60, 120, and 180 minutes and replaced with drug-free assay buffer. Similarly, at the beginning of the experiment, a 100 μL sample was drawn from the donor compartment and replaced with 100 μL drug solution. The Transwell® plates were incubated at 37ºC on an orbital shaker for the duration of

experiment except for the brief sampling times. In the inhibition experiments, either 0.2 μM Ko143 (selective Bcrp inhibitor) or 1 μM of zosuquidar (selective P-gp inhibitor) was added to both apical (A) and basolateral (B) compartments; the inhibitor was present in both compartments during the pre- and post-incubation period.

The apparent permeability (P_{app}) was calculated using the following equation

$$P_{\text{app}} = \frac{\frac{dQ}{dt}}{AC_0} \qquad (1)$$

Where, (*dQ/dt*) is the slope obtained from the initial linear range from the amount transported versus time plot, A is the area of the Transwell® membrane, and C_0 is the initial donor concentration. The efflux ratio and corrected flux ratio were calculated using equations 2 and 3, respectively.

$$\text{Efflux ratio} = \frac{P_{\text{app}}(B \rightarrow A)}{P_{\text{app}}(A \rightarrow B)} \qquad (2)$$

$$\text{Corrected flux ratio} = \frac{\left(\frac{B \rightarrow A}{A \rightarrow B}\right)_{\text{Transfected line}}}{\left(\frac{B \rightarrow A}{A \rightarrow B}\right)_{\text{Wild-type line}}} \qquad (3)$$

Where, A→B represents permeability in apical to basolateral and B→A represents permeability in basolateral to apical direction.

4. 2. 3 In vivo Studies

4. 2. 3. 1 Animals

All of the *in vivo* studies were performed in FVB (wild type), *Mdr1a/b*$^{-/-}$ (P-gp knockout), *Bcrp1*$^{-/-}$ (Bcrp knockout), and *Mdr1a/b*$^{-/-}$*Bcrp1*$^{-/-}$ (triple knockout) mice of either sex from an FVB genetic background (Taconic Farms, Germantown, NY). All animals were 8 to 10 weeks old at the time of experiment. Animals were maintained in a 12 hr light/dark cycle with unlimited access to food and water. All studies were carried out in accordance with the guidelines set by the *Principles of Laboratory Animal Care* (National Institutes of Health, Bethesda, MD) and approved by the Institutional Animal Care and Use Committee (IACUC) of the University of Minnesota.

4. 2. 3. 2 Brain distribution of trametinib in FVB mice

The trametinib i.v. dosing formulation was prepared in a vehicle containing 40% DMSO, 40% propylene glycol and 20% saline. All trametinib dosing solutions were freshly prepared on the day of the experiment. Wild type, *Mdr1a/b*$^{-/-}$, *Bcrp1*$^{-/-}$, and *Mdr1a/b*$^{-/-}$*Bcrp1*$^{-/-}$ mice received an i.v. dose of 5 mg/kg trametinib via the tail vein, and blood and brain samples were collected after 1, 4, 8, 16 and 24 hours post dose. At the end of the desired time point, the animals were euthanized using a CO_2 chamber. Blood was collected via cardiac puncture in heparinized tubes. Plasma was separated by centrifuging whole blood at 3500

rpm for 10 min at 4ºC. The whole brain was removed from the skull and washed with ice-cold PBS and superficial meninges were then removed by blotting with tissue paper. Both brain and plasma samples were stored at -80ºC until further analysis.

4. 2. 3. 3 Steady-state brain distribution of trametinib and combination of dabrafenib-trametinib

To determine the steady state brain and plasma concentrations of trametinib, Alzet osmotic mini pumps (Durect Corporation, Cupertino, CA) were loaded with trametinib (2 mg/mL dissolved in DMSO) to be released for 48 hrs at a rate of 1µL/hr. After initial trametinib loading, mini pumps were primed overnight in sterile saline at 37º C. Pumps were implanted in the peritoneal cavity of wild type, *Mdr1a/b*$^{-/-}$, *Bcrp1*$^{-/-}$, and *Mdr1a/b*$^{-/-}$*Bcrp1*$^{-/-}$ mice as described previously (Mittapalli et al., 2012). Briefly, mice were anesthetized using isofluorane and the abdominal cavity was shaved. A small midline incision was made in the lower abdominal wall under the rib cage. Then a small incision was made directly in the peritoneal membrane and the primed pump was inserted in the cavity. The incision was sutured and the skin was closed using surgical clips. The animals were allowed to recover on a heating pad and once recovered they were moved to their original cages. The animals were sacrificed 48 hrs after the implantation of the pumps, and brain and plasma samples were processed as described above.

Similarly, in another study, Alzet mini-pumps were loaded with trametinib and dabrafenib (2 mg/mL trametinib and 10 mg/mL dabrafenib dissolved in DMSO) to be released for 48 hours at the rate of 1 μL/hr. Pumps were primed overnight and implanted in the peritoneal cavity of wild type and *Mdr1a/b*$^{-/-}$*Bcrp1*$^{-/-}$ mice. These animals were also sacrificed 48 hrs after the implantation of the pumps, and brain and plasma samples were processed as described previously.

4. 2. 4 Analysis of trametinib concentrations using LC-MS/MS

The concentrations of trametinib in cell lysates, assay buffer, plasma and brain homogenate were determined using a sensitive and specific liquid chromatography coupled with tandem mass spectrometry (LC-MS/MS) assay. For brains, three volumes of 5% bovine serum albumin were added and homogenized to get a uniform homogenate. For analysis of unknowns, an aliquot of cell lysate, cell assay buffer, brain homogenate or plasma was spiked with 50 ng of vemurafenib as an internal standard. The samples were then extracted by addition of 10 volumes of ethyl acetate followed by vigorous shaking for 5 min and centrifuged at 7500 rpm for 5 min at 4ºC to separate the organic layer. The organic layer was transferred to microcentrifuge tubes and dried under nitrogen. Samples were reconstituted in 100 µL of mobile phase and transferred into HPLC glass vials. Chromatographic analysis was performed using an AQUITY UPLC® system (Milford, MA, USA). The chromatographic separation was achieved using an Agilent Technologies Eclipse XDB-C18 column (4.6 x 50 mm) with 1.8 µm

Zobrax Rx-SIL as the stationary phase. The mobile phase consisted of 20 mM ammonium formate with 0.1% formic acid and acetonitrile (35:65 v/v), and was delivered at a flow rate of 0.25 mL/min.

The column effluent was monitored using a Waters/Micromass Quattro^{TM} Ultima mass spectrometer (Waters, Milford, MA). The instrument was equipped with an electrospray interface, and controlled by the Masslynx (Version 4.1) data system. The samples were analyzed using an electrospray probe in the negative ionization mode operating at a spray voltage of 2.96 kV for both trametinib and vemurafenib (internal standard). Samples were introduced into the interface through a heated nebulized probe where the source temperature and desolvation temperature was set at 100 ºC and 275 ºC, respectively. The spectrometer was programmed to allow the [MH]- ion of trametinib at *m/z* 613.93 and that of internal standard at *m/z* 488.23 to pass through the first quadrupole (Q1) and into the collision cell (Q2). The collision energy was set at 27V both for trametinib and vemurafenib. The product ions for trametinib (*m/z* 530.79) and vemurafenib (*m/z* 380.89) were monitored through the third quadrupole (Q3). The retention times for trametinib and the internal standard (vemurafenib) were 4.5 and 5.7 minutes, respectively. The assay was sensitive and linear over a range of 1.26 ng/mL to 1500 ng/mL with the coefficient of variation less than 15% over the entire range.

4. 2. 5 Pharmacokinetic Calculations

Pharmacokinetic parameters and metrics from the concentration-time data in plasma and brain were obtained by non-compartmental analysis (NCA) performed using Phoenix WinNonlin 6.2 (Pharsight, Mountain View, CA). The area under the concentration-time profiles for plasma (AUC_{plasma}) and brain (AUC_{brain}) were calculated using the linear trapezoidal method. The sparse sampling module in WinNonlin was used to estimate the standard error around the mean of the AUCs.

4. 2. 6 Statistical Analysis

Data in all experiments represent mean ± SD unless otherwise indicated. Comparisons between two groups were made using an unpaired t-test. One way ANOVA, followed by Bonferonni's multiple comparisons test, was utilized to compare multiple groups. A significance level of $p < 0.05$ was used for all experiments. (GraphPad Prism 5.01 software, GraphPad, San Diego, CA, USA).

4. 3 Results

4. 3. 1 Intracellular accumulation of trametinib

The intracellular accumulation of trametinib was studied in MDCKII WT and P-gp or Bcrp overexpressing cell lines. The cellular accumulation of [^{3}H]-prazosin and [^{3}H]-vinblastine were used as positive controls for Bcrp and P-gp mediated efflux transport, respectively. The accumulation of [^{3}H]-prazosin (**Fig. 4.2A**) was 87% lower in Bcrp overexpressing cells (WT: 100 ± 9.2%; Bcrp: 12.7 ± 1.7%, p< 0.0001). Similarly, the accumulation of [^{3}H]-vinblastine (**Fig. 4.2B**) in P-gp overexpressing cells was ~77% lower compared to WT cells (WT: 100.0 ± 6.8%; MDR1: 22.85 ± 0.7%, p< 0.0001). Trametinib accumulation was approximately 81% lower in Bcrp overexpressing cells compared to WT cells (WT: 100 ± 2.95%; Bcrp: 18.8 ± 1.4%, p<0.0001). The difference in accumulation was abolished when the specific Bcrp inhibitor Ko143 was added (Bcrp: 18.8 ± 1.4%; Bcrp with Ko143: 103.6 ± 1.1%, p<0.0001). Similarly, the accumulation of trametinib was ~45% lower in P-gp overexpressing line compared to its WT control (WT: 100.0 ± 3.5%; MDR1: 55.0 ± 4.2%, p< 0.0001), and the difference in accumulation was abolished (**Fig. 4.2B**) when a specific P-gp inhibitor LY335979 was added (MDR1: 55.0 ± 4.2%; MDR1 with LY: 97.0 ± 2.7%, p< 0.0001). These cellular accumulation data indicate that trametinib is a substrate for both P-gp and Bcrp *in vitro.*

4. 3. 2 Competition assays using prototypical probe substrates

The effect of increasing concentrations of trametinib on probe substrate accumulation was assessed in Bcrp-transfected and MDR1-transfected MDCKII cells. Increasing concentrations of trametinib did not significantly increase the accumulation of prazosin in the Bcrp1-transfected cells **(Fig. 4.3A)**. However, increasing concentrations of trametinib significantly increased (~ 3 fold at 5 μM trametinib) the accumulation of dasatinib in the Bcrp cells **(Fig. 4.3B).** The addition of increasing concentrations of trametinib resulted in an increase in the accumulation of digoxin (~ 4 fold increase at 5 μM trametinib) in the MDCKII-MDR1 cells **(Fig. 4.3C)**. The fold increase in digoxin accumulation in MDCKII-MDR1 cells at 5 μM of trametinib was no different than the effect seen with 1 μM LY335959. These competitive inhibition results suggest that trametinib possibly shares the same binding site on Bcrp as dasatinib and on P-gp as digoxin. Given that dabrafenib and trametinib will be administered as combination therapy, it is important to note that increasing concentrations of trametinib did not significantly increase the intracellular accumulation of dabrafenib in the range from 0.1 to 10 μM in the Bcrp1 **(Fig. 4.4A)** and MDR1 **(Fig. 4.4B)** transfected cells, suggesting no competing interaction between trametinib and dabrafenib in this concentration range.

4. 3. 3 Directional transport studies

The directional flux of trametinib was assessed in MDCKII- wild-type, Bcrp1-transfected, and MDR1-transfected monolayers grown on Transwell membranes. Confluent monolayers with intact tight junctions were formed in 3-4 days. Paracellular leakage was assessed by measuring the transport of [^{14}C]-inulin across the cell monolayers and the % of inulin transported in 120 min was found to be less than 1% in all cell lines. The directional permeability of trametinib was similar in the apical to basal (A-to-B) and B-to-A directions in the wild-type cells (12.8 ± 2.5 versus 12.3 ± 4.7 $\times$ 10$^{\wedge-6}$ cm/sec, respectively; **Table 4.1**). However, in the Bcrp1-transfected cells, the apparent permeability of trametinib in the B-to-A direction was significantly higher than the apparent permeability in the A-to-B direction (19.3 ± 1.96 versus 5.17 ± 2.1 $\times$ 10$^{\wedge-6}$ cm/sec, respectively; $p < 0.05$; Table 4.1) with an efflux ratio of 3.7 **(Table 4.1)**. Treatment with the Bcrp inhibitor Ko143 significantly ($p < 0.05$) decreased the Bcrp1-mediated efflux of trametinib in the B-to-A direction and increased the A-to-B permeability with a resulting efflux ratio of 1.04. The corrected efflux ratio was found to be 3.85 for Bcrp1 mediated bidirectional transport. Similarly, in MDR1-transfected cells, the B-to-A permeability was significantly higher compared to A-to-B permeability, with an efflux ratio of 2.55 (**Table 4.1)**. The presence of LY335979 significantly abolished the difference in directional permeabilities with a resulting efflux ratio of 1.23. The corrected efflux ratio in the MDR1 cells was found to be 2.45. These data further

confirm that trametinib is a substrate for Bcrp1 and MDR1 *in vitro* and suggests that these transporters may be an important factor in the brain distribution of trametinib.

4. 3. 4 Brain distribution of trametinib in different genotypes

The brain distribution of trametinib was studied in FVB wild type, Bcrp1$^{-/-}$, Mdr1a/b$^{-/-}$ and Mdr1a/b$^{-/-}$Bcrp1$^{-/-}$ mice after intravenous administration of 5 mg/kg of trametinib via the tail vein. **Fig. 4.5** shows the plasma and brain concentrations of trametinib in all 4 genotypes at 1, 4, 8, 16, and 24 hours after a single IV dose. The plasma concentrations **(Fig. 4.5A)** were no different between the four genotypes at any given time point. The plasma concentrations of trametinib were 2-30 fold higher than the brain concentrations **(Fig. 4.5B)** in the wild-type and Bcrp1$^{-/-}$ mice. The brain concentrations in the Mdr1a/b$^{-/-}$ and Mdr1a/b$^{-/-}$Bcrp1$^{-/-}$ were 4-20 fold higher than the brain concentrations in the wild-type and the Bcrp1$^{-/-}$ mice. The brain to plasma AUC ratios **(Fig. 4.5C)** in the wild type, Bcrp1$^{-/-}$, Mdr1a/b$^{-/-}$ and Mdr1a/b$^{-/-}$Bcrp1$^{-/-}$ were: 0.148, 0.136, 0.733, 0.675, respectively, resulting in a drug targeting index $(AUC_{brain}/AUC_{plasma})_{knockout}/(AUC_{brain}/AUC_{plasma})_{wild\text{-}type}$ of ~ 5 in both Mdr1a/b$^{-/-}$ and Mdr1a/b$^{-/-}$Bcrp1$^{-/-}$ mice **(Table 4.2),** but there was no significant brain targeting in the Bcrp1$^{-/-}$ mice. These data suggest that P-gp plays a major role, greater than Bcrp, in significantly limiting the brain distribution of trametinib.

4. 3. 5 Steady-state brain distribution of trametinib

The steady state brain distribution of trametinib was examined after a continuous intraperitoneal infusion using Alzet^{TM} osmotic pumps for 48 hrs at 2 µg/hr. As shown in **Fig. 4.6**, the steady-state brain to plasma ratios were 0.28 ± 0.09, 0.14 ± 0.13, 1.53 ± 0.57, 2.45 ± 1.3 in the FVB wild type, Bcrp1$^{-/-}$, Mdr1a/b$^{-/-}$ and Mdr1a/b$^{-/-}$Bcrp1$^{-/-}$ mice, respectively. The B/P ratios at steady state were ~ 5 fold higher in the Mdr1a/b$^{-/-}$ and ~ 9 fold higher in the Mdr1a/b$^{-/-}$Bcrp1$^{-/-}$ mice when compared to wild-type mice. These data indicate that the brain distribution of trametinib is significantly limited due to active efflux at the BBB with P-gp playing a greater role than Bcrp in the mouse, and the steady-state data correspond well with the AUC ratios following a single i.v. dose.

4. 3. 6 Steady state brain distribution of dabrafenib and trametinib in combination

We then examined the steady-state brain distribution of dabrafenib (10 µg/hr) and trametinib (2 µg/hr) when dosed simultaneously as a 48 hours constant intraperitoneal infusion for 48 hours in wild type and *Mdr1a/b$^{-/-}$Bcrp1$^{-/-}$*. The steady-state brain to plasma concentration ratios of dabrafenib in the wild type and *Mdr1a/b$^{-/-}$Bcrp1$^{-/-}$* mice were 0.019 ± 0.02 and 1.09 ± 0.85, respectively **(Fig. 4.7)**. The steady-state brain to plasma concentration ratios of trametinib in the wild type and *Mdr1a/b$^{-/-}$Bcrp1$^{-/-}$* mice were 0.03 ± 0.01 and 0.85 ± 0.38, respectively **(Fig. 4.7)**. The aggregate of these data suggests that both drugs in

the combination of dabrafenib and trametinib suffer from limited brain distribution due to active efflux at the BBB.

4. 4 Discussion

Brain metastases are a significant cause of morbidity and mortality among patients with advanced melanoma (Skibber et al., 1996; Fife et al., 2004; Davies et al., 2011). The last decade has seen remarkable improvements in the treatment of metastatic melanoma. Earlier, dacarbazine and interleukin-2 were the only two systemic agents that were approved for the treatment of metastatic melanoma. The response rates with these two agents were ~10-20% (Comis, 1976; Atkins et al., 1999; Garbe et al., 2011). The discovery of oncogenic mutations in BRAF and its high prevalence in melanoma tumors made it an excellent molecular target. The approval of BRAF inhibitors, vemurafenib and dabrafenib, as well as the MEK inhibitor, trametinib, has tremendously changed the landscape of treatment options for advanced melanoma. Vemurafenib and dabrafenib were approved by the FDA after they showed improved efficacy when compared to dacarbazine in clinical trials (Chapman et al., 2011; Hauschild et al., 2012). Also, in a phase 1 dose escalation clinical trial in melanoma patients with untreated brain metastases, dabrafenib showed a promising reduction in brain tumor size in 90% of the patients (Falchook et al., 2012). Despite the initial success of these two agents, most patients with metastatic melanoma relapse within a year due to the emergence of resistance (Johannessen et al., 2010;

Nazarian et al., 2010; Gowrishankar et al., 2012). The improved duration of response from the combination of BRAF and MEK inhibitors, dabrafenib and trametinib, provides new hope for delaying resistance and improving response. The success of combination therapies in treating brain metastases depends on all agents being effectively delivered to all metastatic sites, including micrometastases that reside behind an intact BBB with functional efflux transporters. In our previous studies, we have shown that both vemurafenib and dabrafenib are substrates for P-gp and BCRP, and their brain distribution is significantly limited due to their interaction with these two important efflux transporters (Mittapalli et al., 2012; Mittapalli et al., 2013). We also observed that dabrafenib has a greater brain distribution when compared to vemurafenib, with the B/P ratio of dabrafenib being greater than that of vemurafenib in both wild-type and *Mdr1a/b*$^{-/-}$*Bcrp*$^{-/-}$ mice. These data suggest that dabrafenib may be a better option than vemurafenib in the treatment of brain metastases. However, for the success of the dabrafenib and trametinib combination in the treatment of brain metastases, it is important to investigate the mechanisms influencing the brain distribution of trametinib, both alone and in combination with dabrafenib.

In the current study, we demonstrate that trametinib is a substrate for P-gp and BCRP in vitro. In vivo, we observe that P-gp plays a greater role than BCRP in limiting trametinib brain distribution. This is the first report of the interaction of trametinib with BCRP and P-gp.

The experiments performed *in vitro* in MDCKII cells that overexpress either murine Bcrp or human MDR1 revealed that trametinib is a substrate for both Bcrp and P-gp (Fig. 4.2; Table 4.1). We observed a significantly lower accumulation of trametinib in the P-gp and Bcrp transfected cells as compared to wild-type (Fig. 4.2). In the presence of specific P-gp and Bcrp inhibitors (LY335979 and Ko-143, respectively) this difference in intracellular accumulation was abolished (Fig. 4.2). The percent accumulation of vinblastine in the presence of LY335979 in the wild-type and MDR1-transfected cells was significantly greater than 100 %, this may be due to the fact that vinblastine was used at a tracer concentration (positive control for functional cells). In comparison, trametinib accumulation at an incubating trametinib concentration of 2 μM was not greatly affected by LY335979, presumably because the higher trametinib concentration (substrate) may be saturating transport, leading to less influence of LY335979 (inhibitor) on the efflux transport clearance.

In P-gp transfected cells, using a prototypical probe substrate, digoxin, for P-gp, we observed a significant increase in intracellular accumulation with increasing concentrations of trametinib starting at 5 μM (Fig. 4.3C). Interestingly, we did not observe a significant increase in intracellular accumulation of BCRP substrate, prazosin, up to a concentration of 25 μM (Fig. 4.3A). In Bcrp cells, we observed a significant increase in accumulation of dual substrate dasatinib, starting at 5 μM

trametinib (Fig. 4.3B). In both, Bcrp and MDR1 cells, we did not observe a significant increase in intracellular dabrafenib with increasing concentrations of trametinib up to 10 μM (Fig. 4.4). It is noteworthy here that this is not a pharmacologically relevant concentration, the average peak concentration observed when patients received 2 mg of trametinib once daily was ~ 0.035 μM (Kim et al., 2013). Using a specific Bcrp inhibitor Ko143 and P-gp inhibitor LY335979, we observed an increase in the intracellular accumulation of trametinib in both Bcrp1 and MDR1 cells. From accumulation studies, we conclude that trametinib is a substrate for both BCRP and P-gp. At 5 μM, trametinib inhibits the active efflux of P-gp probe substrate digoxin and dual substrate dasatinib. This suggests the possibility of trametinib sharing similar binding sites as digoxin and dasatinib on P-gp and BCRP, respectively. Trametinib however, did not inhibit these two transporters in the case of Bcrp probe substrate, prazosin and the dual substrate dabrafenib. This may suggest the interaction of trametinib on a different binding site as compared to these two substrates on the efflux transporters. Importantly, the fact that trametinib (0.1 – 10 μM) does not inhibit Bcrp and P-gp mediated efflux of dabrafenib suggests that at the studied concentrations, the combination of dabrafenib and trametinib may not have any transporter mediated drug-drug interaction in treating brain metastases. From our bidirectional flux studies of trametinib across monolayers of MDCKII wild-type, Bcrp1 transfected and MDR1 transfected cells, we

observed a corrected flux ratio of 3.85 in the Bcrp1 cells and 2.45 in the MDR1 cells (Table 4.1), indicating the involvement of these two efflux transporters in the active efflux of trametinib. The specific inhibitors of Bcrp and P-gp were able to restore the net bidirectional flux of trametinib. All these *in vitro* experimental results, put together, conclusively show that trametinib is a substrate for these two efflux transporters. Based on our current *in vitro* and *in vivo* findings, we have noted a disparity with the current findings and the trametinib product label, which states that trametinib is not a substrate for, or inhibitor of, P-gp or Bcrp. We attribute these differences to be due to the trametinib concentration at which *in vitro* inhibition studies were conducted (0.04 μM). In our studies, we observe trametinib to be a substrate of P-gp and Bcrp. More importantly, we observe that the *in vitro* findings translate *in vivo* with changes in brain distribution in both the P-gp knock-out and triple knock-out mice.

With these results from in vitro experiments, we then investigated the brain distribution of trametinib in mice. After an i.v. dose of trametinib, we observed that the brain concentrations in the wild type and *Bcrp*$^{-/-}$ mice were ~ 1 log unit lower than the plasma concentrations at all measured time points (Fig. 4.5B). However, the brain distribution of trametinib was significantly improved in the *Mdr1a/b*$^{-/-}$ and *Mdr1a/b*$^{-/-}$*Bcrp*$^{-/-}$ mice (Fig. 4.5B). The plasma concentrations were not different in all 4 genotypes at all measured time points (Fig. 4.5A). The AUC_{brain} to AUC_{plasma} ratio (K_P) in the wild-type and *Bcrp*$^{-/-}$ mice were 0.148 and

0.136, respectively while they were 0.733 and 0.675 in the *Mdr1a/b*$^{-/-}$ and *Mdr1a/b*$^{-/-}$*Bcrp*$^{-/-}$ mice (Table 4.2). The remarkable increase in the targeted brain distribution led to a Kp ratio (Kp knockout/Kp wild-type) of ~ 5 in the *Mdr1a/b*$^{-/-}$ and *Mdr1a/b*$^{-/-}$*Bcrp*$^{-/-}$ mice. An important consideration here is the plasma and tissue binding of trametinib. As per the product label, trametinib is 97.4% bound to human plasma proteins. $K_{P,uu}$ would provide useful information regarding brain partitioning and the role of efflux transporters, however, it should be noted here that the magnitude of difference, i.e., fold increase in brain-to-plasma ratio observed between wild-type and knockout mice would not change with correction for free fraction since protein binding is no different between wild-type and knockout mice (Mittapalli et al., 2013). Keeping this in mind, our overall conclusions with regards to the brain penetration of trametinib remain valid.

Also, at steady state, the B/P ratios in the wild-type and *Bcrp*$^{-/-}$ mice were significantly lower (5-9 fold) than in the *Mdr1a/b*$^{-/-}$ and *Mdr1a/b*$^{-/-}$*Bcrp*$^{-/-}$ mice (Fig. 4.6). From simultaneous infusion of dabrafenib and trametinib to steady-state, we observed a significant increase in the B/P ratio in the *Mdr1a/b*$^{-/-}$*Bcrp*$^{-/-}$ mice as compared to wild-type (Fig. 4.7). Also, when infused simultaneously, we observed a decrease in the B/P ratio of trametinib in the wild-type as compared to single agent infusion. A possible explanation for this could be the saturation of influx transporters during co-dosing. It is interesting to note that even though the in vitro cell accumulation and directional flux studies show that trametinib is a

substrate for Bcrp-mediated transport, that fact did not translate into significant effects of Bcrp-mediated transport at the BBB in these mouse models. Here, it is important to think about species differences in the expression of efflux transporters. For example, the expression of BCRP at the human BBB is ~3-times greater as compared to the expression at the mouse BBB, and the expression of P-gp is ~2.5 fold lower at the human BBB as compared to mouse BBB (Uchida et al., 2011). Also, FVB mice express ~ 4 times more P-gp as compared to Bcrp (Agarwal et al., 2012). However, in spite of various differences in transporter expression, rodent models have been widely used to study the brain distribution of drugs. From this study, keeping in mind known differences in transporter expression at the brain capillary endothelium, it may be possible to make correlations to predict potential human exposure related to these two transporters. Also, it should be noted that the findings from this study may be able to guide/explain future clinical results. In the current study, we have observed that active efflux by P-gp plays a major role in keeping trametinib out of the mouse brain. This interpretation of rodent data has to be kept in mind for assessing potential human exposure. In the case of trametinib, it is likely that, together, P-gp and Bcrp will affect its brain distribution in humans. This result is similar to previous findings with another molecularly targeted agent, cediranib (Wang et al., 2012). It is well understood that P-gp and Bcrp may compensate for each other at the BBB in active efflux of dual substrates, i.e., with genetic

knock-out of one transporter (single knock-outs); another transporter can limit substrate brain distribution while in triple knock-outs, there can potentially be a greater than additive effect in the enhancement of brain distribution of dual substrates (Enokizono et al., 2008; Kodaira et al., 2010). Also, given the higher expression of P-gp at the mouse BBB, with substrates of similar affinities, it is common to observe a greater P-gp effect on brain penetration (Agarwal et al., 2011; Agarwal et al., 2012). Taken together, these data clearly indicate that the brain distribution of trametinib is limited by active efflux in an intact BBB model, primarily mediated by P-gp.

The duration of response of single agent BRAF inhibitors is limited by the eventual development of resistance. An understanding of the underlying mechanism of resistance in patients will enable the development of rational combinations. Blocking multiple signaling mechanisms has been shown to overcome resistance to BRAF inhibitors (Villanueva et al., 2010). However, for treatment of brain metastases, combination agents have to be delivered to all metastases in the brain. With the clinical development of a combination of dabrafenib and trametinib, and the fact that both these agents are individually substrates for active efflux, we were interested in understanding the factors that affect the brain distribution of the combination in vivo. When dabrafenib and trametinib were dosed to steady state, we observed a remarkable (> 10 fold) increase in the brain to plasma concentration ratios in the *Mdr1a/b*$^{-/-}$*Bcrp*$^{-/-}$ as

compared to wild-type. These data indicate that the brain distribution of both drugs in the combination is restricted by active efflux at the BBB.

The development of BRAF inhibitors has truly been a breakthrough for the treatment of metastatic melanoma. The addition of combination agents to BRAF inhibitor therapy is a rational method for overcoming resistance. However, given the deadly nature of brain metastases, there is a critical need to address CNS delivery issues of these combinations to achieve a durable response. With the limited delivery of combination agents to the brain, the brain may become a sanctuary site with greater resistance. These findings are clinically relevant as a means to choose rational combinations to ensure the effective treatment of brain metastases.

Figures

Figure 4.1: Chemical structure of trametinib

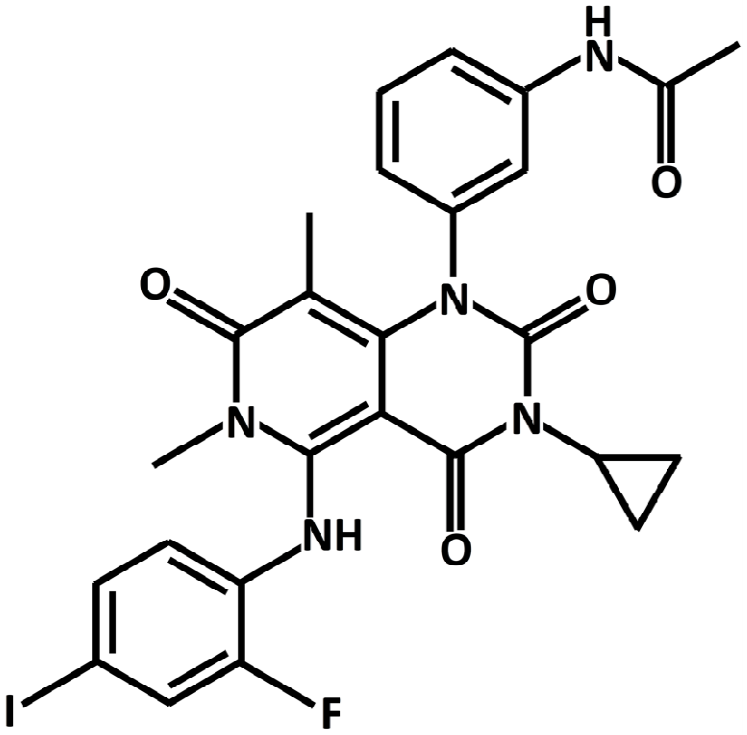

Figure 4.2: In vitro cellular accumulation of trametinib.

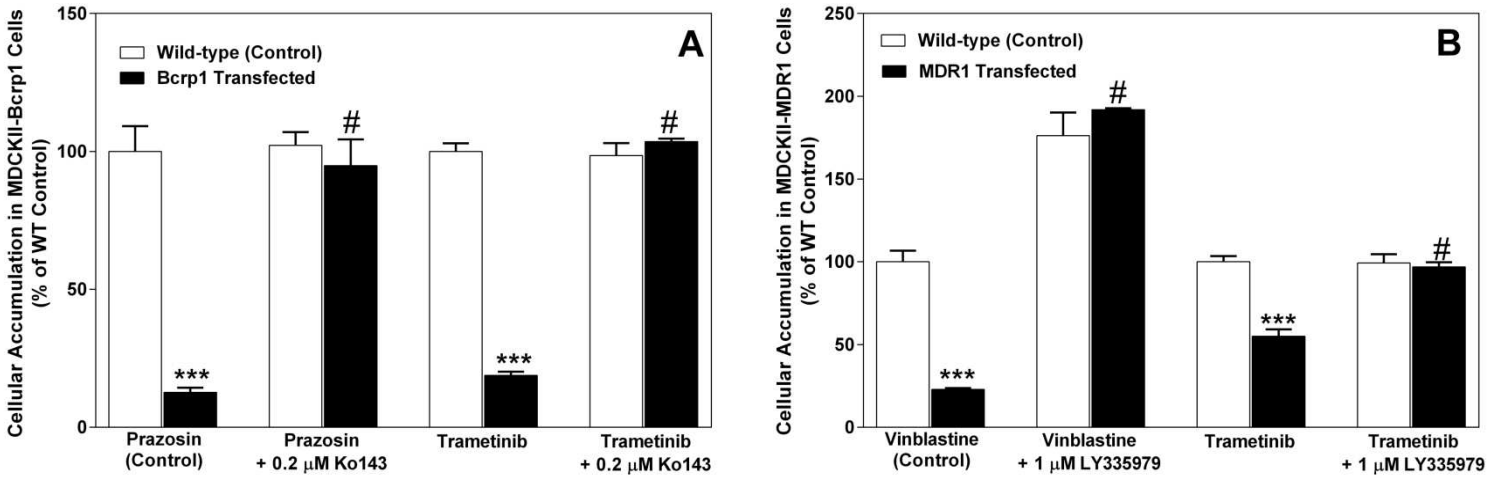

(A) The accumulation of prazosin (prototypical Bcrp probe substrate; positive control) and trametinib in MDCKII-wild-type and Bcrp1-transfected cells with and without specific Bcrp inhibitor Ko-143 (0.2 μM). The accumulation of trametinib and vinblastine (probe substrate for P-gp) in MDR1 cells with and without specific P-gp inhibitor LY335979 (1 μM) is shown in (B). Data represent the mean ± SD.; n=3 for all data points. ***$p < 0.0001$ compared with respective wild-type controls; #$p < 0.001$ compared with the untreated transfected cell line.

Figure 4.3: Competition assays using prototypical probe substrate molecules.

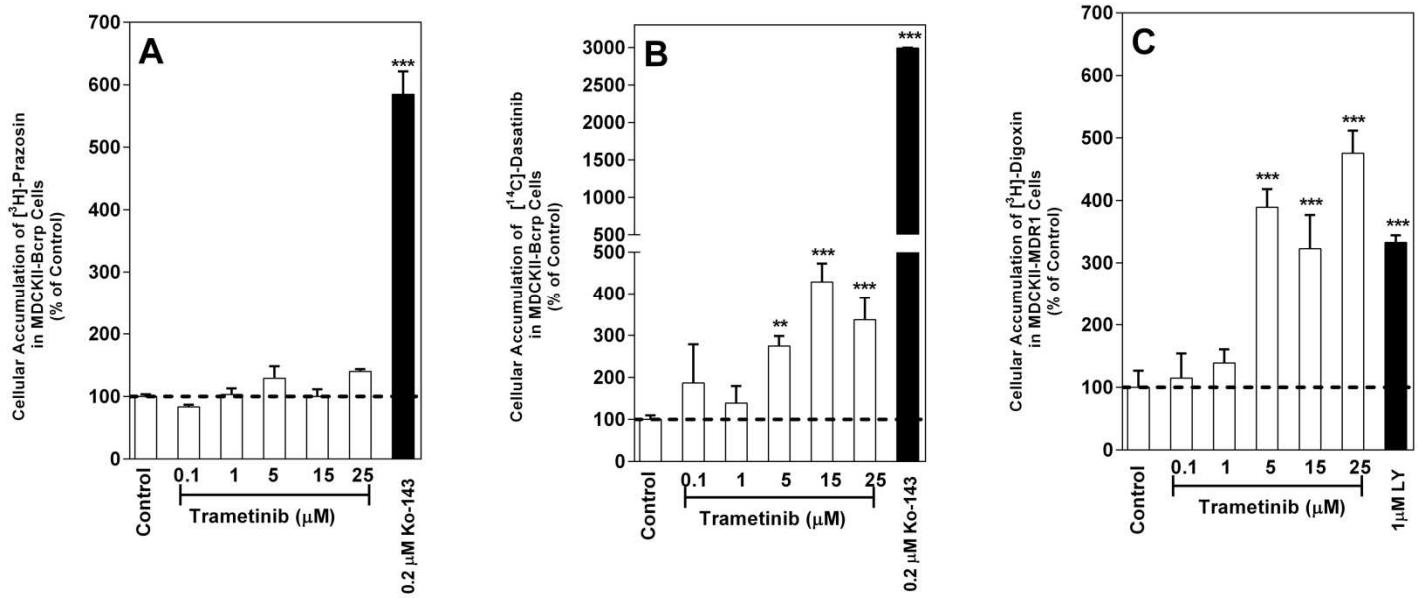

Intracellular accumulation of [^{3}H]-prazosin (Bcrp probe substrate) (A) and [^{14}C]-dasatinib (dual substrate) (B) in Bcrp-1 transfected cells, and [^{3}H]-digoxin (P-gp probe substrate) (C) in MDR1 transfected cells with increasing concentrations of trametinib from 0.1 μM to 25 μM. Ko143: Bcrp inhibitor; LY335979: P-gp inhibitor. Data represent the mean ± SD.; n=3 for all data points. ***$p < 0.0001$, **$p = 0.003$ compared with untreated transfected cells.

Figure 4.4: Intracellular accumulation of dabrafenib in the presence of increasing concentrations of trametinib.

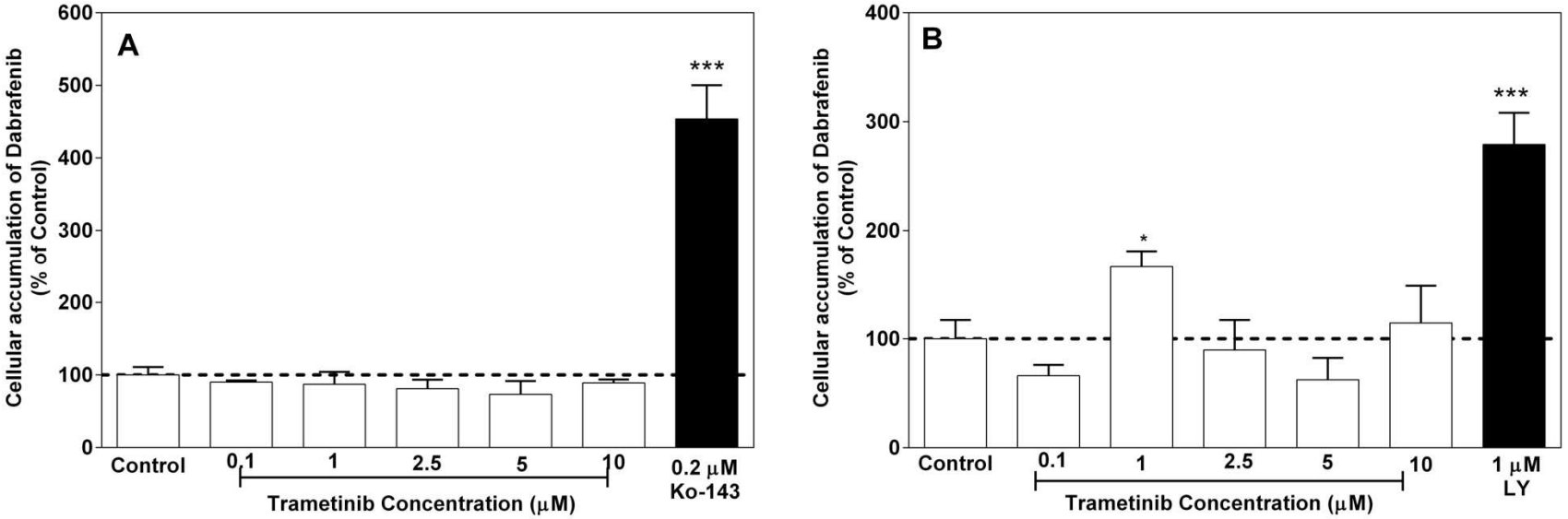

(A) Intracellular accumulation of dabrafenib in Bcrp1 transfected cells in the presence of increasing concentrations of trametinib (0.1-10 μM). The accumulation of dabrafenib in MDR1 cells with increasing concentrations of trametinib from 0.1 μM to 10 μM is shown in (B). Ko-143: Bcrp inhibitor Ko143; LY: P-gp inhibitor LY335979. Data represent the mean ± SD.; n=3 for all data points. ***$p < 0.0001$, *$p = 0.0031$ compared with untreated transfected cells.

Figure 4.5: Brain distribution of trametinib in FVB wild-type, *Bcrp1*$^{-/-}$, *Mdr1a/b*$^{-/-}$ and *Mdr1a/b*$^{-/-}$*Bcrp1*$^{-/-}$ mice.

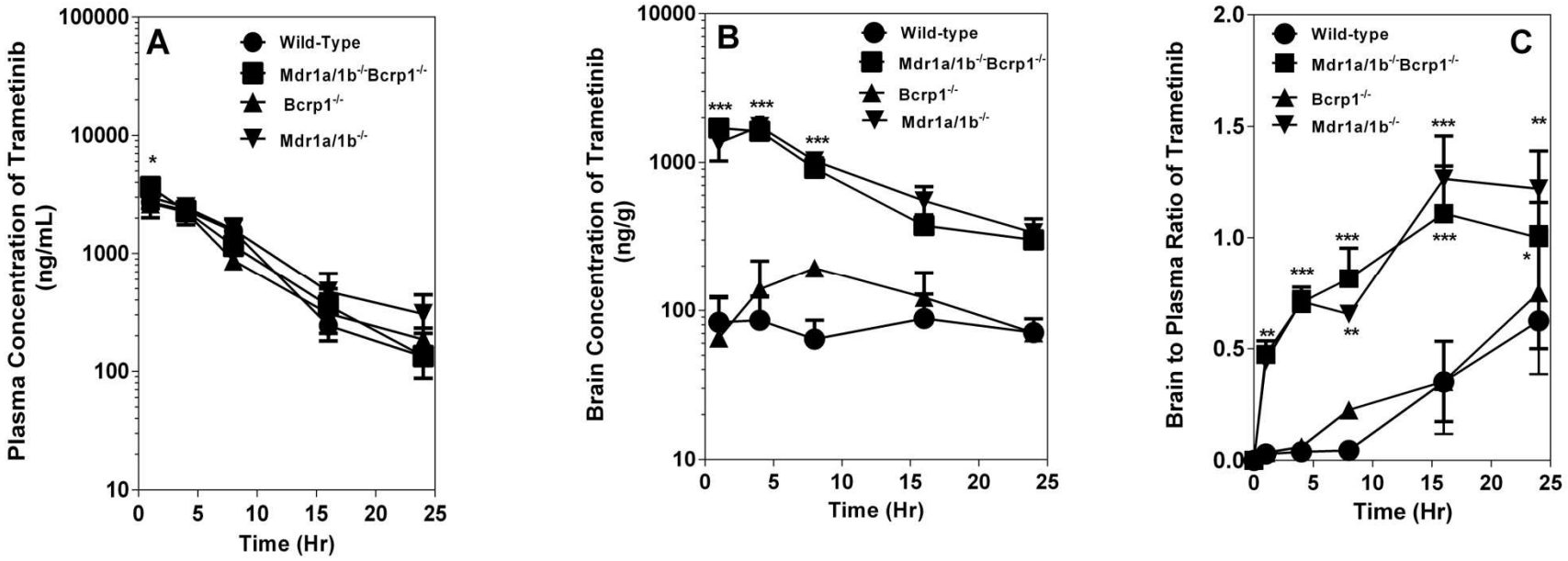

Plasma (A), brain (B), and brain to plasma concentration ratios (C) of trametinib in wild- type, *Bcrp1*$^{-/-}$, *Mdr1a/b*$^{-/-}$ and *Mdr1a/b*$^{-/-}$*Bcrp1*$^{-/-}$ mice after an i.v. dose of 5 mg/kg. Plasma and brain concentrations of trametinib at 1, 4, 8, 16, and 24 hours post dose were determined using LC-MS/MS. Data represent mean ± SD, n = 3-4. *p<0.05, **p<0.001, ***p<0.0001 compared to wild-type.

Figure 4.6: Steady State distribution of trametinib at 2 μg/hr for 48hr.

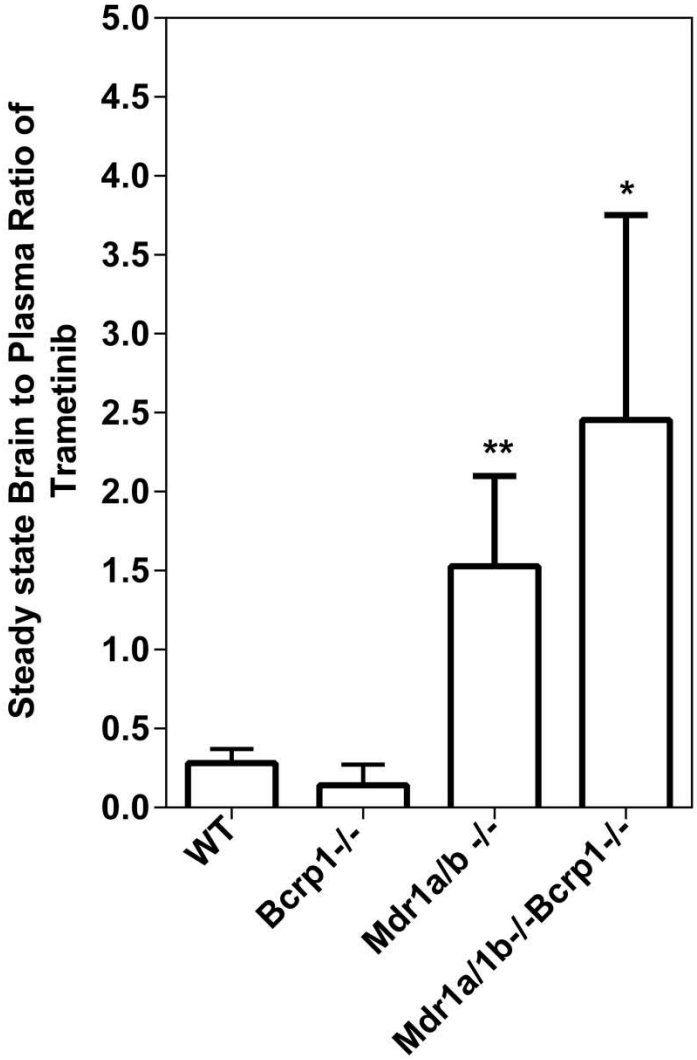

Steady state brain to plasma ratio of trametinib in wild-type, *Bcrp1*$^{-/-}$, *Mdr1a/b*$^{-/-}$, and *Mdr1a/b*$^{-/-}$*Bcrp1*$^{-/-}$ mice. Trametinib was delivered at a constant infusion rate of 2 μg/hr for 48 hrs using Alzet osmotic pumps. Data represent mean ± SD, n = 4-7. **p = 0.004, *p = 0.01 compared to wild-type.

Figure 4.7: Steady State distribution of dabrafenib and trametinib after simultaneous infusion for 48 hours.

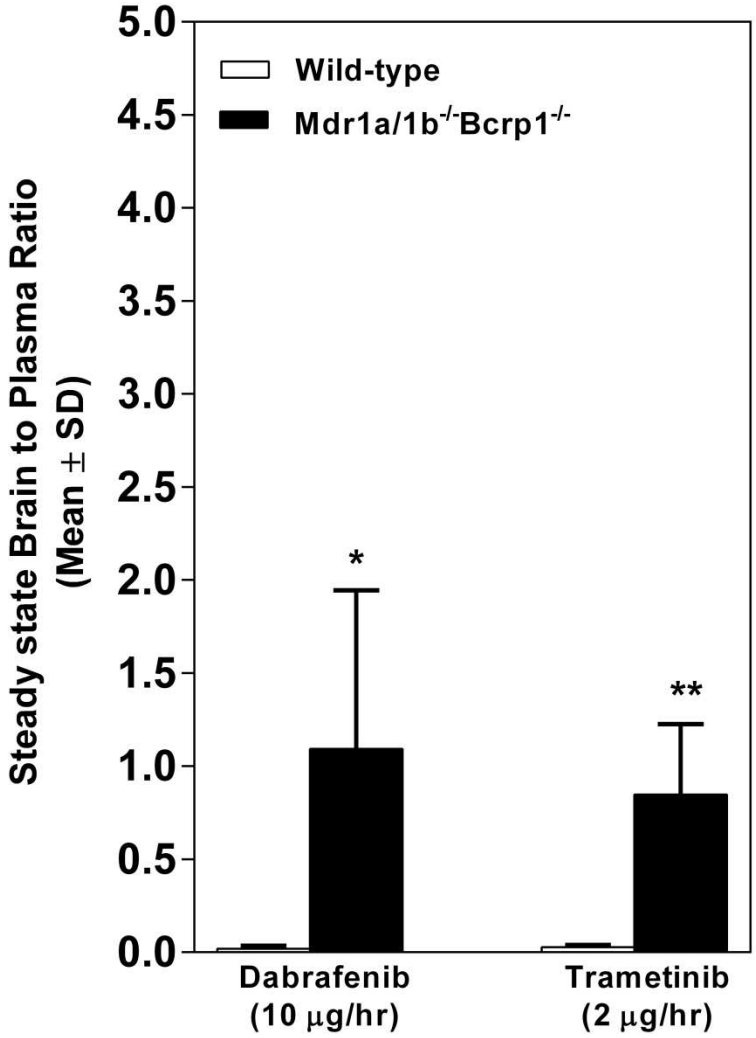

Steady state brain to plasma ratios of dabrafenib and trametinib in wild-type and *Mdr1a/b*$^{-/-}$*Bcrp1*$^{-/-}$ mice. Dabrafenib and trametinib were simultaneously delivered at a constant rate of 10μg/hr and 2μg/hr respectively for 48 hrs using Alzet osmotic pumps. Data represent mean ± SD, n = 4-9. **p = 0.002 compared to dabrafenib B/P ratio in wild-type, *p = 0.05 compared to trametinib B/P ratio in wild-type

Table 4.1: Bidirectional flux of Trametinib in MDCKII-WT, MDCKII-Bcrp1, and MDCKII-WT and MDCKII-MDR1 transfected cells.

Cell line (MDCKII)	Papp (*10^-6 cm/sec)		Efflux Ratio	Corrected Flux Ratio
	A-to-B	B-to-A		
WT (Bcrp)	12.8 ± 2.5	12.3 ± 4.7	0.96	
WT (Bcrp) +0.2 μM Ko-143	12.5 ± 0.9	12.6 ± 1.0	1	
Inulin♦	0.93 ± 0.38	0.37 ± 0.26	0.4	
Bcrp	5.17 ± 2.1 [a]	19.3 ± 1.9 [a]	3.7	**3.85**
Bcrp + 0.2 μM Ko-143	11.7 ± 2.6	12.2 ± 1.6	1.04	
Inulin♦	0.9 ± 0.32	0.93 ± 0.21	1.03	
WT (MDR1)	17.8 ± 1.8	18.6 ± 4.3	1.04	
WT (MDR1) + 1 μM LY335979	8.6 ± 4.9	11.3 ± 1.2	1.3	
Inulin♦	0.12 ± 0.12	0.24 ± 0.14	2	
MDR1	13.8 ± 8 [a]	35.2 ± 1.7 [a]	2.55	**2.45**
MDR1 + 1 μM LY335979	9.3 ± 1.7	11.4 ± 2.9	1.23	
Inulin♦	0.5 ± 0.26	0.62 ± 0.19	1.24	

Papp: Apparent Permeability of trametinib; A, apical; B, basolateral; ER, efflux ratio; MDCKII, Madin-Darby canine kidney II; Papp, apparent permeability of trametinib; WT, wild type. [a] Represent significantly different compared with respective wild-type controls, ♦ Percent transported at 120 minutes was less than 1%.

Table 4.2: Trametinib PK parameters in FVBn wild-type (WT), *Mdr1a/b*$^{-/-}$ (P-gp knockout), *Bcrp1*$^{-/-}$ (Bcrp knockout) and *Mdr1a/b*$^{-/-}$ *Bcrp1*$^{-/-}$ (Triple knockout) after 5 mg/kg i.v. dose (AUC, area under the concentration-time curve; FVB, Friend leukemia virus strain B).

Trametinib i.v. 5 mg/kg								
	Wild Type		Bcrp1-/-		Mdr1a/b-/-		Mdr1a/b-/-Bcrp1-/-	
PK Parameters	Plasma	Brain	Plasma	Brain	Plasma	Brain	Plasma	Brain
Terminal rate constant (hr^{-1})	0.15		0.12		0.11		0.15	
Half life (hr)	4.7		5.6		6.3		4.8	
Clearance (mL/hr)	5.1		6.1		4.7		5.2	
Volume (mL)	37.3		49.6		42.9		36.1	
AUC (0-tlast) µg-hr/mL	26.8 ± 2.8	4.0 ± 0.43	23.0 ± 0.11	3.1 ± 0.30	29.2 ± 1.7	21.4 ± 0.93	27.8 ± 1.6	18.8 ± 0.87
Kp (AUC Brain/ AUC Plasma)	0.15		0.14		0.73		0.68	
Kp ratio (Kp Knock out/Kp wild-type)			**0.92**		**4.9**		**4.6**	

CHAPTER 5: FACTORS INFLUENCING THE CNS DISTRIBUTION OF A NOVEL PI3K/MTOR INHIBITOR GSK2126458: IMPLICATIONS FOR OVERCOMING RESISTANCE TO COMBINATION THERAPY FOR MELANOMA BRAIN METASTASES

Melanoma brain metastases are a major cause of mortality in patients with metastatic melanoma. The presence of brain metastases in a large percentage of patient autopsies suggests a unmet medical need. More recently, a better understanding of the key molecular drivers of melanoma and progression of the disease led to the development of drugs that inhibit specific signaling proteins in the mitogen-activated protein kinase (MAPK) pathway. The significant improvement in overall survival led FDA-approval of BRAF-inhibitors, vemurafenib and dabrafenib, and MEK 1/2 inhibitor, trametinib. However, the emergence of brain metastases and acquired resistance are a huge problem. The combination of dabrafenib and trametinib was FDA-approved after the two-drug combination showed a significant increase in progression-free survival as compared to the single agent arms. Unfortunately, patients acquire resistance to this combination. A promising approach to overcome resistance to acquired resistance to mutations in the MAPK signaling pathway is by simultaneously targeting the phosphoinositide 3-kinase (PI3K/mTOR) signaling pathway, which is deregulated in metastatic melanoma. *In vitro*, GSK2126458, a potent small molecule inhibitor of the PI3 kinase family and mTOR kinase has shown to overcome acquired resistance to dabrafenib and trametinib. In previous studies, we found that vemurafenib, dabrafenib, and trametinib are limited in brain distribution. The purpose of this study was to investigate factors that influence

the brain distribution of GSK2126458, alone and in combination with dabrafenib and trametinib. In vitro studies indicate that GSK212658 is a substrate for both P-gp and Bcrp. The brain distribution of GSK2126458 was significantly greater in the *Mdr1a/b*$^{-/-}$*Bcrp1*$^{-/-}$ (triple knockout) mice as compared to wild-type. At steady-state, the B/P ratio of GSK2126458 was approximately seven-fold higher in triple knockout mice as compared to wild-type. Also, on simultaneous infusion to steady state, we observed that all three drugs, GSK212658, dabrafenib and trametinib were limited in brain distribution due to active efflux by P-gp and Bcrp. Together, these in vivo studies in transgenic mouse models confirmed that active efflux by both P-gp and Bcrp play a significant role in restricting the brain distribution of GSK212658. These results have important implication to the use of GSK212658 as a single agent or in combination with other molecularly-targeted agents for the treatment of melanoma brain metastases.

5. 1 Introduction

Melanoma is a highly aggressive skin cancer with a great propensity for brain metastasis. Currently, melanoma brain metastases are a untreatable and lethal condition in most patients with advanced stages of melanoma. The incidence of melanoma has been steadily escalating over the years and approximately 76000 new cases and ~ 10000 deaths are expected due to this disease in 2014 (Siegel et al., 2014). In early stages of the disease, localized melanoma is curable with a 5-year survival of greater than 90% while disseminated disease (metastatic

melanoma) has an extremely poor prognosis with a 5-year survival of less than 15% (Balch et al., 2009). After lung and breast cancer, melanoma is the third most common cancer to metastasize to the brain (Johnson and Young, 1996).

Patients with one to three brain metastases are often treated with surgical resection or stereotactic radiosurgery, while those with several brain metastases typically receive whole brain radiation (Gibney et al., 2012). Unfortunately, melanomas are highly resistant to radiation and chemotherapy, and patients with brain metastases have a dismal survival of the order of 4 months from first detection despite aggressive therapy (Sampson et al., 1998; Fife et al., 2004). Melanoma brain metastases are the cause of death in nearly 95 % of patients (Sampson et al., 1998).

Patients with multiple brain metastases and extensive peripheral disease can have particularly poor survival, which can be as short as 1-2 months (Gupta et al., 1997; Fife et al., 2004). Incidentally, 50 to 70% of melanoma patients have brain metastases at autopsy (Fife et al., 2004). The presence of brain metastases in such a large proportion of melanoma patients at autopsy is suggestive of a unmet medical need.

There has been significant advancement over the last decade in the treatment of peripheral melanoma metastases based on the discovery and understanding of hallmark molecular events and oncogenic driver mutations that cause disease progression. In melanoma, oncogenic driver mutations in BRAF (v-raf murine

sarcoma viral oncogene homolog) and NRAS (neuroblastoma ras viral oncogene homolog) in the MAPK (mitogen-activated protein kinase) signaling pathway, p53 mutations, and PTEN (phosphatase and tensin homolog) mutations have been identified to play an important role in the progression of the disease (Hodis et al., 2012). The MAPK signaling pathway is known to be highly deregulated in about 80% of melanomas as well as in a wide range of other human cancers (Davies et al., 2002). The discovery of activating mutations in the MAPK pathway, particularly the high prevalence of the valine to glutamic acid substitution mutation at amino acid 600 (V600E; BRAF V600E) in the BRAF protein, led to the development and FDA approval of two BRAF inhibitors, vemurafenib and dabrafenib. This mutation increases BRAF protein catalytic activity by approximately 50-200 fold as compared to wild-type resulting in constitutive activation of the MEK and ERK downstream proteins (Davies et al., 2002; Karasarides et al., 2004; Wan et al., 2004). These two drugs were approved after they showed a remarkable initial efficacy against peripheral tumors (Chapman et al., 2011; Bollag et al., 2012; Falchook et al., 2012). Similarly, trametinib, a mitogen-activated protein kinase kinase (MEK) inhibitor was approved after it showed a 4.8-month progression-free-survival (PFS) compared with 1.5 months in the chemotherapy group in phase 3 clinical trials in patients with BRAF V600E mutation (Flaherty et al., 2012b). However, the emergence of resistance to

MAPK pathway inhibitors is a huge problem and needs to be addressed immediately.

Much of the current clinical data suggests that patients on BRAF inhibitors slowly stop responding to therapy due to the eventual development of resistance and relapse of disease (Puzanov et al., 2011). Several mechanisms may be responsible for this resistance. Mutations in upstream signaling proteins such as RAS or compensatory signaling from other growth factor receptors such as PI3K/mTOR (phosphoinositide 3-kinase/ mammalian target of rapamycin), loss of PTEN, upregulation of cyclinD1 and downregulation of $p27^{Kip1}$ may be driving the reactivation of the MAPK signaling pathway and strengthening the resistance to BRAF inhibitor therapy (Johannessen et al., 2010; Aplin et al., 2011; Gowrishankar et al., 2012). Combination therapy with multiple molecularly-targeted agents is a promising approach that has been pursued to overcome resistance and prolong survival. In this context, the combination of dabrafenib and trametinib was FDA approved after the two drug combination showed a 9.8-month PFS as compared to 5.8 months in the dabrafenib monotherapy arm (Flaherty et al., 2012a). Unfortunately, resistance to BRAF and MEK inhibition occurs eventually via acquired MEK mutations (Wagle et al., 2014). A combination of BRAF or MEK inhibitors with PI3K/mTOR inhibitors is known to overcome acquired resistance *in vitro* (Greger et al., 2012). GSK2126458, a potent ATP competitive inhibitor of the PI3 kinase family and the mTOR kinase is

a promising candidate for combinations (Knight et al., 2010). GSK2126458 was found to be highly specific, orally available and showed a low picomolar inhibitory activity against PI3 kinases and mTOR (Knight et al., 2010).

The efficacy of molecularly-targeted agents and combinations for the successful treatment of melanoma brain metastases requires the sufficient delivery of all agents in the combination across the blood-brain-barrier (BBB) to all target sites in the brain, including those residing behind an intact BBB and are almost always clinically undetectable. The BBB is composed of a monolayer of endothelial cells connected by tight junction proteins and expressing multiple efflux transporter proteins including P-glycoprotein (P-gp) and breast cancer resistance protein (BCRP) that are known to exclude several anticancer drugs from the brain (Ohtsuki and Terasaki, 2007; Agarwal et al., 2011). We have previously demonstrated that vemurafenib, dabrafenib and trametinib are restricted in brain distribution owing to active efflux by P-gp and Bcrp in an intact BBB model (Mittapalli et al., 2012; Mittapalli et al., 2013; Vaidhyanathan et al., 2014). Since GSK2126458 is a promising drug for combination therapy, the purpose of this study was to examine its potential for use in the treatment of melanoma brain metastases. We have evaluated some of the critical factors influencing its brain distribution as a single agent and in combination with dabrafenib and trametinib, with the goal that information from this work will guide the development of effective combinations for melanoma brain metastases.

5. 2 Materials and Methods

5. 2. 1 Chemicals

GSK2126458 [2,4-difluoro-N-(2-methoxy-5-(4-(pyridazin-4-yl)quinolin-6-yl)pyridin-3-yl) benzenesulfonamide], Trametinib [N-[3-[3-cyclopropyl-5-(2-fluoro-4-iodoanilino)-6,8-dimethyl-2,4,7-trioxopyrido[4,3-d]pyrimidin-1-yl]phenyl]acetamide] and dabrafenib (GSK2118436A, N-[3-[5-(2-aminopyrimidin-4-yl)-2-tert-butyl-1,3-thiazol-4-yl]-2-fluorophenyl]-2,6-difluorobenzenesulfonamide) were purchased from Chemietek (Indianapolis, IN). [^{3}H]-Prazosin was purchased from Perkin Elmer Life and Analytical Sciences (Waltham, MA). [^{3}H]-Vinblastine was purchased from Moravek Biochemicals (La Brea, CA). Ko143 [(3S,6S,12aS)-1,2,3,4,6,7,12,12aoctahydro-9-methoxy-6-(2-methylpropyl)-1,4-dioxopyrazino(1',2':1,6) pyrido(3,4-b)indole-3-propanoic acid 1,1-dimethylethyl ester] was purchased from Tocris Bioscience (Ellisville, MO) and zosuquidar [LY335979, (*R*)-4-((1*aR*, 6*R*,10*bS*)-1,2-difluoro-1,1*a*,6,10*b*-tetrahydrodibenzo-(*a*,*e*) cyclopropa (*c*)cycloheptan-6-yl)-((5-quinoloyloxy) methyl)-1-piperazine ethanol, trihydrochloride] was kindly provided Eli Lilly and Co.(Indianapolis, IN). Cell culture reagents were purchased from Invitrogen (Carlsbad, CA). All other chemicals used were of high performance liquid chromatography or reagent grade and were obtained from Sigma-Aldrich (St. Louis, MO).

5. 2. 2 In vitro studies

In vitro studies were performed using polarized Madin-Darby canine kidney-II (MDCK-II) cells. MDCKII-WT and Bcrp1-transfected (MDCKII-Bcrp1) cell lines were gifts from Dr. Alfred Schinkel (The Netherlands Cancer Institute). MDCKII-wild type (WT) and MDR1-transfected (MDCKII-MDR1) cell lines were kindly provided by Dr. Piet Borst (The Netherlands Cancer Institute). Cells were cultured in Dulbecco's modified Eagle's medium supplemented with 10% (v/v) fetal bovine serum and antibiotics (penicillin, 100 U/mL; streptomycin, 100 µg/mL; and amphotericin B, 250 ng/mL). Cells were grown in 25 mL tissue culture treated flasks before seeding for the experiments and were maintained at 37º C in a humidified incubator with 5% CO_2. The growth media for MDCKII-MDR1 additionally contained 80 ng/ml of colchicine to maintain positive selection pressure of P-gp expression.

5. 2. 2. 1 In vitro accumulation studies

The intracellular accumulation of GSK2126458 was performed in 12-well polystyrene plates (Corning Inc. Corning, NY). Briefly, cells were seeded at a density of 2 x 10^5 cells per well and were grown until the cells were ~80% confluent. On the day of experiment the culture media was aspirated and the cells were washed two times with cell assay buffer (122 mM NaCl, 25 mM $NaHCO_3$, 10 mM glucose, 10 mM HEPES, 3 mM KCl, 2.5 mM $MgSO_4$, 1.8 mM $CaCl_2$, and 0.4 mM K_2HPO_4). Then the cells were preincubated with assay buffer

for 30 min, after which the buffer was aspirated and the experiment was initiated by adding 1 mL of GSK2126458 (2 μM) to each well and further incubated for 60 min. The assay plates were incubated at 37º C on an orbital shaker (60 rpm) for the entire duration of the experiment. When the inhibitor was present, it was included in both pre-incubation and accumulation steps. After the incubation period, the drug solution was aspirated and the cells were washed twice with ice cold PBS. Then the cells were lysed by adding 500 μL of 1% Triton X to each well. The solubilized cell fraction was sampled from each well and the concentration of GSK2126458 was determined using liquid chromatography-tandem mass spectrometry (LC-MS/MS) and normalized to protein content (BCA protein assay).

5. 2. 2. 2 Bcrp and P-gp inhibition studies

Inhibition assays were performed using radiolabeled prototypical probe substrates [^{3}H]-prazosin for Bcrp and [^{3}H]-vinblastine for P-gp. The intracellular accumulation of these probe substrates was evaluated in the presence of varying concentrations of GSK2126458 ranging from 0.1 to 50 μM. Briefly, the cells were pre-incubated with increasing concentrations of GSK2126458 for 30 min. After pre-incubation the cells were incubated with substrates along with increasing concentrations of GSK2126458 for 60 min. At the end of the incubation period, the buffer was aspirated and cells were lysed using 1% Triton-X. The radioactivity in solubilized cell fractions was determined by liquid scintillation

counting (LS-6500; Beckman Coulter, Fullerton, CA). The increase in cellular accumulation of substrate as compared to control (no treatment) was measured and reported as a function of GSK2126458 concentration.

5. 2. 3 In vivo Studies

5. 2. 3. 1 Animals

All of the in vivo studies were performed in Friend leukemia virus strain B (FVB) (wild type), *Mdr1a/b*$^{-/-}$ (P-gp knockout), *Bcrp1*$^{-/-}$ (Bcrp knockout), and *Mdr1a/b*$^{-/-}$ *Bcrp1*$^{-/-}$ (triple knockout) mice of either sex from an FVB genetic background (Taconic Farms, Germantown, NY). All animals were 8 to 12 weeks old at the time of experiment. Animals were maintained in a 12 hr light/dark cycle with unlimited access to food and water. All studies were carried out in accordance with the guidelines set by the *Principles of Laboratory Animal Care* (National Institutes of Health, Bethesda, MD) and approved by the Institutional Animal Care and Use Committee (IACUC) of the University of Minnesota.

5. 2. 3. 2 Brain distribution of GSK2126458 after an oral dose in FVB mice

Wild type and *Mdr1a/b*$^{-/-}$*Bcrp1*$^{-/-}$ mice received an oral dose of 10 mg/kg GSK2126458, blood and brain samples were collected after 0.5, 1, 2, 4, 6, and 8 hours post dose. The GSK2126458 p.o. dosing formulation was prepared in a vehicle containing 1% methocel, and 5% DMSO. All GSK2126458 dosing suspensions were freshly prepared on the day of the experiment. At the end of

the desired time point, the animals were euthanized using a CO_2 chamber. Blood was collected via cardiac puncture in heparinized tubes. Plasma was separated by centrifuging whole blood at 3500 rpm for 15 min at 4ºC. The whole brain was removed from the skull and washed with ice-cold PBS and superficial meninges were then removed by blotting with tissue paper. Both brain and plasma samples were stored at -80ºC until further analysis.

5. 2. 3. 3 Steady-state brain distribution of GSK2126458 and a combination of dabrafenib, trametinib, and GSK2126458

To determine the steady state brain and plasma concentrations of GSK2126458, Alzet osmotic mini pumps (Durect Corporation, Cupertino, CA) were loaded with GSK2126458 (2 mg/mL dissolved in DMSO) to be released for 48 hrs at a rate of 1µL/hr. After initial GSK2126458 loading, mini pumps were primed overnight in sterile saline at 37º C. Pumps were implanted in the peritoneal cavity of wild type, *Mdr1a/b*$^{-/-}$, *Bcrp1*$^{-/-}$, and *Mdr1a/b*$^{-/-}$*Bcrp1*$^{-/-}$ mice as described previously (Vaidhyanathan et al., 2014) . Briefly, mice were anesthetized using isofluorane and the abdominal cavity was shaved. A small midline incision was made in the lower abdominal wall under the rib cage. Then a small incision was made directly in the peritoneal membrane and the primed pump was inserted in the cavity. The incision was sutured and the skin was closed using surgical clips. The animals were allowed to recover on a heating pad and once recovered they were moved to their original cages. The animals were sacrificed 48 hrs after the implantation

of the pumps, and brain and plasma samples were processed as described above.

Similarly, in another study, Alzet mini-pumps were loaded with GSK2126458, trametinib and dabrafenib (1 mg/ml GSK2126458, 0.5 mg/mL trametinib and 2.5 mg/mL dabrafenib dissolved in DMSO) to be released for 48 hours at the rate of 1 μL/hr. Pumps were primed overnight and implanted in the peritoneal cavity of wild type, *Mdr1a/b*$^{-/-}$, *Bcrp1*$^{-/-}$, and *Mdr1a/b*$^{-/-}$*Bcrp1*$^{-/-}$ mice. These animals were also sacrificed 48 hrs after the implantation of the pumps, and brain and plasma samples were processed as described previously.

5. 2. 3. 4 Influence of elacridar on the brain distribution of GSK2126458

Elacridar microemulsion was made by preparing a 3 mg/mL solution of elacridar in Cremaphor EL, Carbitol and Captex 355 in a 6:3:1 ratio. This solution was diluted with saline prior to injection. Wild-type mice received vehicle or 10 mg/kg elacridar via an intraperitoneal injection. 1 hour after pretreatment, all mice received 10 mg/kg GSK2126458 orally and were sacrificed 1 hour after the oral dose. Plasma and brains were collected and processed as described earlier.

5. 2. 4 Analysis of GSK2126458, dabrafenib, and trametinib using LC-MS/MS

The concentration of GSK2126458, dabrafenib and trametinib in cell lysates, plasma and brain homogenate were determined using a sensitive and specific

liquid chromatography coupled with tandem mass spectrometry (LC-MS/MS) assay. For brains, three volumes of 5% bovine serum albumin were added and homogenized to get a uniform homogenate. For analysis of unknowns, an aliquot of cell lysate, brain homogenate or plasma was spiked with 10 ng PLX4720 and 10 ng AG1478 as internal standards. The samples were then extracted by addition of 10 volumes of ethyl acetate followed by vigorous shaking for 5 min and centrifuged at 7500 rpm for 5 min at 4ºC to separate the organic layer. The organic layer was transferred to microcentrifuge tubes and dried under a gentle stream of nitrogen. Samples were reconstituted in 100 µL of mobile phase and transferred into HPLC glass vials. Chromatographic analysis was performed using an AQUITY UPLC® system (Milford, MA, USA). The chromatographic separation was achieved using an Agilent Technologies Eclipse XDB-C18 column (4.6 x 50 mm) with 1.8 µm Zobrax Rx-SIL as the stationary phase. The aqueous component (A) of the mobile phase consisted of 20 mM ammonium formate with 0.1% formic acid and the organic mobile phase (B) was acetonitrile and was delivered at a flow rate of 0.25 mL/min. The gradient was as follows, 45% B for the first 3.0 minutes, increased to 70% B minutes in the next 0.5 minutes and maintained at 70% B for next 2.5 minutes, decreased to 45% B within the next 0.5 minutes and maintained at 45%B until 11.0 minutes. The total run time was 11 minutes with a flow rate of 0.25 mL/min. The cassette method involved detection of dabrafenib in the positive ionization mode, and the m/z

transitions were 520.1 →307.1 and 316.1 → 299.9 for dabrafenib and AG1478, respectively. The detection of GSK2126458 and trametinib were in the negative ionization mode with m/z transitions of 412.3 →304.8, 504.0 → 176.9, 613.9 → 530.8 for PLX4720, GSK2126458, trametinib, respectively. The retention times for dabrafenib, AG1478, PLX4720, GSK2126458, and trametinib were 7.26, 4.82, 6.11, 5.25, and 6.96 minutes, respectively.

5. 2. 5 Pharmacokinetic Calculations

Pharmacokinetic parameters and metrics from the concentration-time data in plasma and brain were obtained by non-compartmental analysis (NCA) performed using Phoenix WinNonlin 6.2 (Pharsight, Mountain View, CA). The area under the concentration-time profiles for plasma (AUC_{plasma}) and brain (AUC_{brain}) were calculated using the linear trapezoidal method. The sparse sampling module in WinNonlin was used to estimate the standard error around the mean of the AUCs.

5. 2. 6 Statistical Analysis

Data in all experiments represent mean ± SD unless otherwise indicated. Comparisons between two groups were made using an unpaired t-test. One way ANOVA, followed by Bonferonni's multiple comparisons test; Dunnet's test for comparing versus control was utilized to compare multiple groups. A significance

level of p <0.05 was used for all experiments. (GraphPad Prism 5.01 software, GraphPad, San Diego, CA, USA).

5. 3 Results

5. 3. 1 Intracellular accumulation of GSK2126458

The intracellular accumulation of GSK2126458 was studied in MDCKII WT and P-gp or Bcrp overexpressing cell lines. The cellular accumulation of [^{3}H]-prazosin and [^{3}H]-vinblastine was used as positive controls for Bcrp and P-gp mediated efflux transport, respectively. The accumulation of [^{3}H]-prazosin (**Fig. 5.2A**) was ~70% lower in Bcrp overexpressing cells (WT: 100 ± 3.96%; Bcrp: 29.87 ± 7.72%, p< 0.0001). Similarly, the accumulation of [^{3}H]-vinblastine (**Fig. 5.2B**) in P-gp overexpressing cells was ~41% lower compared to WT cells (WT: 100.0 ± 11.21%; MDR1: 38.63 ± 5.90%, p< 0.0001). GSK2126458 accumulation was approximately 84% lower in Bcrp overexpressing cells compared to WT cells (WT: 100 ± 13.41%; Bcrp: 15.65 ± 7.97%, p<0.0001). Addition of specific Bcrp inhibitor Ko143 significantly increased the accumulation of GSK2126458 in the Bcrp transfected cells (Bcrp: 15.65 ± 7.97%; Bcrp with Ko143: 65.32 ± 12.23%). Similarly, the accumulation of GSK2126458 was ~84% lower in P-gp overexpressing line compared to its WT control (WT: 100.0 ± 5.31%; MDR1: 16.25 ± 1.46%, p< 0.0001). When a specific P-gp inhibitor LY335979 was added (**Fig. 5.2B**), there was a significant increase in the accumulation of GSK2126458

in the MDR1 transfected cells (MDR1: 16.25 ± 1.46%; MDR1 with LY: 213.7 ± 12.05%). These cellular accumulation data indicate that GSK2126458 is a substrate for both P-gp and Bcrp *in vitro.*

5. 3. 2 Competition assays using prototypical probe substrates

The effect of increasing concentrations of GSK2126458 on probe substrate accumulation was assessed in Bcrp-transfected and MDR1-transfected MDCKII cells. Increasing concentrations of GSK2126458 did not significantly increase the accumulation of prazosin in the Bcrp1-transfected cells until a concentration of 25 μM (**Fig. 5.3A)**. We observed a ~ 3-fold and ~ 4-fold increase in prazosin accumulation at 25 μM and 50 μM GSK2126458. Similarly, increasing concentrations of GSK2126458 significantly increased (~ 3 fold at 10 μM GSK2126458) the accumulation of vinblastine in the MDR1 cells **(Fig. 5.3B).** The results of these competitive inhibition studies suggest that GSK2126458 possibly shares the same binding site on Bcrp as prazosin and on P-gp as vinblastine.

5. 3. 3 Plasma and brain pharmacokinetics of GSK2126458

The plasma and brain pharmacokinetics of GSK2126458 was studied in FVB wild-type and Mdr1a/b$^{-/-}$Bcrp1$^{-/-}$ mice after oral administration of 10 mg/kg. **Fig. 5.4** shows the plasma and brain concentrations of GSK2126458 in the two genotypes at 0.5,1,2,4,6, and 8 hours after a single oral dose. The plasma concentrations **(Fig. 5.4A)** were not significantly different between wild-type and

Mdr1a/b$^{-/-}$Bcrp1$^{-/-}$ mice. In the wild-type mice the plasma concentrations were approximately 2 log units higher than the corresponding brain concentrations, indicating the severely restricted brain distribution of GSK2126458. The brain concentrations of GSK2126458 were 3-to 30-fold higher in the Mdr1a/b$^{-/-}$Bcrp1$^{-/-}$ mice as compared to wild-type **(Fig. 5.4B).** These data show the significant role played by P-gp and Bcrp in restricting the brain distribution of GSK212648.

5. 3. 4 Steady-state brain distribution of GSK2126458

The steady state brain distribution of GSK2126458 was examined after a continuous intraperitoneal infusion using Alzet^{TM} osmotic pumps for 48 hrs at 2 µg/hr **(Fig. 5.5)**. The brain concentrations were ~ 5-fold higher in the Mdr1a/b$^{-/-}$ Bcrp1$^{-/-}$ mice as compared to wild-type **(Fig. 5.5A)**. The brain concentrations were not significantly different in the Mdr1a/b$^{-/-}$ and Bcrp1$^{-/-}$ as compared to wild-type and were significantly lower than their corresponding plasma concentrations **(Fig. 5.5A)**. As shown in **Fig. 5.5B**, the steady-state brains to plasma ratios were 0.07 ± 0.01, 0.06 ± 0.03, 0.02 ± 0.0.01, 0.47 ± 0.23 in the FVB wild type, Mdr1a/b$^{-/-}$, Bcrp1$^{-/-}$ and Mdr1a/b$^{-/-}$Bcrp1$^{-/-}$ mice, respectively. The B/P ratios at steady state were ~ 7 fold higher in the Mdr1a/b$^{-/-}$Bcrp1$^{-/-}$ mice when compared to wild-type mice. These data further confirm that the brain distribution of GSK2126458 is significantly impaired due to active efflux at the BBB.

5. 3. 5 Steady state brain distribution of GSK2126458, dabrafenib and trametinib in combination

We then examined the steady-state brain distribution of GSK2126458 (1 µg/hr) dabrafenib (2.5 µg/hr) and trametinib (0.5 µg/hr) when infused simultaneously to steady-state as a 48 hours constant intraperitoneal infusion for 48 hours in wild type, *Mdr1a/b*$^{-/-}$, *Bcrp1*$^{-/-}$and *Mdr1a/b*$^{-/-}$*Bcrp1*$^{-/-}$ mice. The steady-state brain-to-plasma concentration ratios of GSK2126458, dabrafenib and trametinib were significantly higher in the *Mdr1a/b*$^{-/-}$*Bcrp1*$^{-/-}$ mice as compared to wild-type **(Fig. 5.6)**. In addition, the steady-state brain-to-plasma concentration ratios of dabrafenib and trametinib were significantly higher in the *Mdr1a/b*$^{-/-}$ mice as compared to wild-type **(Fig. 5.6)**. The aggregate of these data suggests that all three drugs in the combination suffer from limited brain distribution due to active efflux at the BBB.

5. 3. 6 Influence of elacridar microemulsion on the brain distribution of GSK2126458

Next, we examined the influence of elacridar on the brain distribution of GSK2126458. Wild-type FVBs were pretreated with vehicle or elacridar (10 mg/kg) via an intraperitoneal injection one hour before an oral dose of GSK2126458 (10 mg/kg). The brain-to-plasma concentration ratio of GSK2126458 was ~ 6 fold higher in the elacridar pretreated group as compared

to the vehicle treated group **(Fig. 5.7)**. These results demonstrate that the administration of elacridar as a microemulsion formulation improves the brain distribution of GSK2126458 across the BBB.

5. 4 Discussion

Brain metastases from melanoma are a significant cause of mortality in patients with metastatic melanoma (Fife et al., 2004; Davies et al., 2011). The FDA-approval of BRAF inhibitors, vemurafenib and dabrafenib, MEK inhibitor, trametinib, and dabrafenib-trametinib combination has tremendously changed the treatment options for advanced melanoma. However, the remarkable initial efficacy of these drugs is eventually followed by relapse owing to the development of resistance to therapy (Nazarian et al., 2010a; Nazarian et al., 2010b; Gowrishankar et al., 2012). A combination of agents co-targeting multiple signaling pathways is the approach of choice for delaying/overcoming acquired resistance. It has been previously suggested that targeting MEK, which is downstream of BRAF in the MAPK signaling pathway or PI3K is a valid therapeutic approach to overcome resistance to chronic BRAF inhibition (Villanueva et al., 2010). In this context, the combination of dabrafenib and trametinib proves to be a step in the right direction. However, concomitant MEK mutations observed with the dabrafenib plus trametinib combination suggests that melanomas are capable of switching to alternate signaling pathways. Chronic BRAF inhibition has been known to enhance PI3K/AKT activity via IGF-

1R signaling (Villanueva et al., 2010). GSK2126458 in combination has shown to overcome acquired resistance to dabrafenib in vitro (Greger et al., 2012). The efficacy of a combination of agents in treating melanoma brain metastases will require that all agents in the combination be delivered to all metastatic sites, especially those that reside behind an intact BBB. These metastatic cells that are behind an intact BBB are protected by functional efflux transporters which exclude several anti-cancer drugs. We have previously shown that vemurafenib, dabrafenib, and trametinib are significantly limited in brain distribution due to their interaction with P-gp and BCRP (Mittapalli et al., 2012; Mittapalli et al., 2013; Vaidhyanathan et al., 2014) . We have also shown that the brain distribution of the dabrafenib-trametinib combination is significantly higher in the *Mdr1a/b*$^{-/-}$*Bcrp*$^{-/-}$ mice as compared to wild-type, suggesting that this combination suffers from limited brain distribution due to active efflux at the BBB (Vaidhyanathan et al., 2014) .

In the current study, using in vitro and in vivo models, we demonstrate that GSK2126458 is a substrate for BCRP and P-gp in vitro and in vivo. Also, we demonstrate that the combination of GSK2126458 with dabrafenib and trametinib suffers from active efflux at the BBB. This is the first report investigating the interaction of GSK2126458 with P-gp and BCRP.

The experiments performed in vitro in MDCKII cells that overexpress either murine Bcrp or human MDR1 confirm that GSK2126458 is a substrate for both

Bcrp and P-gp (Fig. 2). We observed a significantly lower accumulation of GK2126458 in P-gp- and Bcrp transfected cells as compared to wild-type (Fig. 2). In the presence of specific inhibitors of P-gp and Bcrp (LY335979 and Ko-143, respectively), this difference in intracellular accumulation was significantly decreased (Fig. 2).

In P-gp transfected cells, using a prototypical probe substrate, vinblastine for P-gp, we observed a significant increase in intracellular accumulation with increasing concentrations of GSK2126458 starting at 10 μM (Fig. 3B). In Bcrp transfected cells, we observed a significant increase in probe substrate prazosin starting at 25 μM (Fig. 3A). At 10 μM and 25 μM, GSK2126458 inhibits the active efflux of vinblastine by P-gp and prazosin by BCRP. It is likely that such high concentrations of GSK2126458 may not be pharmacologically relevant. These data suggest the possibility of GSK2126458 sharing similar binding sites as vinblastine and prazosin on P-gp and BCRP, respectively. All these in vitro results put together, conclusively show that GSK2126458 is a substrate for P-gp and Bcrp. These in vitro findings translate in vivo with changes in brain distribution in the triple knockout mice as compared to wild-type.

Based on our findings from in vitro studies, we went on to investigate the role of P-gp and BCRP in the brain distribution of GSK2126458. After an oral dose of GSK2126458, we observed that the brain concentrations were ~three-twenty-fold higher in *Mdr1a/b*$^{-/-}$*Bcrp*$^{-/-}$ mice as compared to wild-type (Fig. 4.). The plasma

concentrations were not significantly different between wild-type and *Mdr1a/b*$^{-/-}$ *Bcrp*$^{-/-}$.

At steady-state, the brain concentrations in wild-type, *Mdr1a/b*$^{-/-}$, and *Bcrp*$^{-/-}$ were significantly lower than in *Mdr1a/b*$^{-/-}$*Bcrp*$^{-/-}$. The steady-state B/P ratio increased from approximately 0.07 in the wild-types to 0.47 in the triple knockout mice (Fig. 5.). This ~ seven-fold increase in the targeted brain distribution of GSK2126458 further confirms the impact of P-gp and BCRP on the CNS penetration of GSK2126458. Importantly, we did not observe a significant change in the brain distribution of GSK2126458 in the Mdr1a*/b*$^{-/-}$, or *Bcrp*$^{-/-}$ mice as compared to wild-type. This suggests the cooperative role of these two transporters in excluding GSK2126458 from the CNS. Such compensation is well understood, whereby, in the absence of one transporter (single knockout); another transporter can limit substrate brain distribution, while in triple knockouts, there can potentially be a disproportionate enhancement in brain distribution of dual substrates (Kodaira et al., 2010).

When simultaneously infused with dabrafenib and trametinib, we observed a significantly higher B/P ratio for all three drugs in the *Mdr1a/b*$^{-/-}$*Bcrp*$^{-/-}$ as compared to wild-type (Fig. 6.). Also, the brain distribution of dabrafenib and trametinib were significantly higher in the *Mdr1a/b*$^{-/-}$ mice. In the case of trametinib, we had previously observed that its brain distribution was limited

primarily by P-gp (Vaidhyanathan et al., 2014). These data confirm that the brain distribution of all three drugs in combination is limited by active efflux.

Given the poor brain distribution of GSK2126458 and its potential use in combination therapy for the treatment of melanoma brain metastases, we investigated the influence of elacridar on its brain distribution. Pretreatment with elacridar in a microemulsion formulation led to a remarkable six-fold increase in the brain-to-plasma ratio of GSK2126458 in the elacridar pretreatment group as compared to vehicle treated mice (Fig. 7.). The result from this study suggests that the inhibition of P-gp and BCRP with elacridar could be a potential strategy for improving the brain distribution of GSK2126458. This finding is of clinical relevance and the enhancement in brain distribution is a likely strategy for enhancing the efficacy of combination therapies that suffer from active efflux.

With the duration of response of BRAF inhibitors being limited by the development of acquired resistance, delaying resistance for ensuring durable response requires the development of rational combinations. An understanding of the mechanisms of resistance led provided the rationale for combining GSK2126458 with either dabrafenib or trametinib (Greger et al., 2012). However, for success in the treatment of brain metastases, all agents in the combination have to be delivered across the BBB. From our experiments, we observe that all three drugs in the combination are restricted by active efflux at the BBB.

The addition of agents to combinations for success in treating brain metastases has to take into account the potential for active efflux at the BBB. If all drugs in the combination do not reach the brain, there is an increased potential for resistance, possibly making the brain a sanctuary site for further metastases. It is imperative that in addition to the understanding of resistance mechanisms, the potential for active efflux be considered prior to the further development of combination therapies. Our findings are clinically relevant for the choice of rational combinations to ensure effective treatment of melanoma brain metastases.

Figure 5.1: Chemical structure of GSK2126458

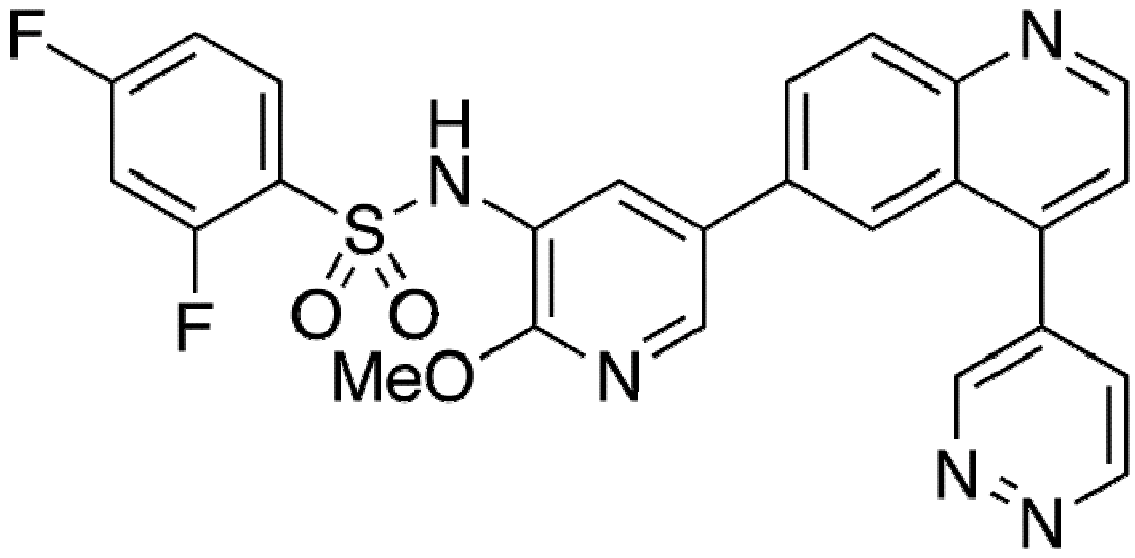

Figure 5.2: In vitro cellular accumulation of GSK2126458

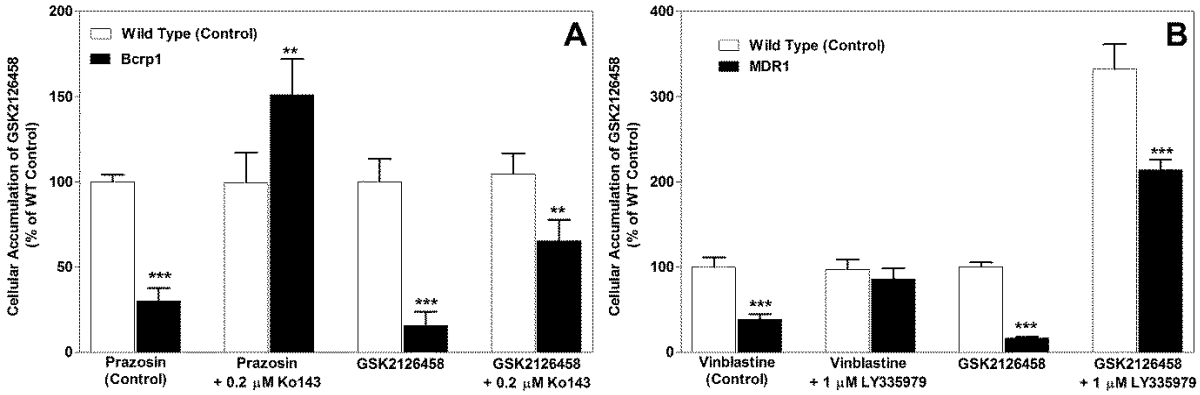

(A) The accumulation of prazosin (prototypical Bcrp probe substrate; positive control) and GSK2126458 in MDCKII-wild-type and Bcrp1-transfected cells with and without specific Bcrp inhibitor Ko-143 (0.2 μM). The accumulation of GSK2126458 and vinblastine (probe substrate for P-gp) in MDR1 cells with and without specific P-gp inhibitor LY335979 (1 μM) is shown in (B). Data represent the mean ± SD.; n=3-6 for all data points. ***$p < 0.0001$, and **$p < 0.05$ compared with respective wild-type controls.

Figure 5.3: Competition assays using prototypical probe substrate molecules

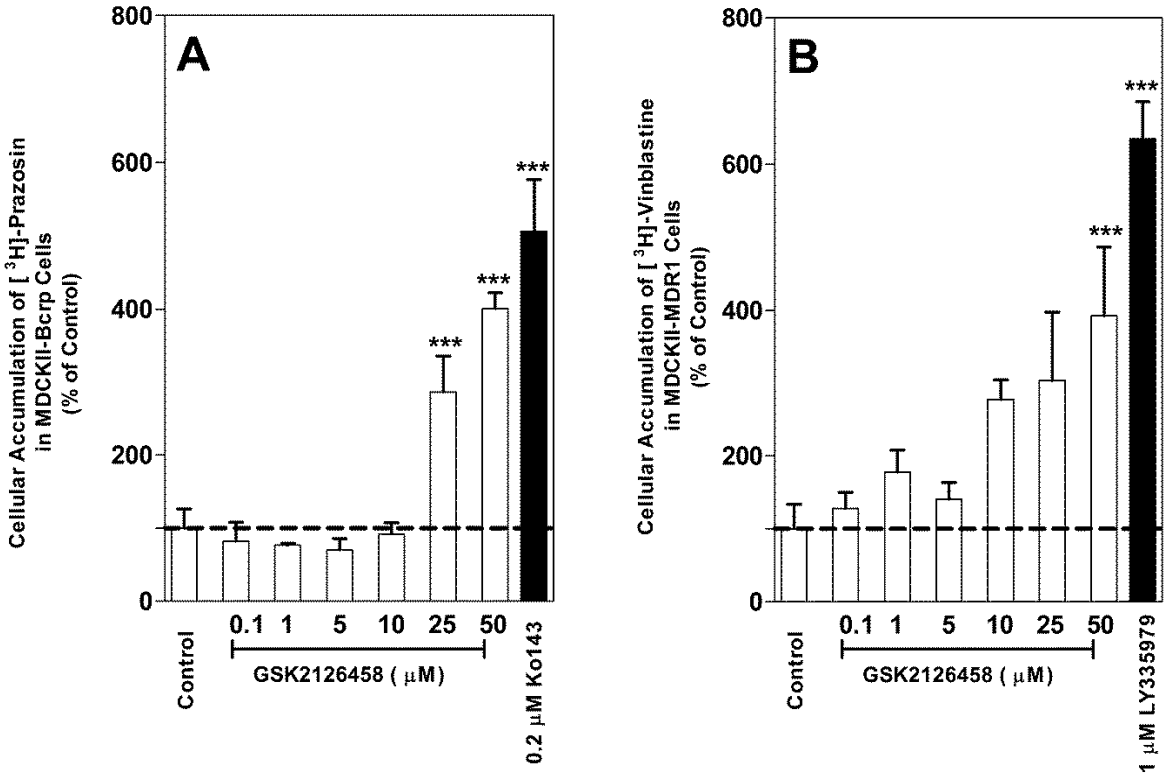

Intracellular accumulation of [^{3}H]-prazosin (Bcrp probe substrate) (A) and [^{3}H]-vinblastine (B) in MDR1 transfected cells with increasing concentrations of GSK2126458 from 0.1 μM to 50 μM. Ko143: Bcrp inhibitor; LY335979: P-gp inhibitor. Data represent the mean ± SD.; n=3 for all data points. ***p <0.0001 compared to respective untreated transfected cells.

Figure 5.4: Brain distribution of GSK2126458 in FVB wild-type, and *Mdr1a/b*$^{-/-}$*Bcrp1*$^{-/-}$ mice.

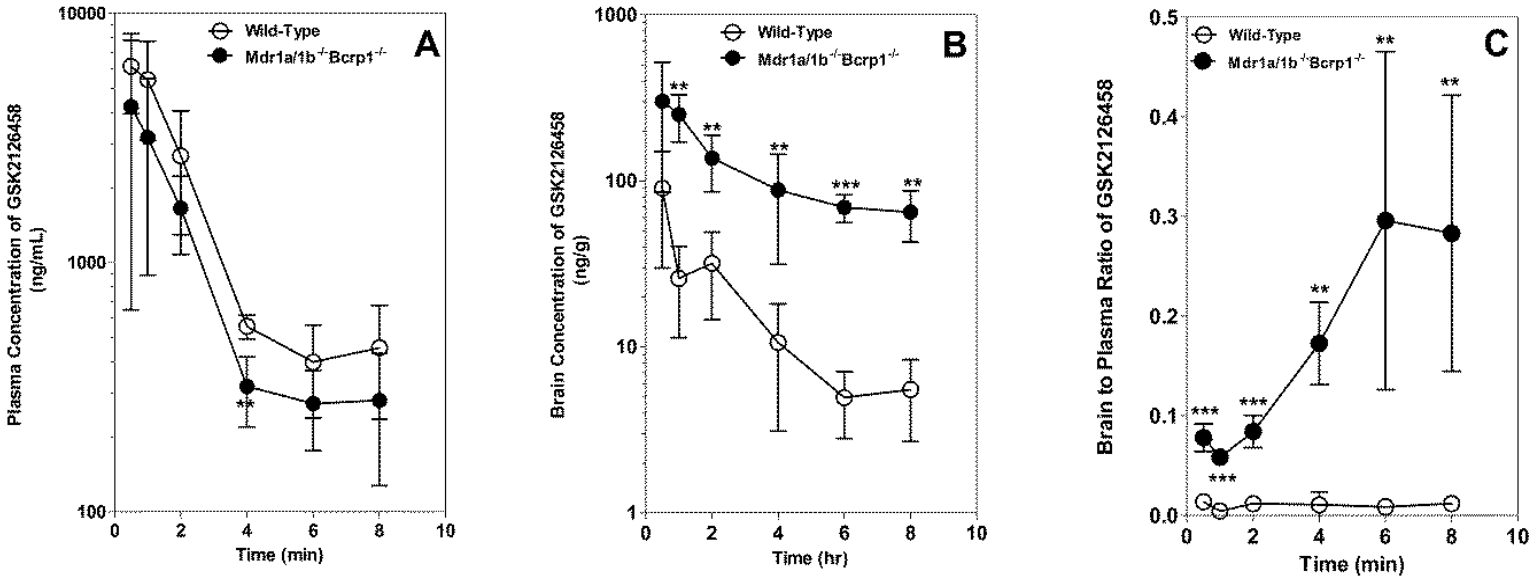

Plasma (A), brain (B), and brain-to-plasma concentration ratios (C) of GSK2126458 in wild- type, and *Mdr1a/b*$^{-/-}$ *Bcrp1*$^{-/-}$ mice after an oral dose of 10 mg/kg.

Plasma and brain concentrations of GSK2126458 at 0.5,1,2, 4, 6, and 8 hours post dose were determined using LC-MS/MS. Data represent mean ± SD, n = 3-4. **p<0.05, ***p≤0.0001 compared to wild-type.

Figure 5.5: Steady State distribution of GSK2126458 at 2 μg/hr for 48hr.

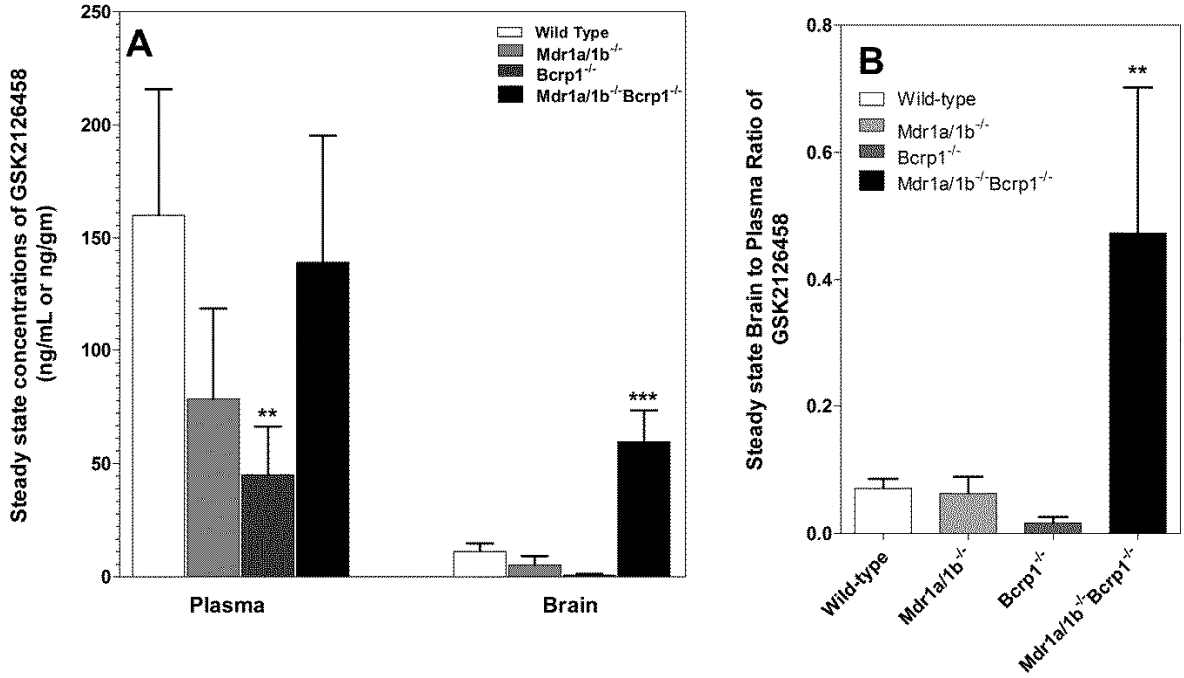

Steady state brain-to-plasma ratio of GSK2126458 in wild-type, *Bcrp1*$^{-/-}$, *Mdr1a/b*$^{-/-}$, and *Mdr1a/b*$^{-/-}$*Bcrp1*$^{-/-}$ mice. GSK2126458 was delivered at a constant infusion rate of 2 μg/hr for 48 hrs using Alzet osmotic pumps. Data represent mean ± SD, n = 3-5. **p < 0.05, ***p < 0.001 compared to wild-type.

Figure 5.6: Steady State distribution of GSK2126458, dabrafenib and trametinib after simultaneous infusion for 48 hours.

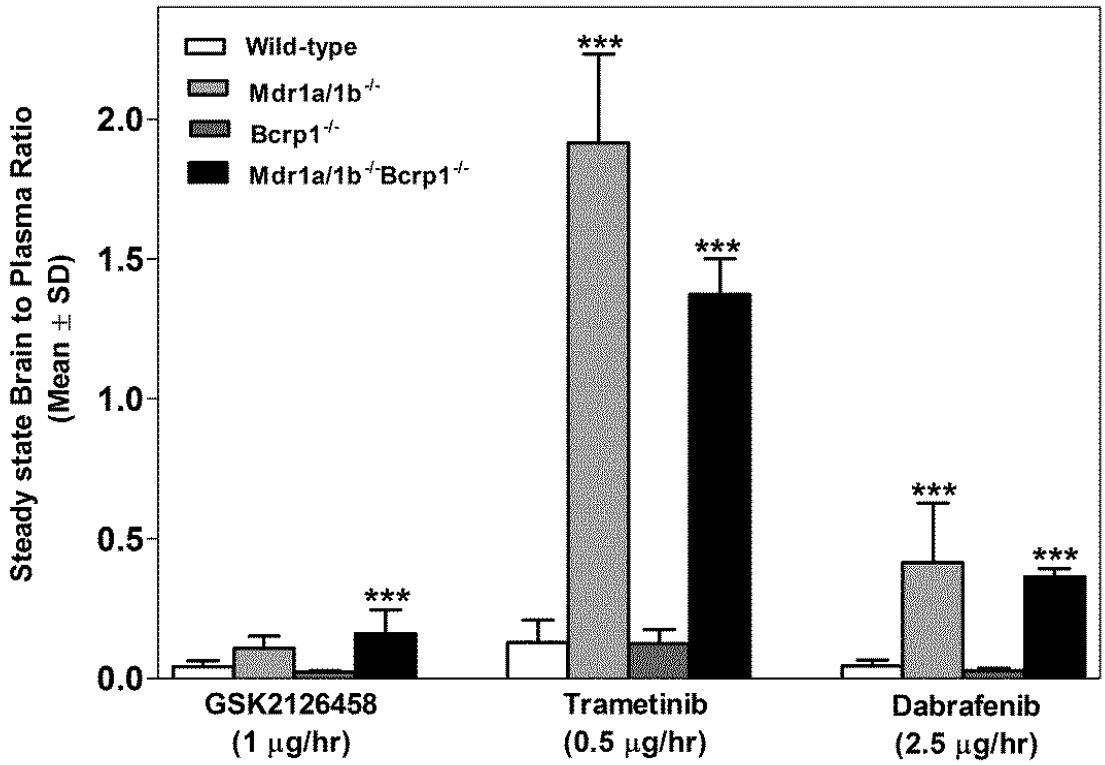

Steady state brain-to-plasma ratios of GSK2126458, dabrafenib and trametinib in wild-type, *Bcrp1*$^{-/-}$, *Mdr1a/b*$^{-/-}$, and *Mdr1a/b*$^{-/-}$*Bcrp1*$^{-/-}$ mice. GSK2126458, dabrafenib and trametinib were simultaneously delivered at a constant rate of 1 µg/hr, 2.5 µg/hr and 0.5 µg/hr respectively for 48 hrs using Alzet osmotic pumps. Data represent mean ± SD, n = 3-4. ***p< 0.05 compared to corresponding B/P ratio in wild-type.

Figure 5.7: Influence of elacridar in a microemulsion formulation on the brain distribution of GSK2126458.

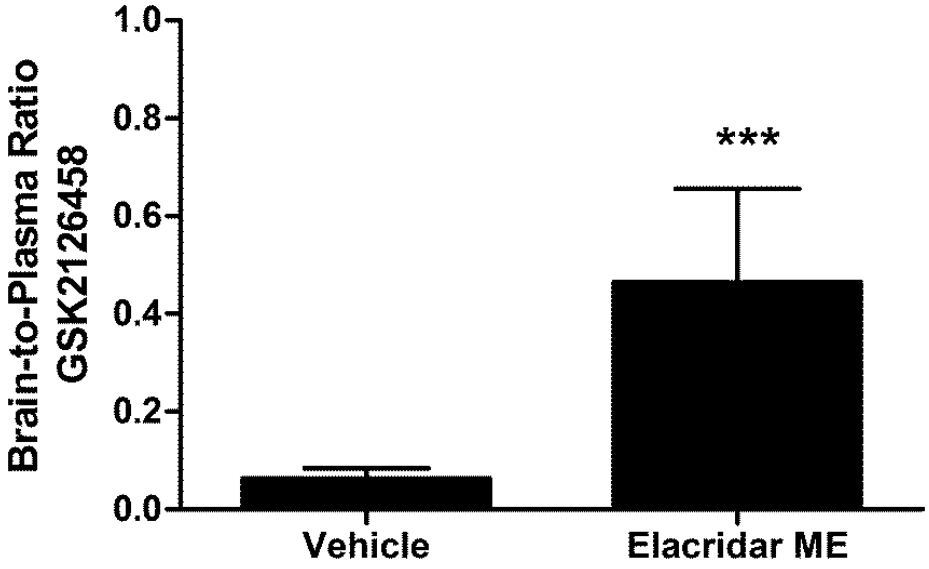

Brain-to-plasma ratio of GSK212658 1 hr post dose after pretreatment with vehicle or elacridar microemulsion (administered 10 mg/kg i.p, 1 hour before oral administration of GSK2126458) in wild-type. Data represent mean ± SD, n = 3-4. *** p = 0.0045 compared to corresponding B/P ratio in vehicle treated wild-type mice.

CHAPTER 6: IMPROVED BIOAVAILABILITY OF ZELBORAF IN A STABLE AMORPHOUS SOLID DISPERSION LEADS TO IMPROVED ANTI-TUMOR RESPONSE IN A NOVEL MELANOMA MOUSE MODEL

The present work indicates the importance of using the most relevant pharmacy-grade formulation of drugs to conduct pre-clinical studies in order to make pertinent conclusions and recommendations for further pre-clinical or clinical investigations. A large proportion of drugs are orally administered and methods to improve oral absorption are critical to the clinical use of low solubility drugs (BCS class II and IV). Vemurafenib (BCS class IV) is a potent FDA-approved BRAF inhibitor that is clinically used to treat metastatic melanoma. During its development, crystalline vemurafenib was reformulated into an amorphous-solid dispersion, termed as “microprecipitated bulk powder (MBP)” before being approved as pharmacy-grade vemurafenib (Zelboraf®). From our oral pharmacokinetic studies in mice, we observe that Zelboraf® has a ~ 2.5 fold higher oral bioavailability as compared to crystalline vemurafenib (non-pharmacy grade). Also, upon oral administration of Zelboraf®and non-pharmacy grade vemurafenib at the same dose, we observed that there was a significantly better anti-tumor response in a flank tumor melanoma model. We also go on to describe the mechanism by which the improved solubility of Zelboraf® in comparison to non-pharmacy grade vemurafenib leads to a significant improvement in plasma exposure and bioavailability.

6. 1 Introduction

Vemurafenib is a BCS class IV (low solubility, low permeability) drug that was reformulated into a amorphous solid dispersion stabilized with a polymer by a solvent-controlled coprecipitation method in order to increase its solubility and oral bioavailability before its FDA approval (Zelboraf®)(Shah et al., 2013). Zelboraf® was shown to provide a significantly higher rate and extent of dissolution than crystalline vemurafenib (Shah et al., 2013). Improving solubility through formulation approaches such as preparing stabilized solid dispersions in polymeric systems have been explored as an option for the improvement of solubility of poorly soluble drugs (Leuner and Dressman, 2000). This method exploits the stabilization of a high energy state (amorphous) of the poorly soluble drug in order to translate the solubility advantage into enhanced absorption and improved bioavailability (Brouwers et al., 2009).

In the case of vemurafenib, the amorphous solid dispersion was prepared using a solvent controlled coprecipitation method using hypromellose acetate succinate (HPMCAS) as the stabilizing enteric polymer (Shah et al., 2013). The formulation of Zelboraf® into a MPB led to achieving efficacious systemic concentrations, which was extremely critical to the clinical success of this drug product. The saturation solubility of the drug formulation also affects the rate of dissolution (Noyes, 1897). Amorphous solids have a higher solubility than crystalline solids,

which has led to an increased focus on the development of amorphous formulations, especially for BCS class II and IV drugs. In the case of vemurafenib, the apparent solubility of the MBP was ~ 30 fold higher than its crystalline counterparts, and this supersaturation was maintained for a sustained period of 4 hours (Shah et al., 2013).

Vemurafenib specifically inhibits the mutant form of the BRAF (v-raf murine sarcoma viral oncogene homolog B) protein that is found to be mutated in a majority of melanoma patients (Davies et al., 2002). BRAF V600 mutations were found to be responsible for the constitutive activation of the MAP kinase signaling pathway leading to uncontrolled cell proliferation and tumor growth. Vemurafenib, approved in August 2011 for the treatment of metastatic melanoma was a remarkable progress in melanoma therapy. Vemurafenib received FDA-approval after showing a substantial improvement in progression-free survival and overall-survival in comparison to dacarbazine in phase 3 clinical trials (Chapman et al., 2011).

Currently, there is a paucity of clinically relevant melanoma mouse models that can be used to understand the progression of the disease and improve treatment options. For our studies, we use a novel patient derived xenograft model, where patient tumor tissue is directly implanted into nude mice, followed by serial passage and expansion. This method is known to preserve the genetic and phenotypic characteristics of the primary patient tumor (Renfrow and Lesser,

2013). In this current study, patient derived M12 BRAF V600E mutant melanoma cells are implanted subcutaneously to represent a flank tumor.

The purpose of this study was to compare the pharmacokinetics and pharmacodynamics (efficacy) of pharmacy-grade Zelboraf® against a non-pharmacy grade vemurafenib in order to understand and delineate the impact of formulation differences on the design and meaningful interpretation of pre-clinical studies. Information from this work will provide a strong basis for making the right choice of formulation to conduct studies in pre-clinical models.

6. 2 Materials and Methods

6. 2. 1 Chemicals

Zelboraf® was purchased from the pharmacy. Non-pharmacy grade vemurafenib was purchased from LC laboratories (Woburn, MA). All other chemicals used were of high-performance liquid chromatography or reagent grade.

6. 2. 2 Animals

Pharmacokinetic studies were performed in Friend leukemia virus strain B (FVB) wild-type mice. Efficacy studies were performed in nude mice implanted with M12 BRAF V600E flank tumors. All animals were 8-12 weeks old at the time of starting the experiment. Animals were maintained in a 12-hour light/dark cycle with unlimited access to food and water. All studies were carried out in accordance with the National Institutes of Health's *Guide for the Care and Use of*

Laboratory Animals (Institute of Laboratory Animal Resources, 1996) and approved by the Institutional Animal Care and Use Committee (IACUC) of the University of Minnesota.

6. 2. 3 Pharmacokinetic Studies

The oral dosing vehicle for non-pharmacy grade vemurafenib was 1% methocel, 5% DMSO and 1% methocel for Zelboraf® . All dosing suspensions were prepared on the day of the experiment. Zelboraf® oral dosing suspension was prepared by gently triturating the Zelboraf® tablet in a mortar-pestle and suspending the powder in 1% methocel. FVBn wild-type mice received 75 mg/kg single oral dose of vemurafenib or Zelboraf® and blood samples were collected after 1, 2, 4,8,12, 16 and 24 hours post-oral dose. At the end of the desired time point, the animals were euthanized using a CO2 chamber. Blood was collected via cardiac puncture in heparinized tubes. Plasma was separated by centrifuging whole blood at 3500 rpm for 10 minutes at 4 degree C. Vemurafenib plasma concentrations were measured using a specific liquid-chromatography- tandem mass spectrometry (LC-MS/MS) method that has been described in detail in our previously published work (Mittapalli et al., 2012).

6. 2. 4 Efficacy studies in a flank melanoma tumor model

M12 cells were obtained from the tumor tissue of a patient diagnosed with melanoma carrying the BRAF V600E mutation. Nude mice were implanted with M12 flank tumors (100,000 cells injected subcutaneously). Once tumors reached a size of 250-300 mm^3, they received vehicle or 75 mg/kg b.i.d of non-pharmacy vemurafenib or Zelboraf® until tumors reach a size of 2000 mm^3 or mice became moribund. During the course of the study, the size of the flank tumor was measured using calipers.

6. 2. 5 Modeling the case of solubility limited absorption and bioavailability

STELLA® 9.0.1 was used to develop a model that describes the impact of improving the solubility of a drug on oral bioavailability. We describe a 2-compartment model with a drug administered orally with first-order absorption from the gut-compartment and first-order elimination from the central compartment (Fig. 6.3). The rate of absorption is directly proportional to the concentration gradient, which in turn increases with an increase in the solubility of the drug or upon achieving its saturation solubility in the gut compartment. A case that involves affecting the concentration achieved in the gut due to formulation differences is simulated and the corresponding changes in plasma pharmacokinetics are observed. The model assumes that the rate of dissolution is a function of the concentration gradient. All rate constants, initial amount in the

gut, and maximum achievable concentration or saturation concentration achievable (C_{sat}) have been arbitrarily assumed in this model. The equations describing the model are listed in Table 6.2.

6. 2. 6 The Noyes-Whitney model and the relationship between saturation solubility and dissolution kinetics:

The Noyes-Whitney model relates surface area, and degree of unsaturation of the solution to the dissolution rate of a drug. For the purpose of this study, we assume that the solubility enhancement of the amorphous formulation far exceeds any differences in surface characteristics of individual nuclei between the amorphous and crystalline formulations. So, the rate of dissolution of the drug molecule can be written as

$$\text{rate of dissolution} = K_{\text{diss}}(C^{sat} - C^{solution}) \qquad (1)$$

where K_{diss} a dissolution rate is constant, C^{sat} is the saturation solubility of the drug formulation, and $C^{solution}$ is the instantaneous concentration of the drug in the gut compartment. Therefore, increasing C^{sat} increases the dissolution rate of the drug.

6. 3 Results and Discussion

6. 3. 1 Improved bioavailability of Zelboraf® in comparison to non-pharmacy grade vemurafenib

Zelboraf® and non-pharmacy grade vemurafenib were given orally to wild-type FVB mice as a suspension. We observed that the plasma concentrations were higher in mice dosed with Zelboraf® as compared to non-pharmacy grade vemurafenib at all measured time points (Fig. 6.1.), possibly an effect of the sustained supersaturation observed for the Zelboraf® formulation.

The area under the curve (AUC) in the Zelboraf® treated mice was ~2.5 fold higher in the Zelboraf® treated mice as compared to non-pharmacy grade vemurafenib (Table 1). The oral bioavailability of Zelboraf® was ~ 100% as compared to 48% for non-pharmacy grade vemurafenib (Table 1). These data confirm that the suspension prepared from pharmacy-grade Zelboraf® has improved oral bioavailability as compared to its crystalline non-pharmacy grade vemurafenib.

6. 3. 2 Improved anti-tumor response of Zelboraf® in the M12 melanoma model

In an efficacy study in M12 flank tumor bearing nude mice that were dosed 75 mg/kg b.i.d Zelboraf® , non-pharmacy grade vemurafenib or vehicle control, we observed that the anti-tumor response measured by tumor volume was significantly better in the Zelboraf® treated group as compared to non-pharmacy grade vemurafenib or vehicle control (Fig. 6.2). Interestingly, we observed that the tumor volumes in the non-pharmacy vemurafenib treated group were similar to the vehicle treated group. This study confirms that the efficacy of vemurafenib is dependent on the formulation and the lower exposure of vemurafenib from the non-pharmacy grade formulation did not lead to a significant response, while the improved bioavailability from the Zelboraf® MBP led to correspondingly higher vemurafenib exposure which translated into significantly higher reduction in flank tumor volume.

6. 3. 3 Modeling the case of solubility limited absorption and bioavailability

In our model, the dissolution rate is proportional to the concentration gradient or the difference between C^{sat} and $C^{solution}$ in the gut (Fig. 6.3). So, an increase in the saturation solubility leads to an increase in the rate of dissolution. This leads to improved exposure and bioavailability of vemurafenib in the MBP (Zelboraf®). On changing the drug from its highly insoluble crystalline form to a stabilized amorphous solid dispersion, a significant increase in the maximum achievable

concentration in the gut is observed. This increase in gut concentration leads to a higher rate of dissolution followed by a higher rate of absorption and improved exposure. We observe that with an increase in C_{sat}, a higher concentration is achieved in the gut, which correspondingly leads to an increase in plasma concentrations (Fig. 6.4).

6. 4 Summary and Conclusions

Our pharmacokinetic studies in mice confirm that the suspension prepared from Zelboraf® (MBP) has a higher overall exposure and oral bioavailability as compared to non-pharmacy grade vemurafenib. The MBP provided a ~ 2.5 fold increase in overall plasma exposure as compared to non-pharmacy grade vemurafenib. From the efficacy studies in the M12 flank melanoma model, we observe that the reduction in tumor volume (efficacy of vemurafenib) is significantly higher when mice receive Zelboraf® as compared to non-pharmacy grade vemurafenib or placebo. These data could indicate that the concentrations achieved from the non-pharmacy grade vemurafenib in the flank tumor are insufficient to block BRAF signaling as compared to Zelboraf®. This is most likely a direct effect of the improved pharmacokinetics of Zelboraf® as compared to the non-pharmacy grade vemurafenib.

From the model describing solubility limited oral bioavailability, we observe that increasing the saturation solubility leads to a greater concentration gradient and improved plasma exposure. Taken together, we conclude that the sustained

increase in solubility of the MBP leads to improved bioavailability and this has to be taken into account in planning studies in pre-clinical models. The choice of formulation has a direct impact on the observed pharmacokinetics and pharmacodynamics and an incorrect choice of formulation could lead to potentially inaccurate conclusions regarding the activity of the drug.

Figures

Figure 6.1: Plasma concentrations of vemurafenib in FVB wild-type at 1, 2,4,8,12,16 and 24 hours after an oral dose of 75 mg/kg Zelboraf® (red) or non-pharmacy grade vemurafenib (black). Data represent mean ± SD., n = 3-4.

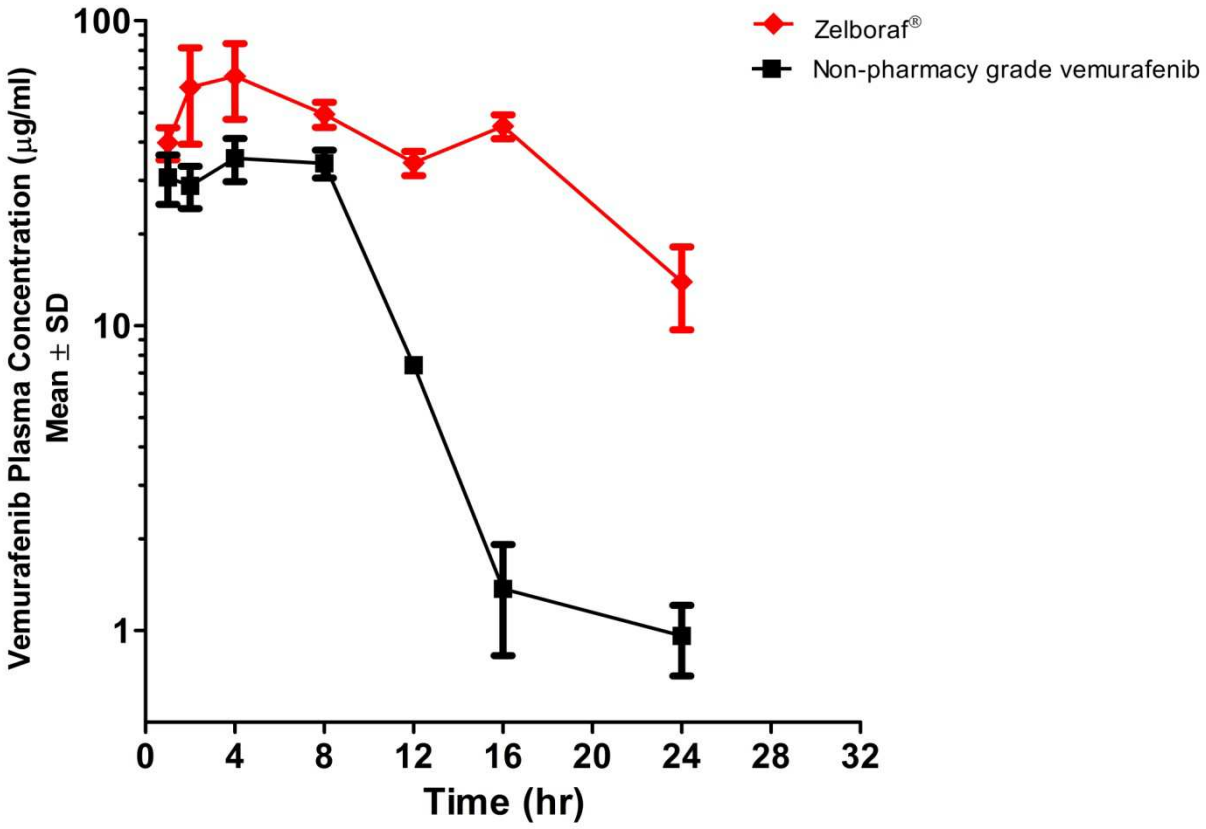

Figure 6.2: Comparison of efficacy of Zelboraf® , non-pharmacy grade vemurafenib, and placebo (vehicle control).

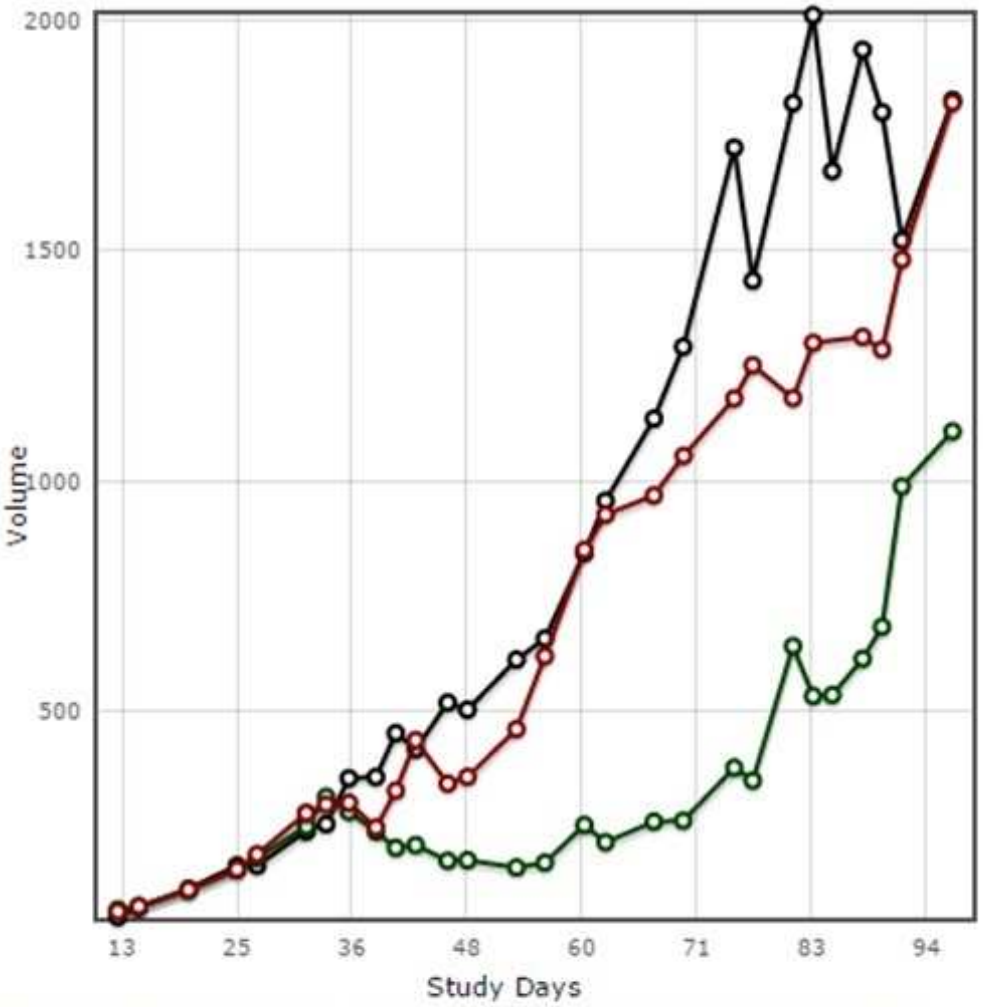

M12 Flank Tumor Volumes (mm^3) Non-pharmacy grade vemurafenib (Brown) versus Zelboraf (Green), placebo (black)

Nude mice bearing flank melanoma tumors (M12) were treated with 75 mg/kg p.o. b.i.d of Zelboraf® , non-pharmacy grade vemurafenib or placebo until placebo treated tumors reached 2000 mm^3 (n=10 per group). At day 72, drug

treatments were stopped, when the placebo treated group reached a tumor size of 1500 mm^3.

Figure 6.3: Model describing a case of solubility limited oral absorption.

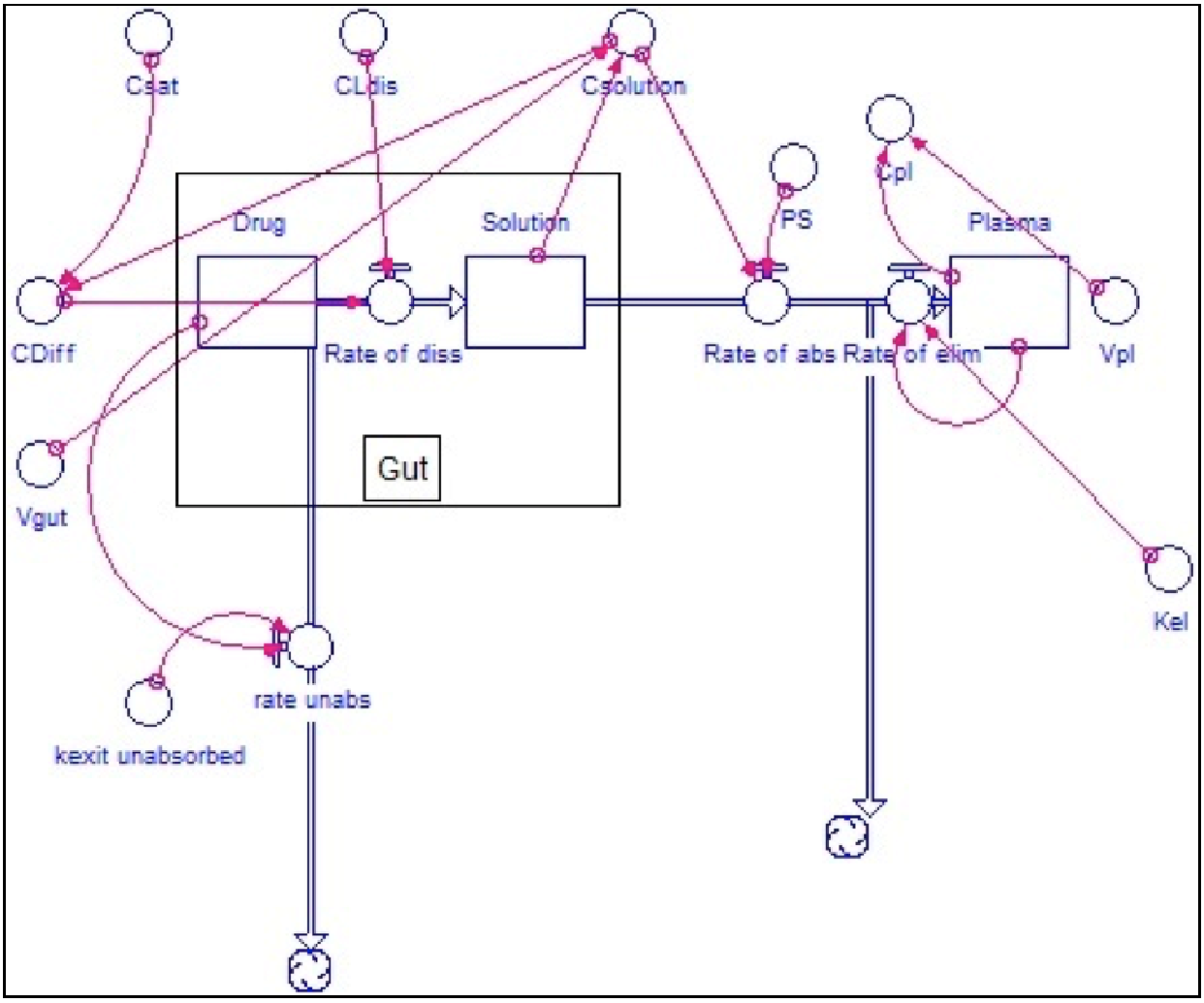

Model assumes that the rate of dissolution is proportional to the concentration gradient, first order absorption and first order elimination. The equations describing this model are listed in Table 6.2.

Figure 6.4: Increase in saturation solubility (similar to the increase between Zelboraf® and non-pharmacy grade vemurafenib) leads to an increase in exposure.

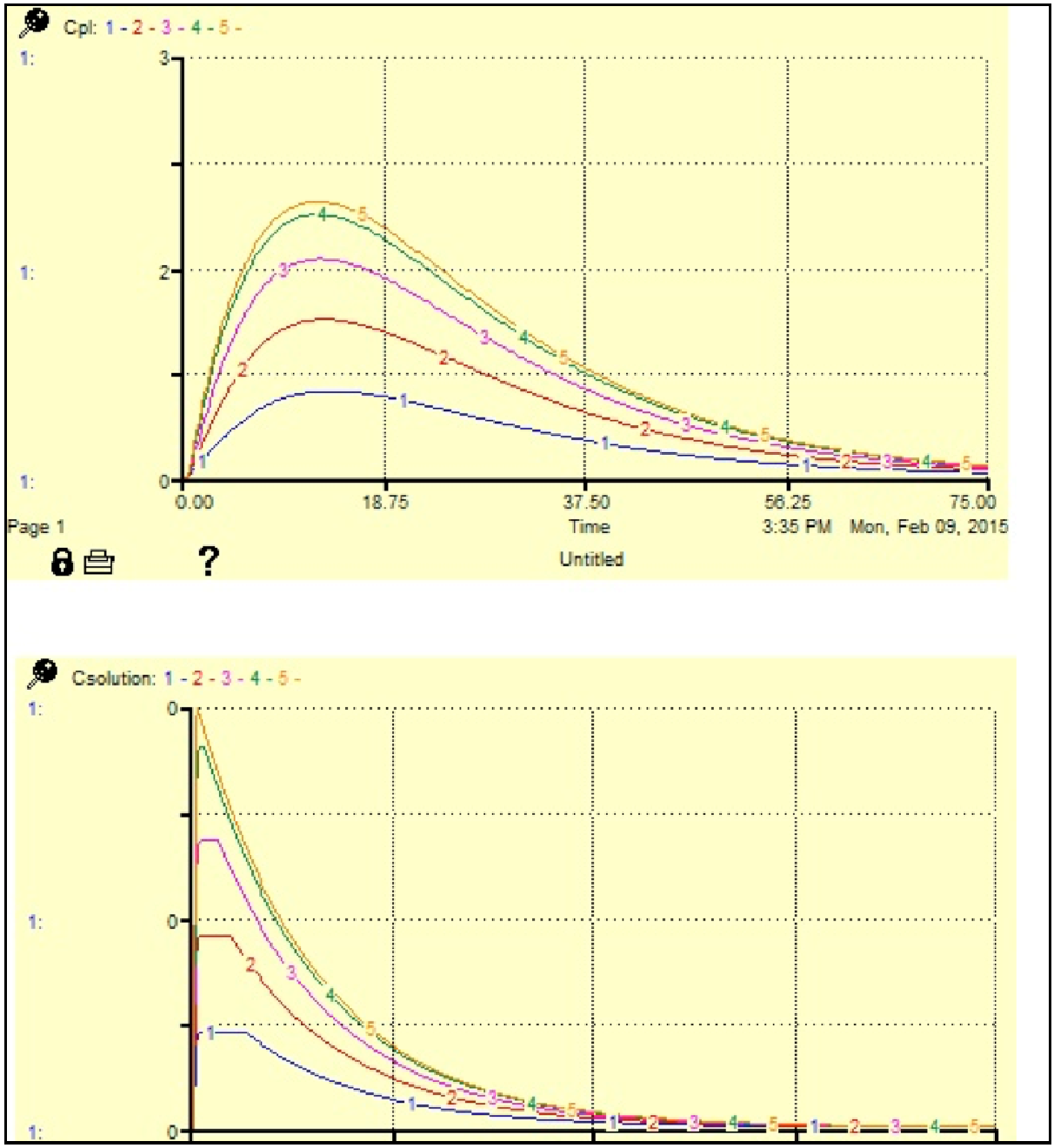

This is seen by the increase in area under the curve, and is also confirmed by the higher concentration of drug in solution (Csolution) in the gut on increasing the saturation solubility of the drug.

Table 6.1: Area under the curve (AUC) and bioavailability of Zelboraf® and non-pharmacy grade vemurafenib. Vemurafenib i.v. AUC is from our previously published work (Mittapalli et al., 2012).

Non-pharmacy grade vemurafenib

		hr*μg/mL	F (%)
Dpo=75mpk	**Mean AUC p.o.**	393.03	
Div = 2.5 mpk	**Mean AUC i.v.**	1663	
AUC iv (min*μg/mL)			
AUC iv(hr.μg/mL)		27.73	**47.24**

Zelboraf®

		hr*μg/mL	F (%)
Dpo=75mpk	**Mean AUC p.o.**	1003.89	
Div = 2.5 mpk	**Mean AUC i.v.**	1663	
AUC iv (min*μg/mL)			
AUC iv(hr.μg/mL)		**27.73**	**120.67**

Table 6.2: Equations describing the model shown in Fig. 6.3.

```
Drug(t) = Drug(t - dt) + (- Rate_of_diss - rate_unabs) * dt

INIT Drug = 1.5


OUTFLOWS:

Rate_of_diss = CLdis*CDiff

rate_unabs = Drug*kexit_unabsorbed

Plasma(t) = Plasma(t - dt) + (Rate_of_abs - Rate_of_elim) *

dt

INIT Plasma = 0


INFLOWS:

Rate_of_abs = Csolution*PS

OUTFLOWS:

Rate_of_elim = Plasma*Kel

Solution(t) = Solution(t - dt) + (Rate_of_diss -

Rate_of_abs) * dt

INIT Solution = 0


INFLOWS:
```

```
Rate_of_diss = CLdis*CDiff

OUTFLOWS:

Rate_of_abs = Csolution*PS

CDiff = Csat-Csolution

CLdis = 10

Cpl = Plasma/Vpl

Csat = 0.25

Csolution = Solution/Vgut

Kel = 0.1

kexit_unabsorbed = 0.5

PS = 0.2

Vgut = 3

Vpl = 0.2
```

CHAPTER 7: RECAPITULATION

Melanoma is a highly aggressive skin cancer with a great propensity for brain metastasis. Currently, brain metastases from melanoma are untreatable and lethal in most patients with advanced disease. The presence of brain metastases in a large proportion of patients at autopsy confirms an unmet medical need. Patients with multiple brain metastases and extensive peripheral disease can have a particularly poor survival; which can be as short as 1-2 months.

Recently, there has been significant advancement in the treatment of peripheral melanoma. With the discovery and better understanding of hallmark molecular events and oncogenic mutations that cause disease progression, there has been a steady increase in the development of molecularly targeted drugs for the treatment of melanoma. In particular, in melanoma, oncogenic driver mutations in BRAF have been known to play an important role in the disease. Vemurafenib and dabrafenib are two BRAF inhibitors that were FDA approved after they showed significant improvement in survival in melanoma patients as compared to conventional therapies. However, the improvement in patient outcomes with BRAF inhibition is short-lived as patients tend to develop resistance to BRAF inhibition. Addition of a MEK inhibitor, trametinib to BRAF inhibition with dabrafenib was also approved as a single agent and in combination for clinical use due to the significant improvement in patient outcomes. Unfortunately, patients on this combination have also shown to develop resistance eventually and relapse with aggressive disease. The emergence of resistance to MAPK

pathway inhibition is a significant problem and needs to be addressed immediately.

A combination of BRAF and MEK inhibitors with PI3K/mTOR inhibition is known to overcome acquired resistance *in vitro*. GSK2126458 is a potent ATP competitive inhibitor of PI3K/mTOR which is a promising candidate for combination therapy.

The efficacy of these molecularly targeted agents and combinations is the sufficient delivery of all agents in the combination across the BBB, also to target sites in the brain that are residing behind an intact BBB, that are almost always undetectable. The BBB is composed of a monolayer of endothelial cells that are connected by tight junction proteins and expressing several efflux transporters. Of particular interest are two important efflux transporter proteins P-glycoprotein (P-gp) and breast cancer resistance protein (Bcrp) that have been previously known to play an important role in excluding several anti-cancer drugs from the brain; limiting the efficacy of chemotherapeutics. The central goal of this dissertation was to understand the influence of active efflux on the brain distribution of these molecularly targeted agents.

The influence of active efflux on the first approved BRAF inhibitor, vemurafenib, was thoroughly studied in the first project using elegant in vitro studies in MDCK II cells and in vivo pharmacokinetic studies in wild-type, P-gp knockout, Bcrp knockout and triple knockout mice (Chapter 2). From our in vitro studies, we were

able to conclude that vemurafenib was a substrate for both P-gp and Bcrp. Also, from our pharmacokinetic studies in mice, we observed that the brain distribution of vemurafenib was severely restricted at the BBB by a cooperative role of both P-gp and Bcrp. At steady-state, the brain-to-plasma ratio increased ~ 80 fold; from 0.01 in the wild-type mice to 1 in the triple knock-out mice (lacking both P-gp and Bcrp).However, the brain distribution of vemurafenib was restricted in the single knockouts; confirming the cooperation of the two transporters.

In continuation of our research plan, we then examined the influence of P-gp and Bcrp on the brain distribution of a second FDA-approved, highly promising BRAF inhibitor, dabrafenib (Chapter 3). From our studies, we were able to conclude that dabrafenib was also restricted in brain distribution by P-gp and Bcrp. The K_p (AUC_{brain}/ AUC_{plasma}) of dabrafenib was ~ 18 fold higher in the triple knockouts (0.42) as compared to wild-type mice (0.023). We also observed that dabrafenib had a higher brain penetration as compared to vemurafenib, suggesting that dabrafenib may be a better choice for the treatment of melanoma brain metastases.

Despite the initial success with vemurafenib and dabrafenib in treating peripheral disease, most patients with metastatic melanoma relapse within one year due to the emergence of resistance to BRAF inhibition. The development of resistance to MAPK signaling blockage by BRAF inhibition is a serious problem that has to be factored in while designing combination therapies. The improved duration of

response from the combination of BRAF and MEK (downstream of BRAF in the MAPK signaling pathway) inhibition (dabrafenib and trametinib) provides new hope for delaying resistance and improving response. However, the success of combination therapies in treating brain metastases depends on all agents being effectively delivered t0 all metastatic sites, including micrometastases that reside behind an intact blood brain barrier. In the light of this problem, we then examined the influence of active efflux of MEK inhibitor, trametinib which was approved for use as a single agent and in combination with dabrafenib for the treatment of metastatic melanoma (Chapter 4). In the case of trametinib, we observed that P-gp played a greater role than Bcrp in restricting its brain distribution in the mouse, while we observed that trametinib was a substrate for both P-gp and Bcrp *in vitro*. The K_p ratio of trametinib in the wild-type and Bcrp knockout mice were 0.148 and 0.136, respectively while they were 0.733 and 0.675 in the P-gp knockout and triple knockout mice. Upon simultaneously infusing dabrafenib and trametinib, we observed that both drugs were restricted in brain distribution in wild-type mice with a significantly higher brain penetration in triple knockouts.

Simultaneous inhibition of multiple signaling pathways is a possible approach for delaying/overcoming acquired resistance. Simultaneously targeting the MAPK and PI3K signaling pathway is a valid therapeutic approach to overcome resistance to chronic MAPK inhibition (BRAF alone, MEK alone or BRAF + MEK

inhibition). In the final chapter (chapter 5), we studied the influence of active efflux on the brain distribution of PI3K/mTOR inhibitor GSK2126458. Using in vitro studies in MDCK II cells, we observed that GSK212658 is a substrate for both P-gp and Bcrp. From pharmacokinetic studies in mice, we observed that GSK2126458 has a severely limited brain distribution in wild-type mice as compared to triple-knockouts. The steady-state B/P ratio increases ~ 7 fold from 0.07 in the wild-type mice to 0.47 in triple knockout mice. Also, we did not observe a significant change in the brain distribution in the P-gp knockout and Bcrp knockout mice as compared to wild-type. The aggregate of these studies confirm the cooperative role of P-gp and Bcrp in restricting the brain distribution of GSK2126458. If all drugs in a combination do not reach the brain, there is an increased potential for resistance, making the brain a sanctuary site for further metastases.

In chapter 6, we investigate the influence of the pharmacy-grade formulation of vemurafenib (Zelboraf®) on the oral bioavailability of vemurafenib in comparison to its non-pharmacy grade counterpart. We observe that the conversion of crystalline drug into an amorphous solid-dispersion leads to a significant increase in bioavailability and efficacy in a melanoma mouse model. The findings of this chapter are critical to the appropriate selection of drug formulations at any stage of pre-clinical or clinical investigation.

Future work on this project will require the study of several different combinations of molecularly targeted agents in a relevant mouse model of melanoma brain metastasis. This will enable a better rational choice of combinations in treating melanoma brain metastases and potentially lead to durable treatment outcomes and lead to substantial delay in resistance.

BIBLIOGRAPHY

CHAPTER 1:

Agarwal S, Hartz AM, Elmquist WF and Bauer B (2011a) Breast cancer resistance protein and P-glycoprotein in brain cancer: two gatekeepers team up. *Curr Pharm Des* **17**:2793-2802.

Agarwal S, Sane R, Oberoi R, Ohlfest JR and Elmquist WF (2011b) Delivery of molecularly targeted therapy to malignant glioma, a disease of the whole brain. *Expert Rev Mol Med* **13**:e17.

Agarwala SS, Kirkwood JM, Gore M, Dreno B, Thatcher N, Czarnetski B, Atkins M, Buzaid A, Skarlos D and Rankin EM (2004) Temozolomide for the treatment of brain metastases associated with metastatic melanoma: a phase II study. *J Clin Oncol* **22**:2101-2107.

Amer MH, Al-Sarraf M, Baker LH and Vaitkevicius VK (1978) Malignant melanoma and central nervous system metastases: incidence, diagnosis, treatment and survival. *Cancer* **42**:660-668.

Aplin AE, Kaplan FM and Shao Y (2011) Mechanisms of resistance to RAF inhibitors in melanoma. *J Invest Dermatol* **131**:1817-1820.

Atkins MB, Kunkel L, Sznol M and Rosenberg SA (2000) High-dose recombinant interleukin-2 therapy in patients with metastatic melanoma: long-term survival update. *Cancer J Sci Am* **6 Suppl 1**:S11-14.

Atkins MB, Lotze MT, Dutcher JP, Fisher RI, Weiss G, Margolin K, Abrams J, Sznol M, Parkinson D, Hawkins M, Paradise C, Kunkel L and Rosenberg SA (1999) High-dose recombinant interleukin 2 therapy for patients with metastatic melanoma: analysis of 270 patients treated between 1985 and 1993. *J Clin Oncol* **17**:2105-2116.

Balch CM, Gershenwald JE, Soong SJ, Thompson JF, Atkins MB, Byrd DR, Buzaid AC, Cochran AJ, Coit DG, Ding S, Eggermont AM, Flaherty KT, Gimotty PA, Kirkwood JM, McMasters KM, Mihm MC, Jr., Morton DL, Ross MI, Sober AJ and Sondak VK (2009) Final version of 2009 AJCC melanoma staging and classification. *J Clin Oncol* **27**:6199-6206.

Bollag G, Tsai J, Zhang J, Zhang C, Ibrahim P, Nolop K and Hirth P (2012) Vemurafenib: the first drug approved for BRAF-mutant cancer. *Nat Rev Drug Discov* **11**:873-886.

Chapman PB, Hauschild A, Robert C, Haanen JB, Ascierto P, Larkin J, Dummer R, Garbe C, Testori A, Maio M, Hogg D, Lorigan P, Lebbe C, Jouary T, Schadendorf D, Ribas A, O'Day SJ, Sosman JA, Kirkwood JM, Eggermont AM, Dreno B, Nolop K, Li J, Nelson B, Hou J, Lee RJ, Flaherty KT and McArthur GA (2011) Improved survival with vemurafenib in melanoma with BRAF V600E mutation. *N Engl J Med* **364**:2507-2516.

Chartrain M, Riond J, Stennevin A, Vandenberghe I, Gomes B, Lamant L, Meyer N, Gairin JE, Guilbaud N and Annereau JP (2012) Melanoma

chemotherapy leads to the selection of ABCB5-expressing cells. *PLoS One* **7**:e36762.

Davies H, Bignell GR, Cox C, Stephens P, Edkins S, Clegg S, Teague J, Woffendin H, Garnett MJ, Bottomley W, Davis N, Dicks E, Ewing R, Floyd Y, Gray K, Hall S, Hawes R, Hughes J, Kosmidou V, Menzies A, Mould C, Parker A, Stevens C, Watt S, Hooper S, Wilson R, Jayatilake H, Gusterson BA, Cooper C, Shipley J, Hargrave D, Pritchard-Jones K, Maitland N, Chenevix-Trench G, Riggins GJ, Bigner DD, Palmieri G, Cossu A, Flanagan A, Nicholson A, Ho JW, Leung SY, Yuen ST, Weber BL, Seigler HF, Darrow TL, Paterson H, Marais R, Marshall CJ, Wooster R, Stratton MR and Futreal PA (2002) Mutations of the BRAF gene in human cancer. *Nature* **417**:949-954.

Eisen T, Ahmad T, Flaherty KT, Gore M, Kaye S, Marais R, Gibbens I, Hackett S, James M, Schuchter LM, Nathanson KL, Xia C, Simantov R, Schwartz B, Poulin-Costello M, O'Dwyer PJ and Ratain MJ (2006) Sorafenib in advanced melanoma: a Phase II randomised discontinuation trial analysis. *Br J Cancer* **95**:581-586.

Falchook GS, Long GV, Kurzrock R, Kim KB, Arkenau TH, Brown MP, Hamid O, Infante JR, Millward M, Pavlick AC, O'Day SJ, Blackman SC, Curtis CM, Lebowitz P, Ma B, Ouellet D and Kefford RF (2012) Dabrafenib in patients

with melanoma, untreated brain metastases, and other solid tumours: a phase 1 dose-escalation trial. *Lancet* **379**:1893-1901.

Fidler IJ (2003) The pathogenesis of cancer metastasis: the 'seed and soil' hypothesis revisited. *Nat Rev Cancer* **3**:453-458.

Fidler IJ (2011) The role of the organ microenvironment in brain metastasis. *Semin Cancer Biol* **21**:107-112.

Fidler IJ, Balasubramanian K, Lin Q, Kim SW and Kim S-J (2010) The Brain Microenvironment and Cancer Metastasis. *Moleculte s and Cells* **30**:93-98.

Fife KM, Colman MH, Stevens GN, Firth IC, Moon D, Shannon KF, Harman R, Petersen-Schaefer K, Zacest AC, Besser M, Milton GW, McCarthy WH and Thompson JF (2004) Determinants of outcome in melanoma patients with cerebral metastases. *J Clin Oncol* **22**:1293-1300.

Flaherty KT, Infante JR, Daud A, Gonzalez R, Kefford RF, Sosman J, Hamid O, Schuchter L, Cebon J, Ibrahim N, Kudchadkar R, Burris HA, 3rd, Falchook G, Algazi A, Lewis K, Long GV, Puzanov I, Lebowitz P, Singh A, Little S, Sun P, Allred A, Ouellet D, Kim KB, Patel K and Weber J (2012a) Combined BRAF and MEK Inhibition in Melanoma with BRAF V600 Mutations. *N Engl J Med*.

Flaherty KT, Robert C, Hersey P, Nathan P, Garbe C, Milhem M, Demidov LV, Hassel JC, Rutkowski P, Mohr P, Dummer R, Trefzer U, Larkin JM, Utikal J, Dreno B, Nyakas M, Middleton MR, Becker JC, Casey M, Sherman LJ,

Wu FS, Ouellet D, Martin AM, Patel K and Schadendorf D (2012b) Improved survival with MEK inhibition in BRAF-mutated melanoma. *N Engl J Med* **367**:107-114.

Fokas E, Steinbach JP and Rodel C (2013) Biology of brain metastases and novel targeted therapies: time to translate the research. *Biochim Biophys Acta* **1835**:61-75.

Gibney GT, Forsyth PA and Sondak VK (2012) Melanoma in the brain: biology and therapeutic options. *Melanoma Res* **22**:177-183.

Goel VK, Lazar AJ, Warneke CL, Redston MS and Haluska FG (2006) Examination of mutations in BRAF, NRAS, and PTEN in primary cutaneous melanoma. *J Invest Dermatol* **126**:154-160.

Guirguis LM, Yang JC, White DE, Steinberg SM, Liewehr DJ, Rosenberg SA and Schwartzentruber DJ (2002) Safety and efficacy of high-dose interleukin-2 therapy in patients with brain metastases. *J Immunother* **25**:82-87.

Gupta G, Robertson AG and MacKie RM (1997) Cerebral metastases of cutaneous melanoma. *Br J Cancer* **76**:256-259.

Hauschild A, Grob JJ, Demidov LV, Jouary T, Gutzmer R, Millward M, Rutkowski P, Blank CU, Miller WH, Jr., Kaempgen E, Martin-Algarra S, Karaszewska B, Mauch C, Chiarion-Sileni V, Martin AM, Swann S, Haney P, Mirakhur B, Guckert ME, Goodman V and Chapman PB (2012) Dabrafenib in BRAF-

mutated metastatic melanoma: a multicentre, open-label, phase 3 randomised controlled trial. *Lancet* **380**:358-365.

Hocker T and Tsao H (2007) Ultraviolet radiation and melanoma: a systematic review and analysis of reported sequence variants. *Hum Mutat* **28**:578-588.

Hodi FS, O'Day SJ, McDermott DF, Weber RW, Sosman JA, Haanen JB, Gonzalez R, Robert C, Schadendorf D, Hassel JC, Akerley W, van den Eertwegh AJ, Lutzky J, Lorigan P, Vaubel JM, Linette GP, Hogg D, Ottensmeier CH, Lebbe C, Peschel C, Quirt I, Clark JI, Wolchok JD, Weber JS, Tian J, Yellin MJ, Nichol GM, Hoos A and Urba WJ (2010) Improved survival with ipilimumab in patients with metastatic melanoma. *N Engl J Med* **363**:711-723.

Hodis E, Watson IR, Kryukov GV, Arold ST, Imielinski M, Theurillat JP, Nickerson E, Auclair D, Li L, Place C, Dicara D, Ramos AH, Lawrence MS, Cibulskis K, Sivachenko A, Voet D, Saksena G, Stransky N, Onofrio RC, Winckler W, Ardlie K, Wagle N, Wargo J, Chong K, Morton DL, Stemke-Hale K, Chen G, Noble M, Meyerson M, Ladbury JE, Davies MA, Gershenwald JE, Wagner SN, Hoon DS, Schadendorf D, Lander ES, Gabriel SB, Getz G, Garraway LA and Chin L (2012) A landscape of driver mutations in melanoma. *Cell* **150**:251-263.

Johnson JD and Young B (1996) Demographics of brain metastasis. *Neurosurg Clin N Am* **7**:337-344.

Joyce JA and Pollard JW (2009) Microenvironmental regulation of metastasis. *Nat Rev Cancer* **9**:239-252.

Karasarides M, Chiloeches A, Hayward R, Niculescu-Duvaz D, Scanlon I, Friedlos F, Ogilvie L, Hedley D, Martin J, Marshall CJ, Springer CJ and Marais R (2004) B-RAF is a therapeutic target in melanoma. *Oncogene* **23**:6292-6298.

Loscher W and Potschka H (2005) Blood-brain barrier active efflux transporters: ATP-binding cassette gene family. *NeuroRx* **2**:86-98.

Luo Y, Ellis LZ, Dallaglio K, Takeda M, Robinson WA, Robinson SE, Liu W, Lewis KD, McCarter MD, Gonzalez R, Norris DA, Roop DR, Spritz RA, Ahn NG and Fujita M (2012) Side population cells from human melanoma tumors reveal diverse mechanisms for chemoresistance. *J Invest Dermatol* **132**:2440-2450.

McCubrey JA, Milella M, Tafuri A, Martelli AM, Lunghi P, Bonati A, Cervello M, Lee JT and Steelman LS (2008) Targeting the Raf/MEK/ERK pathway with small-molecule inhibitors. *Curr Opin Investig Drugs* **9**:614-630.

Miller DM and Flaherty KT (2014) Cyclin-dependent kinases as therapeutic targets in melanoma. *Pigment Cell Melanoma Res* **27**:351-365.

Nikolaou VA, Stratigos AJ, Flaherty KT and Tsao H (2012) Melanoma: new insights and new therapies. *J Invest Dermatol* **132**:854-863.

Ohtsuki S and Terasaki T (2007) Contribution of carrier-mediated transport systems to the blood-brain barrier as a supporting and protecting interface for the brain; importance for CNS drug discovery and development. *Pharm Res* **24**:1745-1758.

Poulikakos PI and Rosen N (2011) Mutant BRAF melanomas--dependence and resistance. *Cancer Cell* **19**:11-15.

Puzanov I, Burnett P and Flaherty KT (2011) Biological challenges of BRAF inhibitor therapy. *Mol Oncol* **5**:116-123.

Ribas A, Kefford R, Marshall MA, Punt CJ, Haanen JB, Marmol M, Garbe C, Gogas H, Schachter J, Linette G, Lorigan P, Kendra KL, Maio M, Trefzer U, Smylie M, McArthur GA, Dreno B, Nathan PD, Mackiewicz J, Kirkwood JM, Gomez-Navarro J, Huang B, Pavlov D and Hauschild A (2013) Phase III randomized clinical trial comparing tremelimumab with standard-of-care chemotherapy in patients with advanced melanoma. *J Clin Oncol* **31**:616-622.

Ribas A, Kim K, Schuchter L, Gonzalez R, Pavlick AC, Weber JS, McArthur GA, Hutson TE, Flaherty KT, Moschos SJ, Lawrence DP, Hersey P, Kefford RF, Chmielowski B, Puzanov I, Li J, Nolop KB, Lee RJ, Joe AK and JA; S

(2011) BRIM-2: An open-label, multicenter phase II study of vemurafenib in previously treated patients with BRAF V600E mutation-positive metastatic melanoma., in *ASCO Annual Meeting;J Clin Oncol 29: 2011 (suppl; abstr 8509)*

Robert C, Thomas L, Bondarenko I, O'Day S, Weber J, Garbe C, Lebbe C, Baurain JF, Testori A, Grob JJ, Davidson N, Richards J, Maio M, Hauschild A, Miller WH, Jr., Gascon P, Lotem M, Harmankaya K, Ibrahim R, Francis S, Chen TT, Humphrey R, Hoos A and Wolchok JD (2011) Ipilimumab plus dacarbazine for previously untreated metastatic melanoma. *N Engl J Med* **364**:2517-2526.

Rochet NM, Dronca RS, Kottschade LA, Chavan RN, Gorman B, Gilbertson JR and Markovic SN (2012) Melanoma brain metastases and vemurafenib: need for further investigation. *Mayo Clin Proc* **87**:976-981.

Sampson JH, Carter JH, Jr., Friedman AH and Seigler HF (1998) Demographics, prognosis, and therapy in 702 patients with brain metastases from malignant melanoma. *J Neurosurg* **88**:11-20.

Schouten LJ, Rutten J, Huveneers HA and Twijnstra A (2002) Incidence of brain metastases in a cohort of patients with carcinoma of the breast, colon, kidney, and lung and melanoma. *Cancer* **94**:2698-2705.

Serrone L, Zeuli M, Sega FM and Cognetti F (2000) Dacarbazine-based chemotherapy for metastatic melanoma: thirty-year experience overview. *J Exp Clin Cancer Res* **19**:21-34.

Shaik N, Giri N, Pan G and Elmquist WF (2007) P-glycoprotein-mediated active efflux of the anti-HIV1 nucleoside abacavir limits cellular accumulation and brain distribution. *Drug Metab Dispos* **35**:2076-2085.

Siegel R, Ma J, Zou Z and Jemal A (2014) Cancer statistics, 2014. *CA Cancer J Clin* **64**:9-29.

Siegel RL, Miller KD and Jemal A (2015) Cancer statistics, 2015. *CA Cancer J Clin* **65**:5-29.

Smalley KS, Haass NK, Brafford PA, Lioni M, Flaherty KT and Herlyn M (2006) Multiple signaling pathways must be targeted to overcome drug resistance in cell lines derived from melanoma metastases. *Mol Cancer Ther* **5**:1136-1144.

Sullivan RJ and Flaherty KT (2013) Resistance to BRAF-targeted therapy in melanoma. *Eur J Cancer* **49**:1297-1304.

Topalian SL, Hodi FS, Brahmer JR, Gettinger SN, Smith DC, McDermott DF, Powderly JD, Carvajal RD, Sosman JA, Atkins MB, Leming PD, Spigel DR, Antonia SJ, Horn L, Drake CG, Pardoll DM, Chen L, Sharfman WH, Anders RA, Taube JM, McMiller TL, Xu H, Korman AJ, Jure-Kunkel M, Agrawal S, McDonald D, Kollia GD, Gupta A, Wigginton JM and Sznol M

(2012) Safety, activity, and immune correlates of anti-PD-1 antibody in cancer. *N Engl J Med* **366**:2443-2454.

Topalian SL, Sznol M, McDermott DF, Kluger HM, Carvajal RD, Sharfman WH, Brahmer JR, Lawrence DP, Atkins MB, Powderly JD, Leming PD, Lipson EJ, Puzanov I, Smith DC, Taube JM, Wigginton JM, Kollia GD, Gupta A, Pardoll DM, Sosman JA and Hodi FS (2014) Survival, durable tumor remission, and long-term safety in patients with advanced melanoma receiving nivolumab. *J Clin Oncol* **32**:1020-1030.

Trunzer K, Pavlick AC, Schuchter L, Gonzalez R, McArthur GA, Hutson TE, Moschos SJ, Flaherty KT, Kim KB, Weber JS, Hersey P, Long GV, Lawrence D, Ott PA, Amaravadi RK, Lewis KD, Puzanov I, Lo RS, Koehler A, Kockx M, Spleiss O, Schell-Steven A, Gilbert HN, Cockey L, Bollag G, Lee RJ, Joe AK, Sosman JA and Ribas A (2013) Pharmacodynamic effects and mechanisms of resistance to vemurafenib in patients with metastatic melanoma. *J Clin Oncol* **31**:1767-1774.

Tsai J, Lee JT, Wang W, Zhang J, Cho H, Mamo S, Bremer R, Gillette S, Kong J, Haass NK, Sproesser K, Li L, Smalley KS, Fong D, Zhu YL, Marimuthu A, Nguyen H, Lam B, Liu J, Cheung I, Rice J, Suzuki Y, Luu C, Settachatgul C, Shellooe R, Cantwell J, Kim SH, Schlessinger J, Zhang KY, West BL, Powell B, Habets G, Zhang C, Ibrahim PN, Hirth P, Artis DR, Herlyn M and Bollag G (2008) Discovery of a selective inhibitor of oncogenic B-Raf

kinase with potent antimelanoma activity. *Proc Natl Acad Sci U S A* **105**:3041-3046.

Uchida Y, Ohtsuki S, Katsukura Y, Ikeda C, Suzuki T, Kamiie J and Terasaki T (2011) Quantitative targeted absolute proteomics of human blood-brain barrier transporters and receptors. *J Neurochem* **117**:333-345.

Villanueva J, Vultur A, Lee JT, Somasundaram R, Fukunaga-Kalabis M, Cipolla AK, Wubbenhorst B, Xu X, Gimotty PA, Kee D, Santiago-Walker AE, Letrero R, D'Andrea K, Pushparajan A, Hayden JE, Brown KD, Laquerre S, McArthur GA, Sosman JA, Nathanson KL and Herlyn M (2010) Acquired resistance to BRAF inhibitors mediated by a RAF kinase switch in melanoma can be overcome by cotargeting MEK and IGF-1R/PI3K. *Cancer Cell* **18**:683-695.

Vultur A, Villanueva J and Herlyn M (2011) Targeting BRAF in advanced melanoma: a first step toward manageable disease. *Clin Cancer Res* **17**:1658-1663.

Wagle N, Emery C, Berger MF, Davis MJ, Sawyer A, Pochanard P, Kehoe SM, Johannessen CM, Macconaill LE, Hahn WC, Meyerson M and Garraway LA (2011) Dissecting therapeutic resistance to RAF inhibition in melanoma by tumor genomic profiling. *J Clin Oncol* **29**:3085-3096.

Wagle N, Van Allen EM, Treacy DJ, Frederick DT, Cooper ZA, Taylor-Weiner A, Rosenberg M, Goetz EM, Sullivan RJ, Farlow DN, Friedrich DC, Anderka

K, Perrin D, Johannessen CM, McKenna A, Cibulskis K, Kryukov G, Hodis E, Lawrence DP, Fisher S, Getz G, Gabriel SB, Carter SL, Flaherty KT, Wargo JA and Garraway LA (2014) MAP kinase pathway alterations in BRAF-mutant melanoma patients with acquired resistance to combined RAF/MEK inhibition. *Cancer Discov* **4**:61-68.

Wan PT, Garnett MJ, Roe SM, Lee S, Niculescu-Duvaz D, Good VM, Jones CM, Marshall CJ, Springer CJ, Barford D and Marais R (2004) Mechanism of activation of the RAF-ERK signaling pathway by oncogenic mutations of B-RAF. *Cell* **116**:855-867.

Wellbrock C, Karasarides M and Marais R (2004) The RAF proteins take centre stage. *Nat Rev Mol Cell Biol* **5**:875-885.

Wolchok JD, Kluger H, Callahan MK, Postow MA, Rizvi NA, Lesokhin AM, Segal NH, Ariyan CE, Gordon RA, Reed K, Burke MM, Caldwell A, Kronenberg SA, Agunwamba BU, Zhang X, Lowy I, Inzunza HD, Feely W, Horak CE, Hong Q, Korman AJ, Wigginton JM, Gupta A and Sznol M (2013) Nivolumab plus ipilimumab in advanced melanoma. *N Engl J Med* **369**:122-133.

CHAPTER 2:

Agarwal S, Sane R, Gallardo JL, Ohlfest JR and Elmquist WF (2010) Distribution of gefitinib to the brain is limited by P-glycoprotein (ABCB1) and breast cancer resistance protein (ABCG2)-mediated active efflux. *J Pharmacol Exp Ther* **334**:147-155.

Agarwal S, Sane R, Ohlfest JR and Elmquist WF (2011) The role of the breast cancer resistance protein (ABCG2) in the distribution of sorafenib to the brain. *J Pharmacol Exp Ther* **336**:223-233.

Agarwal S, Uchida Y, Mittapalli RK, Sane R, Terasaki T and Elmquist WF (2012) Quantitative Proteomics of Transporter Expression in Brain Capillary Endothelial Cells Isolated from P-gp, BCRP, and P-gp/BCRP Knockout Mice. *Drug Metab Dispos*.

Atkins MB, Lotze MT, Dutcher JP, Fisher RI, Weiss G, Margolin K, Abrams J, Sznol M, Parkinson D, Hawkins M, Paradise C, Kunkel L and Rosenberg SA (1999) High-dose recombinant interleukin 2 therapy for patients with metastatic melanoma: analysis of 270 patients treated between 1985 and 1993. *J Clin Oncol* **17**:2105-2116.

Capper D, Berghoff AS, Magerle M, Ilhan A, Wohrer A, Hackl M, Pichler J, Pusch S, Meyer J, Habel A, Petzelbauer P, Birner P, von Deimling A and Preusser M (2011) Immunohistochemical testing of BRAF V600E status in 1,120 tumor tissue samples of patients with brain metastases. *Acta Neuropathol*.

Chapman PB, Hauschild A, Robert C, Haanen JB, Ascierto P, Larkin J, Dummer R, Garbe C, Testori A, Maio M, Hogg D, Lorigan P, Lebbe C, Jouary T, Schadendorf D, Ribas A, O'Day SJ, Sosman JA, Kirkwood JM, Eggermont AM, Dreno B, Nolop K, Li J, Nelson B, Hou J, Lee RJ, Flaherty KT and

McArthur GA (2011) Improved survival with vemurafenib in melanoma with BRAF V600E mutation. *N Engl J Med* **364**:2507-2516.

Chen Y, Agarwal S, Shaik NM, Chen C, Yang Z and Elmquist WF (2009) P-glycoprotein and breast cancer resistance protein influence brain distribution of dasatinib. *J Pharmacol Exp Ther* **330**:956-963.

Comis RL (1976) DTIC (NSC-45388) in malignant melanoma: a perspective. *Cancer Treat Rep* **60**:165-176.

Davies H, Bignell GR, Cox C, Stephens P, Edkins S, Clegg S, Teague J, Woffendin H, Garnett MJ, Bottomley W, Davis N, Dicks E, Ewing R, Floyd Y, Gray K, Hall S, Hawes R, Hughes J, Kosmidou V, Menzies A, Mould C, Parker A, Stevens C, Watt S, Hooper S, Wilson R, Jayatilake H, Gusterson BA, Cooper C, Shipley J, Hargrave D, Pritchard-Jones K, Maitland N, Chenevix-Trench G, Riggins GJ, Bigner DD, Palmieri G, Cossu A, Flanagan A, Nicholson A, Ho JW, Leung SY, Yuen ST, Weber BL, Seigler HF, Darrow TL, Paterson H, Marais R, Marshall CJ, Wooster R, Stratton MR and Futreal PA (2002) Mutations of the BRAF gene in human cancer. *Nature* **417**:949-954.

de Vries NA, Zhao J, Kroon E, Buckle T, Beijnen JH and van Tellingen O (2007) P-glycoprotein and breast cancer resistance protein: two dominant transporters working together in limiting the brain penetration of topotecan. *Clin Cancer Res* **13**:6440-6449.

Fife KM, Colman MH, Stevens GN, Firth IC, Moon D, Shannon KF, Harman R, Petersen-Schaefer K, Zacest AC, Besser M, Milton GW, McCarthy WH and Thompson JF (2004) Determinants of outcome in melanoma patients with cerebral metastases. *J Clin Oncol* **22**:1293-1300.

Garbe C, Eigentler TK, Keilholz U, Hauschild A and Kirkwood JM (2011) Systematic review of medical treatment in melanoma: current status and future prospects. *Oncologist* **16**:5-24.

Ji Z, Flaherty KT and Tsao H (2012) Targeting the RAS pathway in melanoma. *Trends Mol Med* **18**:27-35.

Johannessen CM, Boehm JS, Kim SY, Thomas SR, Wardwell L, Johnson LA, Emery CM, Stransky N, Cogdill AP, Barretina J, Caponigro G, Hieronymus H, Murray RR, Salehi-Ashtiani K, Hill DE, Vidal M, Zhao JJ, Yang X, Alkan O, Kim S, Harris JL, Wilson CJ, Myer VE, Finan PM, Root DE, Roberts TM, Golub T, Flaherty KT, Dummer R, Weber BL, Sellers WR, Schlegel R, Wargo JA, Hahn WC and Garraway LA (2010) COT drives resistance to RAF inhibition through MAP kinase pathway reactivation. *Nature* **468**:968-972.

Johnson JD and Young B (1996) Demographics of brain metastasis. *Neurosurg Clin N Am* **7**:337-344.

Long GV, Menzies AM, Nagrial AM, Haydu LE, Hamilton AL, Mann GJ, Hughes TM, Thompson JF, Scolyer RA and Kefford RF (2011) Prognostic and clinicopathologic associations of oncogenic BRAF in metastatic melanoma. *J Clin Oncol* **29**:1239-1246.

Loscher W and Potschka H (2005) Blood-brain barrier active efflux transporters: ATP-binding cassette gene family. *NeuroRx* **2**:86-98.

McCubrey JA, Milella M, Tafuri A, Martelli AM, Lunghi P, Bonati A, Cervello M, Lee JT and Steelman LS (2008) Targeting the Raf/MEK/ERK pathway with small-molecule inhibitors. *Curr Opin Investig Drugs* **9**:614-630.

Nazarian R, Shi H, Wang Q, Kong X, Koya RC, Lee H, Chen Z, Lee MK, Attar N, Sazegar H, Chodon T, Nelson SF, McArthur G, Sosman JA, Ribas A and Lo RS (2010) Melanomas acquire resistance to B-RAF(V600E) inhibition by RTK or N-RAS upregulation. *Nature* **468**:973-977.

Polli JW, Olson KL, Chism JP, John-Williams LS, Yeager RL, Woodard SM, Otto V, Castellino S and Demby VE (2009) An unexpected synergist role of P-glycoprotein and breast cancer resistance protein on the central nervous

system penetration of the tyrosine kinase inhibitor lapatinib (N-{3-chloro-4-[(3-fluorobenzyl)oxy]phenyl}-6-[5-({[2-(methylsulfonyl)ethyl]amino }methyl)-2-furyl]-4-quinazolinamine; GW572016). *Drug Metab Dispos* **37**:439-442.

Raizer JJ, Hwu WJ, Panageas KS, Wilton A, Baldwin DE, Bailey E, von Althann C, Lamb LA, Alvarado G, Bilsky MH and Gutin PH (2008) Brain and leptomeningeal metastases from cutaneous melanoma: survival outcomes based on clinical features. *Neuro Oncol* **10**:199-207.

Ribas A, Kim K, Schuchter L, Gonzalez R, Pavlick AC, Weber JS, McArthur GA, Hutson TE, Flaherty KT, Moschos SJ, Lawrence DP, Hersey P, Kefford RF, Chmielowski B, Puzanov I, Li J, Nolop KB, Lee RJ, Joe AK and JA; S (2011) BRIM-2: An open-label, multicenter phase II study of vemurafenib in previously treated patients with BRAF V600E mutation-positive metastatic melanoma., in *ASCO Annual Meeting;J Clin Oncol 29: 2011 (suppl; abstr 8509)*

Schinkel AH and Jonker JW (2003) Mammalian drug efflux transporters of the ATP binding cassette (ABC) family: an overview. *Adv Drug Deliv Rev* **55**:3-29.

Siegel R, Ward E, Brawley O and Jemal A (2011) Cancer statistics, 2011: the impact of eliminating socioeconomic and racial disparities on premature cancer deaths. *CA Cancer J Clin* **61**:212-236.

Tsai J, Lee JT, Wang W, Zhang J, Cho H, Mamo S, Bremer R, Gillette S, Kong J, Haass NK, Sproesser K, Li L, Smalley KS, Fong D, Zhu YL, Marimuthu A, Nguyen H, Lam B, Liu J, Cheung I, Rice J, Suzuki Y, Luu C, Settachatgul C, Shellooe R, Cantwell J, Kim SH, Schlessinger J, Zhang KY, West BL, Powell B, Habets G, Zhang C, Ibrahim PN, Hirth P, Artis DR, Herlyn M and Bollag G (2008) Discovery of a selective inhibitor of oncogenic B-Raf kinase with potent antimelanoma activity. *Proc Natl Acad Sci U S A* **105**:3041-3046.

Villanueva J, Vultur A, Lee JT, Somasundaram R, Fukunaga-Kalabis M, Cipolla AK, Wubbenhorst B, Xu X, Gimotty PA, Kee D, Santiago-Walker AE, Letrero R, D'Andrea K, Pushparajan A, Hayden JE, Brown KD, Laquerre S, McArthur GA, Sosman JA, Nathanson KL and Herlyn M (2010) Acquired resistance to BRAF inhibitors mediated by a RAF kinase switch in melanoma can be overcome by cotargeting MEK and IGF-1R/PI3K. *Cancer Cell* **18**:683-695.

Vultur A, Villanueva J and Herlyn M (2011) Targeting BRAF in advanced melanoma: a first step toward manageable disease. *Clin Cancer Res* **17**:1658-1663.

Wagle N, Emery C, Berger MF, Davis MJ, Sawyer A, Pochanard P, Kehoe SM, Johannessen CM, Macconaill LE, Hahn WC, Meyerson M and Garraway LA (2011) Dissecting therapeutic resistance to RAF inhibition in melanoma by tumor genomic profiling. *J Clin Oncol* **29**:3085-3096.

Wan PT, Garnett MJ, Roe SM, Lee S, Niculescu-Duvaz D, Good VM, Jones CM, Marshall CJ, Springer CJ, Barford D and Marais R (2004) Mechanism of activation of the RAF-ERK signaling pathway by oncogenic mutations of B-RAF. *Cell* **116**:855-867.

CHAPTER 3:

Agarwal S, Sane R, Gallardo JL, Ohlfest JR and Elmquist WF (2010) Distribution of gefitinib to the brain is limited by P-glycoprotein (ABCB1) and breast cancer resistance protein (ABCG2)-mediated active efflux. *J Pharmacol Exp Ther* **334**:147-155.

Agarwal S, Sane R, Ohlfest JR and Elmquist WF (2011) The role of the breast cancer resistance protein (ABCG2) in the distribution of sorafenib to the brain. *J Pharmacol Exp Ther* **336**:223-233.

Atkins MB, Lotze MT, Dutcher JP, Fisher RI, Weiss G, Margolin K, Abrams J, Sznol M, Parkinson D, Hawkins M, Paradise C, Kunkel L and Rosenberg SA (1999) High-dose recombinant interleukin 2 therapy for patients with metastatic melanoma: analysis of 270 patients treated between 1985 and 1993. *J Clin Oncol* **17**:2105-2116.

Bailer AJ (1988) Testing for the equality of area under the curves when using destructive measurement techniques. *J Pharmacokinet Biopharm* **16**:303-309.

Bollag G, Hirth P, Tsai J, Zhang J, Ibrahim PN, Cho H, Spevak W, Zhang C, Zhang Y, Habets G, Burton EA, Wong B, Tsang G, West BL, Powell B, Shellooe R, Marimuthu A, Nguyen H, Zhang KY, Artis DR, Schlessinger J, Su F, Higgins B, Iyer R, D'Andrea K, Koehler A, Stumm M, Lin PS, Lee RJ, Grippo J, Puzanov I, Kim KB, Ribas A, McArthur GA, Sosman JA, Chapman PB, Flaherty KT, Xu X, Nathanson KL and Nolop K (2010) Clinical efficacy of a RAF inhibitor needs broad target blockade in BRAF-mutant melanoma. *Nature* **467**:596-599.

Chapman PB, Hauschild A, Robert C, Haanen JB, Ascierto P, Larkin J, Dummer R, Garbe C, Testori A, Maio M, Hogg D, Lorigan P, Lebbe C, Jouary T, Schadendorf D, Ribas A, O'Day SJ, Sosman JA, Kirkwood JM, Eggermont AM, Dreno B, Nolop K, Li J, Nelson B, Hou J, Lee RJ, Flaherty KT and McArthur GA (2011) Improved survival with vemurafenib in melanoma with BRAF V600E mutation. *N Engl J Med* **364**:2507-2516.

Comis RL (1976) DTIC (NSC-45388) in malignant melanoma: a perspective. *Cancer Treat Rep* **60**:165-176.

Dai H, Marbach P, Lemaire M, Hayes M and Elmquist WF (2003) Distribution of STI-571 to the brain is limited by P-glycoprotein-mediated efflux. *J Pharmacol Exp Ther* **304**:1085-1092.

Davies H, Bignell GR, Cox C, Stephens P, Edkins S, Clegg S, Teague J, Woffendin H, Garnett MJ, Bottomley W, Davis N, Dicks E, Ewing R, Floyd Y, Gray K, Hall S, Hawes R, Hughes J, Kosmidou V, Menzies A, Mould C, Parker A, Stevens C, Watt S, Hooper S, Wilson R, Jayatilake H, Gusterson BA, Cooper C, Shipley J, Hargrave D, Pritchard-Jones K, Maitland N, Chenevix-Trench G, Riggins GJ, Bigner DD, Palmieri G, Cossu A, Flanagan A, Nicholson A, Ho JW, Leung SY, Yuen ST, Weber BL, Seigler HF, Darrow TL, Paterson H, Marais R, Marshall CJ, Wooster R, Stratton MR and Futreal PA (2002) Mutations of the BRAF gene in human cancer. *Nature* **417**:949-954.

Davies MA, Liu P, McIntyre S, Kim KB, Papadopoulos N, Hwu WJ, Hwu P and Bedikian A (2011) Prognostic factors for survival in melanoma patients with brain metastases. *Cancer* **117**:1687-1696.

de Vries NA, Zhao J, Kroon E, Buckle T, Beijnen JH and van Tellingen O (2007) P-glycoprotein and breast cancer resistance protein: two dominant transporters working together in limiting the brain penetration of topotecan. *Clin Cancer Res* **13**:6440-6449.

Deeken JF and Loscher W (2007) The blood-brain barrier and cancer: transporters, treatment, and Trojan horses. *Clin Cancer Res* **13**:1663-1674.

Durmus S, Sparidans RW, Wagenaar E, Beijnen JH and Schinkel AH (2012) Oral Availability and Brain Penetration of the B-RAF(V600E) Inhibitor Vemurafenib Can Be Enhanced by the P-Glycoprotein (ABCB1) and Breast Cancer Resistance Protein (ABCG2) Inhibitor Elacridar. *Mol Pharm*.

Falchook GS, Long GV, Kurzrock R, Kim KB, Arkenau TH, Brown MP, Hamid O, Infante JR, Millward M, Pavlick AC, O'Day SJ, Blackman SC, Curtis CM, Lebowitz P, Ma B, Ouellet D and Kefford RF (2012) Dabrafenib in patients with melanoma, untreated brain metastases, and other solid tumours: a phase 1 dose-escalation trial. *Lancet* **379**:1893-1901.

Fife KM, Colman MH, Stevens GN, Firth IC, Moon D, Shannon KF, Harman R, Petersen-Schaefer K, Zacest AC, Besser M, Milton GW, McCarthy WH and Thompson JF (2004) Determinants of outcome in melanoma patients with cerebral metastases. *J Clin Oncol* **22**:1293-1300.

Flaherty KT, Infante JR, Daud A, Gonzalez R, Kefford RF, Sosman J, Hamid O, Schuchter L, Cebon J, Ibrahim N, Kudchadkar R, Burris HA, 3rd, Falchook G, Algazi A, Lewis K, Long GV, Puzanov I, Lebowitz P, Singh A, Little S, Sun P, Allred A, Ouellet D, Kim KB, Patel K and Weber J (2012) Combined BRAF and MEK Inhibition in Melanoma with BRAF V600 Mutations. *N Engl J Med*.

Garbe C, Eigentler TK, Keilholz U, Hauschild A and Kirkwood JM (2011) Systematic review of medical treatment in melanoma: current status and future prospects. *Oncologist* **16**:5-24.

Gibney GT and Sondak VK (2012) Extending the reach of BRAF-targeted cancer therapy. *Lancet* **379**:1858-1859.

Giri N, Agarwal S, Shaik N, Pan G, Chen Y and Elmquist WF (2009) Substrate-dependent breast cancer resistance protein (Bcrp1/Abcg2)-mediated interactions: consideration of multiple binding sites in in vitro assay design. *Drug Metab Dispos* **37**:560-570.

Hauschild A, Grob JJ, Demidov LV, Jouary T, Gutzmer R, Millward M, Rutkowski P, Blank CU, Miller WH, Jr., Kaempgen E, Martin-Algarra S, Karaszewska B, Mauch C, Chiarion-Sileni V, Martin AM, Swann S, Haney P, Mirakhur B, Guckert ME, Goodman V and Chapman PB (2012) Dabrafenib in BRAF-mutated metastatic melanoma: a multicentre, open-label, phase 3 randomised controlled trial. *Lancet* **380**:358-365.

Hawkins BT and Davis TP (2005) The blood-brain barrier/neurovascular unit in health and disease. *Pharmacol Rev* **57**:173-185.

Johannessen CM, Boehm JS, Kim SY, Thomas SR, Wardwell L, Johnson LA, Emery CM, Stransky N, Cogdill AP, Barretina J, Caponigro G, Hieronymus H, Murray RR, Salehi-Ashtiani K, Hill DE, Vidal M, Zhao JJ, Yang X, Alkan O, Kim S, Harris JL, Wilson CJ, Myer VE, Finan PM, Root DE, Roberts TM, Golub T, Flaherty KT, Dummer R, Weber BL, Sellers WR, Schlegel R, Wargo JA, Hahn WC and Garraway LA (2010) COT drives resistance to RAF inhibition through MAP kinase pathway reactivation. *Nature* **468**:968-972.

Kalvass JC, Maurer TS and Pollack GM (2007) Use of plasma and brain unbound fractions to assess the extent of brain distribution of 34 drugs: comparison of unbound concentration ratios to in vivo p-glycoprotein efflux ratios. *Drug Metab Dispos* **35**:660-666.

Lagas JS, van Waterschoot RA, van Tilburg VA, Hillebrand MJ, Lankheet N, Rosing H, Beijnen JH and Schinkel AH (2009) Brain accumulation of dasatinib is restricted by P-glycoprotein (ABCB1) and breast cancer

resistance protein (ABCG2) and can be enhanced by elacridar treatment. *Clin Cancer Res* **15**:2344-2351.

Lockman PR, Mittapalli RK, Taskar KS, Rudraraju V, Gril B, Bohn KA, Adkins CE, Roberts A, Thorsheim HR, Gaasch JA, Huang S, Palmieri D, Steeg PS and Smith QR (2010) Heterogeneous blood-tumor barrier permeability determines drug efficacy in experimental brain metastases of breast cancer. *Clin Cancer Res* **16**:5664-5678.

Long GV, Trefzer U, Davies MA, Kefford RF, Ascierto PA, Chapman PB, Puzanov I, Hauschild A, Robert C, Algazi A, Mortier L, Tawbi H, Wilhelm T, Zimmer L, Switzky J, Swann S, Martin AM, Guckert M, Goodman V, Streit M, Kirkwood JM and Schadendorf D (2012) Dabrafenib in patients with Val600Glu or Val600Lys BRAF-mutant melanoma metastatic to the brain (BREAK-MB): a multicentre, open-label, phase 2 trial. *Lancet Oncol*.

Margolin K, Ernstoff MS, Hamid O, Lawrence D, McDermott D, Puzanov I, Wolchok JD, Clark JI, Sznol M, Logan TF, Richards J, Michener T, Balogh A, Heller KN and Hodi FS (2012) Ipilimumab in patients with melanoma and brain metastases: an open-label, phase 2 trial. *Lancet Oncol* **13**:459-465.

McCubrey JA, Milella M, Tafuri A, Martelli AM, Lunghi P, Bonati A, Cervello M, Lee JT and Steelman LS (2008) Targeting the Raf/MEK/ERK pathway with small-molecule inhibitors. *Curr Opin Investig Drugs* **9**:614-630.

Mittapalli RK, Vaidhyanathan S, Sane R and Elmquist WF (2012) Impact of P-glycoprotein (ABCB1) and breast cancer resistance protein (ABCG2) on the brain distribution of a novel BRAF inhibitor: vemurafenib (PLX4032). *J Pharmacol Exp Ther* **342**:33-40.

Nazarian R, Shi H, Wang Q, Kong X, Koya RC, Lee H, Chen Z, Lee MK, Attar N, Sazegar H, Chodon T, Nelson SF, McArthur G, Sosman JA, Ribas A and

Lo RS (2010) Melanomas acquire resistance to B-RAF(V600E) inhibition by RTK or N-RAS upregulation. *Nature* **468**:973-977.

Nedelman JR, Gibiansky E and Lau DT (1995) Applying Bailer's method for AUC confidence intervals to sparse sampling. *Pharm Res* **12**:124-128.

Polli JW, Olson KL, Chism JP, John-Williams LS, Yeager RL, Woodard SM, Otto V, Castellino S and Demby VE (2009) An unexpected synergist role of P-glycoprotein and breast cancer resistance protein on the central nervous system penetration of the tyrosine kinase inhibitor lapatinib (N-{3-chloro-4-[(3-fluorobenzyl)oxy]phenyl}-6-[5-({[2-(methylsulfonyl)ethyl]amino }methyl)-2-furyl]-4-quinazolinamine; GW572016). *Drug Metab Dispos* **37**:439-442.

Rochet NM, Dronca RS, Kottschade LA, Chavan RN, Gorman B, Gilbertson JR and Markovic SN (2012) Melanoma brain metastases and vemurafenib: need for further investigation. *Mayo Clin Proc* **87**:976-981.

Schinkel AH and Jonker JW (2003) Mammalian drug efflux transporters of the ATP binding cassette (ABC) family: an overview. *Adv Drug Deliv Rev* **55**:3-29.

Siegel R, Ward E, Brawley O and Jemal A (2011) Cancer statistics, 2011: the impact of eliminating socioeconomic and racial disparities on premature cancer deaths. *CA Cancer J Clin* **61**:212-236.

Skibber JM, Soong SJ, Austin L, Balch CM and Sawaya RE (1996) Cranial irradiation after surgical excision of brain metastases in melanoma patients. *Ann Surg Oncol* **3**:118-123.

Sosman JA, Kim KB, Schuchter L, Gonzalez R, Pavlick AC, Weber JS, McArthur GA, Hutson TE, Moschos SJ, Flaherty KT, Hersey P, Kefford R, Lawrence D, Puzanov I, Lewis KD, Amaravadi RK, Chmielowski B, Lawrence HJ, Shyr Y, Ye F, Li J, Nolop KB, Lee RJ, Joe AK and Ribas A (2012) Survival in BRAF V600-mutant advanced melanoma treated with vemurafenib. *N Engl J Med* **366**:707-714.

Laquerre S, Arnone M, Moss K, Yang J, Fisher K, Kane-Carson LS, Smitheman K, Ward J, Heidrich B, Rheault T, Adjabeng G, Hornberger K, Stellwagen J, Waterson A, Han C, Mook RA, Uehling D and King AJ (2009) A selective Raf kinase inhibitor induces cell death and tumor regression of human cancer cell lines encoding B-RafV600E mutation *Mol Cancer Ther* **8** (12 Supple): B88.

Tsao H, Atkins MB and Sober AJ (2004) Management of cutaneous melanoma. *N Engl J Med* **351**:998-1012.

Villanueva J, Vultur A, Lee JT, Somasundaram R, Fukunaga-Kalabis M, Cipolla AK, Wubbenhorst B, Xu X, Gimotty PA, Kee D, Santiago-Walker AE, Letrero R, D'Andrea K, Pushparajan A, Hayden JE, Brown KD, Laquerre S, McArthur GA, Sosman JA, Nathanson KL and Herlyn M (2010) Acquired resistance to BRAF inhibitors mediated by a RAF kinase switch in melanoma can be overcome by cotargeting MEK and IGF-1R/PI3K. *Cancer Cell* **18**:683-695.

CHAPTER 4:

Agarwal S, Hartz AM, Elmquist WF and Bauer B (2011) Breast cancer resistance protein and P-glycoprotein in brain cancer: two gatekeepers team up. *Current pharmaceutical design* **17**:2793-2802.

Agarwal S, Uchida Y, Mittapalli RK, Sane R, Terasaki T and Elmquist WF (2012) Quantitative proteomics of transporter expression in brain capillary endothelial cells isolated from P-glycoprotein (P-gp), breast cancer resistance protein (Bcrp), and P-gp/Bcrp knockout mice. *Drug metabolism and disposition: the biological fate of chemicals* **40**:1164-1169.

Atkins MB, Lotze MT, Dutcher JP, Fisher RI, Weiss G, Margolin K, Abrams J, Sznol M, Parkinson D, Hawkins M, Paradise C, Kunkel L and Rosenberg SA (1999) High-dose recombinant interleukin 2 therapy for patients with metastatic melanoma: analysis of 270 patients treated between 1985 and 1993. *J Clin Oncol* **17**:2105-2116.

Chapman PB, Hauschild A, Robert C, Haanen JB, Ascierto P, Larkin J, Dummer R, Garbe C, Testori A, Maio M, Hogg D, Lorigan P, Lebbe C, Jouary T, Schadendorf D, Ribas A, O'Day SJ, Sosman JA, Kirkwood JM, Eggermont AM, Dreno B, Nolop K, Li J, Nelson B, Hou J, Lee RJ, Flaherty KT and McArthur GA (2011) Improved survival with vemurafenib in melanoma with BRAF V600E mutation. *N Engl J Med* **364**:2507-2516.

Comis RL (1976) DTIC (NSC-45388) in malignant melanoma: a perspective. *Cancer Treat Rep* **60**:165-176.

Davies H, Bignell GR, Cox C, Stephens P, Edkins S, Clegg S, Teague J, Woffendin H, Garnett MJ, Bottomley W, Davis N, Dicks E, Ewing R, Floyd Y, Gray K, Hall S, Hawes R, Hughes J, Kosmidou V, Menzies A, Mould C, Parker A, Stevens C, Watt S, Hooper S, Wilson R, Jayatilake H, Gusterson BA, Cooper C, Shipley J, Hargrave D, Pritchard-Jones K, Maitland N, Chenevix-Trench G, Riggins GJ, Bigner DD, Palmieri G, Cossu A, Flanagan A, Nicholson A, Ho JW, Leung SY, Yuen ST, Weber BL, Seigler HF, Darrow TL, Paterson H, Marais R, Marshall CJ, Wooster R, Stratton MR and Futreal PA (2002) Mutations of the BRAF gene in human cancer. *Nature* **417**:949-954.

Davies MA, Liu P, McIntyre S, Kim KB, Papadopoulos N, Hwu WJ, Hwu P and Bedikian A (2011) Prognostic factors for survival in melanoma patients with brain metastases. *Cancer* **117**:1687-1696.

Enokizono J, Kusuhara H, Ose A, Schinkel AH and Sugiyama Y (2008) Quantitative investigation of the role of breast cancer resistance protein (Bcrp/Abcg2) in limiting brain and testis penetration of xenobiotic compounds. *Drug metabolism and disposition: the biological fate of chemicals* **36**:995-1002.

Falchook GS, Long GV, Kurzrock R, Kim KB, Arkenau TH, Brown MP, Hamid O, Infante JR, Millward M, Pavlick AC, O'Day SJ, Blackman SC, Curtis CM, Lebowitz P, Ma B, Ouellet D and Kefford RF (2012) Dabrafenib in patients with melanoma, untreated brain metastases, and other solid tumours: a phase 1 dose-escalation trial. *Lancet* **379**:1893-1901.

Fife KM, Colman MH, Stevens GN, Firth IC, Moon D, Shannon KF, Harman R, Petersen-Schaefer K, Zacest AC, Besser M, Milton GW, McCarthy WH and Thompson JF (2004) Determinants of outcome in melanoma patients with cerebral metastases. *J Clin Oncol* **22**:1293-1300.

Flaherty KT, Puzanov I, Kim KB, Ribas A, McArthur GA, Sosman JA, O'Dwyer PJ, Lee RJ, Grippo JF, Nolop K and Chapman PB (2010) Inhibition of mutated, activated BRAF in metastatic melanoma. *N Engl J Med* **363**:809-819.

Flaherty KT, Robert C, Hersey P, Nathan P, Garbe C, Milhem M, Demidov LV, Hassel JC, Rutkowski P, Mohr P, Dummer R, Trefzer U, Larkin JM, Utikal J, Dreno B, Nyakas M, Middleton MR, Becker JC, Casey M, Sherman LJ, Wu FS, Ouellet D, Martin AM, Patel K and Schadendorf D (2012) Improved survival with MEK inhibition in BRAF-mutated melanoma. *N Engl J Med* **367**:107-114.

Garbe C, Eigentler TK, Keilholz U, Hauschild A and Kirkwood JM (2011) Systematic review of medical treatment in melanoma: current status and future prospects. *Oncologist* **16**:5-24.

Gibney GT, Forsyth PA and Sondak VK (2012) Melanoma in the brain: biology and therapeutic options. *Melanoma Res* **22**:177-183.

Gowrishankar K, Snoyman S, Pupo GM, Becker TM, Kefford RF and Rizos H (2012) Acquired resistance to BRAF inhibition can confer cross-resistance to combined BRAF/MEK inhibition. *J Invest Dermatol* **132**:1850-1859.

Hauschild A, Grob JJ, Demidov LV, Jouary T, Gutzmer R, Millward M, Rutkowski P, Blank CU, Miller WH, Jr., Kaempgen E, Martin-Algarra S, Karaszewska B, Mauch C, Chiarion-Sileni V, Martin AM, Swann S, Haney P, Mirakhur B, Guckert ME, Goodman V and Chapman PB (2012) Dabrafenib in BRAF-mutated metastatic melanoma: a multicentre, open-label, phase 3 randomised controlled trial. *Lancet* **380**:358-365.

Johannessen CM, Boehm JS, Kim SY, Thomas SR, Wardwell L, Johnson LA, Emery CM, Stransky N, Cogdill AP, Barretina J, Caponigro G, Hieronymus H, Murray RR, Salehi-Ashtiani K, Hill DE, Vidal M, Zhao JJ, Yang X, Alkan O, Kim S, Harris JL, Wilson CJ, Myer VE, Finan PM, Root DE, Roberts TM, Golub T, Flaherty KT, Dummer R, Weber BL, Sellers WR, Schlegel R, Wargo JA, Hahn WC and Garraway LA (2010) COT drives resistance to

RAF inhibition through MAP kinase pathway reactivation. *Nature* **468**:968-972.

Kim KB, Kefford R, Pavlick AC, Infante JR, Ribas A, Sosman JA, Fecher LA, Millward M, McArthur GA, Hwu P, Gonzalez R, Ott PA, Long GV, Gardner OS, Ouellet D, Xu Y, DeMarini DJ, Le NT, Patel K and Lewis KD (2013) Phase II study of the MEK1/MEK2 inhibitor Trametinib in patients with metastatic BRAF-mutant cutaneous melanoma previously treated with or without a BRAF inhibitor. *J Clin Oncol* **31**:482-489.

Kim T, Kim J and Lee MG (2010) Inhibition of mutated BRAF in melanoma. *N Engl J Med* **363**:2261; author reply 2261-2262.

Kodaira H, Kusuhara H, Ushiki J, Fuse E and Sugiyama Y (2010) Kinetic analysis of the cooperation of P-glycoprotein (P-gp/Abcb1) and breast cancer resistance protein (Bcrp/Abcg2) in limiting the brain and testis penetration of erlotinib, flavopiridol, and mitoxantrone. *The Journal of pharmacology and experimental therapeutics* **333**:788-796.

McCubrey JA, Milella M, Tafuri A, Martelli AM, Lunghi P, Bonati A, Cervello M, Lee JT and Steelman LS (2008) Targeting the Raf/MEK/ERK pathway with small-molecule inhibitors. *Curr Opin Investig Drugs* **9**:614-630.

Mittapalli RK, Vaidhyanathan S, Dudek AZ and Elmquist WF (2013) Mechanisms limiting distribution of the threonine-protein kinase B-RaF(V600E) inhibitor dabrafenib to the brain: implications for the treatment of melanoma brain

metastases. *The Journal of pharmacology and experimental therapeutics* **344**:655-664.

Mittapalli RK, Vaidhyanathan S, Sane R and Elmquist WF (2012) Impact of P-glycoprotein (ABCB1) and breast cancer resistance protein (ABCG2) on the brain distribution of a novel BRAF inhibitor: vemurafenib (PLX4032). *The Journal of pharmacology and experimental therapeutics* **342**:33-40.

Nazarian R, Shi H, Wang Q, Kong X, Koya RC, Lee H, Chen Z, Lee MK, Attar N, Sazegar H, Chodon T, Nelson SF, McArthur G, Sosman JA, Ribas A and Lo RS (2010) Melanomas acquire resistance to B-RAF(V600E) inhibition by RTK or N-RAS upregulation. *Nature* **468**:973-977.

Ohtsuki S and Terasaki T (2007) Contribution of carrier-mediated transport systems to the blood-brain barrier as a supporting and protecting interface for the brain; importance for CNS drug discovery and development. *Pharm Res* **24**:1745-1758.

Rochet NM, Dronca RS, Kottschade LA, Chavan RN, Gorman B, Gilbertson JR and Markovic SN (2012) Melanoma brain metastases and vemurafenib: need for further investigation. *Mayo Clin Proc* **87**:976-981.

Sampson JH, Carter JH, Jr., Friedman AH and Seigler HF (1998) Demographics, prognosis, and therapy in 702 patients with brain metastases from malignant melanoma. *J Neurosurg* **88**:11-20.

Skibber JM, Soong SJ, Austin L, Balch CM and Sawaya RE (1996) Cranial irradiation after surgical excision of brain metastases in melanoma patients. *Ann Surg Oncol* **3**:118-123.

Uchida Y, Ohtsuki S, Katsukura Y, Ikeda C, Suzuki T, Kamiie J and Terasaki T (2011) Quantitative targeted absolute proteomics of human blood-brain barrier transporters and receptors. *Journal of neurochemistry* **117**:333-345.

Villanueva J, Vultur A, Lee JT, Somasundaram R, Fukunaga-Kalabis M, Cipolla AK, Wubbenhorst B, Xu X, Gimotty PA, Kee D, Santiago-Walker AE, Letrero R, D'Andrea K, Pushparajan A, Hayden JE, Brown KD, Laquerre S, McArthur GA, Sosman JA, Nathanson KL and Herlyn M (2010) Acquired resistance to BRAF inhibitors mediated by a RAF kinase switch in melanoma can be overcome by cotargeting MEK and IGF-1R/PI3K. *Cancer Cell* **18**:683-695.

Wang T, Agarwal S and Elmquist WF (2012) Brain distribution of cediranib is limited by active efflux at the blood-brain barrier. *The Journal of pharmacology and experimental therapeutics* **341**:386-395.

CHAPTER 5:

Agarwal S, Sane R, Oberoi R, Ohlfest JR and Elmquist WF (2011) Delivery of molecularly targeted therapy to malignant glioma, a disease of the whole brain. *Expert Rev Mol Med* **13**:e17.

Aplin AE, Kaplan FM and Shao Y (2011) Mechanisms of resistance to RAF inhibitors in melanoma. *J Invest Dermatol* **131**:1817-1820.

Balch CM, Gershenwald JE, Soong SJ, Thompson JF, Atkins MB, Byrd DR, Buzaid AC, Cochran AJ, Coit DG, Ding S, Eggermont AM, Flaherty KT, Gimotty PA, Kirkwood JM, McMasters KM, Mihm MC, Jr., Morton DL, Ross MI, Sober AJ and Sondak VK (2009) Final version of 2009 AJCC melanoma staging and classification. *J Clin Oncol* **27**:6199-6206.

Bollag G, Tsai J, Zhang J, Zhang C, Ibrahim P, Nolop K and Hirth P (2012) Vemurafenib: the first drug approved for BRAF-mutant cancer. *Nat Rev Drug Discov* **11**:873-886.

Chapman PB, Hauschild A, Robert C, Haanen JB, Ascierto P, Larkin J, Dummer R, Garbe C, Testori A, Maio M, Hogg D, Lorigan P, Lebbe C, Jouary T, Schadendorf D, Ribas A, O'Day SJ, Sosman JA, Kirkwood JM, Eggermont AM, Dreno B, Nolop K, Li J, Nelson B, Hou J, Lee RJ, Flaherty KT and McArthur GA (2011) Improved survival with vemurafenib in melanoma with BRAF V600E mutation. *N Engl J Med* **364**:2507-2516.

Davies H, Bignell GR, Cox C, Stephens P, Edkins S, Clegg S, Teague J, Woffendin H, Garnett MJ, Bottomley W, Davis N, Dicks E, Ewing R, Floyd Y, Gray K, Hall S, Hawes R, Hughes J, Kosmidou V, Menzies A, Mould C, Parker A, Stevens C, Watt S, Hooper S, Wilson R, Jayatilake H, Gusterson BA, Cooper C, Shipley J, Hargrave D, Pritchard-Jones K, Maitland N, Chenevix-Trench G, Riggins GJ, Bigner DD, Palmieri G, Cossu A, Flanagan A, Nicholson A, Ho JW, Leung SY, Yuen ST, Weber BL, Seigler HF, Darrow TL, Paterson H, Marais R, Marshall CJ, Wooster R, Stratton MR and Futreal PA (2002) Mutations of the BRAF gene in human cancer. *Nature* **417**:949-954.

Davies MA, Liu P, McIntyre S, Kim KB, Papadopoulos N, Hwu WJ, Hwu P and Bedikian A (2011) Prognostic factors for survival in melanoma patients with brain metastases. *Cancer* **117**:1687-1696.

Falchook GS, Long GV, Kurzrock R, Kim KB, Arkenau TH, Brown MP, Hamid O, Infante JR, Millward M, Pavlick AC, O'Day SJ, Blackman SC, Curtis CM, Lebowitz P, Ma B, Ouellet D and Kefford RF (2012) Dabrafenib in patients with melanoma, untreated brain metastases, and other solid tumours: a phase 1 dose-escalation trial. *Lancet* **379**:1893-1901.

Fife KM, Colman MH, Stevens GN, Firth IC, Moon D, Shannon KF, Harman R, Petersen-Schaefer K, Zacest AC, Besser M, Milton GW, McCarthy WH

and Thompson JF (2004) Determinants of outcome in melanoma patients with cerebral metastases. *J Clin Oncol* **22**:1293-1300.

Flaherty KT, Infante JR, Daud A, Gonzalez R, Kefford RF, Sosman J, Hamid O, Schuchter L, Cebon J, Ibrahim N, Kudchadkar R, Burris HA, 3rd, Falchook G, Algazi A, Lewis K, Long GV, Puzanov I, Lebowitz P, Singh A, Little S, Sun P, Allred A, Ouellet D, Kim KB, Patel K and Weber J (2012a) Combined BRAF and MEK inhibition in melanoma with BRAF V600 mutations. *N Engl J Med* **367**:1694-1703.

Flaherty KT, Robert C, Hersey P, Nathan P, Garbe C, Milhem M, Demidov LV, Hassel JC, Rutkowski P, Mohr P, Dummer R, Trefzer U, Larkin JM, Utikal J, Dreno B, Nyakas M, Middleton MR, Becker JC, Casey M, Sherman LJ, Wu FS, Ouellet D, Martin AM, Patel K and Schadendorf D (2012b) Improved survival with MEK inhibition in BRAF-mutated melanoma. *N Engl J Med* **367**:107-114.

Gibney GT, Forsyth PA and Sondak VK (2012) Melanoma in the brain: biology and therapeutic options. *Melanoma Res* **22**:177-183.

Gowrishankar K, Snoyman S, Pupo GM, Becker TM, Kefford RF and Rizos H (2012) Acquired resistance to BRAF inhibition can confer cross-resistance to combined BRAF/MEK inhibition. *J Invest Dermatol* **132**:1850-1859.

Greger JG, Eastman SD, Zhang V, Bleam MR, Hughes AM, Smitheman KN, Dickerson SH, Laquerre SG, Liu L and Gilmer TM (2012) Combinations of

BRAF, MEK, and PI3K/mTOR inhibitors overcome acquired resistance to the BRAF inhibitor GSK2118436 dabrafenib, mediated by NRAS or MEK mutations. *Mol Cancer Ther* **11**:909-920.

Gupta G, Robertson AG and MacKie RM (1997) Cerebral metastases of cutaneous melanoma. *Br J Cancer* **76**:256-259.

Hodis E, Watson IR, Kryukov GV, Arold ST, Imielinski M, Theurillat JP, Nickerson E, Auclair D, Li L, Place C, Dicara D, Ramos AH, Lawrence MS, Cibulskis K, Sivachenko A, Voet D, Saksena G, Stransky N, Onofrio RC, Winckler W, Ardlie K, Wagle N, Wargo J, Chong K, Morton DL, Stemke-Hale K, Chen G, Noble M, Meyerson M, Ladbury JE, Davies MA, Gershenwald JE, Wagner SN, Hoon DS, Schadendorf D, Lander ES, Gabriel SB, Getz G, Garraway LA and Chin L (2012) A landscape of driver mutations in melanoma. *Cell* **150**:251-263.

Johannessen CM, Boehm JS, Kim SY, Thomas SR, Wardwell L, Johnson LA, Emery CM, Stransky N, Cogdill AP, Barretina J, Caponigro G, Hieronymus H, Murray RR, Salehi-Ashtiani K, Hill DE, Vidal M, Zhao JJ, Yang X, Alkan O, Kim S, Harris JL, Wilson CJ, Myer VE, Finan PM, Root DE, Roberts TM, Golub T, Flaherty KT, Dummer R, Weber BL, Sellers WR, Schlegel R, Wargo JA, Hahn WC and Garraway LA (2010) COT drives resistance to RAF inhibition through MAP kinase pathway reactivation. *Nature* **468**:968-972.

Johnson JD and Young B (1996) Demographics of brain metastasis. *Neurosurg Clin N Am* **7**:337-344.

Karasarides M, Chiloeches A, Hayward R, Niculescu-Duvaz D, Scanlon I, Friedlos F, Ogilvie L, Hedley D, Martin J, Marshall CJ, Springer CJ and Marais R (2004) B-RAF is a therapeutic target in melanoma. *Oncogene* **23**:6292-6298.

Knight SD, Adams ND, Burgess JL, Chaudhari AM, Darcy MG, Donatelli CA, Luengo JI, Newlander KA, Parrish CA, Ridgers LH, Sarpong MA, Schmidt SJ, Van Aller GS, Carson JD, Diamond MA, Elkins PA, Gardiner CM, Garver E, Gilbert SA, Gontarek RR, Jackson JR, Kershner KL, Luo L, Raha K, Sherk CS, Sung CM, Sutton D, Tummino PJ, Wegrzyn RJ, Auger KR and Dhanak D (2010) Discovery of GSK2126458, a Highly Potent Inhibitor of PI3K and the Mammalian Target of Rapamycin. *ACS Med Chem Lett* **1**:39-43.

Kodaira H, Kusuhara H, Ushiki J, Fuse E and Sugiyama Y (2010) Kinetic analysis of the cooperation of P-glycoprotein (P-gp/Abcb1) and breast cancer resistance protein (Bcrp/Abcg2) in limiting the brain and testis penetration of erlotinib, flavopiridol, and mitoxantrone. *J Pharmacol Exp Ther* **333**:788-796.

Mittapalli RK, Vaidhyanathan S, Dudek AZ and Elmquist WF (2013) Mechanisms limiting distribution of the threonine-protein kinase B-RaF(V600E) inhibitor

dabrafenib to the brain: implications for the treatment of melanoma brain metastases. *J Pharmacol Exp Ther* **344**:655-664.

Mittapalli RK, Vaidhyanathan S, Sane R and Elmquist WF (2012) Impact of P-glycoprotein (ABCB1) and breast cancer resistance protein (ABCG2) on the brain distribution of a novel BRAF inhibitor: vemurafenib (PLX4032). *J Pharmacol Exp Ther* **342**:33-40.

Nazarian R, Shi H, Wang Q, Kong X, Koya R, Lee H, Chen Z, Lee M-K, Attar N, Sazegar H, Chodon T, Nelson SF, McArthur G, Sosman JA, Ribas A and Lo RS (2010a) Melanomas acquire resistance to B-RAF(V600E) inhibition by RTK or N-RAS upregulation. *Nature*:1-5.

Nazarian R, Shi H, Wang Q, Kong X, Koya RC, Lee H, Chen Z, Lee MK, Attar N, Sazegar H, Chodon T, Nelson SF, McArthur G, Sosman JA, Ribas A and Lo RS (2010b) Melanomas acquire resistance to B-RAF(V600E) inhibition by RTK or N-RAS upregulation. *Nature* **468**:973-977.

Ohtsuki S and Terasaki T (2007) Contribution of carrier-mediated transport systems to the blood-brain barrier as a supporting and protecting interface for the brain; importance for CNS drug discovery and development. *Pharm Res* **24**:1745-1758.

Puzanov I, Burnett P and Flaherty KT (2011) Biological challenges of BRAF inhibitor therapy. *Mol Oncol* **5**:116-123.

Sampson JH, Carter JH, Jr., Friedman AH and Seigler HF (1998) Demographics, prognosis, and therapy in 702 patients with brain metastases from malignant melanoma. *J Neurosurg* **88**:11-20.

Siegel R, Ma J, Zou Z and Jemal A (2014) Cancer statistics, 2014. *CA Cancer J Clin* **64**:9-29.

Vaidhyanathan S, Mittapalli RK, Sarkaria JN and Elmquist WF (2014) Factors influencing the CNS distribution of a novel MEK-1/2 inhibitor: implications for combination therapy for melanoma brain metastases. *Drug Metab Dispos* **42**:1292-1300.

Villanueva J, Vultur A, Lee JT, Somasundaram R, Fukunaga-Kalabis M, Cipolla AK, Wubbenhorst B, Xu X, Gimotty PA, Kee D, Santiago-Walker AE, Letrero R, D'Andrea K, Pushparajan A, Hayden JE, Brown KD, Laquerre S, McArthur GA, Sosman JA, Nathanson KL and Herlyn M (2010) Acquired resistance to BRAF inhibitors mediated by a RAF kinase switch in melanoma can be overcome by cotargeting MEK and IGF-1R/PI3K. *Cancer Cell* **18**:683-695.

Wagle N, Van Allen EM, Treacy DJ, Frederick DT, Cooper ZA, Taylor-Weiner A, Rosenberg M, Goetz EM, Sullivan RJ, Farlow DN, Friedrich DC, Anderka K, Perrin D, Johannessen CM, McKenna A, Cibulskis K, Kryukov G, Hodis E, Lawrence DP, Fisher S, Getz G, Gabriel SB, Carter SL, Flaherty KT, Wargo JA and Garraway LA (2014) MAP kinase pathway alterations in

BRAF-mutant melanoma patients with acquired resistance to combined RAF/MEK inhibition. *Cancer Discov* **4**:61-68.

Wan PT, Garnett MJ, Roe SM, Lee S, Niculescu-Duvaz D, Good VM, Jones CM, Marshall CJ, Springer CJ, Barford D and Marais R (2004) Mechanism of activation of the RAF-ERK signaling pathway by oncogenic mutations of B-RAF. *Cell* **116**:855-867.

CHAPTER 6:

Brouwers J, Brewster ME and Augustijns P (2009) Supersaturating drug delivery systems: the answer to solubility-limited oral bioavailability? *J Pharm Sci* **98**:2549-2572.

Chapman PB, Hauschild A, Robert C, Haanen JB, Ascierto P, Larkin J, Dummer R, Garbe C, Testori A, Maio M, Hogg D, Lorigan P, Lebbe C, Jouary T, Schadendorf D, Ribas A, O'Day SJ, Sosman JA, Kirkwood JM, Eggermont AM, Dreno B, Nolop K, Li J, Nelson B, Hou J, Lee RJ, Flaherty KT and McArthur GA (2011) Improved survival with vemurafenib in melanoma with BRAF V600E mutation. *N Engl J Med* **364**:2507-2516.

Davies H, Bignell GR, Cox C, Stephens P, Edkins S, Clegg S, Teague J, Woffendin H, Garnett MJ, Bottomley W, Davis N, Dicks E, Ewing R, Floyd Y, Gray K, Hall S, Hawes R, Hughes J, Kosmidou V, Menzies A, Mould C, Parker A, Stevens C, Watt S, Hooper S, Wilson R, Jayatilake H, Gusterson BA, Cooper C, Shipley J, Hargrave D, Pritchard-Jones K, Maitland N, Chenevix-Trench G, Riggins GJ, Bigner DD, Palmieri G, Cossu A, Flanagan A, Nicholson A, Ho JW, Leung SY, Yuen ST, Weber BL, Seigler HF, Darrow TL, Paterson H, Marais R, Marshall CJ, Wooster R, Stratton MR and Futreal PA (2002) Mutations of the BRAF gene in human cancer. *Nature* **417**:949-954.

Leuner C and Dressman J (2000) Improving drug solubility for oral delivery using solid dispersions. *Eur J Pharm Biopharm* **50**:47-60.

Mittapalli RK, Vaidhyanathan S, Sane R and Elmquist WF (2012) Impact of P-glycoprotein (ABCB1) and breast cancer resistance protein (ABCG2) on the brain distribution of a novel BRAF inhibitor: vemurafenib (PLX4032). *J Pharmacol Exp Ther* **342**:33-40.

Noyes AA, Whitney, W.R. (1897) The rate of solution of solid substances in their own solutions. *J Am Chem Soc* **19**:930-934.

Renfrow JJ and Lesser GJ (2013) Molecular subtyping of brain metastases and implications for therapy. *Curr Treat Options Oncol* **14**:514-527.

Shah N, Iyer RM, Mair HJ, Choi DS, Tian H, Diodone R, Fahnrich K, Pabst-Ravot A, Tang K, Scheubel E, Grippo JF, Moreira SA, Go Z, Mouskountakis J, Louie T, Ibrahim PN, Sandhu H, Rubia L, Chokshi H, Singhal D and Malick W (2013) Improved human bioavailability of vemurafenib, a practically insoluble drug, using an amorphous polymer-stabilized solid dispersion prepared by a solvent-controlled coprecipitation process. *J Pharm Sci* **102**:967-981.